
Theses and Dissertations

Summer 2018

Nanofiber-enabled multi-target passive sampling device for legacy and emerging organic contaminants

Jiajie Qian
University of Iowa

Follow this and additional works at: <https://ir.uiowa.edu/etd>

 Part of the [Chemical Engineering Commons](#)


Copyright © 2018 Jiajie Qian

This dissertation is available at Iowa Research Online: <https://ir.uiowa.edu/etd/6487>

Recommended Citation

Qian, Jiajie. "Nanofiber-enabled multi-target passive sampling device for legacy and emerging organic contaminants." PhD (Doctor of Philosophy) thesis, University of Iowa, 2018.
<https://doi.org/10.17077/etd.lv1vq3ld>

Follow this and additional works at: <https://ir.uiowa.edu/etd>

 Part of the [Chemical Engineering Commons](#)

NANOFIBER-ENABLED MULTI-TARGET PASSIVE SAMPLING DEVICE FOR LEGACY
AND EMERGING ORGANIC CONTAMINANTS

by

Jiajie Qian

A thesis submitted in partial fulfillment
of the requirements for the Doctor of Philosophy
degree in Chemical and Biochemical Engineering in the
Graduate College of
The University of Iowa

August 2018

Thesis Supervisor: Professor David M. Cwiertny

Copyright by

Jiajie Qian

2018

All Rights Reserved

Graduate College
The University of Iowa
Iowa City, Iowa

CERTIFICATE OF APPROVAL

PH.D. THESIS

This is to certify that the Ph.D. thesis of

Jiajie Qian

has been approved by the Examining Committee
for the thesis requirement for the Doctor of Philosophy degree
in Chemical and Biochemical Engineering at the August 2018 graduation.

Thesis Committee:

David M. Cwiertny, Thesis Supervisor

David G. Rethwisch

Eric E. Nuxoll

Syed Mubeen Jawahar Hussaini

Andres Martinez Araneda

To my family, Thanks for your love and encouragement.

ACKNOWLEDGMENTS

First of all, I would like to express my deepest gratitude to my advisor, Professor David Cwiertyny, for his encouragement, patience, and careful guidance through my Ph.D. study. He shows me an example what a great scientist should look like and teach me how to think more logically and keep moving forward. I really appreciate he took me as his student and gave a chance to work with him.

I would also like to thank Dr. Andres Martinez for all his guidance on my research project. He is always willing to share his experience and listen to my thoughts. He patiently taught the knowledge of sampling methods and made me feel comfortable in this project. Without his help, I cannot complete my research tasks smoothly.

To my previous and current lab mates, Katherine Peter, Katie Greenstein, Edgard Verdugo, Brandon Jennings, Adam Johns, Matt Nagorzanki, Madeline Jensen, Monica McFadden, and Andrew Kral, thanks for all your assistance, friendship and laughter. It is a great experience to work with them.

A special thanks to my lab manager, Deborah Williard, for her conscientious work, which helps maintain a safe lab environment and a good condition for all instruments in our lab. I also want to acknowledge my mentor, Professor Eric Nuxoll, for his concern about study and lift at the University of Iowa. He gave me many useful suggestions about my career deployment.

This project was funded by both Strategic Environmental Research and Development Program (DOD) and Environmental Health Sciences Research Center (the University of Iowa). It was my honor to achieve graduate fellowship which supports me to finish my study.

A huge thanks to my family and girlfriend. Thanks for always supporting and encouraging me without any hesitation. It was a wonderful feeling to hear their voice when I was frustrated sometimes. I appreciate every word from you. Your unconditional trust and love make me successful.

Finally, I would like to thank my coworkers and friends in Iowa for your attention, assistance and company. You make my life more colorful and meaningful.

ABSTRACT

The widespread environmental occurrence of chemical pollutants presents an ongoing threat to human and ecosystem health. This challenge is compounded by the diversity of chemicals used in industry, commerce, agriculture and medicine, which results in a spectrum of potential fates and exposure profiles upon their inevitable release into the environment. This, in turn, confounds risk assessment, where challenges persist in accurate determination of concentrations levels, as well as spatial and temporal distributions, of pollutants in environmental media (e.g., water, air, soil and sediments).

Passive sampling technologies continue to gain acceptance as a means for simplifying environmental occurrence studies and, ultimately, improving the quality of chemical risk assessment. Passive samplers rely on the accumulation of a target analyte into a matrix via molecular diffusion, which is driven by the difference in chemical potential between the analyte in the environment and the sampling media (e.g., sorbent phase). After deployment, the target analyte can be extracted from the sampling media and quantified, providing an integrated, time-weighted average pollutant concentration via a cost-effective platform that requires little energy or manpower when compared to active (e.g., grab) sampling approaches. While a promising, maturing technology, limitations exist in current commercially available passive samplers; they are typically limited in the types of chemicals that can be targeted effectively, can require long deployment times to accumulate sufficient chemical for analysis, and struggle with charged analytes.

In this dissertation, we have designed a next-generation, nanofiber sorbent as a passive sampling device for routine monitoring of both legacy and emerging organic pollutant classes in water and sediment. The polymer nanofiber networks fabricated herein exhibit a high surface area to volume ratio (SA/V values) which shortens the deployment time. Uptake studies of these polymer nanofiber samplers suggest that field deployment could be shortened to less than one day for surface water analysis, effectively operating as an equilibrium passive sampling device, and twenty days for pore water analysis in soil and sediment studies. By comparison, most commercially available passive sampler models generally require at least a month of deployment before comparable analyses may be made.

Another highlight of the nanofiber materials produced herein is their broad target application range. We demonstrate that both hydrophobic (e.g., persistent organic pollutants, or POPs, like PCBs and dioxin) and hydrophilic (e.g., emerging pollutant classes including pesticides, pharmaceuticals and personal care products) targets can be rapidly accumulated with our optimal nanofibers formulations. This suggests that one of our devices could potentially replace multiple commercial passive sampling devices, which often exhibit a more limited range of analyte targets.

We also present several approaches for tailoring nanofiber physical and chemical properties to specifically target particular high priority pollutant classes (e.g., PFAS). Three promising modification approaches validated herein include: (i) fabricating carbon nanotube-polymer composites to capture polar compounds; (ii) introducing surface-segregating cationic

surfactants to target anionic pollutants (e.g., the pesticide 2,4-D and perfluorooctanoic acid or PFOA); and (iii) use of leachable surfactants as porogens to increase nanofiber pore volume and surface area to increase material capacity.

Collectively, outcomes of this work will guide the future development of next generation passive samplers by establishing broadly generalizable structure-activity relationships. All told, we present data related to the influence on the rate and extent of pollutant uptake in polymer nanofiber matrices as a function of both physical (specific surface area, pore volume, and diameter) and chemical (e.g., bulk and surface composition, nanofiber wettability, surface charge) nanofiber properties. We also present modeling results describing sampler operation that can be used to assess and predict passive sampler performance prior to field deployment.

The electrospun nanofiber mats (ENMs) developed as passive sampling devices herein provide greater functionality and allow for customizable products for application to a wide range of chemical diverse organic pollutants. Combined with advances in and expansion of the nanotechnology sector, we envision this product could be made commercially available so as to expand the use and improve the performance of passive sampling technologies in environmental monitoring studies.

PUBLIC ABSTRACT

A diverse range of chemical pollutants enter into the environment, impacting the quality of our water, air and soil, and threatening human health and the health of wildlife. Some pollutants, called persistent organic pollutants or POPs, are the legacy of our industrial past when chemical regulations were more limited. These types of chemicals tend to accumulate in soil and in sediments at the bottom of water bodies, and can persist in these environments for a long time because they are difficult to break down either naturally or in engineered treatment systems. More recent, pollutant concerns have centered on chemicals used widely in agriculture, commerce and medicine. These so-called “emerging” pollutants differ in their behavior from POPs; they prefer to exist in water rather than most soil or sediment systems, and many are designed to be potent and bioactive in humans and wildlife at relatively low levels.

Given the diversity of chemical pollutants in the environment, a persistent challenge is the development of reliable ways to identify the presence and measure the amount of chemicals in water, soil and sediments. This thesis focuses on improving on such monitoring approach, passive samplers. This approach uses specifically designed materials placed in water and soil that effectively function like a sponge, attracting and accumulating chemical pollutants onto and into them. Once collected after their use in the environment, the pollutants can be washed off the passive sampler, collected, and analyzed to determine which pollutants are present and

at what levels in the environment. Passive samplers are advantageous because they are low cost and their use in the environment does not require intense labor or energy demands.

Herein, we improve upon currently commercially available passive samplers by making new materials that are effective toward a wide range of pollutants (e.g., POPs and emerging pollutants), and can more quickly accumulate larger quantities of pollutants. To do this, we rely on nanotechnology, using a process known as electrospinning to make innovative nanomaterials (i.e., materials that have at least one-dimension or structural feature less than 100 nanometers). Electrospinning is a versatile approach for making nanomaterials, specifically nanofibers, with a high degree of control, allowing us to make passive samplers with unique properties ideal for their use in measuring POPs and emerging pollutants. We demonstrate the outstanding performance of these tailored nanofibers using a combination of laboratory studies, as well as field investigations where the passive samplers are used to measure pesticide levels in an Iowa stream.

Collectively, results of this work should help to advance the state-of-the-art in measuring legacy and emerging chemical pollutants using passive sampling technologies, and the materials generated herein may one day have commercial viability for use by researchers beyond the University of Iowa.

TABLE OF CONTENTS

LIST OF TABLES	xiii
LIST OF FIGURES	xvi
CHAPTER 1 INTRODUCTION.....	1
1.1. Organic pollutants in the aquatic environment	1
1.1.1. Hydrophobic Compounds	2
1.1.2. Hydrophilic and Moderately Hydrophobic Compounds.....	4
1.2. Environmental sampling and monitoring methods	5
1.2.1. Passive sampling devices: background and operating principles	6
1.2.2. Kinetic passive samplers	9
1.2.3. Equilibrium passive samplers	11
1.2.4. Current passive sampling materials and technical barriers to further development.....	12
1.3. Potential of Engineered Nanomaterials as Next-Generation Passive Sampling Devices	16
1.3.1. Electrospun nanofiber mats for environmental applications	17
1.3.2. Use of polymer electrospun nanofiber mats as sorbent materials....	18
1.3.3. Tailoring ENM polymer characteristics to improve performance ...	20
1.3.4. Fabrication of polymer ENM nanocomposites to improve performance	22
1.3.5. Imparting chemical functionalization to improve ENM performance: Surfactants	25
1.3.6. Imparting chemical functionalization to improve ENM performance: Post-synthesis chemical processing	27
1.4. Thesis Motivation, Objectives and Overarching Hypotheses	29
1.4.1. Objectives and Hypotheses	29
1.5. Overview and thesis organization	31
CHAPTER 2 DEVELOPMENT AND APPLICATION OF POLYMERIC ELECTROSPUN NANOFIBER MATS AS EQUILIBRIUM-PASSIVE SAMPLER MEDIA FOR ORGANIC COMPOUNDS	35

2.1. ABSTRACT.....	35
2.2. INTRODUCTION	37
2.3 MATERIAL AND METHODS	40
2.4 RESULTS AND DISCUSSION	54
2.5. CONCLUSIONS AND ENVIRONMENTAL IMPLICATIONS	88
CHAPTER 3 POLYMER NANOFIBER-CARBON NANOTUBE COMPOSITES AS A PASSIVE SAMPLING MEDIA FOR POLAR ORGANIC POLLUTANTS	
	90
3.1. ABSTRACT.....	90
3.2. INTRODUCTION	92
3.3. MATERIALS AND METHODS.....	95
3.4 .RESULTS AND DISCUSSION	105
3.5. CONCLUSIONS AND ENVIRONMENTAL IMPLICATIONS	136
CHAPTER 4 SURFACTANT-ASSISTED FABRICATION OF POLYMERIC ELECTROSPUN NANOFIBERS (ENMS): INTEGRATION OF SURFACE FUNCTIONALITIES AND POROSITY TO IMPROVE ORGANIC CHEMICAL UPTAKE.....	
	138
4.1. ABSTRACT.....	138
4.2. INTRODUCTION	140
4.3. MATERIALS AND METHODS	145
4.4. RESULTS AND DISCUSSION	151
4.5. CONCLUSIONS AND ENVIRONMENTAL IMPLICATIONS	172
CHAPTER 5 CONCLUSIONS & FUTURE RESEARCH DIRECTIONS.....	
	175
5.1. Thesis overview	175
5.2. Summary of key findings	177
5.2.1. Polymer electrospun nanofibers are a promising sampling material for both POPs and HMHC.	177
5.2.2. Carbon nanotubes can be integrated into polymer ENMs to enhance performance.....	178
5.2.3. Surfactants can be added to increase surface area and target charged analytes.....	180

5.3. Future research needs	181
5.3.1. Use molecular imprinting techniques to improve ENM selectivity	182
5.3.2. Additional field testing	183
5.3.3. Mechanistic studies with optimized ENMs.	183
5.3.4. Additional environmental applications of ENMs.	184
LITERATURE CITED	186

LIST OF TABLES

Table 1-1. Summary of current functionalized CNT products of Cheap Tubes Inc.	23
Table 2-1. Reagents, physical and chemical properties, and electrospinning synthesis parameters for ENMs investigated herein.	42
Table 2-2. Molecular structures and chemical properties of our organic target analyte suite.	46
Table 2-3. Physical and chemical properties for ENMs investigated herein.	58
Table 2-4. Summary of average measured and predicted ENM-water equilibrium partition coefficients for aniline and nitrobenzene (log units, L/kg) under mixing and static conditions, as well as predicted t ₉₀ % for both mixing and static conditions. For aniline and nitrobenzene, values were also calculated from the sorption isotherms for PAN, PMMA and PS (Figure 2-16).	60
Table 2-5. Summary of average measured ENM-water equilibrium partition coefficients for our hydrophobic model compounds (log units, L/kg) under mixing conditions. Values represent average from 0.5 to 1 day collection samples.	66
Table 2-6. Comparison of measured and predicted ENM-water equilibrium partition coefficients for nitrobenzene (log units, L/kg) for different diameter size of PS under no mixing conditions.	74
Table 2-7. Summary of average and model ENM-water equilibrium partition coefficients and t ₉₀ %s for the 10 hydrophilic and moderately hydrophobic compounds with PAN and PS ENMs (log units, L/kg) under mixing conditions.	82
Table 3-1. Vendor (Cheap Tubes, Inc.) provided characteristics of non-functionalized CNTs (NF-CNT) and oxidized CNTs with carboxylic acid functional groups (COOH-CNT).	96
Table 3-2. Structure and select physicochemical properties of the organic chemical targets investigated here.	97
Table 3-3. Characterization results for synthesized ENM-CNT composites synthesized herein.	105
Table 3-4. Digital (left column, ~25 cm ²) and low-magnification SEM (right column) images of ENM-CNT composites produced herein.	106

Table 3-5. Summary comparing model-estimated and experimentally measured ENM-water equilibrium partition coefficients ($\log K_{\text{ENM-W}}$ values) and $t_{90\%}$ values for select analyte targets on NF-CNT/PAN and COOH-CNT/PAN (at 20% wt. CNT loading).	115
Table 3-6. Values of $\log K_{\text{ENM-W}}$ for NF-CNT/PAN with different average diameters. All ENM-CNT composites were fabricated at 20% wt. of NF-CNT, but the wt.% of PAN was varied to alter average diameter values.	118
Table 3-7. Summary of ENM-water equilibrium partition coefficients for selected model compounds (\log units, L/kg). Values are provided for pure polymers (PS and PAN), as well as composites made with NF-CNT and COOH-CNT. Values determined at pH 7 for an initial chemical concentration of $25\mu\text{M}$ and an ENM loading of ~ 1.5 g/L. Uncertainties represent standard deviations from at least triplicate measurements.....	123
Table 3-8. Summary of K_f and n values from Freundlich model fits to sorption isotherms for diuron and caffeine obtained with CNT/PAN composites. Uncertainties represent standard error associated with regression analysis.....	127
Table 3-9. Values of $\log K_{\text{ENM-W}}$ and C_{ENM} (measured after 48 h) for 2,4-D on CNT/PS and CNT/PAN composites at pH 5 and 7. Uncertainties are standard deviations obtained from the number of replicates (n) indicated.	131
Table 3-10. Values of $\log K_{\text{ENM-W}}$ for atrazine and 2,4-D measured at different temperatures on CNT/PAN composites. Uncertainties associated represent standard deviations from at least three replicate experiments.	131
Table 3-11. Values of $\log K_{\text{ENM-W}}$ and total mass in ENM (M_{ENM} measured after 48 h) for 2,4-D on CNT/PS and CNT/PAN composites in systems with either 50 or 100 mg of ENM mass. Uncertainties are standard deviations obtained from the number of replicates (n) indicated.....	132
Table 3-12. Values of $\log K_{\text{ENM-W}}$ and total mass in ENM (M_{ENM} measured after 48 h) for diuron and atrazine COOH-CNT/PAN and NF-CNT/PAN in systems with either 25, 50 or 100 mg of ENM mass.	133
Table 3-13. Comparison of $\log K_{\text{ENM-W}}$ values for atrazine and 2,4-D on NF-CNT/PAN and COOH-CNT/PAN (20% wt.) measured in model phosphate buffer systems (DI water) and Iowa River Water.	134
Table 4-1. Molecular structures and chemical properties of surfactants investigated herein.	146

Table 4-2. Structure and select physicochemical properties of the organic chemical targets investigated here.....	148
Table 4-3. Surface area, pore volume and average diameters (with standard deviation) of surfactant-modified nanofibers fabricated herein.	152
Table 4-4. Scanning electron microscopy images for surfactant-modified CNT/PAN composites. Both low (left) and high (right) magnification images are shown. ...	154
Table 4-5. Values of $\log K_{\text{ENM-W}}$ for atrazine and 2,4-D as measured in model DI water systems (i.e., 1 mM phosphate buffer), systems containing 5 mg/L of FHA, and in Iowa River water. Values represent mean and standard deviation on $K_{\text{ENM-W}}$ values from at least two experiments.	169
Table 4-6. Values of $\log K_{\text{ENM-W}}$ for atrazine and 2,4-D as measured at 4 °C, 20 °C and 35 °C. Values represent mean and standard deviation on $K_{\text{ENM-W}}$ values from three experiments.	170
Table 4-7. Images of freshly prepared, field deployed, and washed TBAB-modified ENMs. Images are provided both for PAN and COOH-CNT/PAN ENMs. Samples were deployed for 2 days at Muddy Creek, Coralville, IA (USGS 05454090).	171
Table 4-8. Summary of $\log K_{\text{ENM-W}}$ values measured herein with surfactant-modified materials across the target organic analyte suite.	174

LIST OF FIGURES

Figure 1-1. Chemical structure of POPs examples.....	4
Figure 1-2. The octanol-water partition coefficient of selected organic compounds	5
Figure 1-3. Schematic representation of analyte concentration in the sampler material over time, illustrating the two passive sampler operation within the kinetic and equilibrium regimes.	9
Figure 1-4. Schematic of Semi-Permeable Membrane Devices (SPMDs).....	13
Figure 1-5. Schematic of Solid-Phase Microextraction (SPME) Device	13
Figure 1-6. Schematic of Polar Organic Compound Integrative Sampler (POCIS).....	14
Figure 1-7. Schematic of Chemcatcher®	15
Figure 1-8. Sampling rate (in L/d) for POCIS and SPMD as a function of the target analytes hydrophobicity as quantified by logK _{ow} values. The blue and red lines effectively establish the useful monitoring range of pollutant targets for POCIS and SPMD	16
Figure 1-9. Set-up of the lab electrospinning apparatus	18
Figure 1-10. The structural unit of polymers that can be fabricated by electrospinning and may also be beneficial for use in passive sampler applications for legacy and emerging pollutant classes.	20
Figure 1-11. Schematic of (a) coaxial and (b) multiple needles/nozzles electrospinning set-up	21
Figure 1-12. Schematic of carbon nanotubes: single-walled CNT (left), multi-walled CNT (middle) and functionalized CNT (right).....	24
Figure 1-13. Surface functionalization of carbon nanotubes	25
Figure 1-14. Examples of common surfactants for electrospun nanofiber: Sodium dodecyl sulfate (SDS), Alkylphosphonic acids (APA), Sodium dodecylbenzenesulfonate (SDBS), Cetrimonium bromide (CTAB), Tetrabutylammonium bromide (TBAB),Hexadecyltrimethylammonium bromide (HDTMAB).	27
Figure 1-15. The reaction equation of amidoximation reaction on PAN-based ENM	28

Figure 2-1. Set-up of the lab electrospinning apparatus. The left cartoon shows a schematic of an electrospinning apparatus, including high-voltage power supply, spinneret (metallic needle), collector (aluminum foil or metallic drum) and syringe pump. Right photograph shows the laboratory scale electrospinning apparatus used to fabricate all ENMs tested herein.....	41
Figure 2-2. SEM images of fabricated ENMs at low (left) and high (right) magnification. Corresponding recipes and characterization of these ENMs are provided in Table 2-1.....	56
Figure 2-3. Histograms of four batches of PS fabricated. Diameters for at least 100 individual nanofibers within ENMs were quantified via SEM to produce these distributions.....	57
Figure 2-4. Photographs illustrating the handling, manipulation and mechanical strength of a representative PS.....	57
Figure 2-5. Uptake curves with mixing and without mixing for aniline (a, c) and nitrobenzene (b, d) with our five ENMs. The error bars represent one standard deviation from two (w/mixing) and three (static) replicate uptake experiments. Laboratory set up: pH ~ 6.5 (DI water), initial concentrations of aniline: 2 mg/L and nitrobenzene: 3 mg/L, ENM loading ~1.5 g/L. Please note the difference in the x-axis scale for experiments with and without mixing. The light gray area in panels a and b notes a shorter, zoomed in time scale. Lines simply connect data points.....	59
Figure 2-6. Linear regressions (black=aniline, red=nitrobenzene) between equilibrium partition coefficients and (a) water contact angle and (b) specific surface area. Data are shown for PAN (▲), PMMA (▼), PS (●), PVDF(■) and PET (◆). The p-values of the slopes from the regressions are shown as p. Significant is considered with a p-value < 0.05.....	61
Figure 2-7. Comparison of measured equilibrium partition coefficients for (a) aniline and (b) nitrobenzene for all of the ENMs synthesized, and commercially available materials (PS beads, PDMS fiber and LDPE film). Laboratory set up: pH ~ 6.5 (DI water), initial concentrations of aniline: 2 mg/L and nitrobenzene: 3 mg/L, sorbent loading ~1.5 g/L, equilibration time 4 days.....	63
Figure 2-8. Uptake curves for selected PCB congeners and dioxin (TCCD) on ENMs. The error bars represent the standard deviation from two replicate uptake experiments. Laboratory set up: pH ~ 6.5 (DI water), initial concentrations from 0.25 to 5 ng/L, ENM loading ~ 3 g/L. Please note the difference in the y-	

axis scale. Lines simply connect data points.	65
Figure 2-9. Average equilibrium partition coefficients in log units (L/kg) for PAN, PET, PMMA and PS for our model hydrophobic compounds. Uncertainties represent the standard deviation from at least two replicate experiments. Values are also shown in Table 2-5. Laboratory set up: pH ~ 6.5 (DI water), initial concentrations from 0.25 to 5 ng/L, ENM loading ~ 3 g/L.....	65
Figure 2-10. Linear regressions (black=PCB1, red=PCB11, green=PCB29, blue=PCB47, pink=PCB121, cyan=PCB136, grey=Dioxin) between equilibrium partition coefficients and (a) water contact angle and (b) surface area of ENMs. Data are shown for PAN (▲), PMMA (▼), PS (●), PVDF(■) and PET (◆). The p-values of the slopes from the regressions are shown as p. Significant is considered with a p-value < 0.05, and are in bold.	68
Figure 2-11. LogK _{OW} versus logK _{ENM-W} for selected PCB congeners (PCBs 1, 11, 29, 47, 121 and 136) and dioxin in PAN, PS, PMMA and PET. The p-value in parenthesis corresponds to the linear regression.	69
Figure 2-12. Uptake profile of nitrobenzene into PAN, PET, PMMA, PS and PVDF under mixing conditions. K _{ENM-W} values are the average of at least 3 replicates. The curves show the non-linear least squares regression from the one compartment first-order kinetic model. Laboratory set up: pH ~ 6.5 (DI water), initial concentrations of aniline: 2 mg/L and nitrobenzene: 3 mg/L, ENM loading ~1.5 g/L. K _{ENM-W} values are also presented in Figure 2-5b.....	70
Figure 2-13. Time to reach 90% equilibrium (t _{90%}) for (a) aniline and (b) nitrobenzene versus nanofiber diameter of our ENMs. Void circles correspond to mixing experiments, while black triangles are under static conditions. t _{90%} was calculated from Equation 2-3, and the nanofiber diameters are shown in Table 2-3. Line represents the linear regression from the mixing experiments (void circles). See the y-axis break in b).....	71
Figure 2-14. Nitrobenzene uptake into PS as a function of nanofiber diameter. Data are shown for PS with 140, 300 and 560 nm, and uptake experiments were conducted statically (without mixing). For comparison, data for the 140 nm (our standard PS recipe) are also shown from experimental systems were actively mixed. t _{90%} s were calculated from the non-linear least squares regressions (Table 2-6). The curves show the non-linear least squares regression from the one compartment first-order kinetic model. Laboratory set up: pH ~ 6.5 (DI water), initial concentrations of nitrobenzene: 3 ng/L, ENM loading ~ 1.5 g/L.....	74

- Figure 2-15. ENM-water equilibrium partition coefficients (L/kg) for aniline (AN) and nitrobenzene (NB) measured as a function of solution pH for PMMA and PS....77
- Figure 2-16. Sorption isotherms using PAN, PMMA and PS for (a) aniline and (b) nitrobenzene. All linear regressions are statistically significant ($p > 0.001$). Calculated $K_{\text{ENM-W}}$ values from the slopes are presented in Table 2-4. Initial aqueous concentrations for aniline were 1 - 20 mg/L and nitrobenzene were 1 - 29 mg/L. Uncertainties represent the standard deviation from two replicate uptake experiments. When no uncertainty is visible, the bars are smaller than the data symbol.77
- Figure 2-17. Measurements in heterogeneous systems of (a) nitrobenzene pore water concentrations versus time in systems with a model spiked soil, and (b) individual PCB sediment pore water concentrations from IHSC sediment, both using PMMA and PS. IHSC measurements were carried out for 28 days. Error bars represent the standard deviation from two replicate uptake experiments. Lines simply connect data points.....81
- Figure 2-18. Photograph sequence of cleaning for PS (top) and PMMA (bottom) after being exposed to model soils for 5 days. SEM image confirmation was not possible to perform to PMMA due to the amount of soil/organic particles attached to it.....81
- Figure 2-19. PS and PAN uptake curves for our ten hydrophilic and moderately hydrophobic compounds. The error bars represent the standard deviation from two replicate uptake experiments. Laboratory set up: pH ~ 6.5 (DI water), initial concentrations from 2.4 to 6.8 mg/L, ENM loading ~ 1.5 g/L. Please note the difference in the y-axis scale.....84
- Figure 2-20. Average equilibrium partition coefficients of PAN (top panels) and PS (bottom panels) versus octanol-water (K_{OW}) and hexadecane-water ($K_{\text{hexadecane-w}}$)²⁰⁵ partition coefficients, and dissolution constant (D)¹⁷⁶ for our hydrophilic and moderately hydrophobic and hydrophobic analyte suite. When no error bar is visible, the bars are smaller than the data symbol. Uncertainties represent the standard deviation from at least two replicate experiments. Compounds with uptake into ENMs of less than 5% of the total available mass were not included in the regression (Table 2-7). as well as PCBs 187, 206, and 209 due to their uncertainty in the measured equilibrium partition coefficients.....87
- Figure 3-1. Map of the test site for Muddy Creek, Coralville, IA (USGS site: 05454090)... 102

Figure 3-2. Digital picture of sampling site, with inset showing the orientation of sampler during deployment.	102
Figure 3-3. The monthly average temperature of two USGS sites close our measuring site.	103
Figure 3-4. Histograms of nanofiber diameter (measured via SEM for n=200) for ENMs and ENM-CNT composites fabricated herein. Histograms are shown as a function of CNTs mass loading.	108
Figure 3-5. SEM images of ENM-CNT composites. Images are shown for (a) and (c) COOH-CNT/PAN ENM; (b) and (d) NF-CNT/PS ENM. Insets on the right correspond to the areas indicated in (a) and (b) with black boxes. Arrows indicate specific morphological features (e.g., aggregates) due to the presence of CNTs (see text).	109
Figure 3-6. Linear regression analysis for the correlation between ENM composite specific surface area (from BET in m^2/g) and pore volume ($\times 10^{-3} mL/g$) as a function of CNT mass loading (in wt%).	110
Figure 3-7. Linear regression analysis for the correlation between NF-CNT and COOH-CNT surface area (in m^2/g) and pore volume ($\times 10^{-3} mL/g$). NF-CNT mass loading was from 0% to 40%, whereas COOH-CNT mass loading was from 0% to 25%.	111
Figure 3-8. Uptake curves for (a) metolachlor, (b) atrazine, (c) 2,4-D, (d) caffeine, and (e) diuron on ENMs of PAN and CNT-modified PAN. Data represent the accumulation of mass into the ENM over time in g of chemical per kg of mat, as quantified by chemical extraction from the ENM with methanol. Uncertainties represent the standard deviation from three replicate experiments. Experimental conditions: pH 7 (1 mM phosphate); initial concentration of metolachlor: 7.1 mg/L, atrazine: 5.4 mg/L, 2,4-D: 5.5 mg/L, caffeine: 4.8 mg/L and diuron: 5.8 mg/L; ENM loading: $\sim 1.5 g/L$. Experiments were carried out under a static condition.	113
Figure 3-9. Model-estimated $\log K_{ENM-W}$ values obtained from the first-order uptake equation plotted as a function of experimentally measured $\log K_{ENM-W}$ values. To assist with comparison, a 1-to-1 line (dashed) is shown, corresponding to perfect agreement between model-estimated and experimentally measured values.	116

Figure 3-10. Values of $\log K_{\text{ENM-W}}$ as a function of NF-CNT and COOH-CNT mass loading (as wt%) in the ENM composite. Data are shown for (a) diuron and (b) atrazine. Lines represent the results of linear regression analysis on experimental data, where uncertainties associated with individual data points are standard deviation from at least three replicate experiments. The dashed line indicates the $\log K_{\text{ENM-W}}$ value measured for a pure PAN ENM and is provided for comparison. Experimental conditions: pH 7 (1 mM phosphate); initial concentration of diuron: 5.8 mg/L and atrazine: 5.4 mg/L; ENM loading: ~1.5 g/L. Experiments were carried out under a static condition. 117

Figure 3-11. Values of $\log K_{\text{ENM-W}}$ as a function of ENM surface area (from BET in m^2/g). Data are shown for (a) diuron and (b) atrazine. Lines represent the results of linear regression analysis on experimental data, where uncertainties associated with individual data points are standard deviation from at least three replicate experiments. Experimental conditions: pH 7 (1 mM phosphate); initial concentration of diuron: 5.8 mg/L and atrazine: 5.4 mg/L; ENM loading: ~1.5 g/L. Experiments were carried out under a static condition. 119

Figure 3-12. Values of $\log K_{\text{ENM-W}}$ as a function of ENM pore volume ($\times 10^{-3} \text{ mL/g}$). Data are shown for (a) diuron and (b) atrazine. Lines represent the results of linear regression analysis on experimental data, where uncertainties associated with individual data points are standard deviation from at least three replicate experiments. Experimental conditions: pH 7 (1 mM phosphate); initial concentration of diuron: 5.8 mg/L and atrazine: 5.4 mg/L; ENM loading: ~1.5 g/L. Experiments were carried out under a static condition. 119

Figure 3-13. Comparison of $\log K_{\text{ENM-W}}$ values for (a) PAN-based ENMs and (b) PS-based ENMs. Data are shown for pure polymers, as well as composites made with NF-CNT and COOH-CNT. Uncertainties represent standard deviations from at least triplicate measurements. Note: $\log K_{\text{ENM-W}}$ values on CNT/PS for chemicals with an asterisk were estimated by mass balance (see text). 122

Figure 3-14. $\log K_{\text{ENM-W0}}$ VS ENM $\log K_{\text{ENM-W}}$ plots. (a) CNTs modified PAN and (b) CNTs modified PS. To assist with comparison, a 1:1 line (dashed) is shown. Uncertainties associated with individual data points are standard deviation from at least three replicate experiments. 124

Figure 3-15. Correlations between $\log K_{\text{ENM-W}}$ and (a, b) $\log K_{\text{OW}}$ and (c, d) $\log K_{\text{Hexadecane-W}}$ for (left column) CNT/PAN and (right column) CNT/PS. Uncertainties associated with individual data points are standard deviations from at least three replicate experiments. We note that data for 2,4-D is not included in this analysis because it is anionic in our experimental systems. 125

Figure 3-16. Sorption isotherms for (a) diuron and (b) caffeine. Data are shown for NF-CNT/PAN and COOH-CNT/PAN (solid symbols) as well as NF-CNT and COOH-CNT suspensions (open symbols). Please note that the y-axis is broken into two sections to span the range of sorbed concentrations measured across the different sorbents types. Dash lines represent Freundlich isotherm model fits, where K_f and n values are summarized in Table 3-8. Uncertainties associated with individual data points are standard deviations from at least three replicate experiments.	128
Figure 3-17. Reactivity cross correlations between $\log K_d$ values measured in CNT suspensions and $\log K_{ENM-W}$ values measured with CNT-ENM composites. Data are shown (a) CNT/PAN and (b) CNT/PS composites. Uncertainties associated with individual data points are standard deviations from at least three replicate experiments.	130
Figure 3-18. Iowa River water collected at the inlet to the University of Iowa Water Treatment Plan.	133
Figure 3-19. Atrazine concentration in Muddy Creek measured by ENM-CNT composites and active sampling methods. Uncertainties associated with individual data points are standard deviations reflecting the uncertainty associated with measured K_{ENM-W} values and instrument analytical error.	135
Figure 4-1. Chemical structure of Triolein	140
Figure 4-2. Schemes of using surfactants to modify nanofiber surface morphology and property.....	144
Figure 4-3. Histograms of nanofiber diameters for surfactant modified CNT/PAN. Data are shown for analysis of at least 200 nanofibers via SEM images. Average diameters (with standard deviation) are provided for each material.	155
Figure 4-4. Uptake curves for 2,4-D on PAN ENMs with (a) different mass loadings (from 0-30% wt.) of TBAB and (b) 20% wt. of either TBAB or CTAB. Uncertainties represent the standard deviation from three replicate experiments. Experimental conditions: pH 7 (1 mM phosphate); initial 2,4-D concentration of 5.5 mg/L; ENM loading: ~1.5 g/L. Experiments with surfactant-modified PAN were carried out under a static (no mixing) condition, whereas data with unmodified PAN was collected in well-mixed reactor systems.	157

- Figure 4-5. Uptake curves for 2,4-D on PAN-based ENMs modified with 20% wt. (a and c) CTAB and (b and d) TBAB. Data are shown for both PAN- and CNT/PAN composites, with composite data presented for both nonfunctionalized (NF-CNT) and carboxylated (COOH-CNT) CNTs. Uncertainties represent the standard deviation from three replicate experiments. Experimental conditions: pH 7 (1 mM phosphate); initial 2,4-D concentration of 5.5 mg/L; ENM loading: ~1.5 g/L. Experiments with surfactant-modified and CNT-modified PAN were carried out under a static (no mixing) condition, whereas data with unmodified PAN was collected in well-mixed reactor systems. 159
- Figure 4-6. Uptake curves for 2,4-D on (a) TBAB and (b) CTAB modified PAN, NF-CNT/PAN and COOH-CNT/PAN. Data for all materials are shown before and after treatment to promote QAS leaching. Uncertainties represent the standard deviation from three replicate experiments. Experimental conditions: pH 7 (1 mM phosphate); initial 2,4-D concentration of 5.5 mg/L; ENM loading: ~1.5 g/L. Experiments were carried out under a static (no mixing) condition. 160
- Figure 4-7. The uptake curve for PFOA on PAN, CNT/PAs, and TBAB-modified CNT/PAN. Experimental conditions: pH 7 (1 mM phosphate); initial PFOA concentration of 100 µg/L; ENM loading: ~1.5 g/L. Experiments were carried out in well-mixed reactor systems. 161
- Figure 4-8. Uptake curves for (a) atrazine (b) diuron and (c) metolachlor on PAN, CNT/PAN, and TBAB-modified CNT/PAN. Uncertainties represent the standard deviation from three replicate experiments. Experimental conditions: pH 7 (1 mM Potassium phosphate DI in DI water); Initial concentration of atrazine: 5.4 mg/L, diuron: 5.8 mg/L, metolachlor: 7.1 mg/L; ENM loading: ~1.5 g/L. Experiments with surfactant-modified and CNT-modified ENMs were carried out under a static (no mixing) condition, whereas data with unmodified PAN were collected in well-mixed reactor systems. 163
- Figure 4-9. Uptake curves for atrazine on SDS-modified (a) NF-CNT/PAN and (b) COOH-CNT/PAN. Data are shown for two different mass loadings of SDS, 20% and 40% wt. Uncertainties represent the standard deviation from three replicate experiments. Experimental conditions: pH 7 (1 mM phosphate); initial concentration of atrazine: 5.4 mg/L; ENM loading: ~1.5 g/L. Experiments were carried out under a static (no mixing) condition. 165
- Figure 4-10. Uptake curves for (a) atrazine (b) diuron and (c) metolachlor on PAN, CNT/PAN, and SDS-modified CNT/PAN. Uncertainties represent the standard deviation from three replicate experiments. Experimental conditions: pH 7 (1 mM phosphate); initial concentration of atrazine: 5.4 mg/L, diuron:

5.8 mg/L, metolachlor: 7.1 mg/L; ENM loading: ~1.5 g/L. Experiments with surfactant-modified and CNT-modified ENMs were carried out under a static (no mixing) condition, whereas data with unmodified PAN-ENMs was collected in well-mixed reactor systems..... 166

Figure 4-11. Uptake curves for (a) 2,4-D and (b) atrazine in solutions with 5 mg/L of Fluka Humic Acid (FHA). Because of the greater complexity of these solutions, the concentration of analyte associated with the ENM was estimated via mass balance from the difference between the initial aqueous concentration and the concentration measured at each sampling point. Experimental conditions: pH 7 (1 mM phosphate); initial concentration of atrazine: 5.4 mg/L, 2,4-D: 5.5 mg/L; ENM loading: ~1.5 g/L. Experiments with surfactant-modified and CNT-modified ENMs were carried out under a static (no mixing) condition, whereas data with unmodified PAN were collected in well-mixed reactor systems..... 169

CHAPTER 1 INTRODUCTION

1.1 Organic pollutants in the aquatic environment

We live in a chemically dependent society. According to the U.S. Department of Health and Human Services (HHS) National Toxicology Program,¹ more than 80,000 chemicals are currently registered for use in the United States, with another 2,000 introduced annually for various uses in agriculture, medicine, industry and commerce. While diverse, the overwhelming majority of these are organic chemicals, with structures comprised mainly of carbon, hydrogen and oxygen.

Inevitably, through their widespread use and eventual disposal, many of these organic chemicals make their way into the environment, where they can contaminate air, water and soil resources. In these environmental media, organic pollutants represent potential threats to ecosystem and human health. For example, organic pollutants can target and result in adverse health outcomes for the respiratory,^{2,3} immune^{2,4} and reproductive⁵⁻⁷ systems in humans. In fish and other sensitive aquatic and benthic organisms, organic chemicals can function as endocrine disruptors and alter many other physiological functions that have implications for ecosystem structure.^{8,9}

The characteristics of the organic chemical species will determine its fate in the environment and the risk it poses to organisms. For simplicity, and following the nomenclature of others, we can classify organic pollutants broadly into two classes based on their chemical properties. The first class is hydrophobic compounds (hereafter “HCs”), which

are oftentimes also referred to as Persistent Organic Pollutants (or “POPs”) or legacy pollutants.^{10, 11} Due to their chemical properties, HCs are not easily degraded in the environment. Rather, through their hydrophobicity, they tend to sorb to organic carbon and lipid phases in the environment and biota, respectively, thus bioaccumulating and biomagnifying in the food chain.^{12, 13} The second broad class consists of hydrophilic and moderately hydrophobic compounds (hereafter “HMHCs”). Most of these compounds are also known as contaminants of emerging concern (CEC) or emerging pollutants. In contrast to hydrophobic compounds, HMHCs tend to be more water soluble, with greater polarity and charge distributions, and they do not persist in the environment as long as HCs.

As will be detailed in the sections that follow, both classes of chemicals present their own challenges for risk assessment. While HCs and HMHCs differ in many important ways that influence their environmental fate and effects, they share the need for improved environmental monitoring that facilitates chemical identification and quantification. Indeed, improved temporal and spatial trends in the occurrence and abundance of these chemicals in aquatic environments (e.g., surface waters and sediments) would greatly advance risk assessment for human and ecosystems associated with chemical exposure.

1.1.1 Hydrophobic Compounds

Hydrophobic compounds include highly toxic organic chemicals (mostly man-made) such as dioxins,¹⁴ furans,¹⁵ and PCBs¹⁶ (**Figure 1-1**) that were widely produced and used in the industry since World War II. Due to their chemical properties, such as an octanol-water

partition coefficients (K_{ow} values) above 10^4 , the majority of these compounds are not easily dissolved in water but prefer to accumulate in organic carbon phases in the environment and in the lipids of biota.¹⁷ Due to their high bioaccumulative potentials and toxicities, the Stockholm Convention was signed in 2001 by over 150 countries to stop the production and use of POPs.¹⁸

Nevertheless, the extreme chemical stability imparted by their chemical structures makes POP a continued environmental problem today. POPs possess long environmental half-lives ($t_{1/2}$ values, or the time necessary for their concentration decrease by 50%), such that they can be encountered in the environment many years after their production and use has been phased out. For example, the $t_{1/2}$ values of some POPs can exceed 10 years, such as Endrin and Mirex (**Figure 1-1**) in the soil.^{6, 19} Accordingly, their persistence increases the likelihood they bioaccumulate in organisms, either through direct partitioning into organisms (i.e., absorption) or uptake through diet and amplification through the food web.²⁰⁻²² It is also through direct exposure and diet that POPs also threaten human health, where they cause many adverse health outcomes including hypersensitivity, damage to nervous systems, birth defects and cancer.²³⁻²⁷ Although many actions have been taken to control and reduce the usage of POPs, the legacy of large reservoirs of POPs in the environment as a result of their use over the last half-century remains a challenging problem that people must solve.²⁸

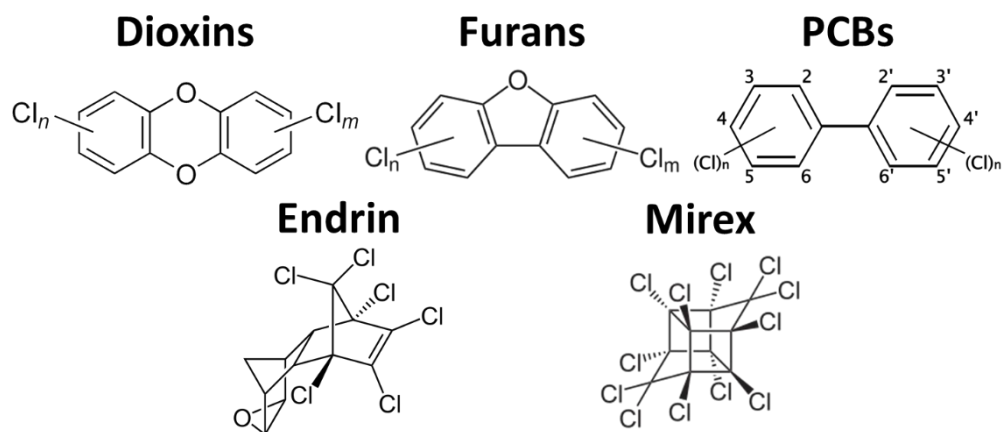


Figure 1-1. Chemical structure of POPs examples

1.1.2 Hydrophilic and Moderately Hydrophobic Compounds

Hydrophilic and moderately hydrophobic compounds (HMHCs) represent a newer class of pollutants more representative of modern chemicals used in industry, commerce, agriculture and medicine.²⁹⁻³⁴ Broadly, they include pesticides, plasticizers, munitions constituents, and pharmaceuticals and personal care products (PPCP). Many of these are not commonly monitored in the environment, as only a small subset is regulated in surface water and drinking water through the Clean Water Act and the Safe Drinking Water Act.^{35, 36} Further, their ecological and human health effects are poorly understood. As such, while they have been extensively investigated over the past several decades and they are likely the subject of future environmental regulations, they are currently referred to as contaminants of emerging concern (CEC).³⁷⁻⁴⁰

As a class and relative to POPs, HMHCs are more water-soluble, as evidenced by their relatively low octanol-water partition coefficient (Hydrophobic: $K_{ow} < 10^2$; moderately

hydrophobic $10^2 < K_{ow} < 10^4$, **Figure 1-2**).^{41, 42} Their high-water solubility results in high mobility in aqueous systems including surface water and groundwater, posing a threat to ecosystem health and increasing the probability that these chemicals can contaminate our drinking water resources or food supply through irrigation.^{43, 44} For example, several studies have confirmed that certain HMHCs can function as endocrine disrupting compounds that alter physiological and reproductive function of a wide range of aquatic organisms, and potentially humans as well.^{38, 45-49}

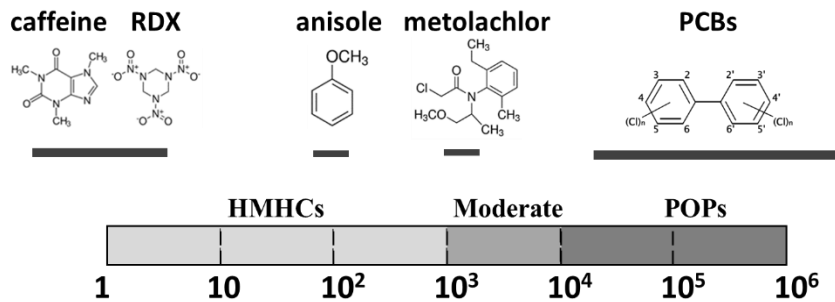


Figure 1-2. The octanol-water partition coefficient of selected organic compounds

1.2 Environmental sampling and monitoring methods

To better establish the environmental occurrence of HMHCs and POPs and identify best management practices to control their environmental fate and exposure risks, it is important to improve monitoring approaches so as to enable higher temporal and spatial resolution related to their environmental abundance. Environmental sampling and monitoring techniques are critical to assessing environmental quality, for both detecting the types and levels of contaminants in air, water, soil and biota, while also tracking their change

over time.^{50, 51} Advances in environmental monitoring have helped to improve environmental protections through regulations, motivate the development of new technologies, and assess the benefits of treatment and management interventions in the field. To further advance these goals, this dissertation focuses on new method development to improve environmental monitoring of POPs and HMHCs in soil, surface waters and sediments.

As background, the two most common methods used to collect environmental samples can be broadly classified as active and passive sampling approaches.⁵²⁻⁵⁴ Grab sampling for water and soil and pumped sampling for air are the most commonly used active sampling methods.^{55, 56} This simply involves collecting and containing a sample of the media for later processing and analysis of its contents.⁵⁷ These active sampling methods require energy, either to push the target phase through a sorbent material or to collect a large volume of sample to be further concentrated in the laboratory. Moreover, highly specialized personnel are often needed to ensure appropriate sample collection, subsequent processing, and operation of all instrumentation involved with these steps.⁵⁸⁻⁶⁰ Because of these requirements, data collected from active sampling tend to be limited in number (i.e., more data requires more energy and personnel), both spatially and temporally.

1.2.1 Passive sampling devices: background and operating principles

Approaches that avoid the labor intensive nature of active sampling, or so-called passive sampling, have the potential to vastly improve temporal and spatial trends of chemicals in the environment in easily deployable monitoring platforms. Passive samplers are

environmental monitoring tools that rely on the accumulation of the target analyte into a matrix via molecular diffusion, which is driven by the difference in chemical potential between the analyte in the environment and the sampling media (e.g., sorbent phase).⁶¹ The use of passive sampling devices as a monitoring method to detect pollutants in the environment was first proposed in the 1970s.⁶² By the end of the 1980s, a growing number of research groups started to develop passive samplers as a new generation of devices for monitoring pollutants in the environment. Various passive samplers have been designed and deployed to collect the freely-dissolved phase of organic pollutants in the air, water, soil and sediment interstitial water, the phase that represents the most readily bioavailable pollutant fraction for exposure and uptake into organisms.^{63, 64}

Compared with conventional active sampling approaches, the passive sampling methods hold several advantages, including:

- Passive samplers do not have any moving parts or require power to operate.
- Integrative passive samplers yield time-weighted average concentrations of pollutants, allowing assessments of chemical exposures that are based not only on abundance but also duration of chemical contact.
- Passive samplers accumulate chemicals from environmental media, thereby increasing the mass collected over time of deployment. This, in turn, improves the detection limits of the analytical methods used to process the chemical recovered from the sampler,

typically gas or liquid chromatography coupled with standard detection methods (e.g., mass spectroscopy (GC/MS or LC/MS) or electron capture detection (GC/ECD)).^{65, 66}

- The cost of the passive samplers is much lower than the conventional active samplers because no energy is required during the monitoring and less organic solvents are used in both the manufacturing process of the sorbent material, as well as the chemical extraction process during sampler analysis.⁶⁷

Passive samplers can be subdivided into two types, kinetic and equilibrium, depending on their operation regime.⁶¹ Generally, analyte exchange between the environmental medium and sorbent phase for a particular analyte is followed by a first-order, one-compartment model.^{61, 68, 69} The uptake process between two separate compartments can be described as;

$$\frac{dC_S(t)}{dt} = C_W(t)k_1 - C_S(t)k_2 \quad (1-1)$$

where $C_S(t)$ is the analyte concentration (mg/g) in the sorbent phase at exposure time t (h), k_1 and k_2 are the uptake (sorption) and elimination (desorption) rate constants (h^{-1}), respectively. $C_W(t)$ is the analyte concentration (mg/L) in the environmental medium at time t , which is assumed to be a constant over the deployment period. Thus, this assumption can be defined as:

$$C_W(t) = C_{W,t=0} = C_W \quad (1-2)$$

$C_{W,t=0}$ is the analyte concentration in the water at time zero. The final model Equation can be integrated by substituting Equation (1-2) into (1-1):

$$C_S(t) = C_W \frac{k_1}{k_2} (1 - e^{-k_2 t}) \quad (1-3)$$

Figure 1-3 illustrates the amount of chemical accumulated in the sampler versus time, as described by Equation 1-3, distinguishing the two main operation regimes of passive sampling devices, either within kinetic or equilibrium sampling regimes. These two modes of operation are further described in the following sections.

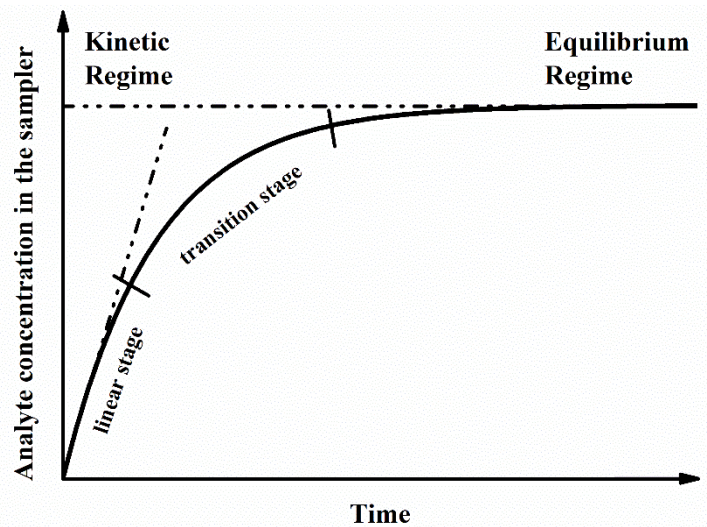


Figure 1-3. Schematic representation of analyte concentration in the sampler material over time, illustrating the two passive sampler operation within the kinetic and equilibrium regimes.⁶¹

1.2.2 Kinetic passive samplers

Kinetic passive samplers are characterized by relatively slow target analyte uptake, which results in a long deployment times typically over several weeks to months to allow for

chemical integration into the sampling materials.^{70, 71} For kinetic passive samplers, therefore, the linear uptake regime in **Figure 1-3** is assumed in analysis and -calculations to determine environmental concentrations. Moreover, selected reference chemicals are needed with kinetic samplers. These reference chemicals are loaded into the sorbent material prior to deployment, and it is assumed that the rate of their desorption (previously quantified in the laboratory) is linearly proportional to the uptake (i.e., sorption) rate of target analytes into the sorbent from the environmental media. Finally, because the concentration gradient of the target analytes between the sorbent phase and the environment is small, it is assumed that the desorption rate of analytes is negligible. Accordingly, Equation 1-3 can be simplified as follows:

$$C_S(t) = C_W k_1 t \quad (1-4)$$

and after rearranging the equation, we obtain the relationship below:

$$M_S(t) = C_W R_S t \quad (1-5)$$

where $M_S(t)$ is the mass (typically in mg) of analyte accumulated in the sorbent phase at exposure time t (in h), and R_S is the volume of water from which analytes were extracted per unit of exposure time (L/h) during the deployment, which is also known as the sampling rate. When $M_S(t)$ is quantified analytically (e.g., via chemical extraction with subsequent quantification via LC/MS or GC/MS) and R_S is estimated by from the reference chemicals, the time-weighted average (TWA) concentration of target contaminants in the environmental

media of interest can be obtained. Kinetic sampling is also often referred to as integrative sampling; semipermeable membrane devices (SPMD), low-density polyethylene (LDPE) strips and the polar organic chemical integrative sampler (POCIS) are all common kinetic passive sampling devices used for legacy and, more recently, emerging pollutant classes.⁷²⁻⁷⁴

1.2.3 Equilibrium passive samplers

For equilibrium samplers, a thermodynamic equilibrium for the target analyte is assumed between the environmental medium and the sorbent phase. In practice, this is most often the case when either the device has been deployed for a long time or the sorption rate of the device is very fast.^{59, 75}

In this case, Equation 1-3 can be simplified as follows:

$$C_S = C_W \frac{k_1}{k_2} = C_W K \quad (1-6)$$

where K the equilibrium partition coefficient between the environmental and sorbent phases (L/kg). Values of K can be measured via laboratory uptake experiments or estimated from predictive poly-parameter linear-free energy relationships (pp-LFERs).⁷⁵ Once the value of K is known, the equilibrium concentration of the target analyte in the relevant environmental media (e.g., water or C_w) can be calculated from C_s , which is measured analytically after sampler extraction. Notably, for devices operating in the equilibrium regime, values of K can be dependent on system variables including temperature, pH and the presence of other

available phases for partitioning (e.g., solid or colloidal particles in the water column).⁷⁶⁻⁷⁸

Accordingly, the potential influence of such environmental factors on values of K must be investigated before an equilibrium sampler is used.

1.2.4 Current passive sampling materials and technical barriers to further development

Currently, passive sampling technologies for water sampling have been developed largely to target either hydrophobic pollutant targets or hydrophilic pollutant targets, but typically not both. Several of the most popular, and in some cases commercially available, passive sampling tools, as well as their active sorbent materials, are described below.

For non-polar (hydrophobic) organic contaminant monitoring, which is typically achieved via chemical absorption or partitioning into the bulk sorbent phase, popular passive sampling materials include:

- **Semi-Permeable Membrane Devices (SPMDs)** are a widely used passive sampling tool for lipophilic chemicals. The sorbent is made of a sandwich low-density polyethylene tubing containing a thin layer of high molecular weight triolein inside (**Figure 1-4**).⁵⁰ The selected hydrophobic chemicals in the aqueous phase can diffuse through the small pores (pore size: ~1 nm) on the polymer film and accumulate in the intermediate layer. Polyethylene Devices (or PEDs) are also a form of modified SPMD.⁷⁹

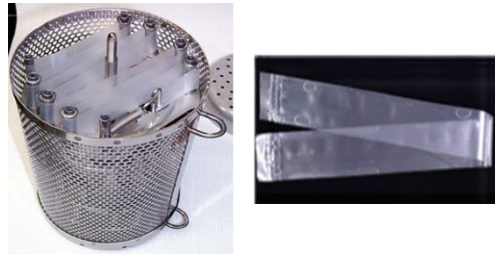


Figure 1-4. Schematic of Semi-Permeable Membrane Devices (SPMDs)⁵⁰

- Solid-Phase Microextraction (SPME) Fibers** are a suite of commercially available non-polar organic pollutant sampling devices. A fiber with diameter less than 100 μm is coated with sorptive materials and fixed between two metal holders (**Figure 1-5**). Common used stationary phases include polydimethylsiloxane (PDMS), polyacrylate, carbowax[®]/divinylbenzene (CW/DVB), and polydimethylsiloxane/divinylbenzene (PDMS/DVB).⁸⁰ Based on the target analyte, one or more stationary phases will be coated on fiber surface. Over hundreds of SPME kits are commercial available in chemical supply companies such as Sigma-Aldrich. As a mature and commercially available product, this device has been designed as a replaceable part which is compatible with GC and HPLC columns.⁸¹

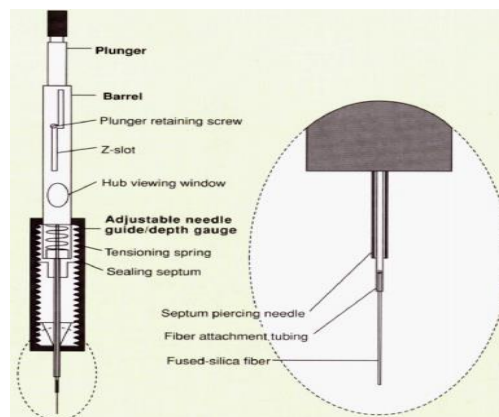


Figure 1-5. Schematic of Solid-Phase Microextraction (SPME) Device⁸²

For polar (hydrophilic) organic contaminant monitoring, which is typically achieved via adsorption or accumulation on the surface of the sorbent phase, popular passive sampling materials include:

- Polar Organic Compound Integrative Sampler (POCIS)** is a kinetic passive sampler for polar organic pollutants. Developed by the USGS, POCIS uses a solid sorbent phase (e.g., Oasis[®] HLB and Triphasic admixture) that is sandwiched between two microporous polyether sulfone membranes (pore size ~100nm, **Figure 1-6**).^{50, 70} The membranes are permeable to water, allowing dissolved chemicals to access and be captured by the solid sorbent layer. Much research has been conducted with POCIS, by far the most mature and reliable approach for polar targets, to analyze emerging pollutants including pharmaceuticals and pesticides in surface waters.^{83, 84}

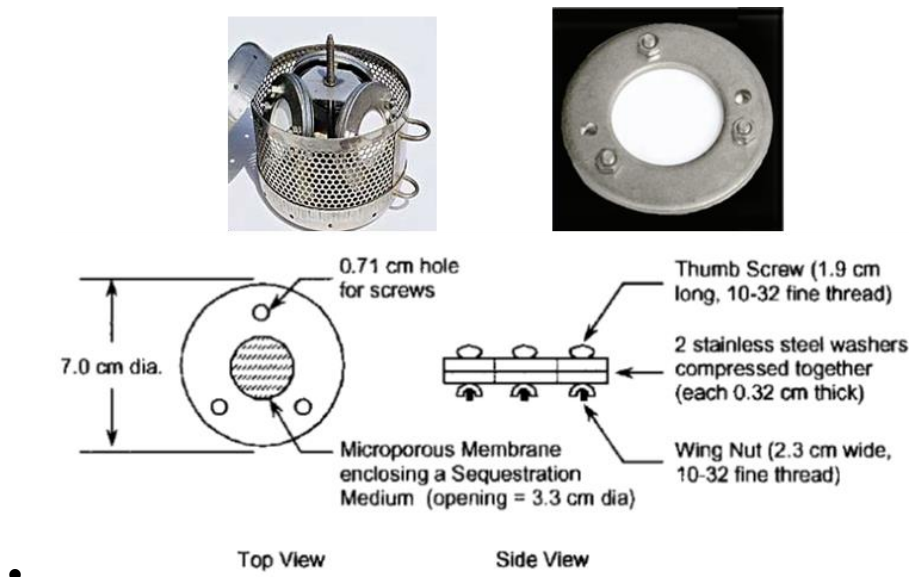


Figure 1-6. Schematic of Polar Organic Compound Integrative Sampler (POCIS)^{50, 70}

- **Chemcatcher**[®] consists of a polytetrafluoroethylene (PTFE) body capable of holding commercially available 47 mm disks of various sorbent phases (**Figure 1-7**). Depending on the target analytes, potential sorbents include divinylbenzene (DVB), Oasis[®] HLB and octadecylsilyl silica gel (C18).^{85, 86} This device is mainly used to measure contaminants in surface water, and produces a time-weighted average concentrations. Originally designed by Professors Richard Greenwood in 2000, Chemcatcher[®] is commercially available and a patented technology across many countries.⁸⁷

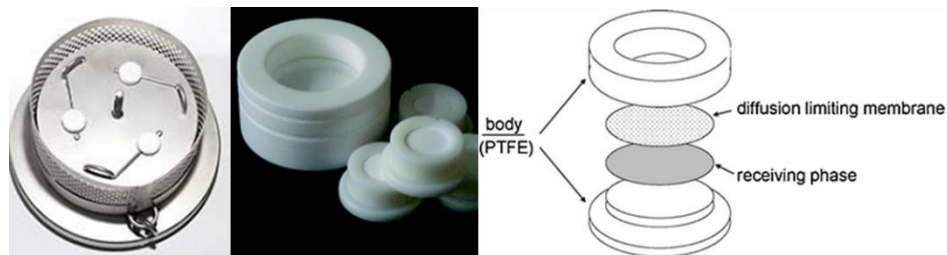


Figure 1-7. Schematic of Chemcatcher[®].^{88, 89}

As previously indicated, current passive sampling devices are designed to monitor for either hydrophilic or hydrophobic compounds, but not both at the same time. For example, **Figure 1-8** illustrates the type of chemicals, based on $\log K_{ow}$ values, that can be monitored using either the hydrophilic sampler POCIS or the SPMD sampler intended for more hydrophobic compounds.⁹⁰ There is little to no overlap in the range of $\log K_{ow}$ values where both are effective. In fact, for chemicals with $\log K_{ow}$ values between 3 and 4, both samplers do not perform well.

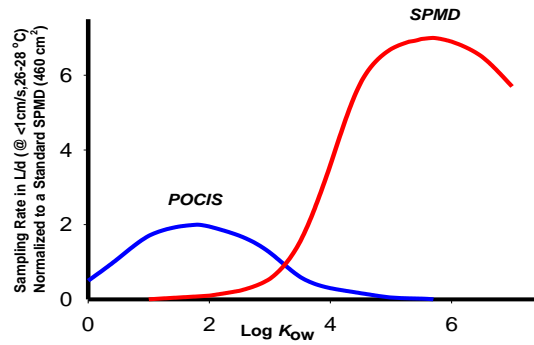


Figure 1-8. Sampling rate (in L/d) for POCIS and SPMD as a function of the target analytes hydrophobicity as quantified by $\log K_{ow}$ values. The blue and red lines effectively establish the useful monitoring range of pollutant targets for POCIS and SPMD⁹⁰

As another challenge to the performance of current passive sampling devices, HMHCs are often present at a very low concentrations in the environment (e.g., ng/L or parts-per-trillion levels).⁹¹ As such, these concentrations currently approach the detection limit of even the most advanced analytical methods.⁹² Thus, improving the sensitivity and capacity of passive sampling devices for HMHCs is both an urgent need and a considerable research and development challenge, especially for equilibrium passive sampling devices that normally exhibit smaller uptake capacities compared with kinetic devices.⁶¹

1.3 Potential of Engineered Nanomaterials as Next-Generation Passive Sampling Devices

Due to existing limitations in passives sampling devices related to their (i) bulk and surface chemistry for targeting chemically diverse target analyte (e.g., HCs and HMHCs) and (ii) limited uptake capacity, particularly for equilibrium passive sampling devices, a new

generation of highly tailorable, high capacity sorbent phases is needed. Nanomaterials, which are generally defined as materials with at least one characteristic dimension or structural features below 100 nm,^{93, 94} hold promise as next generation sorbents in a range of environmental applications.^{95, 96} Nanomaterials are characterized by high surface area to volume ratios (SA/V values), and can often exhibit surface reactivity that is distinct from their larger scale analogs.^{93, 97} In particular, their high surface area makes them ideal for passive sampling, although very little work has been conducted to date considering their use in such applications.

To deploy nanomaterials as sorbents in environmental applications, a challenge is identifying a stable platform that will effectively immobilize nanomaterials and prevent their release into the environment during use. This is not only important for ensuring the reliability and reusability of the nanomaterial in its intended application, but it also limits the risks associated with unintended exposures to engineered nanomaterials, some of which may be toxic to aquatic organisms and humans.⁹⁸⁻¹⁰⁰

1.3.1 Electrospun nanofiber mats for environmental applications

To address the need for robust and environmentally responsible application platforms for engineering nanomaterials, several fabrication routes have been investigated. Among these, electrospinning has emerged as a highly scalable and commercially viable route to the synthesis of a three-dimensional network of nonwoven nanofibers suitable for a range of applications.¹⁰¹

Electrospinning fabricates nanofiber networks or mats by forcing a conductive polymer sol-gel or melt through a metal nozzle and drawing a solution droplet to form fibers in an electric field.^{102, 103} **Figure 1-9** shows the schematic of a standard electrospinning setup. A high voltage is applied to the syringe needle while the collector is connected to ground. The conductive polymer sol-gel is pushed out from the syringe at a steady flow rate and driven by the electric field between needle and collector. The sol-gel forms a Taylor Cone on the needle tip and is then dispersed uniformly to generate the nanofibers. Because of its simplicity and high productivity, the electrospinning setup has been widely used in both academia and industry, where several advantages of this approach have been identified (e.g., a high degree of tailoring nanofiber properties such as composition and diameter) while producing polymer and inorganic nanofibers, as well as their composites, for a range of applications.¹⁰³⁻¹⁰⁵



Figure 1-9. Set-up of the lab electrospinning apparatus

1.3.2 Use of polymer electrospun nanofiber mats as sorbent materials

Polymer electrospun nanofiber mats (ENMs) can be used as potential sorbent materials due to their high SA/V values and the diversity of polymers that can be synthesized via electrospinning. Use of polymer ENMs for the solid-phase extraction (SPE) of organic

chemicals (i.e., to extract organic chemicals from water or other solvents) has been investigated in both aqueous and biological (e.g., plasma) samples.^{106, 107} Beyond the high SA/V values resulting from their nanoscale dimensions, polymer ENMs can also have a high porosity that helps to improve both their selectivity and efficiency for uptake of trace organic chemicals in complex mixtures.¹⁰⁸

Another advantage of electrospinning for such applications is that many different polymers can be fabricated via this approach. Thus, polymer ENMs can be fabricated with physical and chemical properties targeting specific types or classes of chemical analytes. For example, in passive sampling applications, either hydrophobic or hydrophilic polymer ENMs could be fabricated. The repeating structural units for several polymers and co-polymers for which electrospinning synthesis recipes are available are shown in **Figure 1-10**.^{105, 109-117} Notably, the subset of polymers shown possess functional groups that would be ideal for targeting either HCs or HMHCs during passives sampling, and one could envision that multiple polymer ENMs could be integrated into a single device to target a broader spectrum of chemically diverse analytes in a single passive sampling platform.

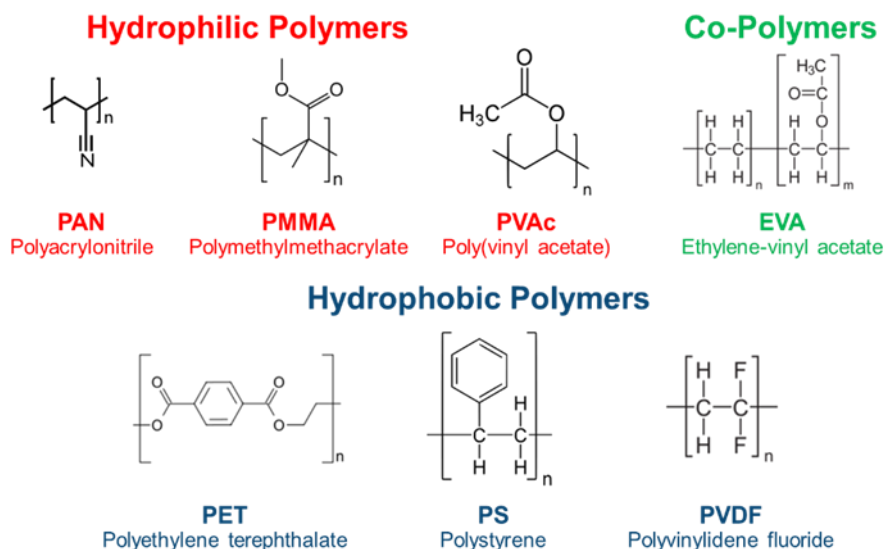


Figure 1-10. The structural unit of polymers that can be fabricated by electrospinning and may also be beneficial for use in passive sampler applications for legacy and emerging pollutant classes.

1.3.3 Tailoring ENM polymer characteristics to improve performance

To improve upon the baseline performance of polymer ENMs in applications related to environmental monitoring and treatment, electrospinning is a highly versatile approach for modifying materials either before synthesis or by post-processing of the resulting nanofiber mat. For example, while the operating principle of electrospinning is straightforward, there are many synthesis parameters that influence the characteristics of the resulting nanofibers including humidity, polymer concentration, sol gel conductivity, applied voltage, flow rate, and needle size. Accordingly, any or all of these variables can be manipulated to help tailor the properties of ENMs, and there are many reviews that have attempted to summarize the effects of different synthesis parameters.^{102, 103} As one example, we can tune polymer nanofiber diameter and thus SA/V values critical to pollutant uptake rates in sorbent

applications, through control of humidity, where low humidity will produce smaller diameter nanofibers.

The composition is also easily tailored through the selection of the precursors used in the preparation of sol gels. Beyond simple polymer nanofibers, advances in this area have involved integration of two or more polymers into one ENM through modifications to the standard electrospinning process. Three common approaches include: (a) preparation of a single electrospinning sol-gel with mixed polymer precursors, which is usually limited to instances where polymers have similar properties and are able to make a homogeneous sol gel mixture;^{118, 119} (b) fabrication of a multi-layer structure, where ENMs are electrospun simultaneously one after another via layer-by-layer deposition of nanofibers and a macrophase separation is created between different polymer layers;^{120, 121} (c) use either a coaxial or multiple needles/nozzles for the simultaneous fabrication of core-shell or multiphasic polymer ENMs, respectively (**Figure 1-11**).^{122, 123}

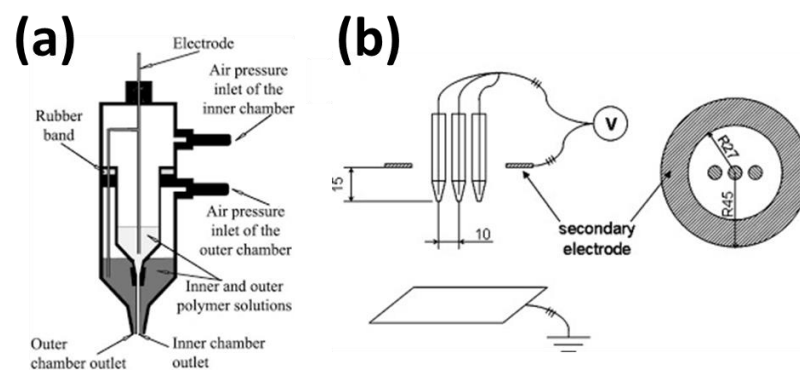


Figure 1-11. Schematic of (a) coaxial and (b) multiple needles/nozzles electrospinning setup^{122, 123}

1.3.4 Fabrication of polymer ENM nanocomposites to improve performance

Beyond polymer composition and ENM morphology, it is also possible to adjust the mat mechanical properties (e.g., flexibility, roughness, and strength) through blending of other nanomaterials into the polymer precursor sol-gel so as to manufacture nanocomposites. Carbon nanotubes (CNTs) and metal or metal oxide nanoparticles are two types of common commercial products used for this purpose.¹²⁴⁻¹²⁶ For example, CNTs are noted for their extreme mechanical strength, and their integration into polymers produces a stronger polymer composite material that is likely more robust during environmental applications.¹²⁶⁻¹²⁹

In addition to structural benefits, integration of other nanomaterials may also impart other beneficial properties related to the physical and chemical nature of the fabricated composites. For example, metal nanoparticles can be used to improve the thermal and electrical conductivity of traditional polymers.^{128, 129} Silver nanoparticles also impart antibacterial activity that can be useful in avoiding biofouling during application of polymer composites in more complex environmental matrices.^{130, 131} During electrospinning, these reactive nanomaterials can easily be mixed into the precursor sol gel solution, so long as the solution is homogeneous (i.e., the nanoparticles are not extensively aggregated), resulting in their distribution throughout the deposited nanofibers and producing multi-functional polymer-ENM composites.

The integration of CNTs into polymer composites offers the potential to not only influence mechanical strength, but also the ability of the polymer to function as a high capacity sorbent during environmental applications. CNTs consist of rolled-up sheets of

graphene, which represents the most thermodynamically stable form of crystalline carbon where carbon atoms are covalently bound to each other in the hexagonal pattern.^{97, 132, 133}

CNTs are divided into two types depending on their number of graphene sheets: single-walled carbon nanotubes (SWNTs) consist of a single, rolled graphene sheet whereas multiple graphene sheets comprise multi-walled carbon nanotubes (MWNTs) (**Figure 1-12**).

CNTs can also be fabricated with different surface functional groups; non-functionalized surfaces are largely hydrophobic because of their carbon structure, but carboxylic acid groups can be introduced via several oxidation routes, while other functional groups (e.g. N-based amines and amides) can be produced with more sophisticated functionalization routes (**Figure 1-13**). All the CNTs products used in this project are purchased from Cheap Tubes Inc. (Cambridgeport, VT). The information of current available functionalized CNTs are listed in **Table 1-1**.

Table 1-1. Summary of current functionalized CNT products of Cheap Tubes Inc.

Primary Surface Group	CNT Type	Graphitized Option	Outer Diameter	Inner Diameter	Length	Functionalization Route
Carboxyl groups (COOH)	SW,DW,MW	Yes	1-80 nm	0.8-5 nm	0.5-50 μ m	CCVD Acid chemistry
Hydroxyl groups (OH)	SW,DW,MW	Yes	1-80 nm	0.8-10 nm	0.5-50 μ m	CCVD Acid chemistry
oxygen groups (COH)	SW,DW,MW	No	1-20 nm	0.8-4 nm	1-30 μ m	Plasma
Amine groups (NH ₂)	SW,DW,MW	No	1-20 nm	0.8-4 nm	1-30 μ m	Plasma
Nitrogen Functionalized (NH)	SW,DW,MW	No	1-20 nm	0.8-4 nm	1-30 μ m	Plasma
Fluorine Functionalized (F _x)	SW,DW,MW	No	1-20 nm	0.8-4 nm	1-30 μ m	CCVD Plasma

CCVD is the abbreviation of catalyzed chemical vapor deposition; SW, DW, MW are the abbreviation of Single-Walled, Double-walled, Multi-Walled respectively. All the information are reported by the manufacturer. Outer diameter, inner diameter and length are selected in the reported range. Generally, outer and inner diameter of SW and DW CNTs are larger than MW CNTs.

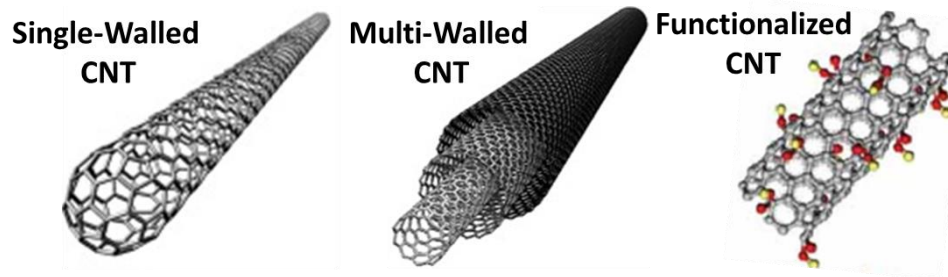


Figure 1-12. Schematic of carbon nanotubes: single-walled CNT (left), multi-walled CNT (middle) and functionalized CNT (right) ^{134, 135}

As a result of their high surface area, environmental application of CNTs have focused on their use as novel sorbents for the removal of organic chemicals from water. ^{130, 136}

Although the high uptake capacity of CNTs is promising, identification of an application platform that effectively immobilizes CNTs during use and prevents their release into the environment (where they may be toxic to exposed organisms) remains a primary challenge. ^{137, 138}

Although polymer-CNT composites represent a promising platform for deploying CNTs in the environment, approaches are needed to ensure that CNTs encapsulated in the polymer remain accessible to solution or other relevant environmental media from which they are to remove target contaminants. Thus, the extent of CNT surface availability, and the porosity of the polymer matrix, may represent key design considerations in developing polymer-CNT composites for environmental applications including next-generation sorbents or passive sampling materials.

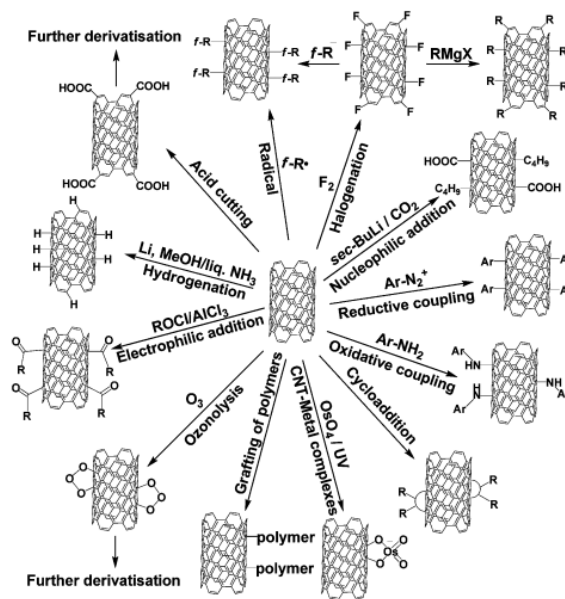


Figure 1-13. Surface functionalization of carbon nanotubes¹³⁹

1.3.5 Imparting chemical functionalization to improve ENM performance: Surfactants

Chemical uptake initiates (and may be limited entirely to) at the nanofiber surface, such that changing its surface physical and chemical properties will likely influence nanofiber activity toward various dissolved target analytes.¹⁴⁰ One approach that has previously been used to alter the surface chemistry of polymer nanofibers is through the use of surfactants that impart specific reactive surface sites.¹⁴¹ Surfactants are the surface active agents that can reduce the surface tension between two phases (e.g. liquid-liquid, gas-liquid and liquid-solid phase).^{142, 143} Specifically for electrospun polymer nanofibers, a useful subset of surfactants are those that are surface segregating,^{141, 144} during fabrication, the surfactants migrate to the surface of the polymer so as to minimize the free energy of interaction between the surfactants and the polymer bulk. Thus, surface-segregating surfactants hold the advantage of

being able to be blended homogeneously into the sol gel precursor solution, but concentrate on the nanofiber surface during the fabrication process. Surface-segregating surfactants including cationic quaternary ammonium salts (QAS) were initially used in the production of antibacterial nanofiber materials for wound dressing,¹⁴⁵ as the QAS functionality is also a potent biocide. Subsequently, prior work by our group integrated surface-segregating QAS including CTAB and TBAB (**Figure 1-14**) for uptake of metal anions (e.g., chromate and arsenate), as in addition to their antimicrobial activity, the quaternary ammonium groups are analogous to groups used in strong base anion exchange resins for oxyanion removal.

There remain some practical challenges to these surfactant modified materials. First, outside of their use in metal binding, their activity in promoting uptake of charged organic molecules has not yet been investigated. Another potential problem is that the charge imparted to the surface of the nanofibers will promote fouling; for example, the presence of positively charged quaternary ammonium sites may hasten interaction with non-target, negatively charged species including dissolved organic matter and even bacteria, which carry a net negative surface charge. Alternately, it could be envisioned that the integration on an anionic surfactant, like sodium dodecyl sulfate (SDS) could be used to avoid biofouling issues.¹⁴⁶

A final practical consideration is the long-term stability of the surfactant embedded in the polymer matrix. Retention is dependent on the strength of the physical and chemical interactions between the hydrocarbon chain and the polymer matrix, and thus for weaker

interactions leaching of the surfactant into water over time is a possible concern.¹⁴⁷ This would result in a loss of surface active sites over time, and a declining performance in the surfactant modified materials over their application lifetime, as was observed for CTAB-modified polymers for metal uptake.¹⁴⁵ However, Peter *et al.* recently reported on an approach to take advantage of the leaching surfactants from PAN nanofibers to intentionally improve their porosity, which in turn increased the amount of surface area available for metal cation uptake.¹⁴¹

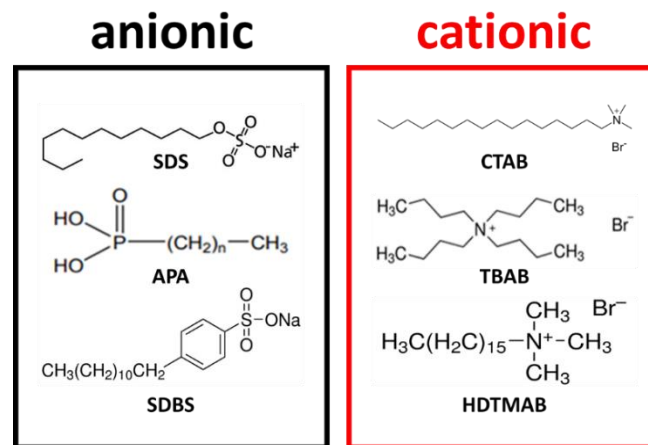


Figure 1-14. Examples of common surfactants for electrospun nanofiber: Sodium dodecyl sulfate (SDS),^{141, 148} Alkylphosphonic acids (APA),^{149, 150} Sodium dodecylbenzenesulfonate (SDBS),¹⁵¹ Cetrimonium bromide (CTAB),¹⁵² Tetrabutylammonium bromide (TBAB),¹⁵³ Hexadecyltrimethylammonium bromide (HDTMAB).¹⁴⁸

1.3.6 Imparting chemical functionalization to improve ENM performance: Post-synthesis chemical processing

Even after ENMs have been synthesized, many other post-processing treatments can be used to impart and improve functionality. A common approach is to use chemical reactions to change functional groups within the polymer matrix. For example, PAN-based

ENMs can be amidoximated via their reaction with hydroxylammonium chloride in an acidic environment (shown in **Figure 1-15**).^{154, 155} Via this reaction, the nitrile group originally present in PAN is replaced by amidoxime groups, which are active sites for binding and complexation of many species including metals (like uranium).¹⁵⁶ The new amidoxime functional group may also be useful for binding of organic pollutants via Van der Waals forces and hydrogen bonding. Moreover, after amidoximation, Das *et al.* proposed further chemical processing to form a poly(imide dioxime) structure that also can be used to improve the sorption performance of anionic species.¹⁵⁷ However, the disadvantage of using such chemical reactions is that they are restricted to polymers with reactive structural elements (e.g., PAN), and the processes may alter the strength and the integrity of the ENM in cases of extensive chemical reaction.

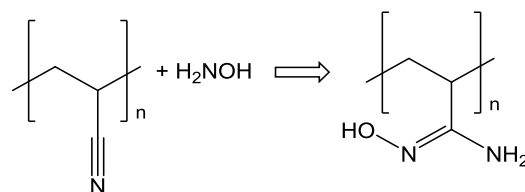


Figure 1-15. The reaction equation of amidoximation reaction on PAN-based ENM

There are other post-functionalizing methods that can be considered. If an ENM is synthesized with more than one polymer (or copolymer), UV- or plasma treatment can be used to etch one domain to create an organized nanostructure in the ENM that would increase the sampling rate of the device.¹⁵⁸⁻¹⁶⁰ Carbonization and oxidation are another two

approaches that can enhance the ENMs mechanical performance and bring in oxygen-containing functional groups, respectively.¹⁶¹⁻¹⁶⁴

1.4 Thesis Motivation, Objectives and Overarching Hypotheses

To address persistent technical obstacles in the development and application of passive sampling devices including a relatively narrow range of target analytes (based on K_{ow} values), poor selectivity and low sensitivity, we propose to use polymer electrospun nanofiber mats (ENMs) as a sorbent material for multi-target passive sampling devices for monitoring legacy and emerging pollutant classes in the aqueous and sediment pore water phases. To achieve this overall research goal, several synthesis and optimization methods will be used to tailor the chemical and physical properties of ENMs to improve their uptake of both POPs and HMHCs. This includes tuning the composition and morphology of polymer ENMs, the fabrication of polymer-CNT ENM composites, and surfactant-modified materials with surface chemistries specifically designed to target polar HMHCs.

1.4.1 Objectives and Hypotheses

Specific research objectives to achieve the overall research goal include:

- **Objective 1:** Synthesize via electrospinning a suite of chemically diverse polymer ENMs and characterize their physical and chemical properties.

- **Objective 2:** Using a suite of structurally analogous model compounds exhibiting a range of $\log K_{ow}$ values, establish the physical and chemical characteristics governing pollutant uptake on polymer ENMs.
- **Objective 3:** Focusing on the optimal polymer materials (based on equilibration time, largest partitioning coefficients and recovery rate), utilize chemical modifications and fabrication of polymer-CNTs composites to improve further material performance and functionality (e.g., absorption capacity, equilibrium time, stability, strength and anti-fouling).
- **Objective 4:** Design a multi-target passive sampling device with modified nanofibers and evaluate the device performance toward real-world targets in systems representative of contaminated sediments and surface waters.

To address these objectives, there are several hypotheses guiding the development of novel passive sampling materials in this work. They are:

- **Hypothesis 1:** The ability of an ENM to sorb polar organic pollutants will scale with its wettability, solubility of its monomeric unit, and N and O contents.
- **Hypothesis 2:** The sorption capacity of ENMs will increase with surface area and porosity of the nanofibers.
- **Hypothesis 3:** Functionalized carbon nanotubes and ionic surfactants can be used to introduce surface chemical sites to the ENM that will improve the sorption capacity and

uptake rates, specifically for polar compounds, by promoting specific and electrostatic binding interactions.

- **Hypothesis 4:** Inclusion of quaternary ammonium surfactants and carbon nanotubes, both of which exhibit antimicrobial activity, will prevent nanofibers from biofouling in complex environments (e.g., surface waters and sediments), and facilitate the use of modified polymer ENMs over pure polymer ENMs for field applications.

1.5 Overview and thesis organization

The dissertation contains a total of five chapters, including the current Introduction, three chapters of original research to test the above hypothesis and achieve stated research objectives, and one Conclusion chapter that summarizes key findings while also proposing several avenues of future research. Please note that all of the content in Chapter 2 has been published in *Environmental Science Processes & Impacts*.¹²⁵ The contents of each research chapter are briefly summarized below.

Chapter 2 demonstrates that polymer ENMs are good sampling sorbent materials for POPs, achieve 4-log unit values of K_{ENM-W} that are on par with current POPs passive sampling devices. However, not all of the seven types of polymer ENMs were effective for the HMHC analyte suite. Based on uptake experiments, the three most promising polymers for ENMs were determined to be polyacrylonitrile (PAN), polystyrene (PS), and polymethyl methacrylate (PMMA). Chapter 2 also confirms that ENMs are flexible and strong materials

with a high reproducibility during fabrication. pH-edge and isotherm experiments were also conducted with select ENMs to verify that K_{ENM-W} values our optimal sampling materials are independent of pH and environmental pollutants concentrations. Further, ENM passive samplers perform as equilibrium samplers because of their short equilibration time (<2 days in the most cases). The first attempt of environmental deployment of our ENMs was conducted with sediment from Indiana Harbor and Ship Canal (IHSC) to measure PCBs concentration in the sediment pore water. ENM performance toward POPs and HMHCs are also compared with other commercial products involving polyethylene (PE) membrane and polydimethylsiloxane (PDSM) fiber to ensure our ENMs have a broader testing range than currently available products.

Chapter 3 is focused on using CNT nanocomposites to improve the performance of selected hydrophilic (PAN-based) and hydrophobic (PS-based) ENMs. Both nonfunctionalized CNTs and carboxylated CNTs are used to tailor ENM sorbent activity. We find that the fiber morphology changes after inclusion of CNTs, as monitored by scanning electron microscopy (SEM). Focusing on ENM-CNT composites toward a suite of HMHCs, values of K_{ENM-W} and measured sorption capacities are far greater for CNT-amended materials relative to pure polymer ENMs. CNTs can not only introduce new sites for organic pollutant uptake but also create more porous nanostructures that increase reactive surface area and promote uptake rate. Further, the uptake of HMHCs can be increased by increasing the mass loading of CNTs in the nanofiber composite. In Chapter 3, we also measure the equilibrium

partition coefficient of target analytes in aqueous CNT suspensions (K_d values) and examine possible correlations among different partition coefficient values (i.e., in CNT suspensions versus on ENM-CNT composites) to better understand the sorption mechanism of CNT-enabled passive sampling materials. Field deployment of ENM-CNT composites was conducted at Muddy Creek, IA (USGS site 05454090) to measure atrazine, a corn herbicide, with these new sampling materials producing concentrations comparable to active sampling methods (i.e., aqueous grab samples) conducted by the USGS.

Chapter 4 demonstrates that the addition of cationic and anionic surfactants into the electrospinning precursor sol-gel can be used to enhance organic pollutant sorption on ENMs. ENMs are modified with two types of cationic quaternary ammonium salts to improve uptake of 2,4-dichlorophenoxyacetic acid (2,4-D), an anionic herbicide. We find that as the mass loading of cationic surfactants in the ENM (both pure polymer and polymer-CNT composites) is increased, so too is the uptake of 2,4-D and other anionic targets (PFOA). The anionic surfactant SDS is also used as a porogen in this Chapter, where its intentional removal (via leaching) from the polymer matrix increases ENM porosity and, thus, reactive surface area. For both cationic and anionic surfactant modified materials, tests were also conducted with neutral targets (e.g., atrazine, diuron and metolachlor), with the surfactant modified materials showing performance benefits even when simple electrostatic interactions are not solely at play. Through experiments in complex environmental media (the Iowa River), it is found that there is little to no interference from common non-target species (e.g.,

organic matter) present in environmental matrices for these surfactant modified materials, suggesting great promise for their application in the field.

CHAPTER 2 DEVELOPMENT AND APPLICATION OF POLYMERIC ELECTROSPUN NANOFIBER MATS AS EQUILIBRIUM-PASSIVE SAMPLER MEDIA FOR ORGANIC COMPOUNDS

2.1 ABSTRACT

We fabricated a suite of polymeric electrospun nanofiber mats (ENMs) and investigated their performance as next-generation passive sampler media for environmental monitoring of organic compounds. Electrospinning of common polymers [e.g., polyacrylonitrile (PAN), polymethyl methacrylate (PMMA), and polystyrene (PS), among others] yielded ENMs with reproducible control of nanofiber diameters (from 70 to 340 nm). ENM performance was investigated initially with model hydrophilic (aniline and nitrobenzene) and hydrophobic (selected PCB congeners and dioxin) compounds, generally revealing fast chemical uptake into all ENMs that was well described by a one compartment, first-order kinetic model. Typical times to reach 90% of equilibrium ($t_{90\%}$) were ≤ 7 days under mixing conditions for all ENMs, and < 0.5 days for the best performing materials under static (i.e., no mixing) conditions. Collectively, these short equilibrium timescales suggest that ENMs may be used in the field as an equilibrium-passive sampler, at least for our model compounds. Equilibrium partitioning coefficients (K_{ENM-W} , L/kg) averaged 2 and 4.7 log units for the hydrophilic and hydrophobic analytes, respectively. PAN, PMMA and PS were prioritized for additional studies because they exhibited not only the greatest capacity for simultaneous uptake of the entire model suite ($\log K_{ENM-W} \sim 1.5 - 6.2$), but also fast uptake. For these optimized ENMs, rates uptake into PS were limited by diffusion into the nanofiber, PMMA was limited by aqueous phase diffusion to the

nanofiber surface, and the rate-determine step for PAN was analyte specific. Sorption isotherms also revealed that the environmental application of these optimized ENMs would occur within the linear uptake regime. We examined ENM performance for the measurement of pore water concentrations from spiked soil and freshwater sediments. Soil and sediment studies not only yielded reproducible pore water concentrations and comparable values to other passive sampler materials, but also provided practical insights into ENM stability and fouling in such systems. Further, fast uptake for a suite of structurally diverse hydrophilic and moderately hydrophobic compounds were obtained for PAN and PS, with $t_{90\%}$ ranging from 0.01 to 4 days with mixing and K_{ENM-W} values ranging from 1.3 to 3.2 log units. Our findings show promise for the development and use of ENMs as equilibrium-passive samplers for a range of organic pollutants across soil/sediment and water systems.

2.2 INTRODUCTION

Accurately measuring the abundance of organic chemical pollutants in contaminated water and sediment systems is critical for effective management and risk assessment. However, these measurements are complicated by the diverse physicochemical properties of both legacy and emerging pollutant classes, as well as variables arising from system complexity (e.g., low target concentrations, sorption to dissolved organic matter, and pollutant ionization). For this purpose, the use of passive sampling devices has increased remarkably over the last decade, particularly for the determination of the freely dissolved sediment pore water and surface water concentrations of hydrophobic contaminants.^{63, 165-168}

To date, relatively less attention has been focused on passive samplers for hydrophilic and moderately hydrophobic contaminants.^{70, 92, 168-172} Alvarez *et al.*⁷⁰ were among the first to develop and field deploy passive samplers operating in the linear uptake stage for measurement of polar compounds in surface water (the so-called Polar Organic Chemical Integrative Samplers, or POCIS). They focused on organic compounds with logarithmic octanol-water partitioning coefficients (i.e., $\log K_{OW}$ values) less than 4, with field results for two herbicides and a naturally occurring hormone yielding good agreement with conventional sampling and measurement methods. MacLeod *et al.* performed one of the first POCIS laboratory calibration for 25 pharmaceuticals and personal care products (PPCPs), which also included field deployment,¹⁷³ concluding that POCIS can be used as a quantitative tool for measuring PPCPs in water systems. Harman *et al.*¹⁷⁴ and Mori *et al.*¹⁷⁵ reviewed and summarized calibration

methods and sampling rates for more than 100 hydrophilic analytes using POCIS. Both studies agreed that even though POCIS is a useful device to measure hydrophilic and moderately hydrophobic compounds in aquatic systems, there remains a lack of standardization for calibration methods, and that the use of laboratory sampling rates in field measurements can increase uncertainty when environmental time-weighted average (TWA) concentrations are calculated.

A passive sampler characterized by rapid uptake that operates in an equilibrium partitioning regime could reduce such uncertainties. Equilibrium-passive samplers hold the promise of higher precision and accuracy for field measurements because their calculations of field concentrations only depend on equilibrium partition coefficients, which can be readily measured in the laboratory. Equilibrium partitioning eliminates the need for spiking performance reference compounds, which are needed to account for sampling rates during field deployment of kinetic passive samplers. Further, shorter sampling times is highly desirable for capturing spatial and temporal variability in dynamic pollutant systems. To the best of our knowledge, only three equilibrium-passive sampler materials consisting of plastic films have been developed to date for measurement of hydrophilic and moderately hydrophobic analytes.^{169, 170, 176} Although the uptake capacity for these materials may be lower than, for example, POCIS, their ability to achieve equilibrium over a short sampling period, even under static conditions, represents an important advance for passive environmental sampling techniques.

Here, we aim to develop a new, nanomaterial-enabled platform for equilibrium-passive sampling devices. Our approach uses electrospinning, a nanofiber fabrication method that offers superior control over the material properties exhibited by the resulting electrospun nanofiber mats (or ENM).^{102, 177} Accordingly, we investigated how the physical and chemical properties of various polymeric ENMs influence their performance as passive sampling materials toward a suite of hydrophilic (i.e., $\log K_{OW} < 2$), moderately hydrophobic (i.e., $\log K_{OW}$ ranging from 2 to 4.5), and hydrophobic (i.e., $\log K_{OW} > 4.5$) compounds. We anticipated that the high surface-area-to-volume ratio (SA/V values) of the nanofiber mats would promote faster uptake of target organic compounds into the ENM.^{102, 178} As has been reported for hydrophobic compounds, the size and geometry of the sampler device, often described by its SA/V ratio, play an important role for uptake rates. Specifically, increasing the SA/V ratio corresponds to a faster sampling device.^{178, 179} For our ENMs, this SA/V ratio is inversely proportional to the nanofiber radius (i.e., $SA/V = 2/r$), which we propose represents a critical design parameter for tuning and optimizing ENM performance.

To test this hypothesis, we fabricated seven ENMs from different polymers and tested their sorption performance against a suite of eight hydrophilic, four moderately hydrophobic, and ten hydrophobic compounds. Scanning electron microscopy, water contact angle and specific surface area measurements were used to characterize the fabricated ENMs. Initially, ENM performance experiments focused on aniline and nitrobenzene as model hydrophilic compounds and selected PCB congeners and dioxin as model hydrophobic compounds.

Optimal ENMs from initial studies were then tested across a broader range of conditions (e.g., pH, target concentration, nanofiber diameter and in soil and sediment systems) and against a larger suite of hydrophilic and moderately hydrophobic compounds.

2.3 MATERIAL AND METHODS

ENM fabrication. We synthesized seven ENMs from ethylene-vinyl acetate (EVA); polyacrylonitrile (PAN); polyethylene terephthalate (PET); polymethyl methacrylate (PMMA); polystyrene (PS); polyvinyl acetate (PVAc); and polyvinylidene fluoride (PVDF). These polymers were selected due to their different chemical functionalities, providing materials across the spectrum from hydrophobic (e.g., PS and PVDF) to hydrophilic (e.g., PAN and PMMA) (**Table 2-1**).

ENMs were fabricated using a custom-built electrospinning apparatus that has been described in detail elsewhere (**Figure 2-1**).¹⁶¹ ENM synthesis recipes were adapted from previously published methods.^{103, 180} All reagents and ENM fabrication parameters are summarized in **Table 2-1**. Briefly, polymers were dissolved in an appropriate organic solvent and thermally mixed at 60 °C for 4 h to obtain a homogenous sol-gel as an electrospinning precursor solution. The sol-gel was cooled to room temperature, and transferred into a 12 mL syringe, which was then mounted on a syringe pump. A needle was used to expel the sol-gel, with the needle tip connected to a high-voltage power supply. During synthesis, the flow rate of the sol-gel from the syringe was controlled, as well as the needle-tip voltage. A grounded,

rotating metal drum collector (covered with Al foil) was used to collect deposited ENMs, located a fixed distance from the needle tip. All electrospinning was conducted under a controlled environment within a custom environmental chamber, where temperature and humidity were fixed at a desired value between 20 °C to 28 °C and 16% to 20%, respectively. Chemical properties of each fabricated ENM, including the molecular weight and repeating structural units of each polymer, are listed in **Table 2-1**.

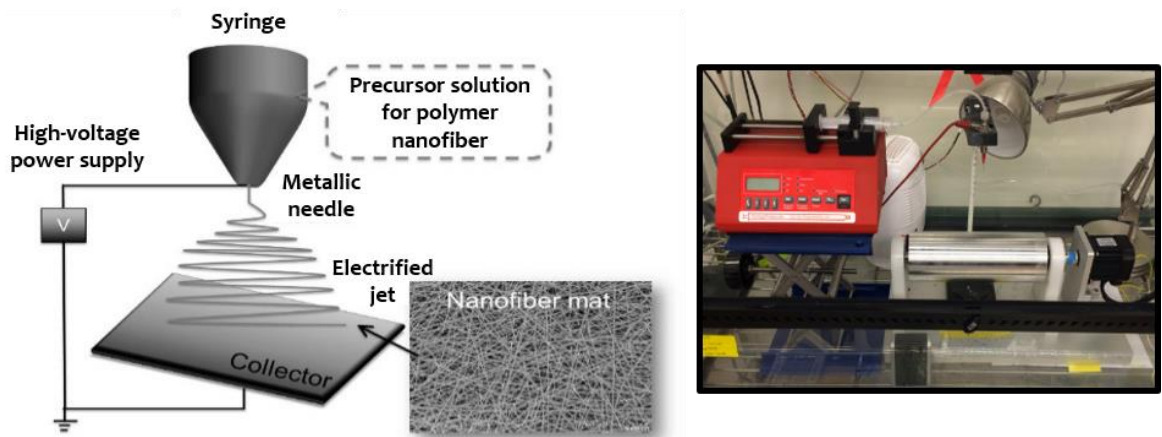


Figure 2-1. Set-up of the lab electrospinning apparatus. The left cartoon shows a schematic of an electrospinning apparatus, including high-voltage power supply, spinneret (metallic needle), collector (aluminum foil or metallic drum) and syringe pump. Right photograph shows the laboratory scale electrospinning apparatus used to fabricate all ENMs tested herein.

Table 2-1. Reagents, physical and chemical properties, and electrospinning synthesis parameters for ENMs investigated herein.

Reagent Details	PAN	PS	PMMA	PET	PVDF
Physical and Chemical Properties of Polymers					
Repeating structural unit					
Ave. Mw	~150,000	~280,000	~996,000	n.m.	~534,000
Monomer formula	C ₃ H ₃ N	C ₈ H ₈	C ₅ H ₈ O ₂	C ₈ H ₆ O ₄ And C ₂ H ₆ O ₂	C ₂ H ₂ F ₂
Hydrogen bond* O or N content (w %)	H-acceptor (1)	No	H-acceptor (2)	H-acceptor (4)	H-acceptor (2)
Aromatic bond**	0	6	0	6/0	0
Density (g/cm ³)	1.2	1.0	1.2	1.4	1.8
Hydrophobicity of functional group	Hydrophilic	Hydrophobic	Hydrophilic	Hydrophobic	Hydrophobic
ENM hydrophobicity (measured water contact angle)	Hydrophilic	Hydrophobic	Hydrophobic	Hydrophobic	Hydrophobic
Electrospinning Receipt and Synthesis Parameters					
Solvent (v/v)	DMF	DMF	5:1 DMF: GAA	1:1 DCM:TFA	25:9 Acetone : DMA
Polymer to solvent ratio (w/w)	0.087	0.11	0.071	0.071	0.14
Polymer weight (%)	8	10	6.6	6.6	12
Distance needle-collector (cm)	10	10	10	10	10
Voltage (kV)	13	17	9	16	22
Pump flow (mL/h)	0.5	0.3	0.3	0.4	0.7
Needle gauge size	25G	25G	25G	23G	25G

*Hydrogen bond is a chemical bond in which a hydrogen atom of one molecule is attracted to an electronegative atom, especially a nitrogen, oxygen or fluorine atom, usually of another molecule. The numbers of electronegative atoms that accept covalent bonds in each polymer repeat unit are listed in parentheses.¹⁸¹

**Based on Hückel's rule, the numbers of aromatic bond are counted by delocalized electrons in each polymer repeat unit.

ENM Characterization. Nanofiber diameters were measured from scanning electron microscopy (SEM) and analysis of resulting SEM images using ImageJ software. Typically, 100 nanofiber diameters were measured per ENM sample, allowing size distributions with

mean and standard deviation (i.e., histograms of nanofiber diameters) to be quantified. Specific surface area of ENMs was measured using a Micromeritics ASAP 2020 surface area and pore size analyzer (N₂-BET). The water contact angle, which uses wettability to assess ENM hydrophobicity/hydrophilicity, was obtained using a Rame-Hart model 100 contact angle goniometer equipped with a Thor Laboratories 6-60× magnification microscope lens and high-resolution CMOS camera. For this analysis, 10 μL of DI water was used as the wetting liquid, dispensed and collected by an Eppendorf EDOS 5222 Electronic Dispensing System at 1 μL/s. If the angle between the material and the water drop is lower than 90°, the material is considered hydrophobic, and if the angle is more than 90°, the material is considered hydrophilic. Stability of ENMs during analytical processing (e.g., solvent extraction) was also examined across a range of pH values (2 to 12) and in various organic solvents (e.g., methanol, acetonitrile).

Target Analyte Suite. The suite of hydrophilic and moderately hydrophobic (i.e., log *K_{OW}* ranging from -0.07 to 4.5) target chemicals consisted of aniline, anisole, atrazine, caffeine, benzylamine, diuron, β-Estradiol, nitrobenzene, phenol, p-nitrophenol, trinitrotoluene (TNT) and 1, 3, 5-Trinitroperhydro-1, 3, 5-triazine (RDX), all of which were purchased from Sigma-Aldrich (with purity ≥ 98%). Stock solutions (from 1.1-6,800 μg/L) for each compound were prepared in deionized (DI) water. The hydrophobic chemical suite consisted of PCB1, PCB11, PCB29, PCB47, PCB121, PCB136, PCB187, PCB206, PCB209 and 2,3,7,8-tetrachlorodibenzodioxin (dioxin), all purchased from AccuStandard, Inc. A mixed stock solution (100 - 2,000 mg/L) for PCBs was prepared in hexane, as well as for dioxin (200 mg/L).

Solvents were purchased from Sigma-Aldrich and Fisher chemical (purity \geq 99% in all cases).

Table 2-2 summarizes key chemical properties for the target chemicals.

Table 2-2. Molecular structures and chemical properties of our organic target analyte suite.

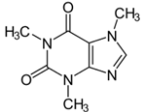
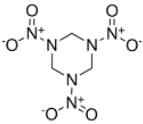
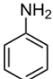
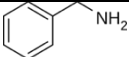
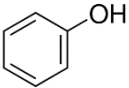
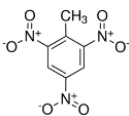
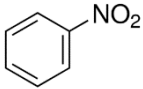
Compound	Structure	MW (g/mol)	Log K_{ow}	Water solubility (room temperature) (g/100 mL)	Aromatic bonds	Hydrogen bonds (count)*	pKas (25 °C)	Charge @ pH ≈ 6.5
Caffeine		194.19	-0.07	2	10	H-donor (0) H-acceptor (6)	0.52, 14 **	Neutral
RDX		222.12	0.9	0.004	0	H-donor (0) H-acceptor (12)	-15	Neutral
Aniline		93.13	0.9	3.6	6	H-donor (2) H- acceptor (1)	4.9	Protonated (neutral)
Benzylamine		107.16	1.1	100	6	H-donor (2) H- acceptor (1)	9.1	Protonated (positive)
Phenol		94.11	1.5	8.2	6	H-donor (1) H- acceptor (1)	9.9	Deprotonated (neutral)
TNT		227.13	1.6	0.013	6	H-donor (0) H-acceptor (9)	0.65, 12.0**	Neutral
Nitrobenzene		123.06	1.9	0.2	6	H-donor (0) H-acceptor (3)	4.0 (0 °C)	Neutral

Table 2-2. Molecular structures and chemical properties of our organic target analyte suite.

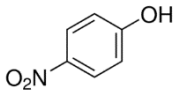
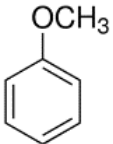
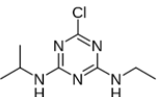
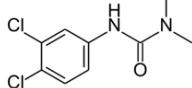
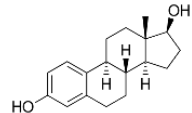
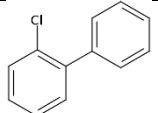
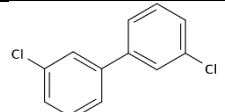
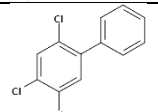
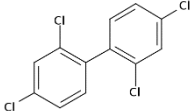
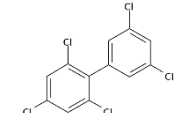
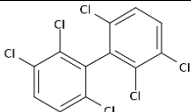
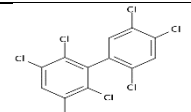
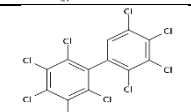
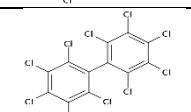
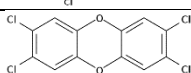
Compound	Structure	MW (g/mol)	Log K_{ow}	Water solubility (room temperature) (g/100 mL)	Aromatic bonds	Hydrogen bonds (count)*	pKas (25 °C)	Charge @ pH ≈ 6.5
p-Nitrophenol		139.11	1.9	1.6	6	H-donor (1) H- acceptor (4)	7.2	Partially deprotonated (partially negative)
Anisole		108.14	2.1	0.16	6	H-donor (0) H-acceptor (1)	-4.8	Neutral
Atrazine		215.68	2.6	0.007	6	H-donor (2) H- acceptor (5)	2.3	Protonated (neutral)
Diuron		233.09	2.7	0.0042	6	H-donor (1) H- acceptor (3)	14	Protonated (positive)
β-Estradiol		272.38	4.0	0.00213	6	H-donor (2) H- acceptor (2)	10	Deprotonated (neutral)
PCB1		188.65	4.6	4.75*10 ⁻⁰⁴	12	H-donor (0) H- acceptor (0)		Neutral
PCB11		223.09	5.3	6.09*10 ⁻⁰⁵	12	H-donor (0) H- acceptor (0)		Neutral
PCB29		257.54	5.6	2.19*10 ⁻⁰⁵	12	H-donor (0) H- acceptor (0)		Neutral

Table 2-2. Molecular structures and chemical properties of our organic target analyte suite.

Compound	Structure	MW (g/mol)	Log K_{ow}	Water solubility (room temperature) (g/100 mL)	Aromatic bonds	Hydrogen bonds (count)*	pKas (25 °C)	Charge @ pH ≈ 6.5
PCB47		291.99	5.9	7.45×10^{-06}	12	H-donor (0) H- acceptor (0)		Neutral
PCB121		326.43	6.6	2.62×10^{-06}	12	H-donor (0) H- acceptor (0)		Neutral
PCB136		360.88	6.2	2.73×10^{-06}	12	H-donor (0) H- acceptor (0)		Neutral
PCB187		395.32	7.2	8.65×10^{-07}	12	H-donor (0) H- acceptor (0)		Neutral
PCB206		464.21	8.1	5.67×10^{-08}	12	H-donor (0) H- acceptor (0)		Neutral
PCB209		498.66	8.2	2.65×10^{-08}	12	H-donor (0) H- acceptor (0)		Neutral
Dioxin		321.97	6.8	$2.0E \times 10^{-08}$	12	H-donor (0) H- acceptor (2)		Neutral

* Hydrogen bond is a chemical bond in which a hydrogen atom of one molecule is attracted to an electronegative atom, especially a nitrogen, oxygen or fluorine atom, usually of another molecule. The numbers of electronegative atoms that accept covalent bonds and electropositive hydrogen atoms that participate covalent bonds in each chemical are listed in this table.

** Caffeine and TNT contain a weak base and a weak acid corresponding to pK_a values of 0.52 and 14, and 0.65 and 12, respectively.

Sorption and Uptake Experiments. Protocols for time-dependent uptake experiments were adapted from previous passive sampler development studies.^{61, 182} Initial experiments with the entire suite of ENMs were performed with aniline and nitrobenzene (model hydrophilic chemicals), as well as the entire collection of PCB congeners and dioxin (model hydrophobic chemicals) in aqueous solutions. Partition coefficients (K_{ENM-w} , L/kg) between the concentration of the chemical of interest in the ENM and the aqueous phase were used to evaluate ENM performance, as shown in the Equation. 2-1

$$K_{ENM-w} = \frac{C_{ENM}}{C_w} \quad (2-1)$$

where C_{ENM} and C_w are the experimentally measured concentrations of the chemical in the ENM and aqueous phase, respectively.

Experiments used an initial aqueous concentration of ~ 2.8 mg/L for aniline and nitrobenzene, and 0.1 to 100 ng/L for PCBs and dioxin. Amber glass vials were filled completely with solution (i.e., ~40 mL so that there was no headspace) and ~0.05 g of ENM was added (~ 20 cm²). Vials were then sealed with Teflon-lined screw caps and placed on a rotator on which they were tumbled slowly end-over-end (~ 8 rpm). Samples were periodically collected for measurement of both the aqueous and sorbed phase concentrations after 3, 7, and 11 h, and 1, 2, 3 and 5 d for aniline and nitrobenzene. A shorter sampling interval of 3, 5, and 8 h and 1 day was used for PCBs and dioxin.

For select ENMs with optimal performance, additional uptake studies were conducted. To complement actively mixed experiments, studies considered uptake rates in static systems

(i.e., without mixing) for aniline and nitrobenzene were carried out. These were conducted over 8 days to measure partitioning under conditions most representative of passive sampling applications. We also explored the influence of ENM surface area-to-volume ratio (SA/V values) by exploring nitrobenzene uptake as a function of the nanofiber diameter (which was tuned by varying polymer concentration in the sol-gel and humidity during synthesis).

Aniline and nitrobenzene sorption was also measured across a range of pH values (from 5.5 to 9), where solutions buffered at pH 5.5 and 6 used 10 mM of 2-(N-morpholino) ethanesulfonic acid buffer, at pH 7 and 8 used 10 mM of 2- [4-(2-hydroxyethyl) piperazin-1-yl] ethanesulfonic acid, and at pH 9 used 5 mM of sodium borate buffer. To determine ENM capacity, sorption isotherm experiments were also conducted with aniline and nitrobenzene. These experiments followed the aforementioned protocol for rate experiments, but the initial aqueous concentration of each compound was varied from 1 to 29 mg/L at a fixed ENM loading (0.05 g). Optimal ENMs were also used to measure uptake of our entire suite of hydrophilic and moderately hydrophobic compound targets. These compounds were tested with an initial concentration between 2.3 and 6.8 mg/L at pH ~ 6.5 (in DI water). The testing period varied from 3 to 8 days depending on the equilibrium time for each chemical.

Uptake Experiments in Soil and Sediment Systems. To evaluate optimal ENM performance under environmentally relevant conditions, uptake experiments were conducted in systems containing a model soil amended with nitrobenzene. Experiments used a sandy loam commercially acquired through AGVISE laboratories (Northwood, ND and Benson, MN)

marketed as “LBLS”, which contained an organic carbon fraction of 3%.¹⁸³ The soil was first mixed with DI water (50% v/v), and then sterilized with 30 mM of sodium azide (NaN_3) while mixing for 2 weeks. After this time period, the soil was spiked with nitrobenzene to achieve an initial concentration of ~ 10 mg/L. The suspension was once again tumbled for two additional weeks to achieve solid-water equilibrium partitioning for nitrobenzene. Using these equilibrated systems, 30 g of wet soil was then combined with ~ 0.05 g of ENM in a clean amber glass vial. After ENM addition, vials were tumbled end-over-end, and samples were collected after 5, 10, 15, 20 and 25 days.

At each sampling point, the ENM was removed, gently wiped with a paper towel to remove superficial residual soil, and rinsed with a small volume (~ 50 to 100 mL) of DI water. We note that to confirm removal of soil via this wiping and washing procedure, SEM images of cleaned ENMs were collected. Moreover, samples of the DI wash water were collected for analysis to measure any loss of target analyte through this cleaning procedure. After cleaning, ENMs were analyzed for sorbed nitrobenzene concentration as described before.

As a final performance test of our ENMs, sediment pore water measurements from highly PCB contaminated sediments collected from the Indiana Harbor and Ship Canal (IHSC), Indiana were carried out. We have previously measured and reported the PCB sediment pore water concentrations using PDMS fiber.¹⁶⁷ Sampling and handling of the sediments are presented in details elsewhere.¹⁶⁷ Around 0.1 g of ENM was placed in a clean

amber glass bottle (250 mL) with Teflon liner cap, with sediment and deionized water (~100 g), and gently shaken (80 rpm and ~25°C) for 28 days.

Uptake Modeling. Analyte uptake and accumulation into the ENM was modeled using a one compartment, first-order kinetic model:^{170, 178}

$$C_{ENM} = \frac{k_1}{k_2} \times C_W \times (1 - \exp(-k_2 \times t)) \quad (2-2)$$

where C_{ENM} and C_W are the concentrations of the analyte in the ENM and in the water as function of time (mg/L), respectively; k_1 and k_2 are the uptake and elimination rate constants (h^{-1}), respectively; and t is time (h). Time-series of C_{ENM} and C_W data were input into Equation 2-2, and a non-linear least squares analysis (performed in Excel using the embedded Solver tool) was used to solve for k_1 and k_2 . Further, K_{ENM-W} can be calculated from the ratio of k_1 and k_2 , while the time required to reach 90% of equilibrium can be estimated via Equation 2-3. Estimation of the uncertainty of the calculated parameters was performed by the “jackknife” method.¹⁸⁴

$$t_{90\%} = \frac{\ln 10}{k_2} \quad (2-3)$$

Analytical Methods. High performance liquid chromatography with diode array detector (LC/DAD, Agilent 1100 Series HPLC) was used to measure hydrophilic and moderately hydrophobic compounds in both the aqueous phase and in ENM extracts corresponding to the sorbed phase. All analyses followed previously published methods.^{143, 185-191} For aqueous phase analysis, 1 mL of aqueous sample was transferred to an amber autosampler vial, and immediately analyzed. For analysis of the sorbed phase, ENM-bound

mass was extracted by mixing the ENM with 10 mL of methanol for 2 d, after which 1 mL of methanol was collected and analyzed.

PCBs and dioxin were measured using a published method from our group that is also used by others.^{167, 192} For the aqueous phase, 20 mL of sample was spiked with 25 ng of a PCB solution (PCB14, PCB65-d and PCB166) as a surrogate standard. The surrogate congeners were used to estimate any losses during the cleanup and extraction procedures. The mixture was vortexed for 1 minute and subsequently mixed with 8 mL of hexane. This solution was tumbled for 5 minutes, after which the hexane layer was separated from the water. The extracted hexane was concentrated using a Turbo Vap unit to around 0.5 mL and transferred to a gas chromatography (GC) vial. An internal standard consisting of 50 ng of PCB30-d and PCB204 was spiked into this concentrated solution. For analysis of the sorbed phase, the ENM was first spiked with 25 ng of a PCB surrogate standard and then tumbled with 40 mL of hexane for 12 h. The hexane was recovered via pipette and concentrated using a Turbo Vap unit to approximately 1 mL. An internal standard consisting of 50 ng of PCB30-d and PCB204 was then spiked into this concentrated solution. PCBs and dioxin were then measured using gas chromatography with tandem mass spectrometry (GC-MS/MS, Agilent 7000) in multiple reaction monitoring mode.

QA/QC. Laboratory blanks consisted of DI water, methanol, hexane and unused ENMs were analyzed in parallel with experimental samples. No contamination was found in any of the blanks analyzed. Further, a mass balance approach was carried out to calculate recoveries

of aniline, nitrobenzene, PCBs and dioxin. In general, recoveries ranged from 50% to 110% through all the experiments. In the case of replicated measurements of aniline, nitrobenzene, PCBs and dioxin in the aqueous phase of ENM-containing systems, a relative standard deviation (RSD) of 7%, 3%, 16% and 16% were obtained, respectively. Because we used an internal standard method to quantify PCBs and dioxin, we also determined the recoveries of the surrogate standards that were spiked into our samples prior to sample extraction and cleanup. For these compounds, the recoveries of PCB14, PCB-d65 and PCB166 averaged $87 \pm 7\%$, $85 \pm 9\%$ and $88 \pm 6\%$, respectively.

2.4 RESULTS AND DISCUSSION

Synthesis and Characterization of ENMs. ENMs of PAN, PET, PMMA, PS and PVDF met criteria that made them most promising for application in passive sampling. These materials could be reproducibly fabricated using electrospinning, and they also showed no signs of degradation or dissolution in water across a range of pH values (from 2-12) and in various organic solvents commonly used for extraction (e.g., methanol and acetonitrile). We note that while PVAc could be fabricated by electrospinning, it dissolved readily in methanol, and numerous attempts and approaches to fabricate EVA-ENM via electrospinning were unsuccessful. Thus these two ENMs were not further investigated.

Figure 2-2 shows SEM images of the five viable ENMs. All consisted of well-defined nanofibers with average diameters ranging from ~70 to 350 nm. Nanofiber diameters were

relatively uniform and without beading, as evidenced by the small standard deviation associated with measured size distributions (**Table 2-3**). Further, all recipes resulted in good batch-to-batch reproducibility. For PS, for example, three replicate batches fabricated over several months produced average diameters of 150 ± 40 , 140 ± 20 and 140 ± 30 nm (**Figure 2-3**). Generally, ENMs exhibited modest N₂-BET specific surface areas typically in the range of 5 - 30 m²/g (**Table 2-3**).

Measured water contact angles mostly matched expectations of polymer hydrophilicity and hydrophobicity from characteristics of their monomeric unit (**Table 2-1**). Hydrophobic ENMs (water contact angles > 90°) were PVDF > PMMA > PET > PS, while PAN was hydrophilic (water contact angle < 90°). The exception was PMMA; although it contains a presumed hydrophilic carboxylate ester functional group,¹⁹³ the measured water contact angle of 120° suggests our PMMA-ENM behaves more as a hydrophobic material.

Simple mechanical testing indicated that all the ENMs were able to support a reasonable load, and they could be twisted and stretched without significant deformation (**Figure 2-4**). Thus, all ENMs are sufficiently robust and durable such that application in the field as a passive sampler media and subsequent handling in the laboratory during sample processing should not be prohibitive.

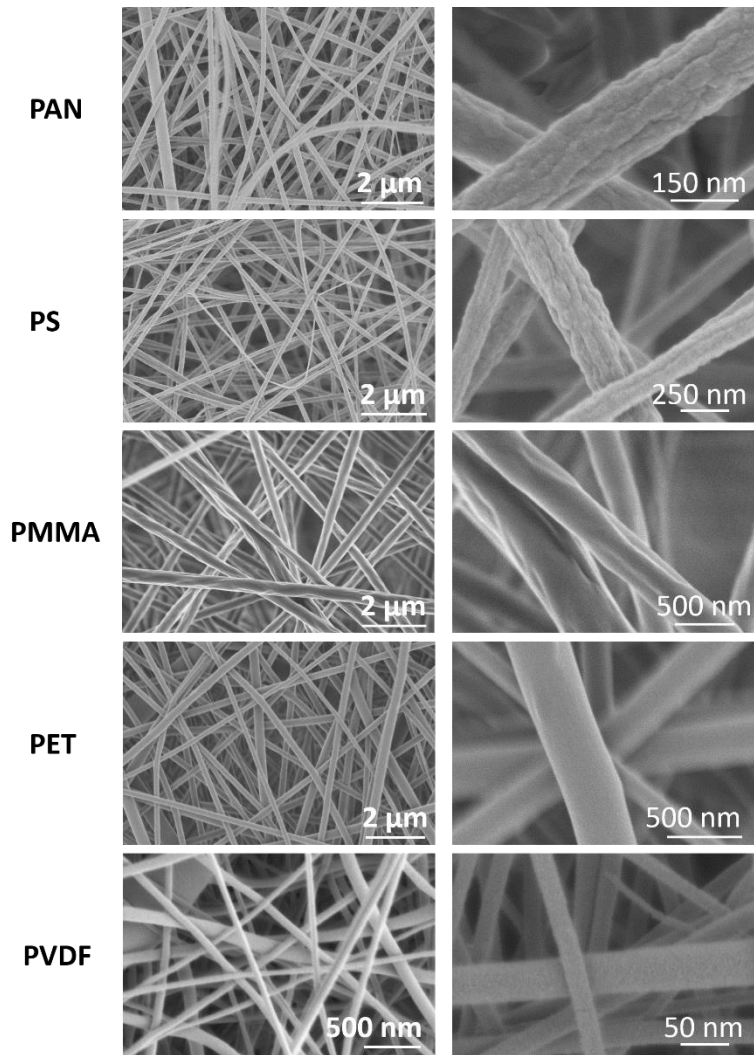


Figure 2-2. SEM images of fabricated ENMs at low (left) and high (right) magnification. Corresponding recipes and characterization of these ENMs are provided in **Table 2-1**.

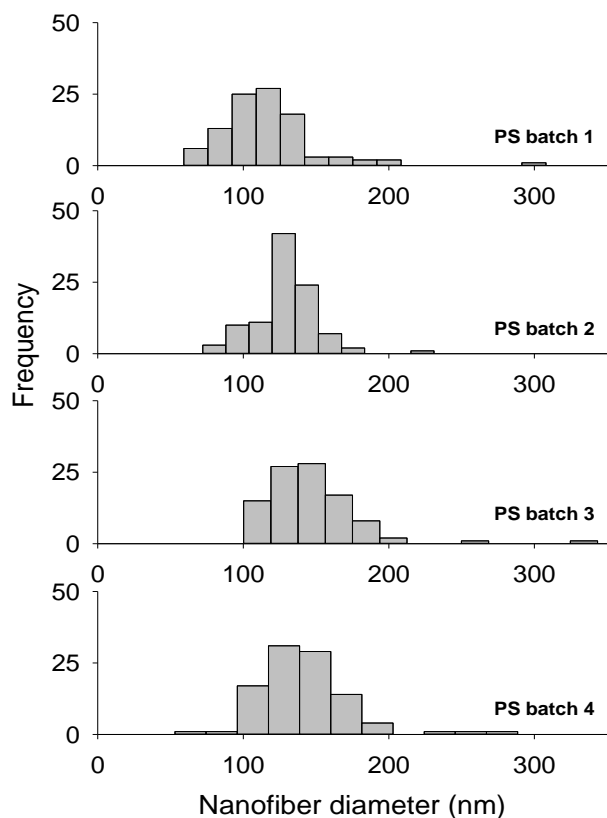


Figure 2-3. Histograms of four batches of PS fabricated. Diameters for at least 100 individual nanofibers within ENMs were quantified via SEM to produce these distributions.

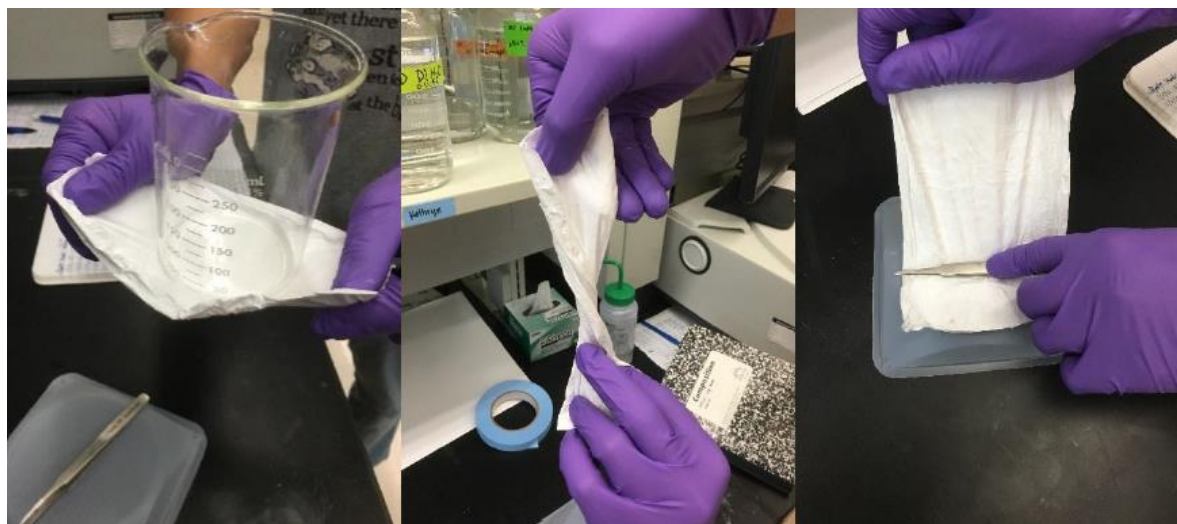


Figure 2-4. Photographs illustrating the handling, manipulation and mechanical strength of a representative PS.

Table 2-3. Physical and chemical properties for ENMs investigated herein.

Property	PAN	PS	PMMA	PET	PVDF
Average diameter (nm)*	160 ± 30 (n = 7)	140 ± 30 (n = 4)	340 ± 50 (n = 6)	70 ± 20 (n = 4)	50 ± 10 (n=5)
Surface area (m ² /g)	12 ± 0.50	27 ± 3.5	6.1 ± 1.4	7.1 ± 2.2	16 ± 0.2
Water contact angle (°)	44 ± 6.2	109 ± 9.9	119 ± 5.1	117 ± 7.5	135 ± 5.4

* Fiber diameters were measured from SEM images using ImageJ software. Typically, 100 nanofiber diameters were measured per ENM sample, allowing size distributions to be calculated for all synthesized materials. n = number of replicate syntheses.

Trends in ENM Performance with Model Compounds. *Aniline and nitrobenzene.*

With mixing, both model hydrophilic chemicals exhibited very fast uptake to all ENMs, shown by the minimum change in experimentally measured partition coefficients after 0.4 d (**Figure 2-5**). Thus, equilibrium partition coefficients were calculated from the average data collected from 2 to 5 days. Average K_{ENM-W} values ranged from 0.7 to 2.8 log units (L/kg), although the extent of sorption varied depending on both the ENM and the model compound target (**Table 2-2**). For example, values of K_{ENM-W} were typically ~1 log unit higher for nitrobenzene than aniline, but both compounds exhibited similar K_{ENM-W} values on PAN. We note that no inhibitory or competitive effects were observed when experiments were conducted with analyte mixtures relative to individual analyte experiments.

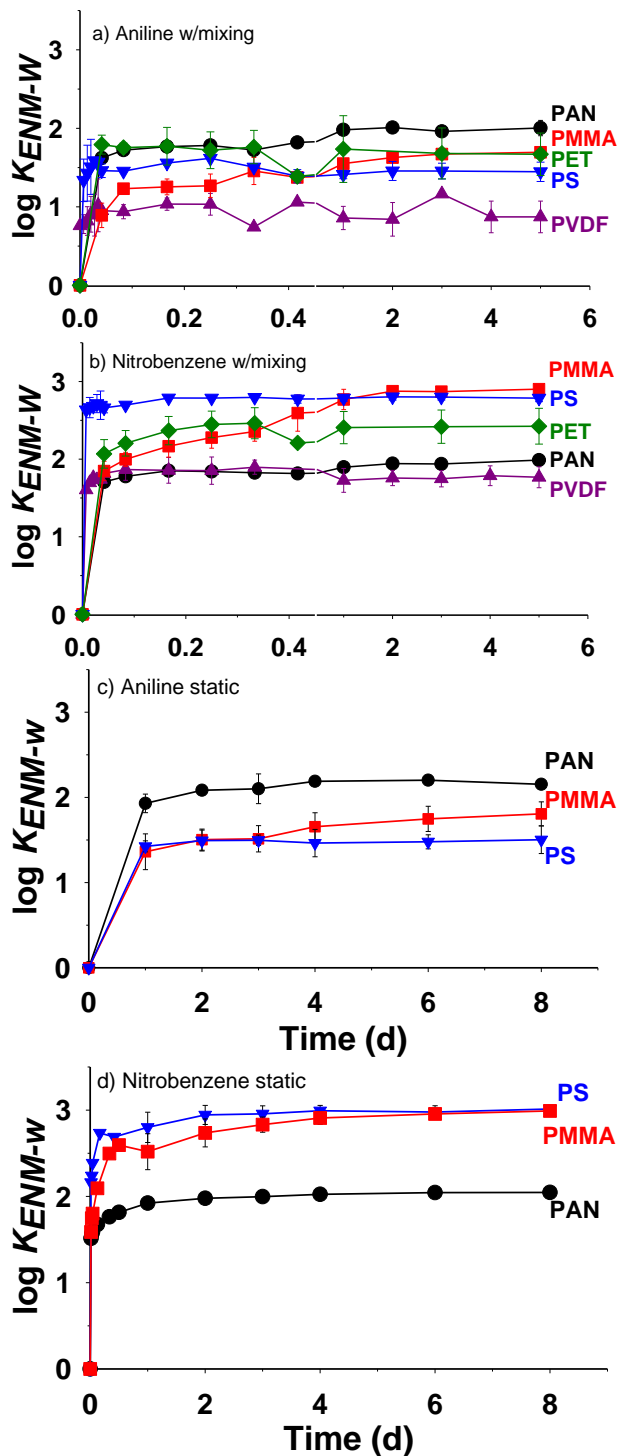


Figure 2-5. Uptake curves with mixing and without mixing for aniline (a, c) and nitrobenzene (b, d) with our five ENMs. The error bars represent one standard deviation from two (w/mixing) and three (static) replicate uptake experiments. Laboratory set up: pH ~ 6.5 (DI water), initial concentrations of aniline: 2 mg/L and nitrobenzene: 3 mg/L, ENM loading ~1.5 g/L. Please note the difference in the x-axis scale for experiments with and without mixing. The light gray area in panels a and b notes a shorter, zoomed in time scale. Lines simply connect data points.

Table 2-4. Summary of average measured and predicted ENM-water equilibrium partition coefficients for aniline and nitrobenzene (log units, L/kg) under mixing and static conditions, as well as predicted $t_{90\%}$ for both mixing and static conditions. For aniline and nitrobenzene, values were also calculated from the sorption isotherms for PAN, PMMA and PS (**Figure 2-16**).

ENM	Aniline						
	Log K_{ENM-W} (L/kg)					$t_{90\%}$ (d)	
	Measured (n = 10) ^a	Measured static (n ≥ 3)	Isotherm ^b	Model mixing	Model static	Mixing	Static
PAN	1.9 ± 0.06	2.1 ± 0.04	1.8 ± 0.6	1.9 ± 0.04	2.1 ± 0.03	2.2 ± 0.4	2.4 ± 0.2
PMMA	1.7 ± 0.1	1.9 ± 0.06	2.1 ± 1.0	1.8 ± 0.05	2.0 ± 0.02	7.3 ± 1.2	12 ± 0.6
PS	1.5 ± 0.03	1.5 ± 0.02	1.7 ± 1.0	1.5 ± 0.03	1.5 ± 0.02	0.01 ± 0.01	0.01 ± 0.01
PET	1.7 ± 0.04			1.6 ± 0.01		0.01 ± 0.01	
PVDF	0.9 ± 0.1			1.0 ± 0.02		0.3 ± 0.07	
ENM	Nitrobenzene						
	Log K_{ENM-W} (L/kg)					$t_{90\%}$ (d)	
	Measured (n = 10) ^a	Measured static (n ≥ 3)	Isotherm ^b	Model mixing	Model static	Mixing	Static
PAN	1.9 ± 0.1	1.9 ± 0.08	1.8 ± 0.3	1.9 ± 0.01	2.0 ± 0.03	0.1 ± 0.03	0.4 ± 0.2
PMMA	2.8 ± 0.2	2.9 ± 0.05	2.9 ± 1.1	2.9 ± 0.01	3.0 ± 0.02	1.2 ± 0.06	4.5 ± 0.6
PS	2.8 ± 0.01	2.9 ± 0.09	2.6 ± 1.2	2.8 ± 0.01	2.8 ± 0.02	0.03 ± 0.01	0.1 ± 0.01
PET	2.4 ± 0.09			2.5 ± 0.02		0.1 ± 0.01	
PVDF	1.8 ± 0.06			1.9 ± 0.01		0.02 ± 0.01	

^a Equilibrium partition coefficients were calculated from the average data collected from 2 to 5 days under mixing conditions. ^b From linear regression from the sorption isotherms, **Figure 2-16**. Sorption isotherms using **PAN, PMMA and PS for (a) aniline and (b) nitrobenzene**. Linear regressions yielded very strong correlations ($R^2 \geq 0.93$, $p < 0.0001$) with the exception of aniline sorbed to PS, which was also statistical significant ($R^2 = 0.7$, $p = 0.0004$), but not as strong as the other correlations

For aniline, the overall trend in partitioning was as follows: PAN > PMMA ≈ PET > PS >> PVDF, spanning a range of 1-log unit from the ENM with the most to least uptake capacity. Although the five ENMs exhibit different chemical properties (**Table 2-1**), aniline uptake was generally greatest on the hydrophilic ENMs (**Table 2-3**). For example, although measured water contact angles for our ENMs clustered into two groups as either hydrophilic (40-60°) or hydrophobic (100-140°), we observed a clear negative correlation ($p = 0.003$) between $\log K_{ENM-W}$ values and increasing water contact angles (i.e., hydrophobic surfaces; see **Figure 2-6**). Conversely, no significant correlation was observed between the $\log K_{ENM-W}$ and ENM specific surface area from BET ($p = 0.1$).

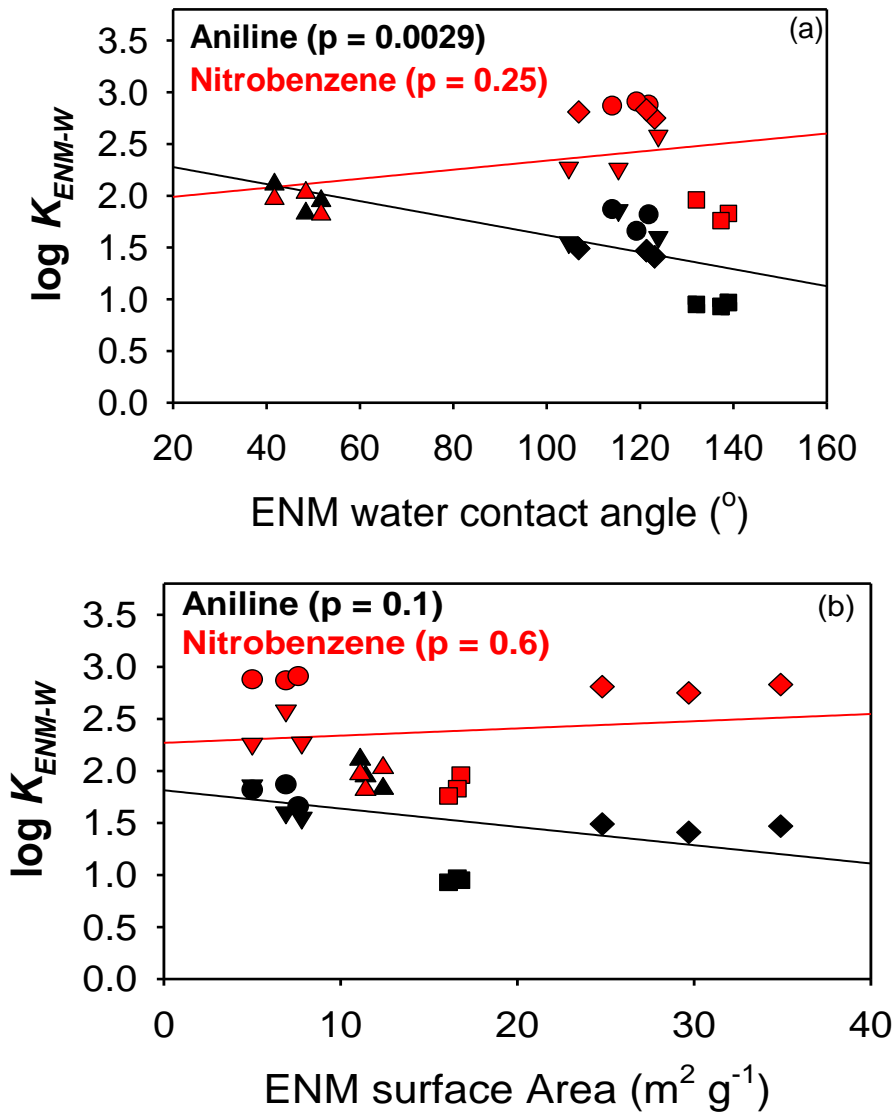


Figure 2-6. Linear regressions (black=aniline, red=nitrobenzene) between equilibrium partition coefficients and (a) water contact angle and (b) specific surface area. Data are shown for PAN (▲), PMMA (▼), PS (●), PVDF (■) and PET (◆). The p-values of the slopes from the regressions are shown as p. Significant is considered with a p-value < 0.05.

Nitrobenzene yielded a different trend in uptake, PMMA ~ PS > PET > PAN ~ PVDF, although a similar range of 1-log unit was observed across measured partitioning coefficients. Based upon measured water contact angles, nitrobenzene uptake was greatest on moderately

hydrophobic polymers (**Table 2-1, Table 2-3**), whereas the most hydrophilic (PAN) and most hydrophobic (PVDF) ENMs performed poorly. Unlike aniline, therefore, no significant correlation ($p = 0.25$) was found between $\log K_{ENM-W}$ values and water contact angles for nitrobenzene (**Figure 2-6**). As with aniline, no correlation was obtained between the $\log K_{ENM-W}$ and ENM specific surface area ($p = 0.6$).

For comparison, we also measured partition coefficients for aniline and nitrobenzene using conventional, commercially available passive sampling materials under the same experimental conditions. These included polystyrene beads, PDMS fiber and a low-density polyethylene (LDPE) film, many of which have been used in research and development of passive sampling materials, albeit mostly for hydrophobic compounds.^{167, 168, 192} Results showed that no uptake on LDPE was observed for either analyte, while PS beads and PDMS fibers produced aniline K_{ENM-W} values that were at least 75% smaller than those measured for the best ENMs (**Figure 2-7**). Uptake of nitrobenzene was not measurable over our standard experimental timescale for any of the commercial materials, further highlighting the dearth of passive sampling materials currently available for some polar analytes outside of POCIS.

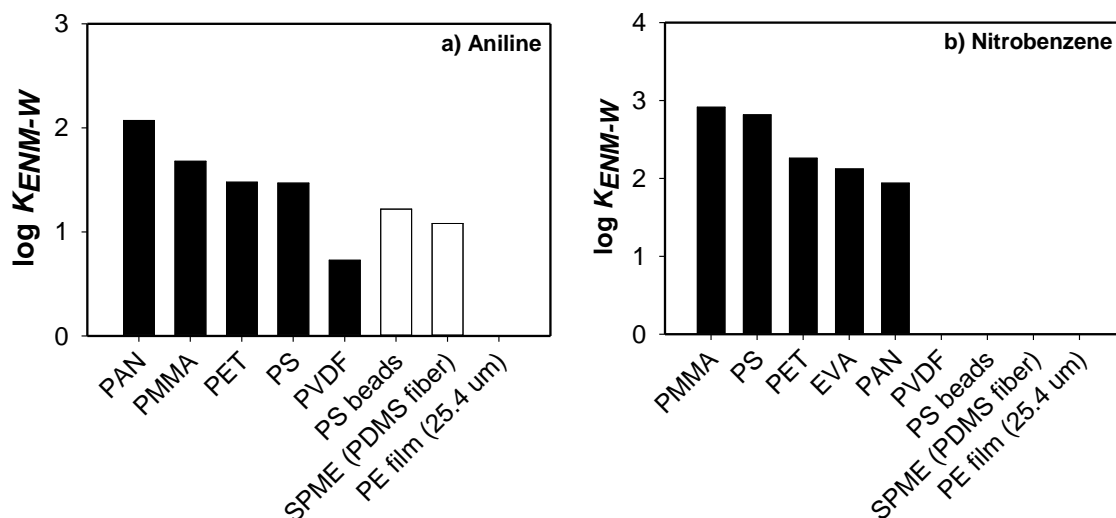
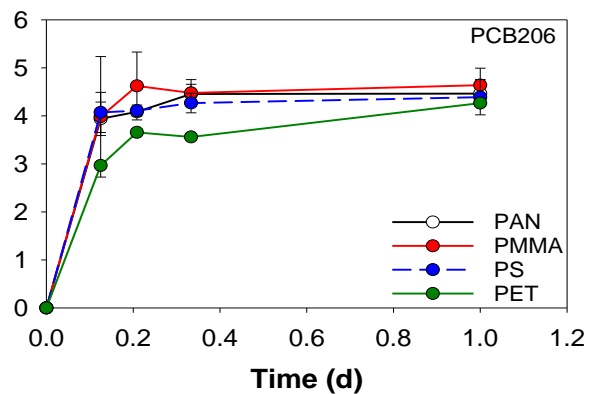
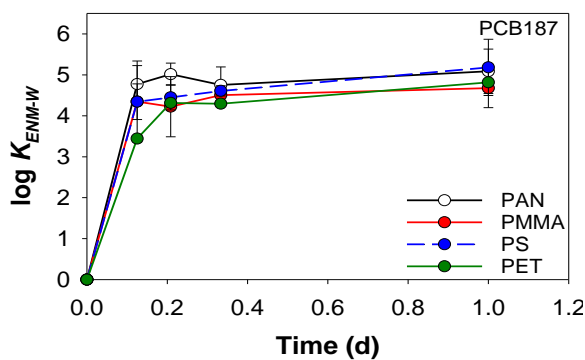
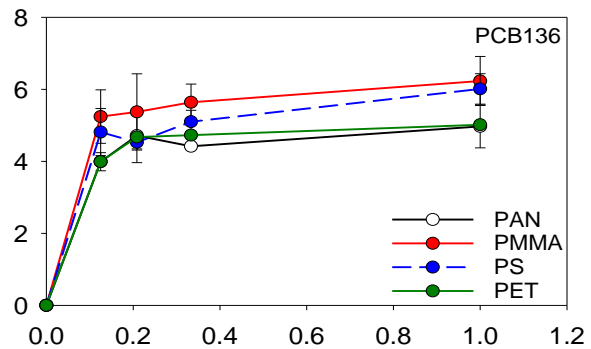
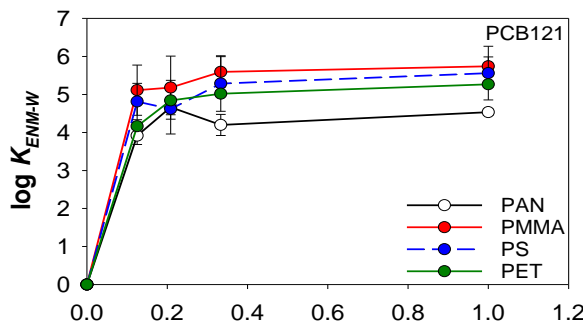
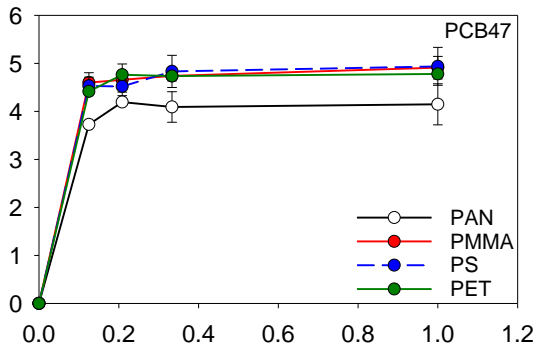
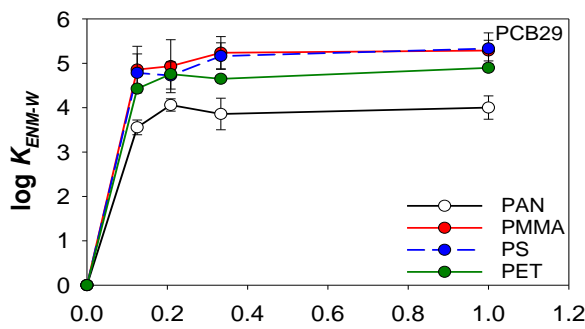
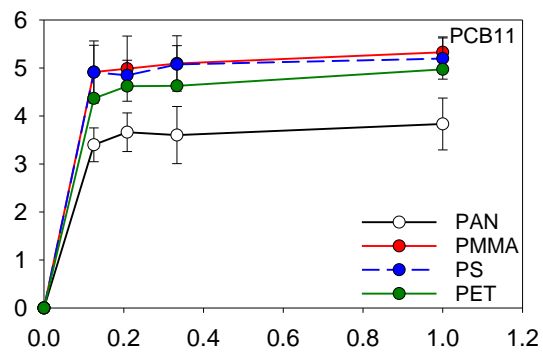
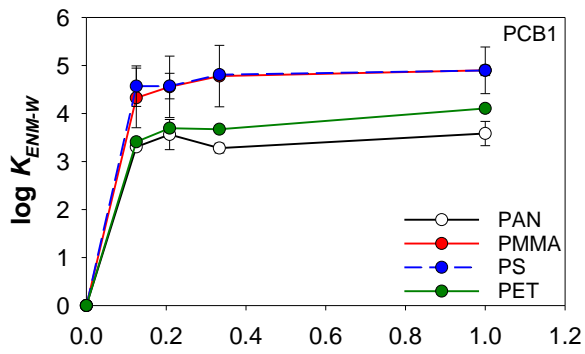


Figure 2-7. Comparison of measured equilibrium partition coefficients for (a) aniline and (b) nitrobenzene for all of the ENMs synthesized, and commercially available materials (PS beads, PDMS fiber and LDPE film). Laboratory set up: pH ~ 6.5 (DI water), initial concentrations of aniline: 2 mg/L and nitrobenzene: 3 mg/L, sorbent loading ~1.5 g/L, equilibration time 4 days.

PCBs and Dioxin. Because PVDF performed most poorly toward aniline and nitrobenzene and our goal was to identify materials suitable for passive samplers targeting chemicals with a broad range of $\log K_{OW}$ values, PVDF was not considered in studies with PCBs and dioxin. Once again, the remaining four ENMs exhibited relatively fast equilibration times (< 0.5 d) for both selected PCB congeners and dioxin under mixing conditions in the laboratory (**Figure 2-8**). Average K_{ENM-W} values from samples collected at 0.5 and 1 day ranged from 3.2 to 6.4 log units (L/kg) across the ENMs (**Figure 2-9, Table 2-5**), which are comparable to estimated partition coefficients previously reported for commercially available passive sampler materials (e.g., POM film, PDMS glass fiber and LDPE film).^{63, 194}



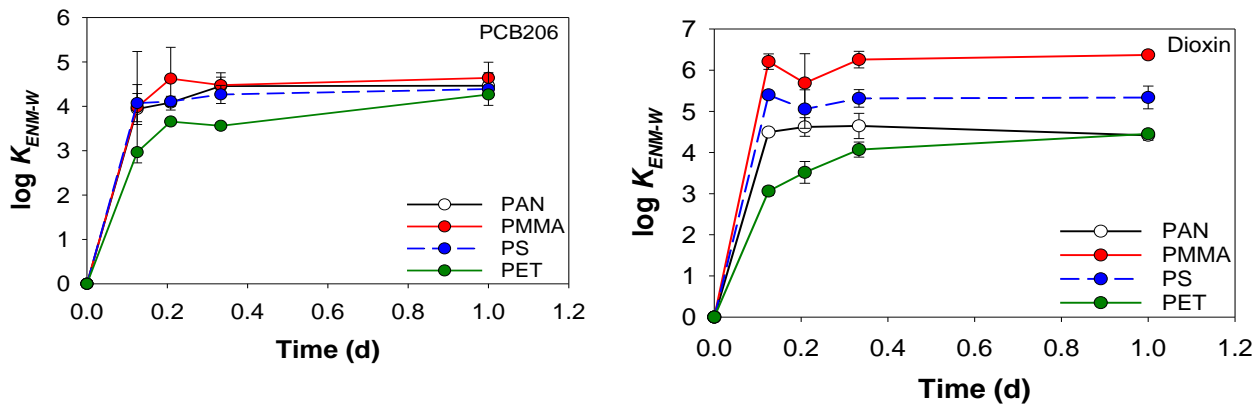


Figure 2-8. Uptake curves for selected PCB congeners and dioxin (TCCD) on ENMs. The error bars represent the standard deviation from two replicate uptake experiments. Laboratory set up: pH ~ 6.5 (DI water), initial concentrations from 0.25 to 5 ng/L, ENM loading ~ 3 g/L. Please note the difference in the y-axis scale. Lines simply connect data points.

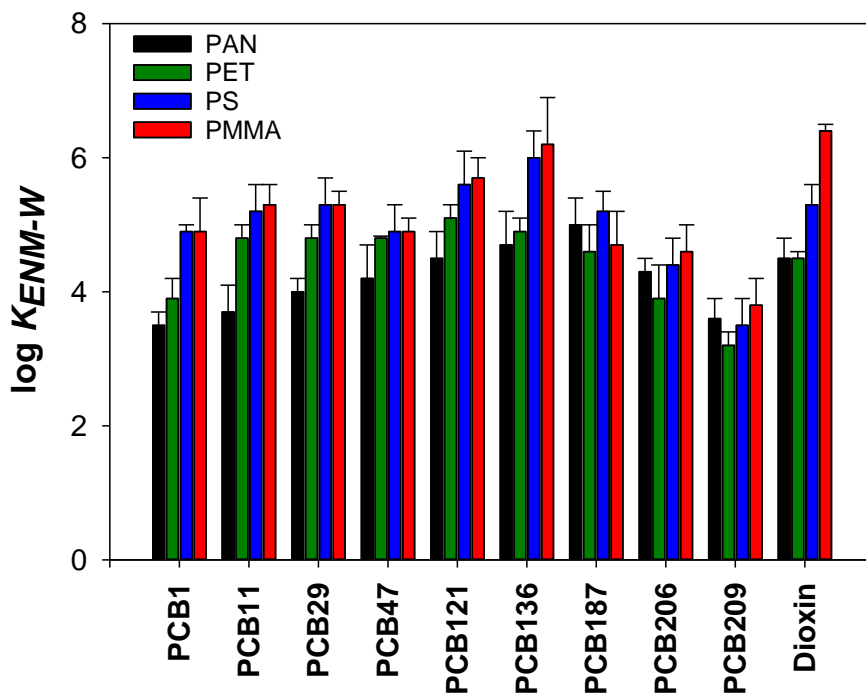


Figure 2-9. Average equilibrium partition coefficients in log units (L/kg) for PAN, PET, PMMA and PS for our model hydrophobic compounds. Uncertainties represent the standard deviation from at least two replicate experiments. Values are also shown in **Table 2-5**. Laboratory set up: pH ~ 6.5 (DI water), initial concentrations from 0.25 to 5 ng/L, ENM loading ~ 3 g/L.

Table 2-5. Summary of average measured ENM-water equilibrium partition coefficients for our hydrophobic model compounds (log units, L/kg) under mixing conditions. Values represent average from 0.5 to 1 day collection samples.

Compound	PAN	PMMA	PS	PET	PVDF
PCB1 (n=3)	3.5 ± 0.2	4.9 ± 0.5	4.9 ± 0.1	3.9 ± 0.3	n.m.
PCB11 (n=3)	3.7 ± 0.4	5.3 ± 0.3	5.2 ± 0.4	4.8 ± 0.2	n.m.
PCB29 (n=3)	4.0 ± 0.2	5.3 ± 0.2	5.3 ± 0.4	4.8 ± 0.2	n.m.
PCB47 (n=3)	4.2 ± 0.5	4.9 ± 0.2	4.9 ± 0.4	4.8 ± 0.03	n.m.
PCB121 (n=3)	4.5 ± 0.4	5.7 ± 0.3	5.6 ± 0.5	5.1 ± 0.2	n.m.
PCB136 (n=3)	4.7 ± 0.5	6.2 ± 0.7	6.0 ± 0.4	4.9 ± 0.2	n.m.
PCB187 (n=3)	5.0 ± 0.4	4.7 ± 0.5	5.2 ± 0.3	4.6 ± 0.4	n.m.
PCB206 (n=3)	4.3 ± 0.2	4.6 ± 0.4	4.4 ± 0.4	3.9 ± 0.5	n.m.
PCB209 (n=3)	3.6 ± 0.3	3.8 ± 0.4	3.5 ± 0.4	3.2 ± 0.2	n.m.
Dioxin (n=4)	4.5 ± 0.3	6.4 ± 0.1	5.3 ± 0.3	4.5 ± 0.1	n.m.

Unexpectedly, we observed a decrease in the K_{ENM-W} on all ENMs for highly chlorinated congeners (e.g., see results for PCBs 187, 206 and 209 in **Figure 2-9**). Others have also observed this phenomenon and several explanations have been proffered. These include insufficient time for the system to achieve equilibrium between phases, differences in the extraction processes and thickness of the sampling materials,^{195, 196} and physicochemical properties of materials and analytes,¹⁷⁰ while still others did not provide an explanation.¹⁹⁷ We speculate that the reduction in partition coefficients for these congeners may be due these highly hydrophobic congeners not completely dissolving into the aqueous solution, such that our reported K_{ENM-W} values may not actually reflect the extent of their partitioning into ENMs. Thus, these PCB congeners were removed from further analysis.

Generally, the overall trend in partitioning for PCBs and dioxin was as follows: PMMA ≈ PS > PET > PAN (**Figure 2-9, Table 2-5**). PAN yielded the lowest equilibrium partition coefficients, as might be expected for the uptake of strongly hydrophobic targets on

a hydrophilic substrate (**Table 2-3**). Conversely, more hydrophobic PMMA (water contact angle $\approx 120^\circ$) yielded the highest equilibrium partition coefficients. A significant correlation was found between the equilibrium partition coefficients and the water contact angle for PCB congeners 1 to 121 ($p < 0.05$), but no significant correlation was found for PCB136 nor dioxin ($p > 0.05$) (**Figure 2-10**). Further, no significant relationship existed between $\log K_{ENM-W}$ values and ENM surface area. For PCB congeners 1 to 136 and dioxin, positive correlations between $\log K_{ENM-W}$ and $\log K_{OW}$ ($p < 0.05$) were observed for each ENM (**Figure 2-11**). Thus, ENM hydrophobicity (as water contact angle) and/or compound K_{OW} values generally predict ENM performance toward PCBs and dioxin.

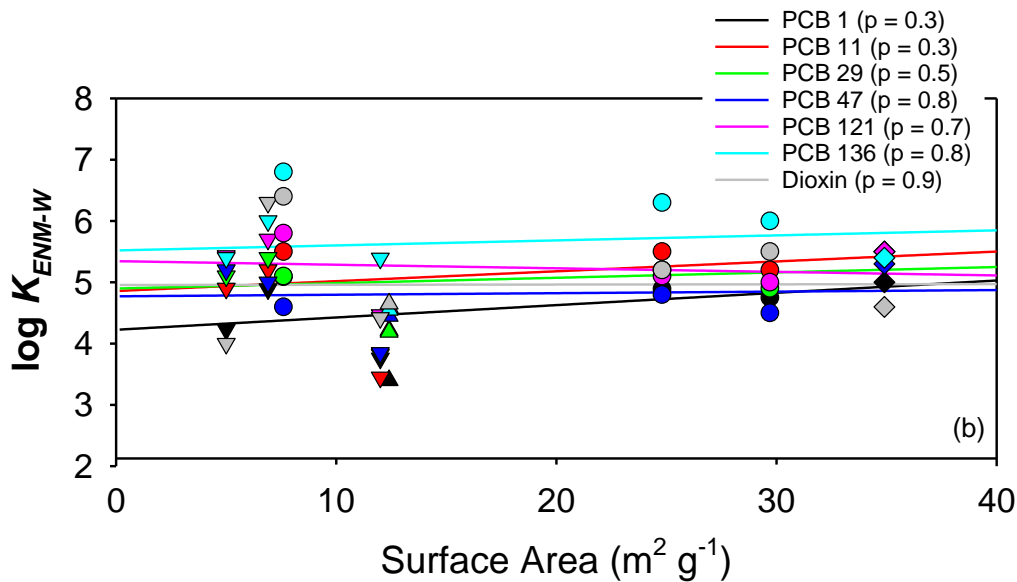
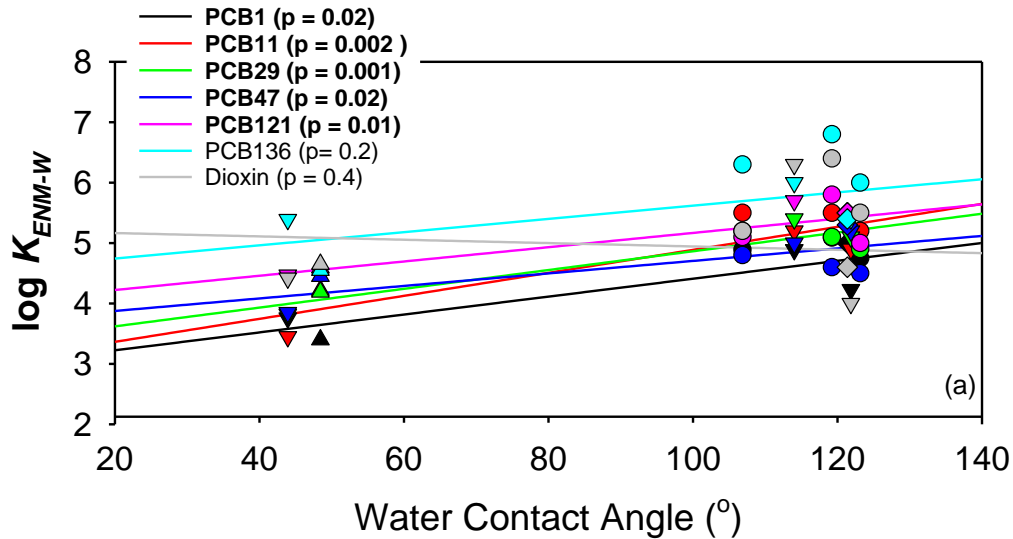


Figure 2-10. Linear regressions (black=PCB1, red=PCB11, green=PCB29, blue=PCB47, pink=PCB121, cyan=PCB136, grey=Dioxin) between equilibrium partition coefficients and (a) water contact angle and (b) surface area of ENMs. Data are shown for PAN (\blacktriangle), PMMA (\blacktriangledown), PS (\bullet), PVDF (\blacksquare) and PET (\blacklozenge). The p-values of the slopes from the regressions are shown as p. Significant is considered with a p-value < 0.05 , and are in bold.

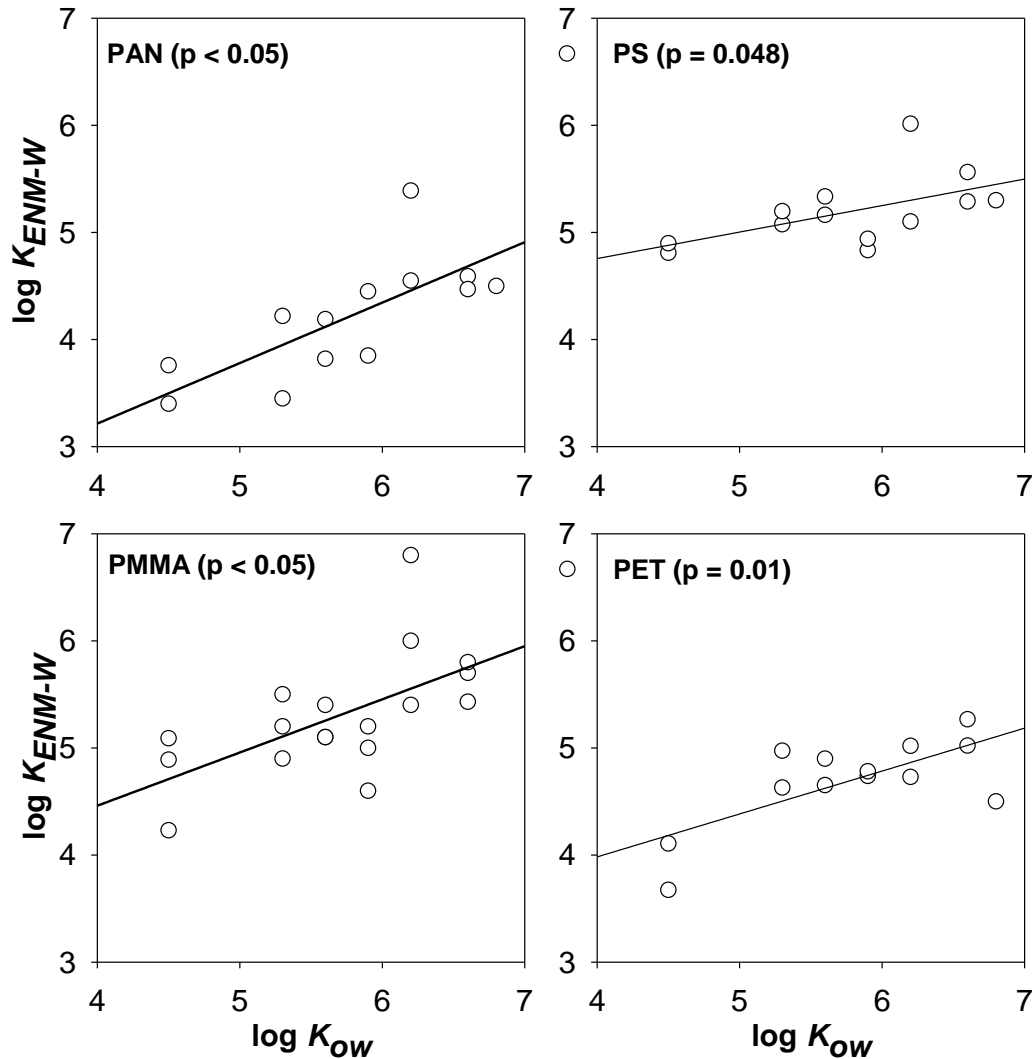


Figure 2-11. $\log K_{ow}$ versus $\log K_{ENM-W}$ for selected PCB congeners (PCBs 1, 11, 29, 47, 121 and 136) and dioxin in PAN, PS, PMMA and PET. The p-value in parenthesis corresponds to the linear regression.

Modeling Uptake Rates and Timescales for Model Compounds into ENMs

Because of rapid PCB and dioxin uptake (i.e., equilibrium was generally achieved during the first two sampling periods), we elected to focus our efforts to model analyte uptake to our polar model compounds, nitrobenzene and aniline. Time-dependent experimental C_w and C_{ENM} data, and resulting equilibrium partition coefficients, were well-described by the one

compartment, first-order kinetic model (Equation 2-2; see **Figure 2-12**), as others have also observed for passive sampler materials.^{170, 178, 198} Accordingly, using model outputs for k_2 we calculated $t_{90\%}$ values for the 5 ENMs, with estimates ranging from 0.01 ± 0.01 to 7.3 ± 1.2 days for aniline and nitrobenzene under mixing conditions in the laboratory (**Table 2-4**).

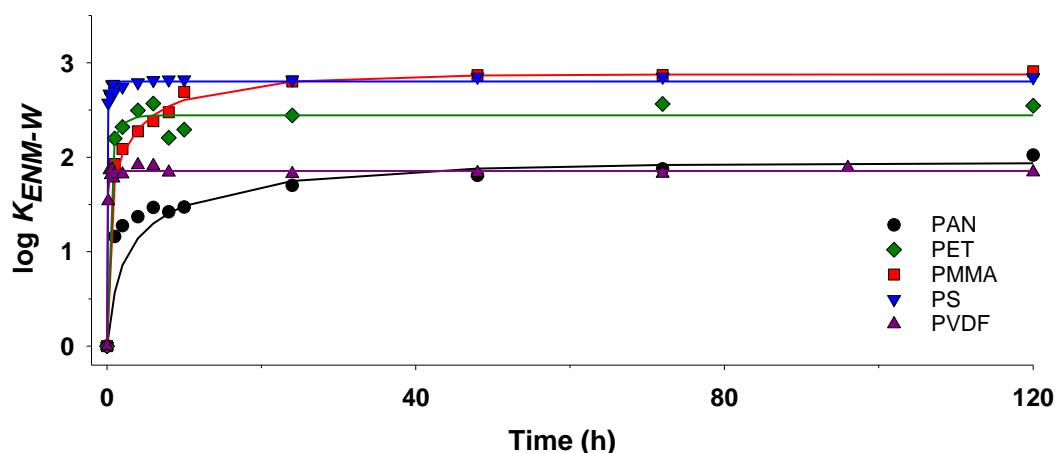


Figure 2-12. Uptake profile of nitrobenzene into PAN, PET, PMMA, PS and PVDF under mixing conditions. K_{ENM-W} values are the average of at least 3 replicates. The curves show the non-linear least squares regression from the one compartment first-order kinetic model. Laboratory set up: pH ~ 6.5 (DI water), initial concentrations of aniline: 2 mg/L and nitrobenzene: 3 mg/L, ENM loading ~1.5 g/L. K_{ENM-W} values are also presented in **Figure 2-5b**.

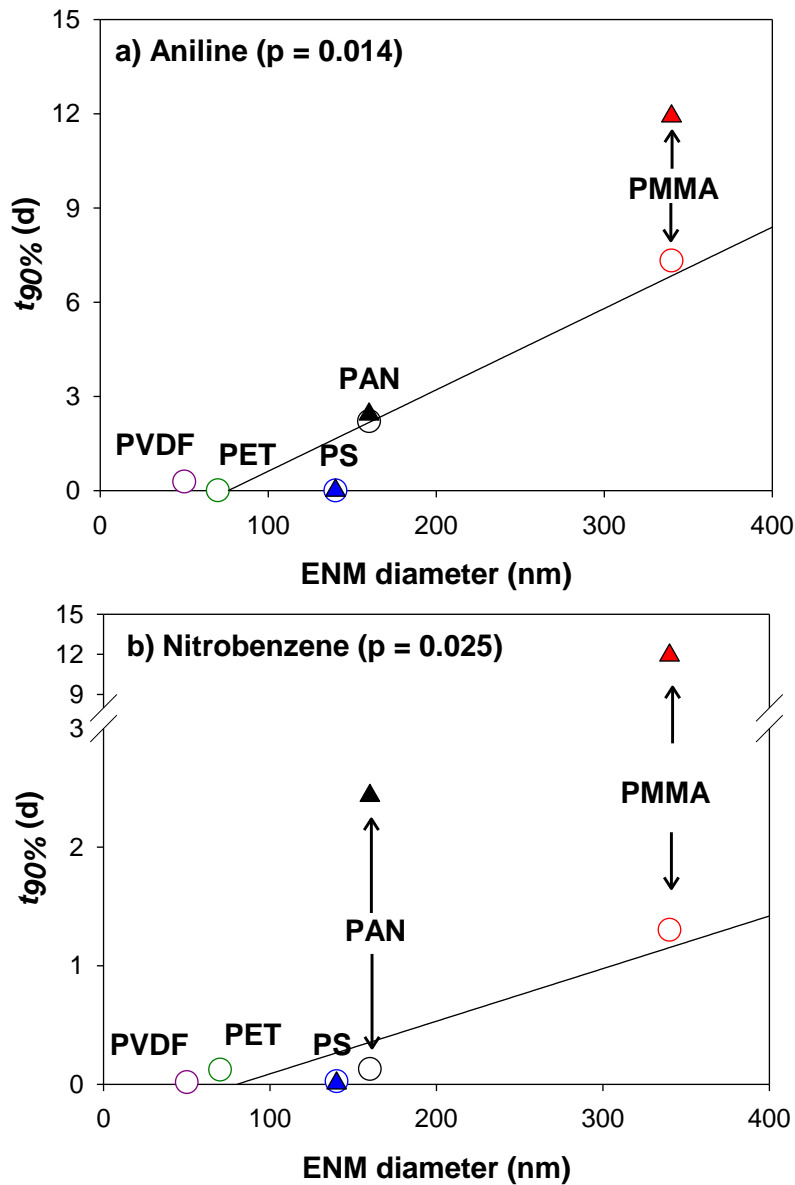


Figure 2-13. Time to reach 90% equilibrium ($t_{90\%}$) for (a) aniline and (b) nitrobenzene versus nanofiber diameter of our ENMs. Void circles correspond to mixing experiments, while black triangles are under static conditions. $t_{90\%}$ was calculated from Equation 2-3, and the nanofiber diameters are shown in **Table 2-3**. Line represents the linear regression from the mixing experiments (void circles). See the y-axis break in b).

The longer time to achieve equilibrium for PMMA ($t_{90\%} = 1.2 \pm 0.06$ and 7.3 ± 1.2 days for nitrobenzene and aniline, respectively) is likely related to its larger diameter compared to other ENMs such as PAN and PS (**Table 2-3**). Indeed, we observed a positive correlation ($p < 0.025$) between $t_{90\%}$ and nanofiber diameter for both aniline and nitrobenzene across the suite of ENMs investigated (**Figure 2-13**). Such a relationship implies that thinner nanofibers can produce faster uptake rates and in turn will require less time to reach equilibrium in the field, consistent with conventional wisdom that a higher SA/V (or in this case $2/r$) ratio corresponds to a faster sampling device.^{178, 179, 199} Notably, there was no relationship between $t_{90\%}$ and K_{ENM-W} , suggesting that faster uptake rates do not negatively impact ENM sorption capacity.

Additional uptake experiments were conducted using PAN, PMMA and PS without mixing (i.e., static conditions). These systems, intended to mimic passive sampling conditions in the field, resulted in nearly equivalent K_{ENM-W} values when compared to results from well-mixed systems, and time-dependent uptake once again followed the one compartment, first-order model (Equation 2-2, **Table 2-4**). Because no change in the sorption capacity was observed between mixing and static conditions, we conclude that changes in the uptake kinetics do not affect ENM sorption capacity (**Table 2-4**).

Changes in $t_{90\%}$ values between mixed and unmixed systems lend insight into the rate-determine steps in analyte sorption on ENMs. For example, PMMA exhibited longer equilibrium times in unmixed ($t_{90\%} = 12 \pm 0.6$ and 4.5 ± 0.6 days for aniline and

nitrobenzene, respectively) relative to mixed systems, presumably due to its larger nanofiber diameter or smaller SA/V ratio. (**Figure 2-13**). This increase is consistent with diffusion across the aqueous boundary layer being rate-limiting in analyte uptake. In contrast, little to no change in $t_{90\%}$ values was observed for either nitrobenzene or aniline on PS in mixed and unmixed systems, suggesting that uptake is mostly controlled by diffusion into the nanofiber. PAN produced a mixed result, where uptake rates of aniline were the same with and without mixing, while $t_{90\%}$ values for nitrobenzene increased significantly in static relative to well-mixed systems. Thus, rate controls for PAN appear analyte dependent. We note that water boundary rate-limiting uptake into LDPE strips has been reported for hydrophobic compounds ($\log K_{OW} > 4.5$) under low flow conditions.²⁰⁰⁻²⁰²

Influence of Nanofiber Diameter on ENM Performance. To further evaluate the effect of nanofiber diameter on uptake rates, we fabricated two larger diameter variations of PS ENMs (with average diameters of 300 and 560 nm) and compared their performance toward nitrobenzene under static conditions with that of our standard 140 nm diameter PS ENM (**Figure 2-14**). Measured K_{ENM-W} values were invariant across all nanofiber diameters (**Table 2-6**). Although we cannot directly compare our ENM with plastic sheets as passive sampler materials, this independence of equilibrium partition coefficient with respect to material thickness has also been demonstrated for PE.²⁰³

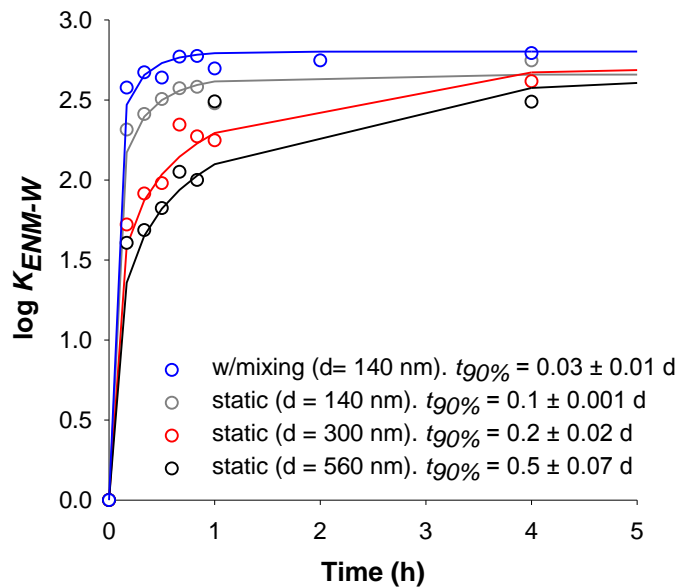


Figure 2-14. Nitrobenzene uptake into PS as a function of nanofiber diameter. Data are shown for PS with 140, 300 and 560 nm, and uptake experiments were conducted statically (without mixing). For comparison, data for the 140 nm (our standard PS recipe) are also shown from experimental systems were actively mixed. $t_{90\%}$ s were calculated from the non-linear least squares regressions (**Table 2-6**). The curves show the non-linear least squares regression from the one compartment first-order kinetic model. Laboratory set up: pH ~ 6.5 (DI water), initial concentrations of nitrobenzene: 3 ng/L, ENM loading ~ 1.5 g/L.

Table 2-6. Comparison of measured and predicted ENM-water equilibrium partition coefficients for nitrobenzene (log units, L/kg) for different diameter size of PS under no mixing conditions.

Nanofiber Diameter (nm)	Log K_{ENM-W} (L/kg)		$t_{90\%}$ (d)
	Measured	Model	
140 ^a	2.8 ± 0.01	2.8 ± 0.01	0.03 ± 0.01
140	2.9 ± 0.09	2.8 ± 0.02	0.1 ± 0.01
300	2.7 ± 0.1	2.8 ± 0.01	0.2 ± 0.02
560	2.8 ± 0.1	2.8 ± 0.01	0.5 ± 0.07

^a Experiments performed under mixing conditions (**Table 2-4**).

A decrease in uptake kinetics was observed with increasing nanofiber diameter.

Utilizing Equations 2-2 and 2-3, values of $t_{90\%}$ increased from 0.03 ± 0.01 to 0.5 ± 0.07 days with an increase in diameter from 140 to 560 nm. Recall, for 140 nm nanofibers, $t_{90\%}$ values

were equivalent in mixed and unmixed systems. For PS ENMs, therefore, these diameter-dependent uptake data may suggest a shift in the rate determining step from solid-phase to aqueous-phase diffusion above some critical nanofiber diameter. Nevertheless, this behavior is consistent with the established relationship between the uptake rate and the surface area-to-volume (SA/V values) ratio of the sampling device,¹⁷⁹ where a high SA/V ratio results in a faster diffusive exchange between both phases.¹⁷⁸

Collectively, these results illustrate the promise of electrospinning for tailoring the fabrication of a sampling device with short equilibration times without diminishing overall (per unit mass) sorption capacity, as the same K_{ENM-W} values were obtained for all PS nanofiber diameters explored (**Figure 2-14**). Moreover, these relative short equilibration times, even for the static experiments, strongly suggest that our ENMs can be deployed as equilibrium-passive samplers in the field and over timescales considerably shorter than the 20 to 40-day sampling periods typically utilized for water and sediment pore water passive samplers.

Influence of System on the Performance of Optimal ENMs. From the experiments with model compounds, PAN, PMMA and PS were selected as the most promising material for further development as passive sampling materials. PMMA and PS yielded the highest K_{ENM-W} values toward our model compounds, on average 2.2 ± 0.7 log units (**Table 2-4**). PAN was also included, in part because it showed a slightly better performance toward

aniline than the rest of the ENMs, but also due to how commonly it is used for electrospinning and its ease of fabrication.²⁰⁴

Influence of pH on ENM Performance. We found that K_{ENM-W} were generally independent of pH for both aniline (i.e., anilinium cation) and nitrobenzene (**Figure 2-15**) We specifically tested the effect of pH on the sorption capacity on PMMA and PS because preliminary sorption experiments indicated that both ENMs yielded, in general, the highest K_{ENM-W} values for these two compounds. While further work is merited, a slight pH dependence observed for aniline at low pH may reflect different modes of uptake on PMMA and PS. For example, PMMA exhibited more uptake at lower pH values, where a greater fraction of the aniline mass is positively charged (roughly ~20% of total aniline mass is positively charged at pH 5.5. $pK_a = 4.9$). Meanwhile, aniline uptake is essentially independent across pH on PS, but notably lower than on PMMA. We propose that the greater net uptake of aniline on PMMA, as well as the slight pH-dependence in partition coefficients in more acidic regimes, reflects a favorable role for electrostatic or specific binding interactions in uptake. In contrast, uptake of aniline on PS may be limited to only hydrophobic exclusion (presumably localized to the aromatic ring of aniline) and nonspecific interactions (e.g., van der Waals), the driving force for which would be independent of pH.

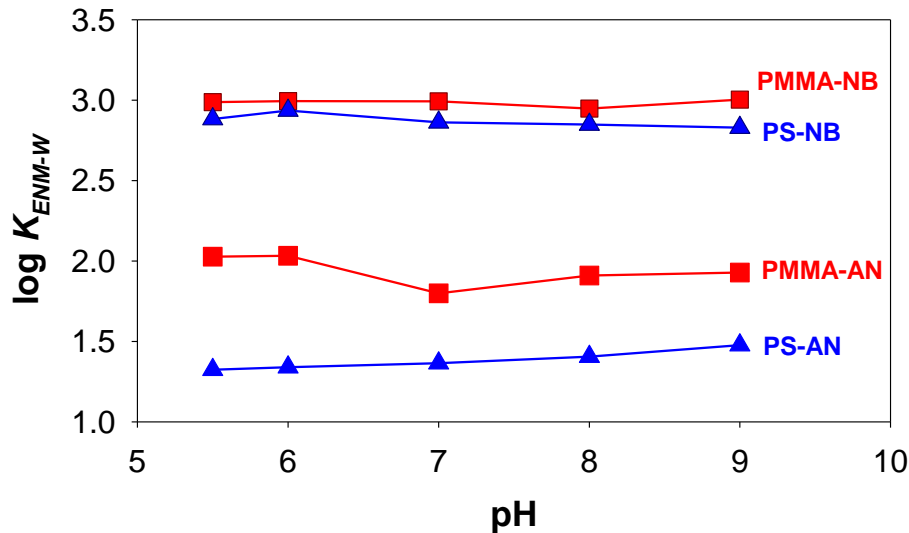


Figure 2-15. ENM-water equilibrium partition coefficients (L/kg) for aniline (AN) and nitrobenzene (NB) measured as a function of solution pH for PMMA and PS. Laboratory set up: initial aniline and nitrobenzene concentrations 2 mg/L and 3 mg/L, respectively, ENM loading ~1.5 g/L. Experiments were performed for 5 days. pH was controlled using commercially available buffers (MES, HEPES, AMPSO and BioXtra).

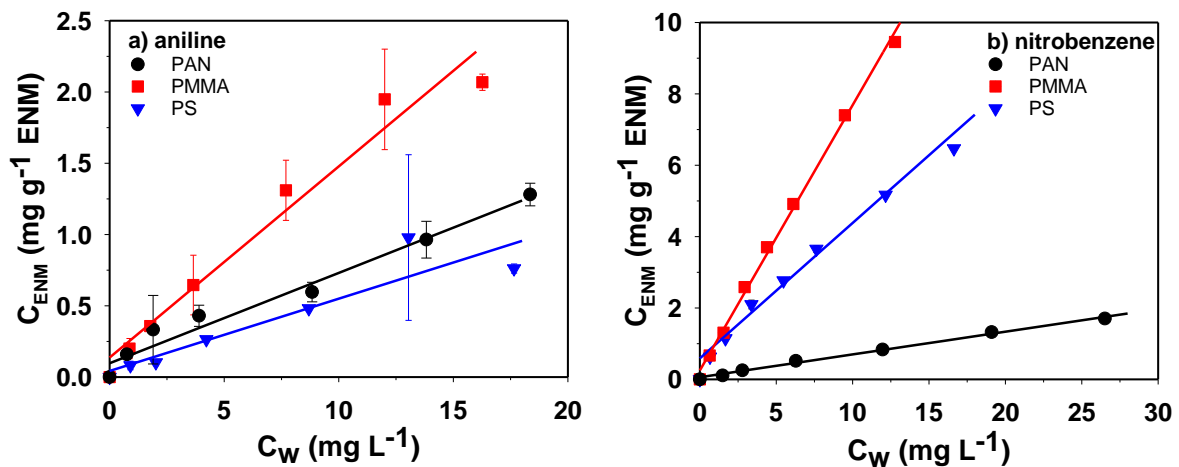


Figure 2-16. Sorption isotherms using PAN, PMMA and PS for (a) aniline and (b) nitrobenzene. All linear regressions are statistically significant ($p > 0.001$). Calculated K_{ENM-W} values from the slopes are presented in **Table 2-4**. Initial aqueous concentrations for aniline were 1 - 20 mg/L and nitrobenzene were 1 - 29 mg/L. Uncertainties represent the standard deviation from two replicate uptake experiments. When no uncertainty is visible, the bars are smaller than the data symbol.

Sorption Isotherms to Establish ENM Capacity. Isotherm experiments using PAN, PMMA and PS with aniline and nitrobenzene assessed whether ENM application at environmentally relevant concentrations would be limited by their uptake capacity. Linear sorption isotherms were obtained for aniline and nitrobenzene on all ENMs (**Figure 2-16**), allowing ENM-water equilibrium partition coefficients to be calculated from linear regression analyses of the isotherm slope. This value was comparable to those calculated at each sampling point during aforementioned time-dependent uptake experiments (**Table 2-4**).

Isotherm results indicate that ENMs operate in a linear uptake regime, where K_{ENM-W} values are independent of the aqueous concentration, up to ~25 mg/L (for our model compounds). This linear concentration range far exceeds concentrations likely to be encountered at contaminated sites where ENMs would be deployed. Thus, during field deployment, partitioning of polar targets should scale linearly with the dissolved concentration in surface or sediment pore water and not be subject to a saturation regime that would complicate accurate analysis of field concentrations. Moreover, this behavior suggests aniline and nitrobenzene uptake occurs primarily via absorption (i.e., bulk uptake into nanofibers rather than surface adsorption-limited). Indeed, we found no significant correlation ($p \geq 0.1$) between K_{ENM-W} values and ENM surface area (**Figure 2-6** and **Figure 2-10**), as might be expected for an adsorptive process.

Freely-Dissolved Pore Water Measurements in Soil and Sediment Systems. Pore water nitrobenzene concentrations in spiked soils using PMMA and PS are shown in **Figure**

2-17a. The pore water concentration was calculated using the mass of the chemical accumulated in the ENM (m_i), the mass of the ENM used in the experiment (m_{ENM}), and the K_{ENM-W} values measured in our aqueous-phase uptake experiments (**Table 2-4**) according to Equation 2-4.

$$C_{Pwi} = m_i / m_{ENM} \times K_{ENM-w} \quad (2-4)$$

Both ENMs achieved rapid equilibrium with pore water nitrobenzene (~ 1 day), as we have previously demonstrated in aqueous systems. Effectively, PMMA and PS were equivalent in their performance, with equilibrium pore water concentrations ranging between 1.7 and 2.9 mg/L for these samples. However, an important practical distinction is that PS was far more resistant to fouling from organic matter in these sterilized soil systems. After 5 d of mixing with soil, PS was considerably easier to clean of debris and wash than PMMA (**Figure 2-18**). For example, after a gentle mechanical cleaning with a paper towel and a light rinse with a small volume of DI water [for which loss of nitrobenzene was minimal (< 5%)], the PS was nearly the same color as when freshly synthesized. SEM images of the rinsed PS also revealed no residual soil particles or organic residues (**Figure 2-18**). In contrast, PMMA remained covered in soil and organic particles that were observable to the naked eye. More aggressive washing necessary to clean PMMA possible led to loss of compounds in the wash water, which we believe contributed to the slightly greater relative standard deviation (RSD) of the pore water concentration for PMMA (~20%) relative to PS (~10%).

With anthropogenically impacted sediment from the IHSC, 28 d experiments with

PMMA and PS revealed the occurrence of many individual PCB congeners based on detection with gas chromatography. However, here we report only the congeners for which we had already measured equilibrium partition coefficients (**Table 2-5**). Sediment pore water concentrations (from Equation 2-4) for our nine PCB congeners (PCB1, 11, 29, 47, 121, 136, 187, 206 and 209) ranged from 0.2 to 230 ng/L. It is most probable that the calculated concentrations of PCBs 187, 206 and 209 are overestimated due to our low equilibrium partition coefficients obtained for those three congeners. Both PMMA and PS performed similarly, with no significant difference observed between their measured sediment pore water concentrations (**Figure 2-17b**), although PS was once again easier to clean than PMMA. Further, these individual PCB concentrations are within the range and follow the same trend among congeners for published sediment pore water concentrations for the same IHSC sediment but using PDMS fiber (range from 0.4 to 60 ng/L).¹⁶⁷ Further, PMMA and PS proved to be more sensitive than PDMS fiber; while it was possible to detect PCBs 206 and 209 on ENMs, these congeners were not amenable to analysis via PDMS fiber.

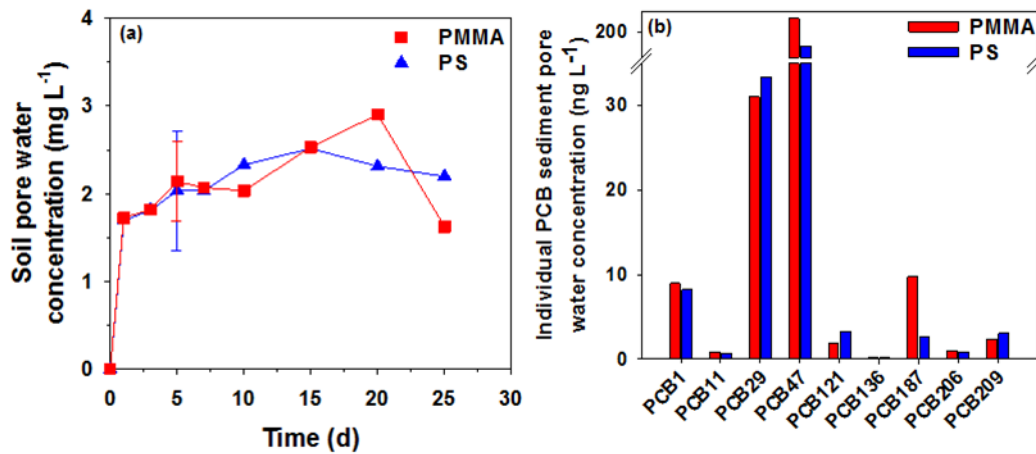
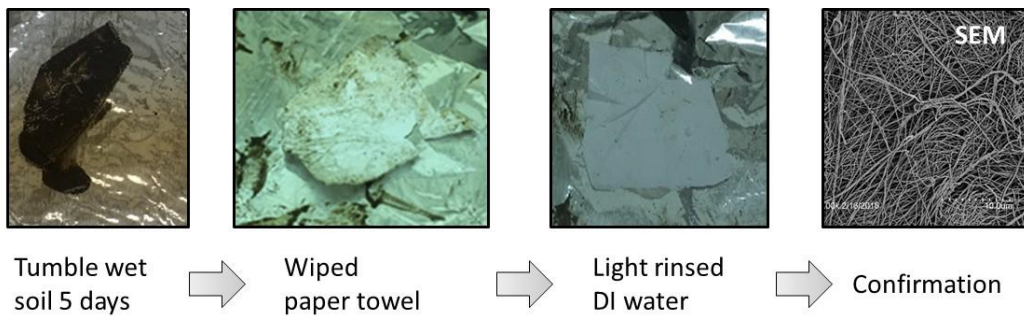


Figure 2-17. Measurements in heterogeneous systems of (a) nitrobenzene pore water concentrations versus time in systems with a model spiked soil, and (b) individual PCB sediment pore water concentrations from IHSC sediment, both using PMMA and PS. IHSC measurements were carried out for 28 days. Error bars represent the standard deviation from two replicate uptake experiments. Lines simply connect data points.

PS



PMMA



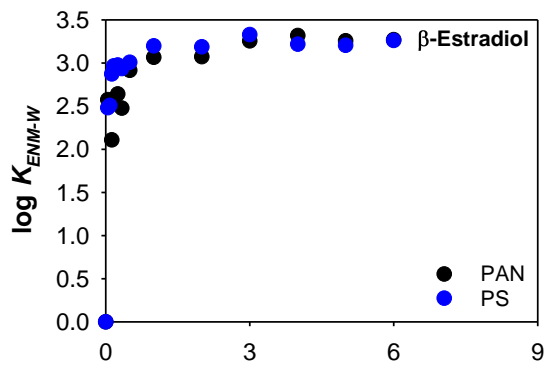
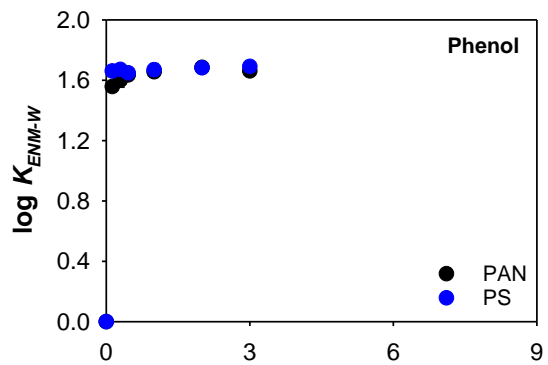
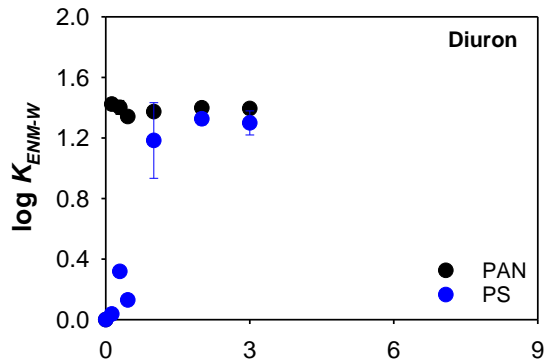
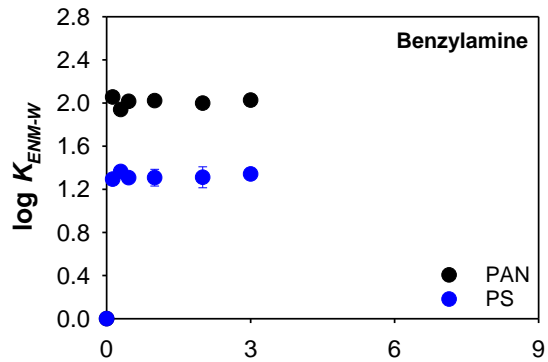
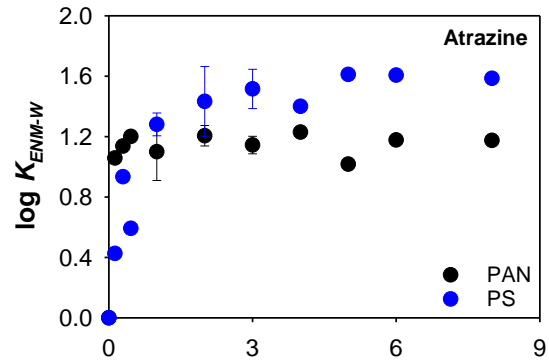
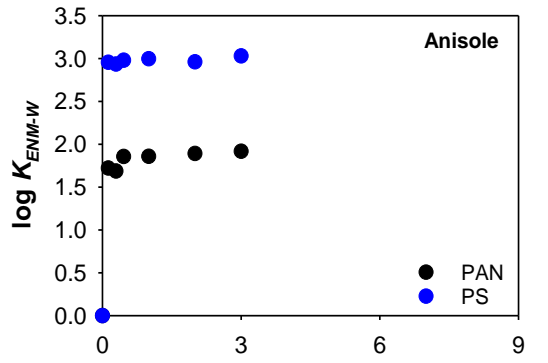
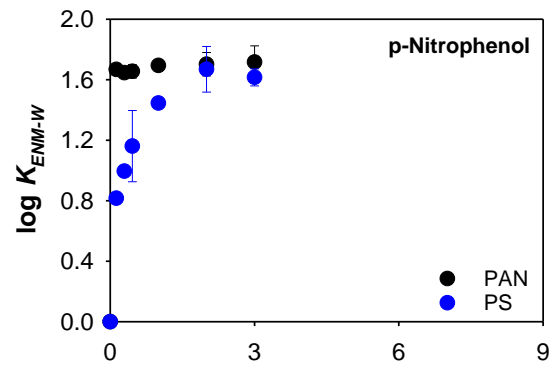
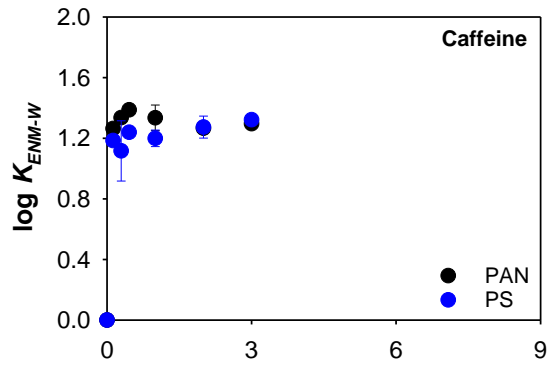
Figure 2-18. Photograph sequence of cleaning for PS (top) and PMMA (bottom) after being exposed to model soils for 5 days. SEM image confirmation was not possible to perform to PMMA due to the amount of soil/organic particles attached to it.

Uptake of Hydrophilic and Moderately Hydrophobic Compounds. As a final test of our ENMs, uptake experiments under mixing conditions with ten additional hydrophilic and moderately hydrophobic compounds on PAN and PS were performed. Concentration profiles (**Figure 2-19**) revealed fast uptake, as described before with our model compounds. In general, equilibrium partition coefficients were measured from samples collected after 1 day. Most $\log K_{ENM-W}$ values were similar to those measured for aniline and nitrobenzene, with an average of 2.0 ± 0.7 log units. Larger values (i.e., > 2.7 log units) were occasionally observed; this was the case for 17β -estradiol on both PAN and PS, as well as for TNT and anisole on PS (**Table 2-7, Figure 2-19**).

Table 2-7. Summary of average and model ENM-water equilibrium partition coefficients and $t_{90\%}$ s for the 10 hydrophilic and moderately hydrophobic compounds with PAN and PS ENMs (log units, L/kg) under mixing conditions.

Analytes	PAN			PS		
	Log K_{ENM-W} (L/kg)		$t_{90\%}$	Log K_{ENM-W} (L/kg)		$t_{90\%}$
	Measured	Model	(day)	Measured	Model	(day)
Aniline (n =10)	1.9 ± 0.06	1.9 ± 0.04	2.2 ± 0.4	1.5 ± 0.03	1.5 ± 0.01	0.01 ± 0.01
Anisole (n=6)	1.9 ± 0.04	1.9 ± 0.01	0.4 ± 0.12	3.1 ± 0.05	3.0 ± 0.02	0.1 ± 0.1
Atrazine (n=4)	1.2 ± 0.1 ^a	1.1 ± 0.01	0.01 ± 0.01	1.6 ± 0.01	1.6 ± 0.01	4.2 ± 0.3
Benzylamine (n=6)	2.0 ± 0.03	2.0 ± 0.01	0.01 ± 0.01	1.3 ± 0.06	1.3 ± 0.01	0.1 ± 0.02
β -Estradiol (n=6)	3.2 ± 0.2	3.4 ± 0.02	1.1 ± 0.1	3.2 ± 0.1	3.2 ± 0.01	0.2 ± 0.1
Caffeine (n=6)	1.3 ± 0.05 ^a	1.3 ± 0.02	0.1 ± 0.03	1.3 ± 0.07 ^a	1.2 ± 0.02	0.11 ± 0.13
Diuron (n=6)	1.4 ± 0.02 ^a	1.4 ± 0.01	0.01 ± 0.01	1.3 ± 0.1 ^a	1.4 ± 0.1	3.1 ± 1.8
Nitrobenzene (n = 10)	1.9 ± 0.1	1.9 ± 0.01	0.1 ± 0.03	2.8 ± 0.01	2.8 ± 0.01	0.03 ± 0.01
Phenol (n=6)	1.7 ± 0.02 ^a	1.6 ± 0.01	0.2 ± 0.07	1.7 ± 0.03 ^a	1.7 ± 0.01	0.1 ± 0.05
p-Nitrophenol (n=6)	1.7 ± 0.06	1.8 ± 0.01	0.1 ± 0.1	1.6 ± 0.1	1.7 ± 0.1	2.5 ± 1.3
RDX (n=6)	1.8 ± 0.03 ^a	1.9 ± 0.01	0.1 ± 0.01	1.8 ± 0.1 ^a	1.8 ± 0.01	0.2 ± 0.04
TNT (n=6)	1.9 ± 0.03	1.9 ± 0.01	0.2 ± 0.1	2.8 ± 0.01	2.7 ± 0.02	1.5 ± 0.2

^aLess than 5% of the total aqueous mass was sorbed to the ENM.



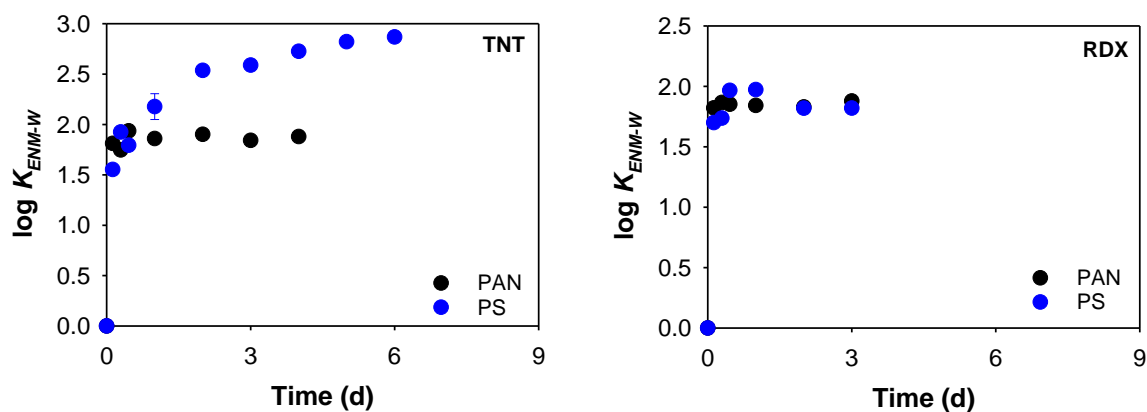


Figure 2-19. PS and PAN uptake curves for our ten hydrophilic and moderately hydrophobic compounds. The error bars represent the standard deviation from two replicate uptake experiments. Laboratory set up: pH ~ 6.5 (DI water), initial concentrations from 2.4 to 6.8 mg/L, ENM loading ~ 1.5 g/L. Please note the difference in the y-axis scale.

Again, hydrophilic and moderately hydrophobic compound uptake into PAN and PS was well-described by the one compartment, first-order kinetic model. Calculated values of $t_{90\%}$ ranged from 0.01 ± 0.01 to 4.2 ± 0.3 days, consistent with PAN and PS exhibiting relatively short equilibration times with the suite of analytes tested. We note that uptake rates, and consequently $t_{90\%}$ values, for some analytes depended on the ENM tested. For example, anisole uptake occurred 3-fold faster on PS than on PAN, whereas p-nitrophenol uptake was 30 times faster on PAN than PS. Interestingly, for these two analytes the ENM with the higher K_{ENM-W} value also exhibited the faster uptake rate, a scenario ideal for the development of an equilibrium-passive sampler. This was not always the case, however. For example, TNT uptake was faster on PAN, but PS produced the greater sorption capacity. Nevertheless, results with this analyte suite reveal the potential for producing not only a fast, but also a high capacity equilibrium-passive sampling device from polymeric ENMs.

Reasonably strong correlations ($R^2 \geq 0.83$ and $p < 0.05$) were obtained when the equilibrium partition coefficients of all investigated analytes (except PCB187, 206 and 209) were plotted as a function of K_{OW} , hexadecane-water ($K_{hexadecane-w}$)²⁰⁵ partition coefficient, and the dissolution constant (D),¹⁷⁶ as shown in **Figure 2-20**. $K_{hexadecane-w}$ has been suggested by others to better predict equilibrium partition coefficients of moderately and hydrophobic compounds into sorbent materials,^{76, 206} and D expresses the distribution of both the neutral and the ionic fraction of the analyte between the K_{OW} for the basic analyte and for the acidic analyte.¹⁷⁶

The dissociation constant (D) calculations were obtained from the following expressions,¹⁷⁶ and used in **Figure 2-20**.

$$D_{Base} = \frac{K_{OW}}{(1+10^{pKa-pH})} \quad (2-5)$$

$$D_{Acid} = \frac{K_{OW}}{(1+10^{pH-pKa})} \quad (2-6)$$

We note that $\log K_{ENW-W}$ values for our moderately hydrophobic compounds on PAN were relatively insensitive to these descriptors, whereas PS seemed to show a better correlation across all of the analytes tested and the descriptors used. This suggests that PAN may be most promising for rather constant performance across a range of polar targets, while classical paradigms for hydrophobic partitioning may govern uptake capacity on PS. Nevertheless, this correlation analysis suggests that it may be possible to estimate with a low

degree of uncertainty the equilibrium partition coefficients on PAN and PS for a diverse type of analytes using these chemical properties.

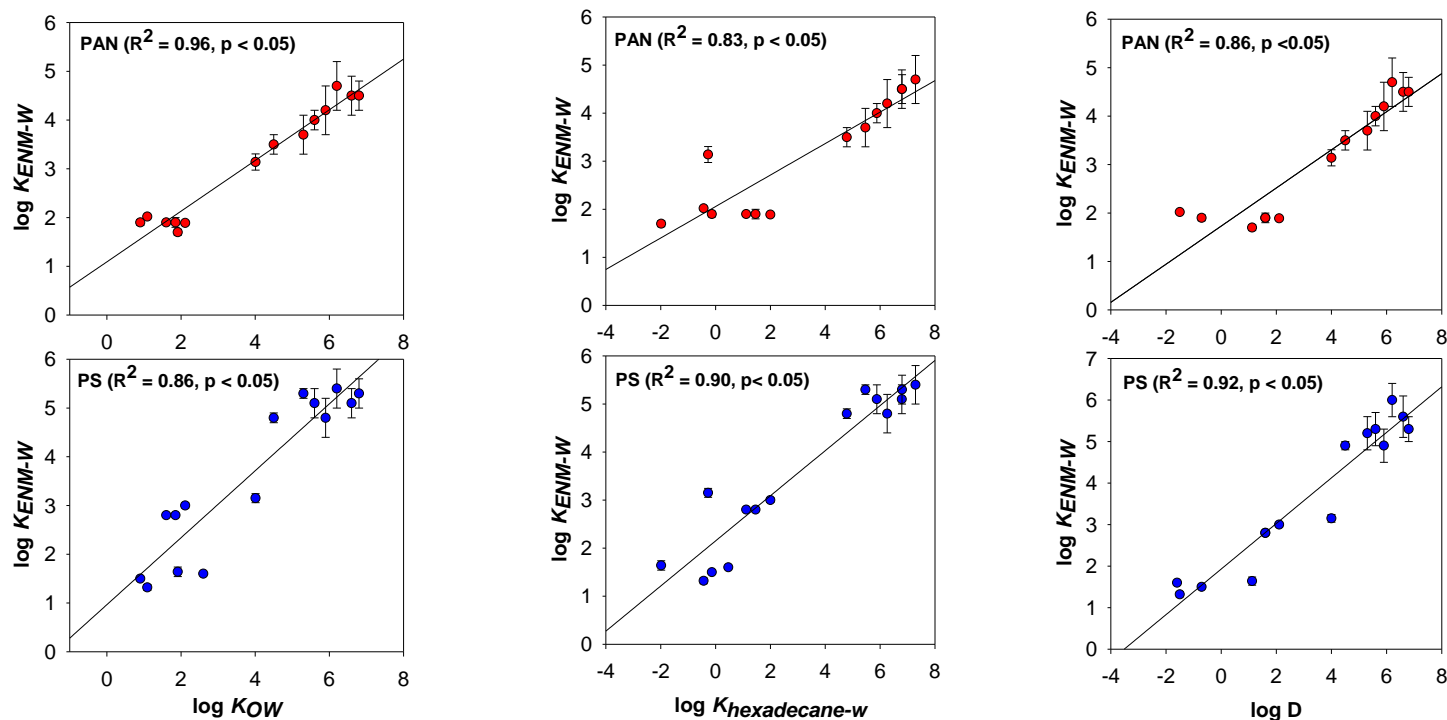


Figure 2-20. Average equilibrium partition coefficients of PAN (top panels) and PS (bottom panels) versus octanol-water (K_{OW}) and hexadecane-water ($K_{hexadecane-w}$)²⁰⁵ partition coefficients, and dissolution constant (D)¹⁷⁶ for our hydrophilic and moderately hydrophobic and hydrophobic analyte suite. When no error bar is visible, the bars are smaller than the data symbol. Uncertainties represent the standard deviation from at least two replicate experiments. Compounds with uptake into ENMs of less than 5% of the total available mass were not included in the regression (**Table 2-7.** Summary of average and model ENM-water equilibrium partition coefficients and $t_{90\%s}$ for the 10 hydrophilic and moderately hydrophobic compounds with PAN and PS ENMs (log units, L/kg) under mixing conditions.), as well as PCBs 187, 206, and 209 due to their uncertainty in the measured equilibrium partition coefficients.

2.5 CONCLUSIONS AND ENVIRONMENTAL IMPLICATIONS

Electrospun nanofiber mats (ENMs) provide a promising sorbent for passive sampling materials targeting organic contaminants in water and sediment environments. ENMs possess nanoscale features, but also exist as a robust bulk, macroscopic material. Their tunable nanofiber properties (e.g., diameter and surface area) make them ideal for applications that rely on uptake rate and pollutant partitioning. High surface area-to-volume ratios (SA/V values) can lead to improved uptake rates and shorter times to achieve equilibrium. For passive sampling, these ENM performance characteristics translate into shorter field deployments and easier analytical detection.

Across several polymers considered, PAN, PMMA and PS ENMs were most promising. They exhibited rapid (with and without mixing) uptake with $t_{90\%}$ values from 0.008 to 7 days and equilibrium partitioning coefficients ranging from 1.3 to 6.4 log units (L/kg) for hydrophilic, moderately hydrophobic and hydrophobic targets alike. From results with model compounds, these materials provide comparable performance or better to commercially available passive sampling materials and more traditional research alternatives, although a direct comparison to POCIS remains needed. Indeed, POCIS and Chemcatcher™ generally show higher equilibrium partitioning coefficients, from 1 to 4 log units for hydrophilic and moderately hydrophobic compounds, but sometimes there is no accumulation of the analytes into their different sorbent phases (e.g., Triclosan and Dicamba),^{182, 198} and with longer time to reach equilibrium.¹⁹⁸

We contend, therefore, that these ENMs have the potential to be applied to a broad spectrum of pollutant targets, simultaneously, with only a single sorbent material. We also demonstrated ENM performance in complex settings (e.g., soil and sediment), while also revealing important

practical considerations associated with their use; for example, PS had limited organic matter fouling relative to PMMA in soil and sediment.

While the results shown here are promising, further improvement on selectivity and capacity, are likely needed. Further, device scales up with integration of ENMs into a passive sampling device, and ultimately field demonstration and validation, will be needed to fully realize the promise of ENMs as next-generation passive sampling materials.

CHAPTER 3 POLYMER NANOFIBER-CARBON NANOTUBE COMPOSITES AS A PASSIVE SAMPLING MEDIA FOR POLAR ORGANIC POLLUTANTS

3.1 ABSTRACT

Carbon nanotubes (CNTs) are promising sorbent materials for many organic pollutants because of their high external surface area and tunable surface chemistry. Here, we integrated two types of multi-walled CNTs, both with and without surface carboxyl ($-\text{COOH}$) functional groups, into polymeric electrospun nanofiber mats (ENMs) that we have previously developed for passive sampling applications. Although inclusion of CNTs did not alter the hydrophobicity of polyacrylonitrile (PAN) and polystyrene (PS) based ENMs, ENM-CNT composites exhibited a slight increase in average diameter, greater specific surface area and pore volume. In uptake experiments with a suite of 11 polar and moderately hydrophobic (i.e., $\log K_{ow} < 4.5$) chemicals, the sorption capacity of ENM-CNT composites increased anywhere from 2- to 50-fold relative to unmodified polymer ENMs. As with unmodified polymers, pollutant uptake with ENM-CNT composites was rapid in all cases. Sorption kinetic followed a first-order uptake model, from which we determined that it took less than 20 minutes for most to reach 90% equilibrium. Across the suite of pollutant targets, equilibrium partition coefficients between the ENM-CNT composites and water (K_{ENM-W} values as L/kg) were 2-log units in most cases. We observed no clear correlation between partition coefficients measured with ENM-CNT composites and those measured in CNT suspensions, indicating that the composite materials exhibit unique performance that cannot be directly attributed to the individual components from which they are constructed. Isotherm experiments with select targets (pesticides diuron and atrazine) revealed no signs of saturation even at much higher levels than found in the environment ($\gg 100$'s $\mu\text{g/L}$)

with uptake capacities ranging from 1.5 to 4.5 mg/g. However, these capacities were far lower than those measured in CNTs suspensions and thus are consistent with the loss of available surface area expected upon CNT integration into the polymeric nanofiber. To increase uptake capacity, we demonstrated a linear relationship between $\log K_{ENM-W}$ and the abundance of CNTs (as wt. %) in the composite, although thresholds in CNT content were encountered above which electrospinning was not feasible (~25% wt. for -COOH functionalized CNTs and 40% wt. for non-functionalized CNTs). Additional studies revealed that composite performance is not adversely affected in complex aquatic media (e.g., Iowa River water), and their deployment at Muddy Creek, IA yield atrazine concentrations in surface water that generally agreed with values obtained by USGS through more traditional analysis of grab samples. Collectively, these results suggest that high capacity, rapid uptake ENM-CNT composites are more promising materials for passive sampling and related environment applications than pure polymer ENMs.

3.2 INTRODUCTION

Many organic chemicals from industry, medicine and commerce are now ubiquitous in terrestrial and aquatic environments,²⁰⁷⁻²¹⁰ but the human health and ecosystem risks associated with their occurrence remain difficult to assess. A common challenge in risk assessment is determining chemical exposure, which involves not just accurate quantification of environmental concentrations but also the appropriate timescales over which exposure occurs. Passive sampling devices, which collect chemicals over a relatively long-time period via molecular diffusion between the analyte and sorbent, represent an easy-to-operate, low cost, and robust tool for assessing these aspects of environmental occurrence. Although the favorable attributes of passive samplers have led to their widespread use in the environmental monitoring of both legacy and emerging organic pollutant classes,^{211, 212} there remain opportunities to improve upon their performance, both to expand the universe of chemicals amenable to this approach and to improve the spatial and temporal resolution of resulting occurrence data.

Nanotechnology holds tremendous promise for improving the performance of passive sampling devices through innovation in the materials used for chemical sequestration. The high surface-area to volume ratios of engineered nanomaterials, along with other features that can be manipulated at the nanoscale (e.g., surface roughness and porosity), are ideal for technologies relying on partitioning processes (e.g., adsorption and absorption), including passive samplers.^{102, 178} For example, we have previously shown in Chapter 2 that polymeric electrospun nanofiber mats (ENMs) can provide fast, albeit somewhat limited, chemical uptake across a broad spectrum of legacy (e.g., PCBs and dioxin) and emerging (e.g., diuron and β -estradiol) organic pollutant classes. Specifically, for a matrix of five different polymers and 19 organic pollutants ranging from hydrophilic to hydrophobic, we quantified equilibrium partition

coefficients between ENMs and water (or $K_{\text{ENM-W}}$ values) of 1.1- and 4.7-log units, and observed rapid uptake with time to reach 90% equilibrium ($t_{90\%}$) of < 7 days with mixing.¹²⁵ For optimally performing materials [e.g., polyacrylonitrile (PAN) and polystyrene (PS)], we observed very fast chemical uptake, with $t_{90\%}$ values < 1 day even under a static (i.e., no-mixing) conditions during uptake experiments.

The benefit of electrospinning for production of passive sampling materials is the high degree of tunability in material properties during nanofiber synthesis. In our earlier work, the primary material variable explored for optimizing ENM performance was the nature of the polymer, ranging from hydrophobic (e.g., polyvinylidene fluoride or PVDF) to hydrophilic (e.g., PAN). Control of this property via electrospinning is trivial, however, and simply depends on the polymer precursor used in the electrospinning solution. We also considered the diameter of the nanofibers as a performance variable, where we tuned the diameter of PAN by altering polymer concentration and relative humidity during synthesis. Our expectation was for ENMs consisting of smaller diameter nanofibers to exhibit greater uptake capacity (i.e., larger $K_{\text{ENM-W}}$ values), which is preferred because this allows less material to be used during passive sampler deployment while also improving the detection limits of analytical methods used to quantify the chemicals extracted from ENMs. However, we discovered that nanofiber diameter (and thus surface area) only improved the rate, but not the extent, of chemical uptake. Not only does this result imply that chemical uptake is driven by absorption (i.e., into the nanofiber bulk such that ENM capacity is controlled by available mass) rather than adsorption (i.e., onto the nanofiber surface such that ENM capacity is controlled by available surface area), it also requires alternative pursuits to increase ENM uptake capacity.

To pursue this goal, we herein produce polymer ENM composites with carbon nanotubes (CNTs) via electrospinning and evaluate their performance (i) relative to pure polymer ENMs and (ii) toward a suite of 11 polar and moderately hydrophobic (i.e., $\log K_{ow} < 4.5$) chemicals representative of traditional and emerging pollutant classes. CNTs are known to exhibit many attractive features for environmental applications including their excellent tensile strength,¹²⁸ antimicrobial activity,¹³⁷ tunable surface chemistry through functionalization,²¹³ and high sorption capacity for organic chemicals.^{214, 215} However, to harness CNTs as a next-generation sorbent material, they will need to be deployed in a supported network that limits their release but still allows sufficient access to their surface active sites responsible for pollutant uptake. For example, in our prior work with electrospun carbon nanofibers (CNFs), we found that integration of CNTs greatly enhanced organic micropollutant uptake;¹⁶¹ a similar approach may also be viable to improve the uptake capacity of polymer ENMs for passive sampling applications.

Accordingly, we have produced polymer ENM composites with two types of multi-walled CNTs, those with and without surface carboxyl groups, through the simple integration of CNTs into the electrospinning precursor solution. Our focus on non-functionalized CNTs (hereafter “NF-CNT”) and surface carboxylated CNTs (hereafter “COOH-CNT”) allow us to determine how CNT surface chemistry influences composite behavior as a sorbent for polar and moderately hydrophobic pollutant classes. Moreover, to better understand mechanisms of pollutant uptake, we not only examined trends in ENM-CNT composite performance as a function of material properties (e.g., CNT type and loading, composite hydrophobicity), but also directly compared the sorption behavior of composites to that measured with CNT dispersions. Performance studies also examined how ENM-CNT composites perform in complex media, simulating the types of environments (e.g., surface water and sediments) where passive samplers

are most often deployed, and a limited field deployment study targeting surface water concentrations of atrazine was conducted to validate the practical viability of these materials.

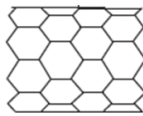
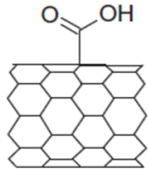
3.3 MATERIALS AND METHODS

Reagents. All reagents used for ENM fabrication were used as received including polyacrylonitrile (PAN; MW ~150,000; Sigma-Aldrich), polystyrene (PS; MW ~280,000; Sigma-Aldrich), tetrabutylammonium bromide (TBAB; $\geq 99\%$; Sigma-Aldrich) and N,N-dimethylformamide (DMF; 99.8%; VWR International). Carbon nanotubes (CNTs) were acquired from Cheap Tubes, Inc. (Cambridgeport, VT). Both carboxylated (COOH-CNT) and non-functionalized (NF-CNT) CNTs were used, and their characteristics are summarized in

Table 3-1.

The target analyte suite used in uptake experiments consisted of anisole (neat, $\geq 99.9\%$), metolachlor (neat, $\geq 99.9\%$), *S*-metolachlor (neat, $\geq 99.9\%$), aniline (liquid, $\geq 99.5\%$), nitrobenzene (liquid, $\geq 99.0\%$), caffeine (powder, $\geq 99.0\%$), *p*-nitrophenol (powder, $\geq 99.5\%$), atrazine (powder, 99.1%), diuron (powder, $\geq 98.0\%$), 2,4-dichlorophenoxyacetic acid (2.4-D; crystalline, $\geq 98.0\%$) and phenol (crystalline, $\geq 99.0\%$). The structure and select chemical properties of these chemical targets are summarized in **Table 3-2**. All were purchased from Sigma-Aldrich and used as received. Stock solutions (from 2.3 to 7.1 g/L) of each chemical were prepared in methanol (Fisher Chemical, optima grade, $\geq 99.9\%$) and stored in a refrigerator ($\sim 3\text{ }^{\circ}\text{C}$) until use. Uptake experiments were conducted in 1 mM potassium phosphate buffer (Fisher Scientific, crystalline, $\geq 99.0\%$) deionized (DI) water (Thermo Scientific, Barnstead™ GenPure™ ultrapure water system) solution at pH 7.

Table 3-1. Vendor (Cheap Tubes, Inc.) provided characteristics of non-functionalized CNTs (NF-CNT) and oxidized CNTs with carboxylic acid functional groups (COOH-CNT).

	NF-CNT	COOH-CNT
Surface Functionality		
Wall Type	Multi-walled CNT	Multi-walled CNT
Outer Diameter	< 8 nm	< 8 nm
Length	0.5 – 2.0 μm	0.5 – 2.0 μm
Purity	> 95 w.t. %	> 95 w.t. %
Ash	< 1.5 w.t. %	< 1.5 w.t. %
Functional Content	N.M.	3.86 w.t. %(COOH groups)

Electrospinning. ENMs were synthesized using a customized electrospinning apparatus, which has been described in Chapter 2, as well as in the related published work.¹²⁵ For production of ENM-CNT composites, we modified our standard polymer ENM fabrication procedures to accommodate precursor solutions of homogenous suspensions of CNTs and polymer precursors. In general, CNTs (4.4 – 35 mg/mL) were sonicated in DMF for 5 hours to promote dispersion and minimize the presence of CNT aggregates. Next, the polymer precursor was added to this CNT/DMF suspension and mixed (Eppendorf, ThermoMixer® C) at 60 °C for 5 hours to produce the polymer-CNT sol-gel used for electrospinning ENM-CNT composites. The resulting sol-gel was then transferred into a 12 mL syringe and delivered via syringe pump through a 25G metal needle at a flow rate of 0.5 mL/h (we note that a 23G needle was used for composites with 25% by mass of COOH-CNT to avoid needle clogging issue during the fabrication). Depending on the relative mass ratio of polymer and CNTs, a voltage between 14 and 16 kV was applied to the needle tip. An aluminum foil covered, grounded spinning drum was used to collect the deposited ENMs, and was located at a distance of 10 cm from the needle tip. During electrospinning, relative humidity was controlled at 18 (\pm 2) %, and the temperature was fixed at 28 °C.

Table 3-2. Structure and select physicochemical properties of the organic chemical targets investigated here.

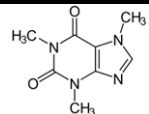
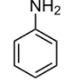
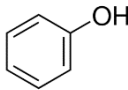
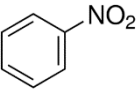
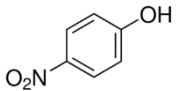
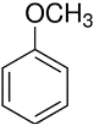
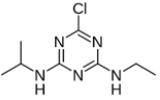
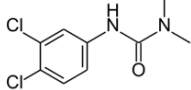
Compound	Structure	MW (g/mol)	Log K _{ow}	Water solubility (room temperature) (g /100 mL)*	Aromatic bonds	Hydrogen bonds (count)**	pKas (25 °C)*	Charge @ pH ≈ 7	Molar refractivity (cm ³)*
Caffeine		194.19	-0.07	2	10	H-donor (0) H-acceptor (6)	0.52, 14 **	Neutral	46
Aniline		93.13	0.9	3.6	6	H-donor (2) H-acceptor (1)	4.9	Protonated (neutral)	30
Phenol		94.11	1.5	8.2	6	H-donor (1) H-acceptor (1)	9.9	Deprotonated (neutral)	28
Nitrobenzene		123.06	1.9	0.2	6	H-donor (0) H-acceptor (3)	4.0 (0 °C)	Neutral	33
p-Nitrophenol		139.11	1.9	1.6	6	H-donor (1) H-acceptor (4)	7.2	Partially deprotonated (partially negative)	32
Anisole		108.14	2.1	0.16	6	H-donor (0) H-acceptor (1)	-4.8	Neutral	33
Atrazine		215.68	2.6	0.007	6	H-donor (2) H-acceptor (5)	2.3	Protonated (neutral)	59
Diuron		233.09	2.7	0.0042	6	H-donor (1) H-acceptor (3)	14	Protonated (positive)	59

Table 3-2. Structure and select physicochemical properties of the organic chemical targets investigated here.

Compound	Structure	MW (g/mol)	Log K _{ow}	Water solubility (room temperature) (g /100 mL)*	Aromatic bonds	Hydrogen bonds (count)**	pK _{as} (25 °C)*	Charge @ pH ≈ 7	Molar refractivity (cm ³)*
2,4-D		221.04	2.8	0.054	6	H-donor (1) H- acceptor (3)	2.98	Deprotonated (negative)	49
Metolachlor		283.79	3.13	0.053	6	H-donor (0) H- acceptor (3)	1.45	Neutral	80.1
S-Metolachlor		283.79	2.89	0.0488	6	H-donor (0) H- acceptor (3)	1.45	Neutral	80.1

* All the data are collected from PubChem database operating by National Center for Biotechnology Information (NCBI)

** Hydrogen bond is a covalent effect happening when a hydrogen atom is attracted by nitrogen, oxygen or fluorine atom. The numbers of electronegative atoms that accept covalent bonds and electropositive hydrogen atoms that participate covalent bonds in each chemical are listed in this table.

Material characterization. ENM-CNT composites were imaged using a Hitachi S-4800 scanning electron microscope (SEM). SEM images were analyzed using Image J software to determine the distribution and average of nanofiber diameters from sizing of at least 200 individual nanofibers. Specific surface area and total pore volume measurements for ENM-CNT composites were conducted using a Micromeritics ASAP 2020 surface area and pore size analyzer. Surface area was quantified using a seven point N₂-BET adsorption isotherm, whereas the Barrett-Joyner-Halenda (BJH) method was applied to measure pore volume.²¹⁶ Surface hydrophobicity was evaluated using water contact angle measurements conducted on a Rame-Hart Model 100 contact angle goniometer. For analysis, a 10 µL droplet of deionized (DI) water was spread and withdrawn at a flow rate of 1 µL/s, which was controlled by an Eppendorf EDOS 5222 Electronic Dispensing System automatically.

Sorption experiments with ENM-CNT composites. Stock solutions of target analytes were prepared in methanol at a concentration of 25 mM (from 2.3 g/L to 7.1 g/L). To initiate uptake experiments, the stock solution was diluted in 1 mM potassium phosphate buffer prepared in deionized (DI) water at pH 7 to an initial concentration of 25 µM and transferred to a 40 mL amber glass vial. Sorption measurements were conducted at room temperature (~ 20 °C). All experiments were conducted at pH 7 with the exception of those conducted in Iowa River water, which was used at its ambient pH (~7.9) without adjustment and remained stable at this value during experiments. Sorption experiments with ENM-CNT composites were conducted in systems that were either mixed or static (i.e., not mixed). For experiments with mixing, reactors were mixed end-over-end on a labquake rotator (Barnstead/Thermolyne Model 415110) at a speed of 8 rpm over a 2 day experimental duration. ENM-CNT mass loading in each reactor was 1.25 ± 0.05 g/L.

For analysis, samples were collected over time, with each data point collected from a sacrificial sample of an identically prepared set of reactors. Analysis quantified both the amount of target analyte remaining in solution, as well as the mass of analyte bound to the ENM-CNT composite as a result of sorption. To analyze the bound fraction, methanol was used as the extraction solvent according to the protocols outlined in Chapter 2 and in the related published work.¹²⁵ For environmental water samples (Iowa River sample), all aqueous samples were first filtered through a 0.22 μm nylon membrane filter (Celltreat Scientific Products) prior to analysis via HPLC as described below.

Sorption experiments with CNT suspensions. For sorption studies with CNT suspensions, CNT mass loadings (between 0.03 g/L and 0.3 g/L) were used to measure single-point K_d values (C_{CNT}/C_w) for each chemical. The initial chemical concentration in the aqueous phase was between 2.3 g/L to 7.1 g/L, and different initial concentrations were used to ensure there was residual chemical in the aqueous phase once the system achieved equilibrium. Preliminary investigations revealed uptake in CNT suspensions to be very fast, with most sorption occurring in the first 30 minutes after addition of the chemical to the CNT suspension, even without mixing (i.e., static condition). Nevertheless, we conducted these CNT suspensions experiment over 8 hours to ensure equilibrium. At this time, samples were collected from the suspensions, and the CNTs were removed by a 0.22 μm Nylon filter prior to analysis by HPLC. Analysis of the sample was used to measure C_w , which depending on the target analyte was typically anywhere between 10-90% of the initial mass present in the system. Values of C_{CNT} were then determined from the difference between the initial mass added to the reactor and the remaining mass in solution at equilibrium.

Field testing of ENM-CNT composites. A quadrature metallic frame (9.5 cm × 9.5 cm) with a circular hole (diameter: 7 cm) in its middle was used to hold the ENM used in field testing. A piece of an ENM (approximately 11 cm × 21cm; ~ 450 mg) was folded and sandwiched between the metal pieces, and the open edge of frame was tightened by two self-locking zip ties. After assembly, the frame with ENM was wrapped in aluminum foil and placed into a zip lock bag. An extra ENM of similar mass was also covered with aluminum foil and taken to the monitoring site for use as a filed blank reference sample.

The deployment location was Muddy Creek, Coralville, IA (USGS 05454090; **Figure 3-1** and **Figure 3-2**). Muddy Creek is part of the Iowa River watershed with a drainage area of 22.5 km². USGS started recording discharge from Muddy Creek in November 2006,¹²⁰ along with quality data. The Creek was an impaired segment (excessive indicator bacteria) of the Iowa River on the 2004 Iowa 303(d) list.²¹⁷ For example, urban and (primarily) agriculture inputs contributed nitrogen (as nitrate and ammonia) into the Creek's water at a level of 7 mg/L as N. Moreover a dissolved phosphorus concentration of 0.04 mg/L was also reported for the water in this region.²¹⁸ This site was chosen due to previous reports of higher pesticide concentration by the USGS based upon their routine grab sampling at the site.^{219, 220} Monthly average temperature histograms of two nearby USGS sites where the temperature was monitored throughout the year are provided in **Figure 3-3**.

Both NF-CNT/PAN and COOH-CNT/PAN ENMs were deployed approximately 100 meters upstream from the discharge point of the Coralville wastewater treatment plant (**Figure 3-1**). At the site, the ENM-containing frame was tied to a metal rod, which was then inserted into the sediment at the bottom of the creek. Once inserted, the ENM was in contact with the surface

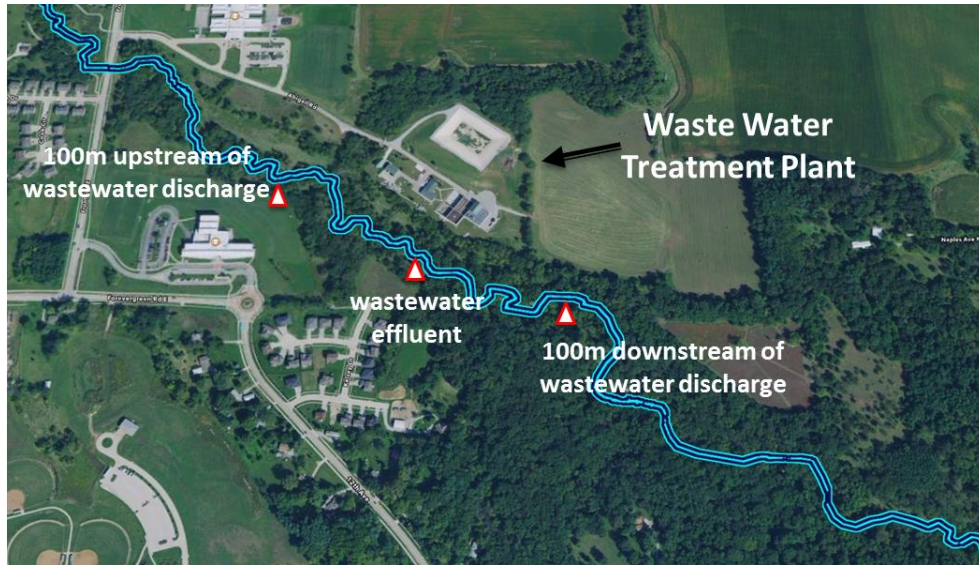


Figure 3-1. Map of the test site for Muddy Creek, Coralville, IA (USGS site: 05454090)



Figure 3-2. Digital picture of sampling site, with inset showing the orientation of sampler during deployment.

water of the Creek, but not the underlying sediment. After 48 hours, the sampler was collected and once again covered in aluminum foil during transport back to the laboratory.

For ENM processing and analysis, the field-recovered ENM was first rinsed by DI water to remove any coarse grain sandy particles or loose dirt on the material surface. Methanol was

then used to extract the target organic analyte, atrazine, via immersion and mixing for 24 hours. The extract liquor was then filtered through a 0.22 μm Nylon filter prior to analysis by HPLC with mass spectrometry detection according to the methods described below.

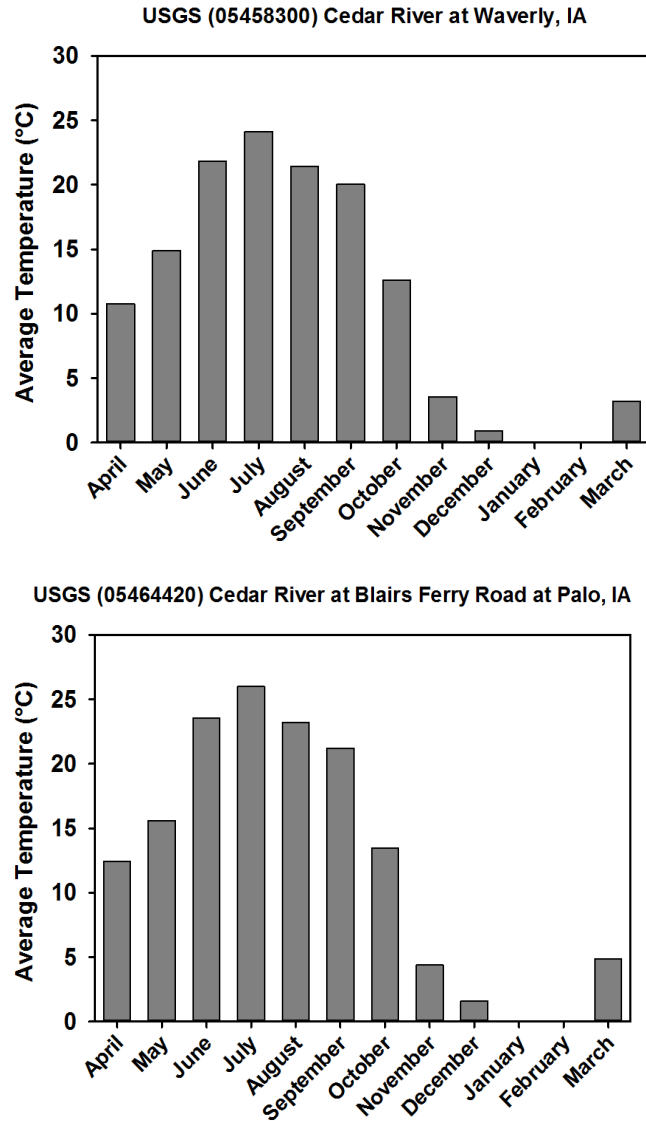


Figure 3-3. The monthly average temperature of two USGS sites close our measuring site.

Analytical methods. A high-performance liquid chromatography with a diode array detector (LC/DAD, Agilent 1100 series HPLC) was used to measure both aqueous samples and methanol extracts of ENM-CNT composites. HPLC methods for each chemical were adapted from previously published methods.^{187-189, 212, 221-224} For aqueous phase analysis, 1 mL of aqueous sample was transferred to an amber autosampler vial, and immediately analyzed. For analysis of the sorbed phase, ENM-bound mass was extracted by mixing the ENM with 10 mL of methanol for 1 d, after which 1 mL of methanol was collected and analyzed.

Field samples were analyzed using liquid chromatography with tandem mass spectrometry (Agilent Technologies 1260 Infinity LC with 6460 MS/MS) equipped with an electrospray ionization (ESI) source operating in multiple reaction monitoring (MRM) mode. The mobile phase was 50% water:50% acetonitrile, the method was isocratic and the column was a Poroshell 120 SB-C18 (2.1 x 50 mm, 7.7 μ M, Agilent Technologies).

3.4 RESULTS AND DISCUSSION


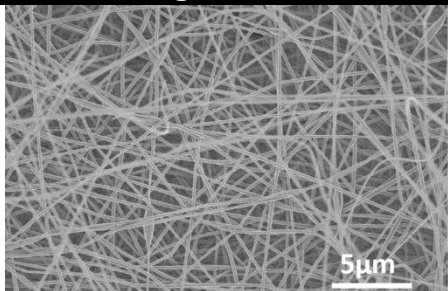

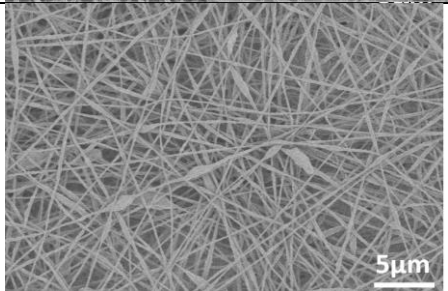

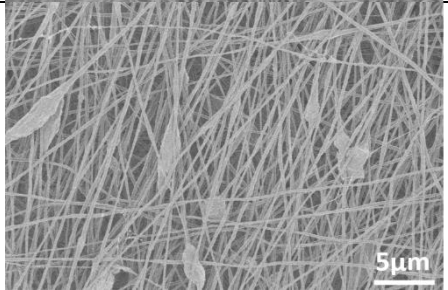
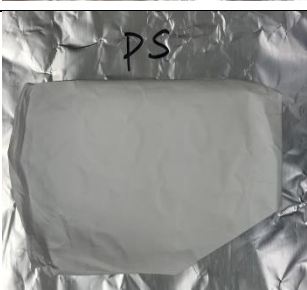
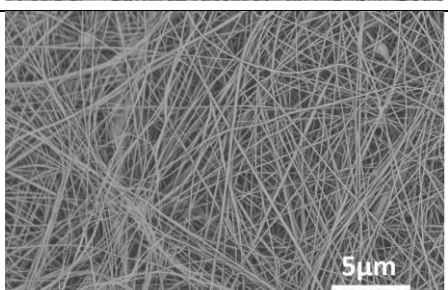
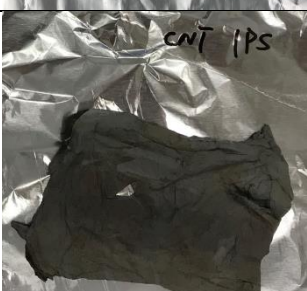
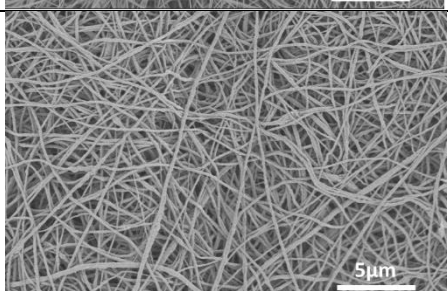
Synthesis and characterization of ENM-CNTs. For ENM-CNT composites prepared from PAN and PS, **Table 3-3** summarizes select physical and chemical properties expected to influence material sorption capacity and uptake rate. Also provided for comparison are characterization results from Chapter 2 for unmodified PAN and PS ENMs.

Table 3-3. Characterization results for synthesized ENM-CNT composites synthesized herein.

	Surface Area (m ² /g) ^a n = 6	Pore Volume (10 ⁻³ mL/g) ^a n = 3	Water Contact Angle (°) ^b n = 8	Diameter (nm) ^c n = 3
PS	35 ± 7.0	76 ± 3.0	118 ± 2.0	140 ± 30
20% NF-CNT/PS	48 ± 2.0	168 ± 3.0	123 ± 6.0	150 ± 20
20% COOH-CNT/PS	43 ± 2.0	140 ± 3.0	130 ± 5.0	150 ± 30
PAN	12 ± 0.5	23 ± 1.7	44 ± 6.2	160 ± 30
10% NF-CNT/PAN	15 ± 1.0	35 ± 2.2	43 ± 5.0	230 ± 60
20% NF-CNT/PAN	15 ± 2.4	37 ± 8.0	47 ± 2.0	210 ± 50
30% NF-CNT/PAN	19 ± 0.7	48 ± 3.0	51 ± 1.0	250 ± 70
40% NF-CNT/PAN	22 ± 1.6	78 ± 3.0	49 ± 4.0	210 ± 50
10% COOH-CNT /PAN	14 ± 0.5	38 ± 1.0	45 ± 2.0	220 ± 40
15% COOH-CNT /PAN	15 ± 0.3	37 ± 1.0	50 ± 2.0	240 ± 50
20% COOH-CNT /PAN	17 ± 2.0	43 ± 6.0	43 ± 3.0	200 ± 40
25% COOH-CNT /PAN	17 ± 0.5	52 ± 2.0	48 ± 1.0	250 ± 50

a Surface area and pore volume were measured by BET by using a seven-point adsorption isotherm, and BJH methods respectively; b Water contact angles were measured from digital images of contact angle goniometry by using ImageJ software. Both right and left contact angles were counted for each liquid droplet. Values < 90° are wettable (hydrophilic) surfaces; c Diameters were measured from SEM images by using ImageJ software. Uncertainties represent the standard deviation from at least three replicate experiments. Typically, 100 nanofibers were measured per ENM sample. n = number of replicate syntheses.

Table 3-4. Digital (left column, ~25 cm²) and low-magnification SEM (right column) images of ENM-CNT composites produced herein.

	Digital Photo	Low Magnification SEM
PAN		
20% NF-CNT/PAN		
20% COOH-CNT/PAN		
PS		
20% NF-CNT/PS		

From SEM images (see low magnification images shown in **Table 3-4**) histograms of nanofiber diameters were constructed (**Figure 3-4**), with averages values (with standard deviation) summarized in **Table 3-3**. For PAN, the inclusion of CNTs generally increased the average nanofiber diameter within the mat, although rarely to the extent to be statistically significant given the standard deviation associated with sizing measurements via SEM. Further, there was no systematic relationship between nanofiber diameter and increasing CNT loading within PAN, nor was there any difference resulting from integration of oxidized or non-functionalized CNTs. Although a greater number of CNT loadings were considered for PAN-based ENMs, these same trends in composite size were also observed with PS-based ENMs, where integration of either oxidized or non-functionalized CNTs had no significant influence on average nanofiber diameter or distribution.

Via higher magnification SEM imaging of ENM-CNTs (**Figure 3-5**), some noteworthy features regarding nanofiber morphology were observed. First, both low- and high-magnification images revealed the presence of CNT aggregates in the composite material, appearing as large

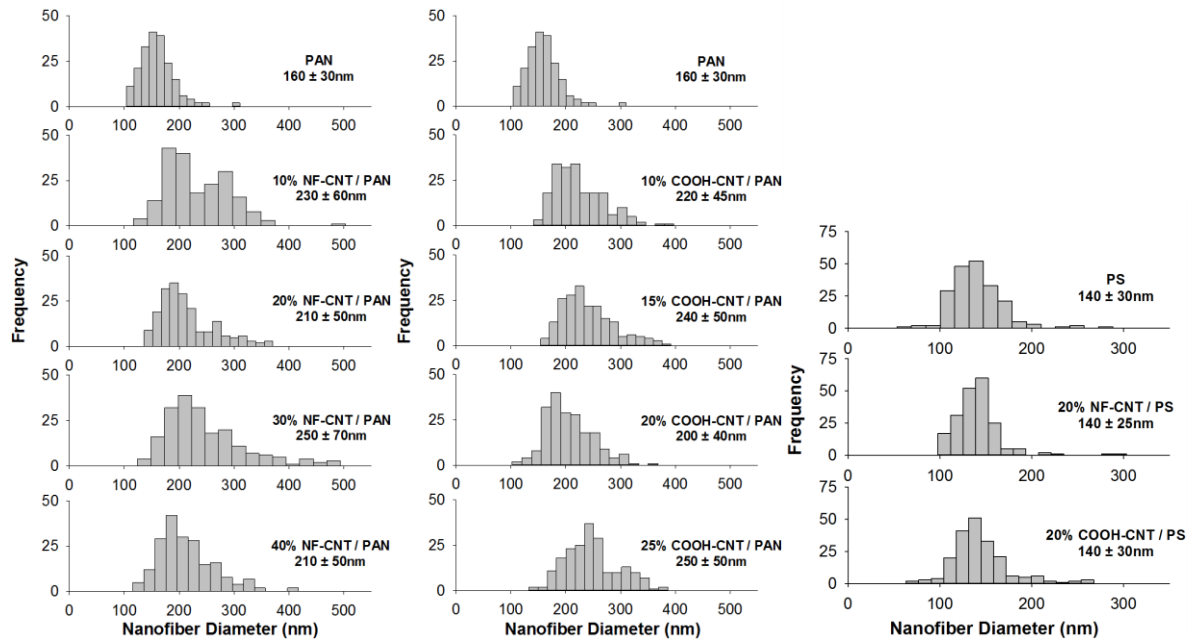


Figure 3-4. Histograms of nanofiber diameter (measured via SEM for $n=200$) for ENMs and ENM-CNT composites fabricated herein. Histograms are shown as a function of CNTs mass loading.

clumps of CNTs embedded or encapsulated by the polymer that are randomly distributed across and within the ENM. Generally, in the ENM with higher CNT loadings, the structure is more heterogeneous, with evidence of beads or clumping resulting from non-dispersed, large aggregates of CNT (see the feature indicated with two arrows in **Figure 3-5a**). Second, composites exhibited surface features and roughness that are unique compared to unmodified polymers,¹²⁵ and thus we presume attributable to the integration of CNTs (see features indicated with one arrow in the high magnification insets of **Figure 3-5**). Because SEM resolution is insufficient to image isolated CNTs, we assume that the surface roughness and other features reflect smaller CNT aggregates with different morphologies within the polymer nanofiber. We also noticed that integration of CNTs resulted in the formation of some very thin nanofibers with

diameters on the order of ~80 nm, although these thin fibers were not sufficiently numerous to greatly increase the distribution of nanofiber diameters (based on standard deviation) reported in

Table 3-3.

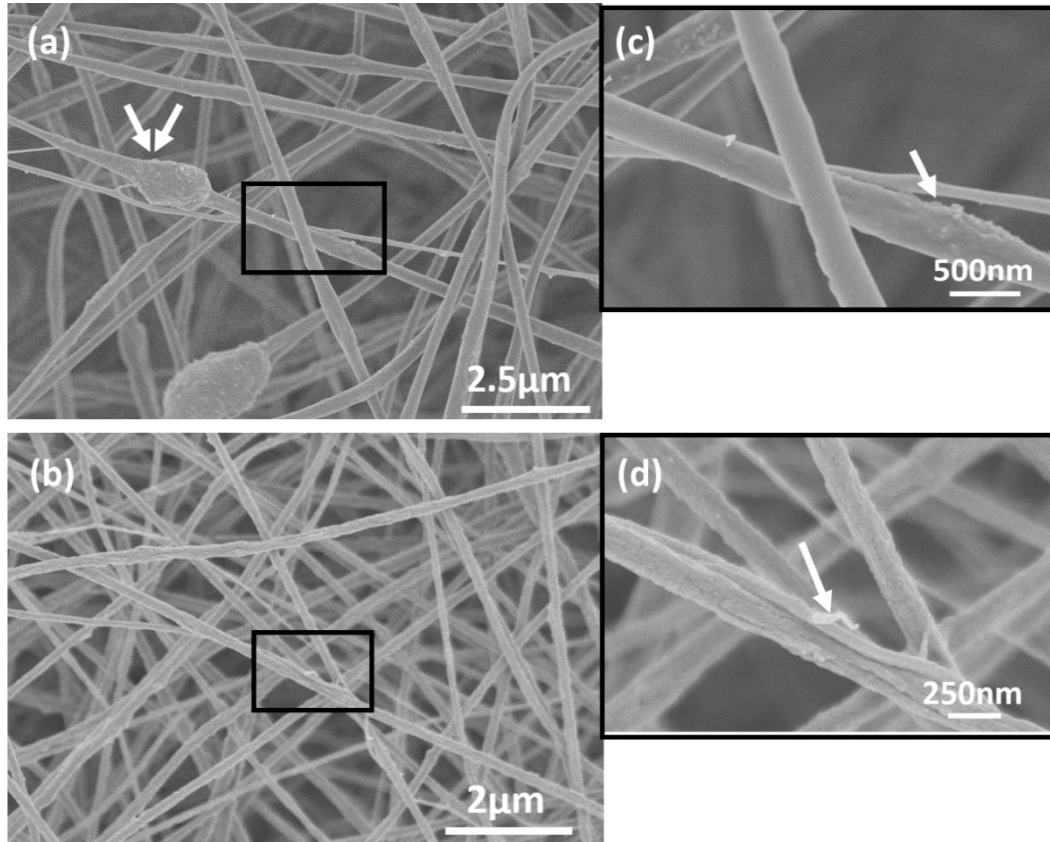


Figure 3-5. SEM images of ENM-CNT composites. Images are shown for (a) and (c) COOH-CNT/PAN ENM; (b) and (d) NF-CNT/PS ENM. Insets on the right correspond to the areas indicated in (a) and (b) with black boxes. Arrows indicate specific morphological features (e.g., aggregates) due to the presence of CNTs (see text).

Surface area and pore volume. For both PS- and PAN-based ENMs, increasing CNT mass loading increased the specific surface area and pore volume of the composite. The increase in surface area was modest for both PAN and PS composites, whereas the increase of pore volume was more significant, increasing 2-to-3-fold in some cases (e.g., see pore volume results

for PAN composites in **Table 3-3**). As shown in the regression analyses conducted in **Figure 3-6**, both surface area and pore volume scale with CNT mass loading, increasing roughly linearly. Given that the average diameters of ENM-CNT composites were either comparable or

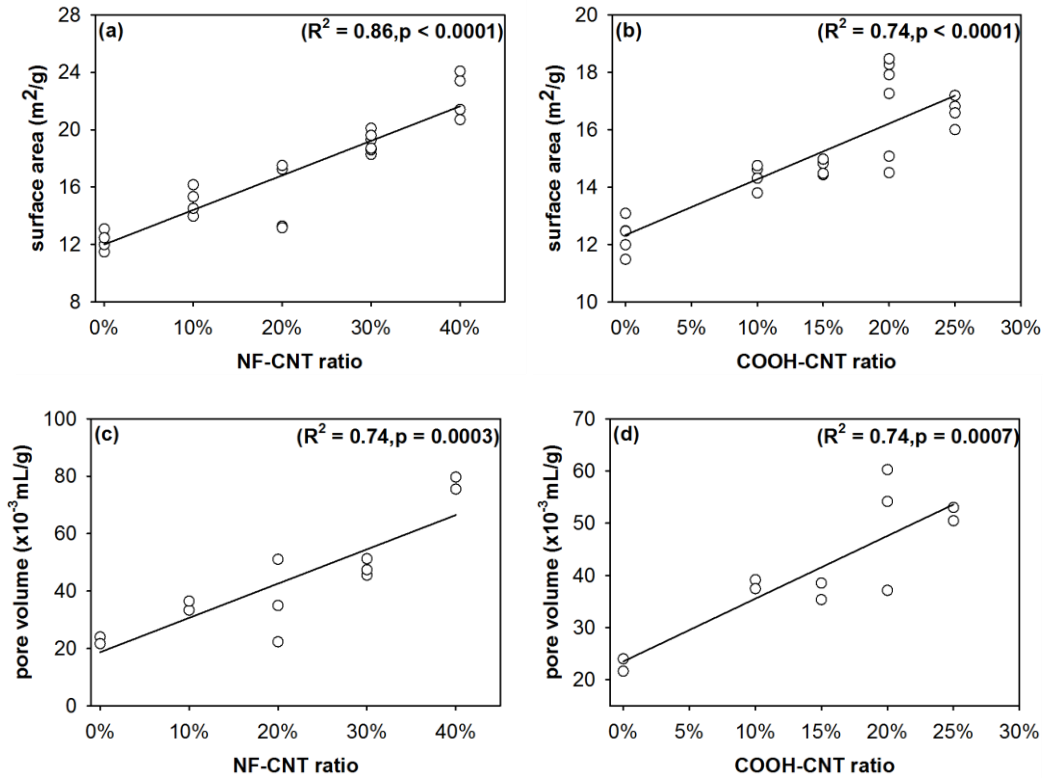


Figure 3-6. Linear regression analysis for the correlation between ENM composite specific surface area (from BET in m²/g) and pore volume (×10⁻³ mL/g) as a function of CNT mass loading (in wt%).

greater than the pure polymer ENMs, it is reasonable to conclude that the slight increases in surface area are due to porosity, presumed to be internal to the fibers, generated via integration of CNTs into the polymer matrix. Not surprisingly, therefore, we also observed a strong correlation between measured specific surface area and pore volume for both NF-CNT and COOH-CNT composites (**Figure 3-7**). We note that because of the high viscosity of polymer sol gels

containing CNTs, the highest mass loadings of NF-CNT and COOH-CNT that could be easily electrospun (i.e., without needle clogging) were 40% and 25%, respectively. Although not investigated herein, higher mass loadings of CNTs may be achievable upon introduction of additional agents to the sol gel to increase the viscosity (e.g., surfactants).

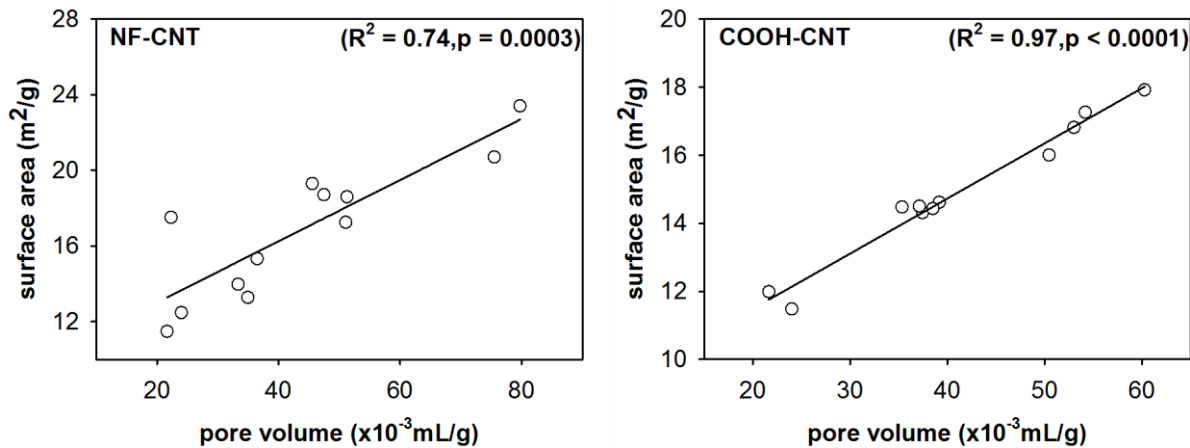


Figure 3-7. Linear regression analysis for the correlation between NF-CNT and COOH-CNT surface area (in m^2/g) and pore volume ($\times 10^{-3}$ mL/g). NF-CNT mass loading was from 0% to 40%, whereas COOH-CNT mass loading was from 0% to 25%.

Surface hydrophobicity and hydrophilicity. Somewhat unexpectedly, we observed a negligible influence of CNT inclusion on ENM-CNT hydrophobicity as measured by water contact angle. Mats of PS are hydrophobic, with a water contact angle greater than 90° (118 ± 2) and consistent with low wettability. There was no change in the measured water contact angle after integration of either type of CNT, despite the presence of carboxylic acid moieties on oxidized CNTs, which would be expected to increase composite hydrophilicity, and the hydrophobic nature of NF-CNTs. Likewise, the nature of the PAN surface, a hydrophilic

polymer with water contact angle of 44 ± 6 , was unaffected by the inclusion of NF- and COOH-CNTs across the range of mass loadings considered.

Influence of CNT inclusion on ENM composite sorption performance. Figure 3-8 presents uptake curves for five model organic pollutants, metolachlor, atrazine, 2,4-D, caffeine, and diuron, on PAN-based composites with 20 wt.% of either NF-CNT or COOH-CNT. Data are shown for the mass of chemical accumulated in the nanofiber mat over time (in g chemical per kg mat), which was quantified analytically after extraction of the ENM with methanol. Also, data obtained with a pure polymer ENM are provided for comparison. We note that all uptake curves for ENM-CNTs were collected under static experimental conditions (i.e., without mixing), whereas uptake data on pure PAN were collected with mixing.

In all cases, the inclusion of 20% wt. CNT substantially increased chemical uptake, in many cases by more than an order of magnitude. For example, caffeine exhibits little to no uptake on PAN, whereas ~ 0.5 g caffeine per kg of ENM was observed with CNT-modified systems. For all chemicals, COOH-CNTs resulted in greater uptake than NF-CNTs. Recall from **Table 3-3** that 20% wt. of NF-CNTs in PAN produced composites with a surface area and pore volumes statistically equivalent to that of PAN composites with 20% wt. COOH-CNTs. Thus, the enhanced chemical uptake on ENM-CNT composites cannot simply be rationalized by physical changes to the ENM structure that produce a higher capacity sorbent through gains in surface area and pore volume. While these changes no doubt promote uptake, the improved performance of CNT-containing composites appears to also reflect specific chemical interactions between the composite and the organic chemical targets,^{225, 226} particularly when carboxylic acid groups are present on the CNT surface.

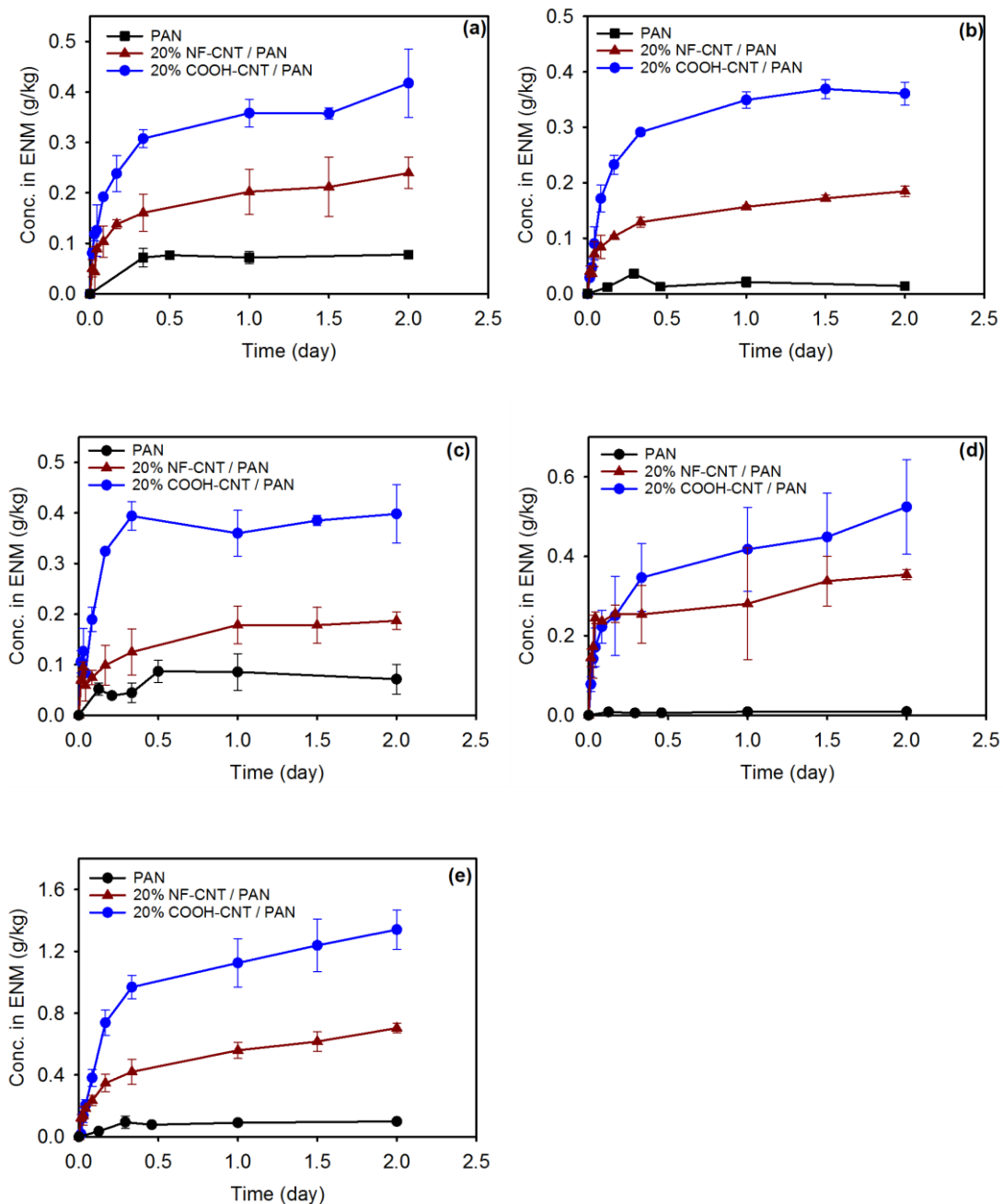


Figure 3-8. Uptake curves for (a) metolachlor, (b) atrazine, (c) 2,4-D, (d) caffeine, and (e) diuron on ENMs of PAN and CNT-modified PAN. Data represent the accumulation of mass into the ENM over time in g of chemical per kg of mat, as quantified by chemical extraction from the ENM with methanol. Uncertainties represent the standard deviation from three replicate experiments. Experimental conditions: pH 7 (1 mM phosphate); initial concentration of metolachlor: 7.1 mg/L, atrazine: 5.4 mg/L, 2,4-D: 5.5 mg/L, caffeine: 4.8 mg/L and diuron: 5.8 mg/L; ENM loading: ~1.5 g/L. Experiments were carried out under a static condition.

For both COOH- and NF-CNTs, chemical uptake was rapid, especially so for unmixed experimental systems. In both cases, equilibrium was typically achieved in less than 2 days, which is comparable to the timeframes observed with pure polymer ENMs in Chapter 2 and in our related published research.¹²⁵ To more quantitatively evaluate chemical uptake, a one compartment, first-order kinetic model (Equation 3-1) was used to describe chemical uptake data.

$$C_{ENM} = \frac{k_1}{k_2} \times C_W \times (1 - \exp(-k_2 \times t)) \quad (3-1)$$

In Equation 3-1, k_1 and k_2 are uptake and elimination rate constants (h^{-1}), C_{ENM} and C_W are the chemical concentrations in the ENM and water (mg L^{-1}), respectively, and t is time (h).

Furthermore, the equilibrium partitioning coefficient between the ENM and water (the K_{ENM-W} value) of these model curves can be estimated from the ratio of k_1 and k_2 . These model values for K_{ENM-W} could then be compared to experimentally measured values according to Equation 3-2 to help assess the quality of the kinetic model in describing our experimental uptake data. In Equation 3-2,

$$K_{ENM-w} = \frac{C_{ENM}}{C_W} = \left(\frac{m_{total}}{m_w} - 1 \right) \times \frac{V}{M} \quad (3-2)$$

m_{total} is total chemical mass (in g) added to the reactor, m_w is the chemical mass (in g) remaining in the aqueous phase at equilibrium, V is the total volume (in L) of solution, and M is the mass of ENM in the reactor (in g). Thus, based on the **Error! Reference source not found.**, the value of K_{ENM-w} goes up when the chemical mass remaining in the water at equilibrium goes down. Finally, from the first-order kinetic model in Equation 3-1, we were also able to calculate $t_{90\%}$ values (Equation 3-3), which is the time necessary to reach 90% of system equilibrium (i.e., steady state), from the model fit k_2 value.

$$t_{90\%} = \frac{\ln 10}{k_2} \quad (3-3)$$

Model results are provided in **Table 3-5**. For model-derived $\log K_{ENM-W}$ values, good agreement was observed when compared to the experimental value determined from analysis of the aqueous and ENM-associated chemical concentrations at equilibrium. Indeed, plots of model-derived $\log K_{ENM-W}$ values as a function of experimentally measured values (**Figure 3-9**) illustrate data either directly on or immediately adjacent to the 1-to-1 line, suggesting uptake data for these five analytes appear well-described by the one-compartment model. Under static (i.e., no mixing) experimental conditions, $t_{90\%}$ values for all compounds were less than 20 minutes for CNT-modified ENMs, which were faster than those of pure polymer ENMs.¹²⁵ The fast equilibrium between target chemicals and ENM-CNT is unique relative to current commercially available passive sampling tools, and supports our intended use of these materials as equilibrium-passive sampling devices to improve the temporal resolution of passive sampling data.

Table 3-5. Summary comparing model-estimated and experimentally measured ENM-water equilibrium partition coefficients ($\log K_{ENM-W}$ values) and $t_{90\%}$ values for select analyte targets on NF-CNT/PAN and COOH-CNT/PAN (at 20% wt. CNT loading).

Analytes	20% NF-CNT/PAN			20% COOH-CNT /PAN		
	$\log K_{ENM-W}$ (L/kg)			$\log K_{ENM-W}$ (L/kg)		
	Measured	Model	$t_{90\%}$ (h)	Measured	Model	$t_{90\%}$ (h)
Metolachlor	1.8 ± 0.05	1.7 ± 0.03	0.1 ± 0.03	1.6 ± 0.05	1.6 ± 0.03	0.2 ± 0.02
Atrazine	1.5 ± 0.06	1.4 ± 0.07	0.2 ± 0.1	1.8 ± 0.07	1.8 ± 0.02	0.3 ± 0.05
2.4-D	1.4 ± 0.03	1.4 ± 0.03	0.06 ± 0.01	1.8 ± 0.02	1.8 ± 0.03	0.09 ± 0.01
Caffeine	1.5 ± 0.1	1.5 ± 0.01	0.07 ± 0.01	1.8 ± 0.3	1.8 ± 0.04	0.06 ± 0.01
Diuron	2.1 ± 0.1	1.9 ± 0.09	0.2 ± 0.02	2.4 ± 0.1	2.5 ± 0.1	0.7 ± 0.01

Our experiments also show that the extent of chemical uptake can be tuned by varying the concentration (by wt%) of CNTs embedded into the polymer nanofibers, with increasing CNT loading generally increasing chemical partitioning into the mat. In **Figure 3-10**, data are

shown across a range of wt% for both NF-CNTs (up to 40%) and COOH-CNTs (up to 20%) targeting either diuron or atrazine, with data for a pure PAN ENM provided for comparison (see the dashed line). We observed linear relationships between $\log K_{ENM-W}$ values and CNT mass loading for PAN composites (**Figure 3-10**), with regression p values ≤ 0.02 and correlation coefficients (R^2 values) ≥ 0.97 . This dependence of chemical uptake on the CNT content

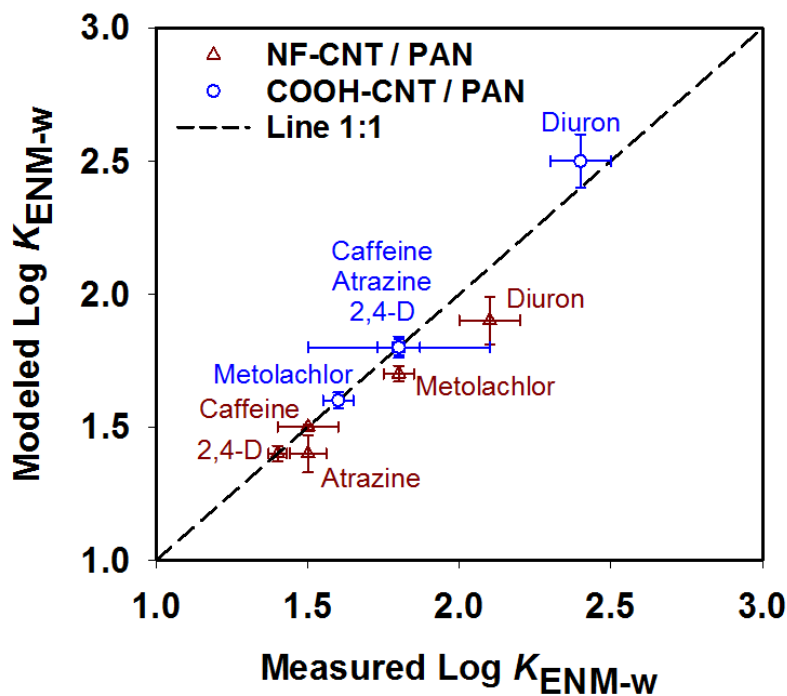


Figure 3-9. Model-estimated $\log K_{ENM-W}$ values obtained from the first-order uptake equation plotted as a function of experimentally measured $\log K_{ENM-W}$ values. To assist with comparison, a 1-to-1 line (dashed) is shown, corresponding to perfect agreement between model-estimated and experimentally measured values.

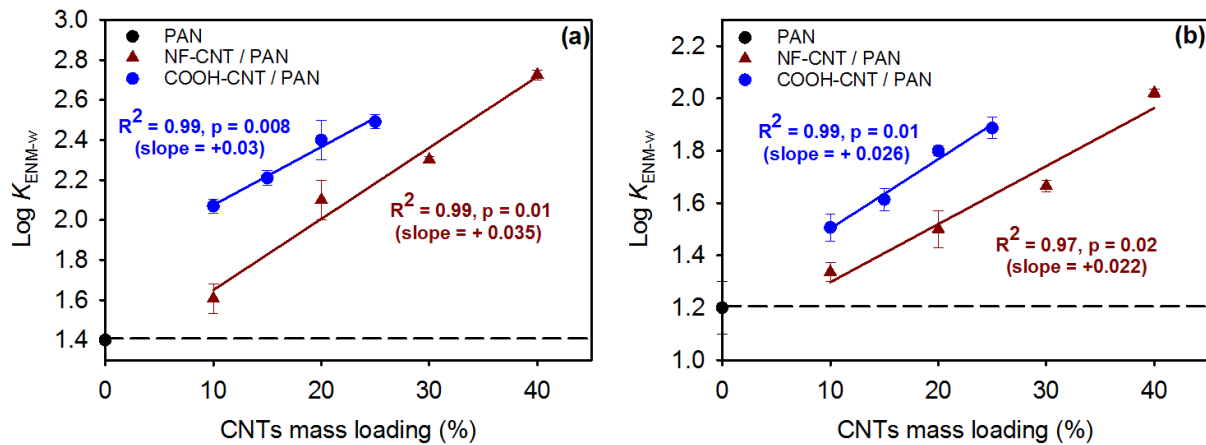


Figure 3-10. Values of $\log K_{ENM-W}$ as a function of NF-CNT and COOH-CNT mass loading (as wt%) in the ENM composite. Data are shown for (a) diuron and (b) atrazine. Lines represent the results of linear regression analysis on experimental data, where uncertainties associated with individual data points are standard deviation from at least three replicate experiments. The dashed line indicates the $\log K_{ENM-W}$ value measured for a pure PAN ENM and is provided for comparison. Experimental conditions: pH 7 (1 mM phosphate); initial concentration of diuron: 5.8 mg/L and atrazine: 5.4 mg/L; ENM loading: ~1.5 g/L. Experiments were carried out under a static condition.

of the composite implies a key role of the embedded CNTs in chemical partitioning, similar to what we previously observed for composites of carbon nanofibers where embedded CNTs functioned as the active sorbent site.¹⁶¹ As shown in **Figure 3-11** and **Figure 3-12**, composite surface area and pore volume remain useful predictors of overall contaminant uptake, with larger $\log K_{ENM-W}$ values being observed for composites with greater surface area and pore volume. However, there is still a clear distinction between these correlations for COOH-CNT and NF-CNTs, suggesting that gains in surface area from induced pore volume are not solely responsible for higher organic chemical partitioning in CNT-containing composite ENMs.

Given the impact of composite surface area on chemical uptake, a final performance variable that we considered was the average diameter of the composite nanofiber mat, where

smaller diameter nanofibers are expected to exhibit greater surface area. In our prior work with pure polymer ENMs, we found that smaller diameter nanofibers resulted in faster rates of chemical uptake via diffusive exchange but did not impact equilibrium $\log K_{EMN-W}$ values. Here, we prepared three sizes of NF-CNT/PAN nanofiber mats by varying the wt% of PAN used in the electrospinning precursor solution while holding the relative mass of non-functionalized CNTs constant at 20% wt. Across the average diameters of 70 (± 20), 210 (± 50), and 320 (± 90) nm for these NF-CNT/PAN composites, equilibrium $\log K_{EMN-W}$ values for caffeine, diuron, atrazine and metolachlor were unchanged (see **Table 3-6**).

It is notable that $\log K_{EMN-W}$ values scale with changes in surface area resulting from increasing CNT mass loading in ENM-CNT composites, but they do not vary with the surface area of the nanofiber composites (at a fixed CNT mass loading) when surface area is changed by altering the average nanofiber diameter. Taken together, this implies that increases in chemical uptake with increasing CNT mass loading are primarily driven by the introduction of new binding sites, presumably on the surface of CNTs that remain accessible to solution in the near surface region, and not simply increasing surface area of the composite.

Table 3-6. Values of $\log K_{EMN-W}$ for NF-CNT/PAN with different average diameters. All ENM-CNT composites were fabricated at 20% wt. of NF-CNT, but the wt.% of PAN was varied to alter average diameter values.

	6% PAN (70 \pm 20 nm)	8.5% PAN (210 \pm 50 nm)	10% PAN (320 \pm 90nm)
Caffeine	1.5 \pm 0.05	1.5 \pm 0.1	1.6 \pm 0.08
Diuron	2.2 \pm 0.06	2.1 \pm 0.1	2.3 \pm 0.08
Atrazine	1.5 \pm 0.03	1.5 \pm 0.07	1.7 \pm 0.05
Metolachlor	1.7 \pm 0.05	1.8 \pm 0.05	1.8 \pm 0.009

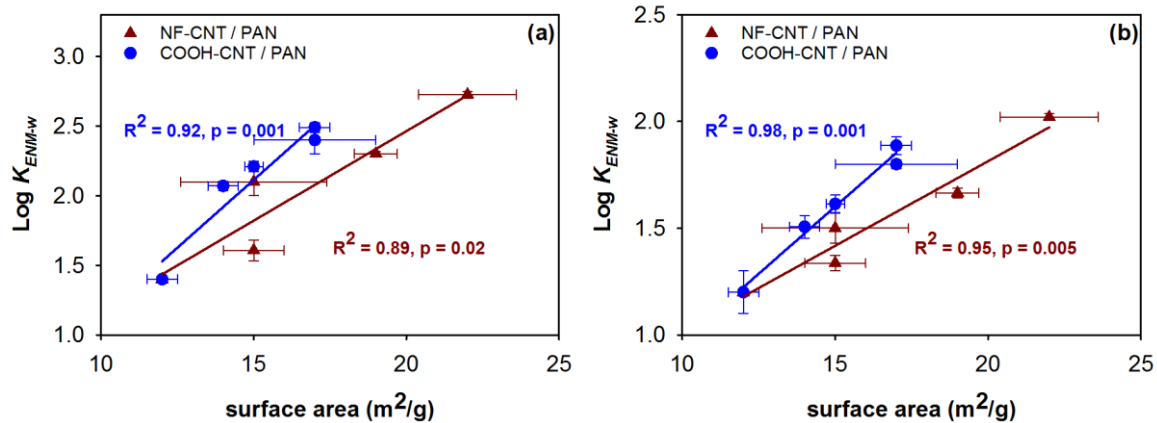


Figure 3-11. Values of $\log K_{ENM-W}$ as a function of ENM surface area (from BET in m^2/g). Data are shown for (a) diuron and (b) atrazine. Lines represent the results of linear regression analysis on experimental data, where uncertainties associated with individual data points are standard deviation from at least three replicate experiments. Experimental conditions: pH 7 (1 mM phosphate); initial concentration of diuron: 5.8 mg/L and atrazine: 5.4 mg/L; ENM loading: ~ 1.5 g/L. Experiments were carried out under a static condition.

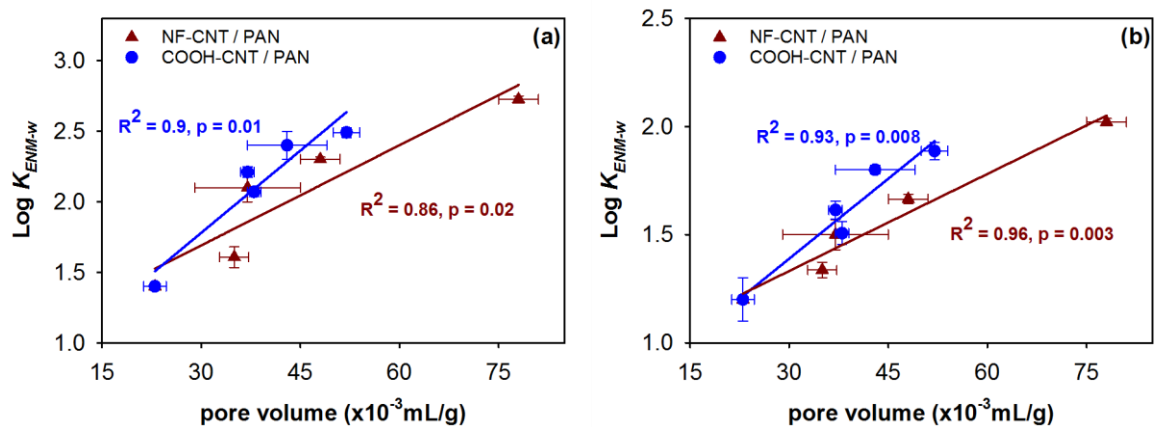


Figure 3-12. Values of $\log K_{ENM-W}$ as a function of ENM pore volume ($\times 10^{-3}$ mL/g). Data are shown for (a) diuron and (b) atrazine. Lines represent the results of linear regression analysis on experimental data, where uncertainties associated with individual data points are standard deviation from at least three replicate experiments. Experimental conditions: pH 7 (1 mM phosphate); initial concentration of diuron: 5.8 mg/L and atrazine: 5.4 mg/L; ENM loading: ~ 1.5 g/L. Experiments were carried out under a static condition.

Influence of the polymer matrix on ENM composite sorption performance. To more systematically explore the influence of the polymer matrix on ENM-CNT performance, we examined the uptake of 11 hydrophilic and moderately hydrophilic compounds (HMHCs) on two types of ENM-CNT composites (at 20% wt.) fabricated from PAN and polystyrene (PS). Values of $\log K_{EMN-W}$ for the model compound suite are displayed in **Figure 3-13** and tabulated in **Table 3-7**.

Generally, the behavior of PAN-based composites was as expected from our initial results exploring a smaller subset of organic targets. Values of $\log K_{EMN-W}$ (i.e., chemical partitioning into the ENM) increased with CNT/PAN formulations relative to unmodified PAN mats for all 11 organic targets, and the composites with COOH-CNTs outperformed composites fabricated with NF-CNTs. However, the extent of increase in $\log K_{EMN-W}$ for CNT/PAN composites was highly variable and dependent on the organic target; the largest increases (0.7 to 1-log unit) were observed for diuron, *p*-nitrophenol, and 2,4-D, while more modest increases (~0.1 to 0.3-log units) were measured for aniline and phenol. This variable impact of CNTs on uptake is visualized in **Figure 3-14a**, which compares $\log K_{EMN-W}$ values for the CNT/PAN composites with those values measured with unmodified PAN (labeled $\log K_{EMN-W0}$ values). Also shown in **Figure 3-14a** is a 1-to-1 line (i.e., indicating when the $\log K$ values are equal for both CNT/PAN and unmodified PAN). Data points falling above the dashed line indicate higher partitioning into CNT-containing materials, which is the case for the overwhelming majority of organic targets on CNT/PAN composites.

Somewhat different behavior was observed for PS-based composites, where $\log K_{EMN-W}$ values increased for some, but not all, chemical targets upon the integration of CNTs.

For example, there were several instances where neither NF-CNTs nor COOH-CNTs significantly improved uptake (e.g., phenol, nitrobenzene, *p*-nitrophenol) and even one instance, anisole, where partitioning was lower on CNT-containing composites. The oftentimes comparable performance of CNT/PS composites and unmodified PS is visualized in **Figure 3-14b**, where data for several HMHCs fall on or near the 1-to-1 line, indicative of equivalent $\log K_{EMN-W}$ values. Only for atrazine, diuron, 2,4-D and metolachlor (both a racemic mixture and enantiomerically pure *S*-metolachlor) did both NF- and COOH-CNTs increase partitioning, typically with COOH-CNTs better promoting uptake.

We note that for caffeine, diuron, and 2,4-D, extraction of mass bound to CNT/PS was less effective using methanol, producing recoveries of only 10-40% that were well below recoveries of other HMHCs on other ENMs using methanol (typically >90%). Accordingly, $\log K_{EMN-W}$ values reported for these chemicals on NF-CNT/PS and COOH-CNT/PS were estimated using mass balance (i.e., the difference between the initial and equilibrium aqueous concentration was assumed to be the PS-based ENM associated mass) rather than analytically measured C_W and C_{ENM} values.

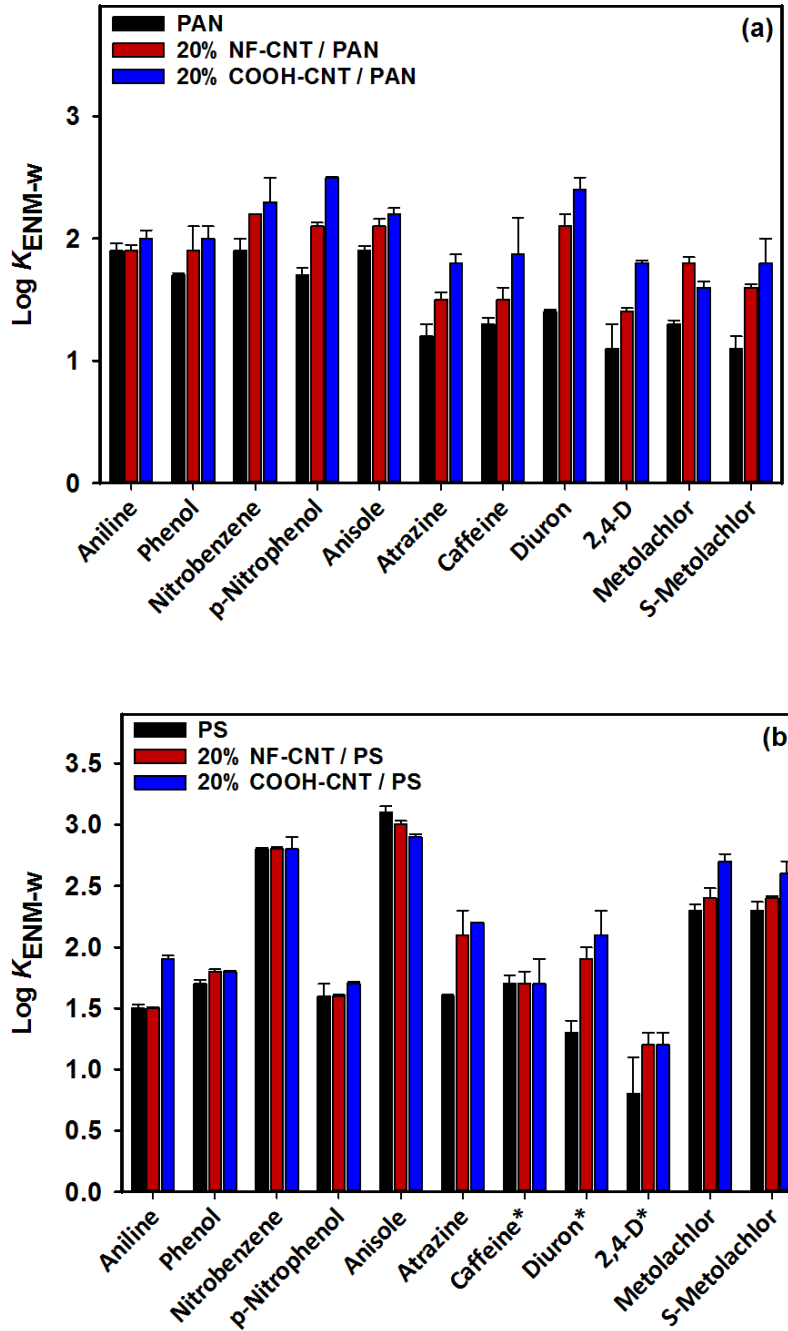


Figure 3-13. Comparison of $\log K_{ENM-W}$ values for (a) PAN-based ENMs and (b) PS-based ENMs. Data are shown for pure polymers, as well as composites made with NF-CNT and COOH-CNT. Uncertainties represent standard deviations from at least triplicate measurements. Note: $\log K_{ENM-W}$ values on CNT/PS for chemicals with an asterisk were estimated by mass balance (see text).

Table 3-7. Summary of ENM-water equilibrium partition coefficients for selected model compounds (log units, L/kg). Values are provided for pure polymers (PS and PAN), as well as composites made with NF-CNT and COOH-CNT. Values determined at pH 7 for an initial chemical concentration of 25 μ M and an ENM loading of ~1.5 g/L. Uncertainties represent standard deviations from at least triplicate measurements.

Compound	PAN	20% NF-CNT PAN	20% COOH- CNT PAN	PS	20% NF-CNT PS	20% COOH-CNT PS
Aniline (<i>n</i> =2)	1.9 \pm 0.06	1.9 \pm 0.05	2.0 \pm 0.07	1.5 \pm 0.03	1.5 \pm 0.01	1.9 \pm 0.03
Phenol (<i>n</i> =2)	1.7 \pm 0.02 ^a	1.9 \pm 0.2	2.0 \pm 0.1	1.7 \pm 0.03 ^a	1.8 \pm 0.02	1.8 \pm 0.01
Nitrobenzene (<i>n</i> =2)	1.9 \pm 0.1	2.2 \pm 0.004	2.3 \pm 0.2	2.8 \pm 0.01	2.8 \pm 0.02	2.8 \pm 0.1
4-Nitrophenol (<i>n</i> =2)	1.7 \pm 0.06	2.1 \pm 0.03	2.5 \pm 0.007	1.6 \pm 0.1	1.6 \pm 0.01	1.7 \pm 0.02
Anisole (<i>n</i> =2)	1.9 \pm 0.04	2.1 \pm 0.06	2.2 \pm 0.05	3.1 \pm 0.05	3.0 \pm 0.03	2.9 \pm 0.02
Atrazine (<i>n</i> =3)	1.2 \pm 0.1 ^a	1.5 \pm 0.07	1.8 \pm 0.02	1.6 \pm 0.01	2.1 \pm 0.2	2.2 \pm 0.004
Caffeine (<i>n</i> =3)	1.3 \pm 0.05 ^a	1.5 \pm 0.1	1.8 \pm 0.3	1.7 \pm 0.07 ^a	1.7 \pm 0.1	1.7 \pm 0.2
Diuron (<i>n</i> =3)	1.4 \pm 0.02 ^a	2.1 \pm 0.1	2.4 \pm 0.1	1.3 \pm 0.1 ^a	1.9 \pm 0.1	2.1 \pm 0.2
2,4-D (<i>n</i> =6)	1.1 \pm 0.2 ^a	1.4 \pm 0.02	1.8 \pm 0.03	0.8 \pm 0.3 ^a	1.2 \pm 0.1 ^a	1.2 \pm 0.1 ^a
Metolachlor (<i>n</i> =3)	1.3 \pm 0.03	1.8 \pm 0.05	1.6 \pm 0.05	2.3 \pm 0.05	2.4 \pm 0.08	2.7 \pm 0.06
s-Metolachlor (<i>n</i> =3)	1.1 \pm 0.1	1.6 \pm 0.03	1.8 \pm 0.2	2.3 \pm 0.07	2.4 \pm 0.02	2.6 \pm 0.1

^a Less than 5% of the total aqueous mass was sorbed into the ENM.

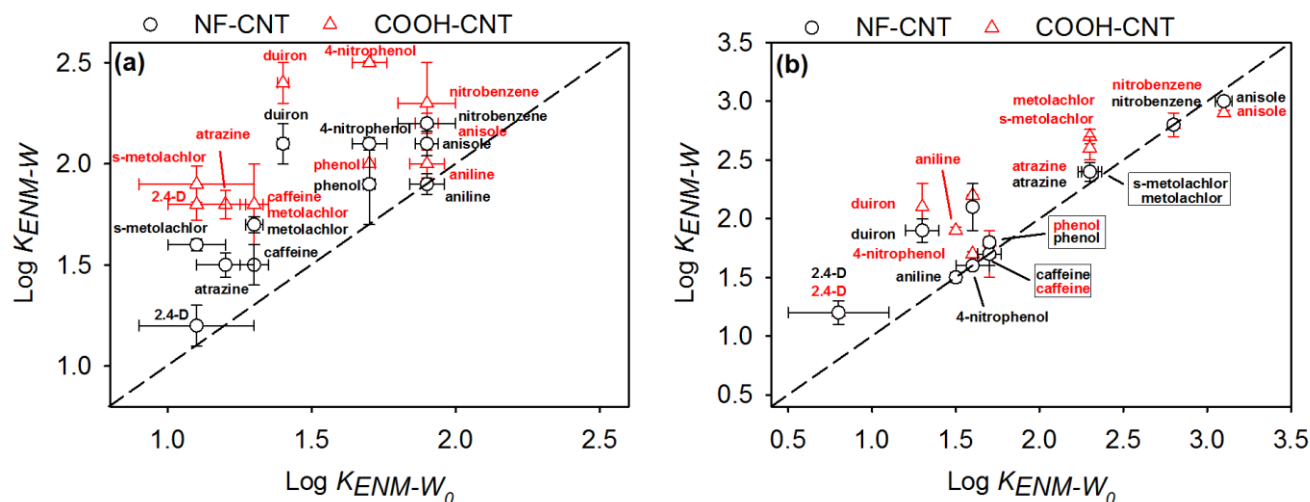


Figure 3-14. $\text{Log}K_{ENM-W_0}$ VS ENM $\text{log}K_{ENM-W}$ plots. (a) CNTs modified PAN and (b) CNTs modified PS. To assist with comparison, a 1:1 line (dashed) is shown. Uncertainties associated with individual data points are standard deviation from at least three replicate experiments.

Insights from chemical structure-ENM activity relationships. To better understand the chemical characteristics driving organic partitioning into ENM-CNTs, we assembled chemical structure-ENM activity relationships from known physicochemical properties of our target analyte suite and measured $\text{log}K_{EMN-W}$ values (**Figure 3-15**). We focused particularly on measures of compound hydrophobicity via potential dependencies of $\text{log}K_{EMN-W}$ values on either octanol-water partitioning coefficients ($\text{log}K_{ow}$ values) or hexadecane-water partitioning coefficients ($\text{log}K_{Hexadecane-w}$) values. While $\text{log}K_{ow}$ values have long been used as a measure of organic chemical hydrophobicity, some have suggested that $\text{log}K_{Hexadecane-w}$ may better predict equilibrium partitioning of moderately hydrophobic compounds on sorbent materials typically used in passive sampling devices.^{76, 227}

For CNT-modified PAN mats (**Figure 3-15a** and **Figure 3-15c**), there was no clear relationship with either descriptor. The lack of dependence of $\log K_{EMN-W}$ values on compound hydrophobicity suggests that partitioning is likely occurring via some other mechanism, likely involving more specific binding interactions (e.g., hydrogen bonding, van der Waals forces). From an application standpoint, the relative independence of $\log K_{EMN-W}$ values on compound hydrophobicity for CNT/PAN ENMs is encouraging, particularly for the aim of developing a passive sampling material suitable for targeting a wide range of chemically diverse pollutants (e.g., from polar to hydrophobic).

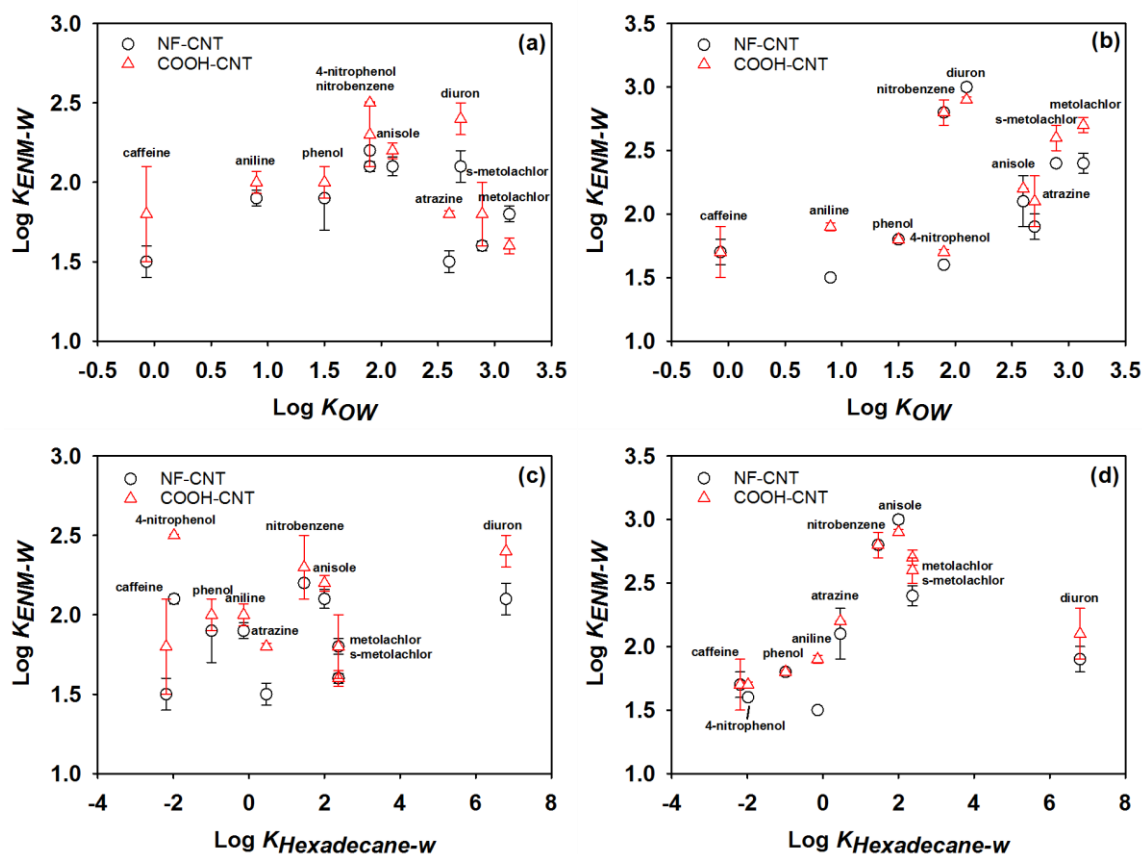


Figure 3-15. Correlations between $\log K_{ENM-W}$ and (a, b) $\log K_{OW}$ and (c, d) $\log K_{Hexadecane-W}$ for (left column) CNT/PAN and (right column) CNT/PS. Uncertainties associated with individual data points are standard deviations from at least three replicate experiments. We note that data for 2,4-D is not included in this analysis because it is anionic in our experimental systems.

For CNT/PS composites, structure-activity relationships provide evidence that hydrophobic partitioning contributes to chemical uptake. Values of $\log K_{EMN-W}$ were effectively equivalent (between ~1.5-2.0) for most compounds with $\log K_{ow} < 2$. However, $\log K_{EMN-W}$ were greater than 2.0, and in some cases considerably, for the majority of chemicals with $\log K_{ow}$ values > 2 . This clustering suggests that for moderately hydrophobic chemicals, hydrophobic partitioning helps to drive uptake on NF-CNT/PS and COOH-CNT/PS. More evidence for this behavior is provided from comparisons with $\log K_{Hexadecane-w}$ values, where a clear linear correlation exists between increasing $\log K_{EMN-W}$ and $\log K_{Hexadecane-w}$ values, with the exception of diuron. For PS-based materials, $\log K_{Hexadecane-w}$ values appear to be a better predictor of organic compound partitioning than $\log K_{ow}$ values. Furthermore, relative to CNT/PAN, CNT/PS composites may be best-suited for analysis of moderately hydrophobic and hydrophobic pollutant classes.

Comparing ENM-CNT sorption capacity and reactivity trends to CNT suspensions.

To explore the sorption capacity of ENM-CNT composites, and determine whether it was sufficiently in excess of probable environmental concentrations to be encountered during passive sampling applications, we conducted sorption isotherms with PAN-based ENM composites. Isotherms were collected at pH 7 with both COOH-CNT and NF-CNT composites using diuron and caffeine (up to ~40 mg/L initial concentration) as model organic pollutant targets.

Generally, isotherms were non-linear for both COOH-CNT and NF-CNT composites. No clear plateau in uptake was observed, as would be expected for Langmuir-type sorption. Thus, we modeled all isotherms according to the Freundlich isotherm model (Equation 3-4), which empirically relates the ENM-bound mass to that remaining in solution at equilibrium:

$$C_{ENM} = K_F \cdot C_W^{1/n} \quad (3-4)$$

In Equation 3-4, K_f (L/g) is the Freundlich sorption coefficient and n (dimensionless) is a measure of isotherm non-linearity. Results of these Freundlich model fits were obtained via linear regression analysis after log-log transformation of Equation 3-4, and model outputs (K_f and n) are summarized in **Table 3-8**.

Table 3-8. Summary of K_f and n values from Freundlich model fits to sorption isotherms for diuron and caffeine obtained with CNT/PAN composites. Uncertainties represent standard error associated with regression analysis.

Sorbent	Diuron			Caffeine		
	K_f (L/g)	n	R^2	K_f (L/g)	n	R^2
NF-CNT/PAN	0.44 ± 0.04	2.5 ± 0.18	0.99	0.12 ± 0.03	1.6 ± 0.19	0.97
COOH-CNT/PAN	1.25 ± 0.08	2.6 ± 0.14	0.99	0.34 ± 0.03	2.4 ± 0.16	0.99

The largest values of K_f were observed for diuron, consistent with its higher affinity for CNT/PAN (e.g., the uptake of diuron approached 4 mg/g at the highest initial concentration considered compared to only 1.5 mg/g for caffeine). Diuron isotherms also exhibited the greatest degree of non-linearity (based on the larger n values). For field applications, this non-linearity is not ideal, as it suggests that $\log K_{\text{ENM-w}}$ values may be dependent on the aqueous concentration of the target analyte. However, the concentrations considered in these isotherm experiments (up to ~40 mg/L) are far in excess of environmentally relevant concentrations (at most 10-100's of $\mu\text{g/L}$). As we previously observed for pure polymer ENMs in Chapter 2, it is likely chemical uptake at the lower concentrations more representative of surface waters and sediments can be reasonably approximated as linear, which would enable the use of $\log K_{\text{ENM}}$ value for calculating environmental concentrations according to Equation 3-2.

Also in **Figure 3-16**, we present sorption isotherms for diuron and caffeine in suspensions (typically between 0.03-0.05 g/L) of COOH-CNTs and NF-CNTs powders at pH 7.

These data are provided to compare the relative capacity of freely dispersed CNTs to CNTs embedded into PAN composites, where we anticipate the integration of CNTs with PAN will result in some loss of capacity due to loss of CNT surface upon immobilization in the PAN matrix.

Indeed, isotherm results indicate that sorption capacity (in mg of chemical per g of sorbent) of CNTs powders is ~100-fold larger than that of CNT-ENMs. Even after normalizing diuron and caffeine uptake on composites to the percentage of CNT mass within the ENMs (20% wt.), the sorption capacity of nanofiber embedded CNTs is only ~5% of that in CNT suspensions. Thus, through the process of embedding the CNTs into the polymer matrix, a considerable amount of sorption capacity is lost presumably through CNT aggregation²²⁸ and direct interaction between CNT and PAN.^{215, 229}

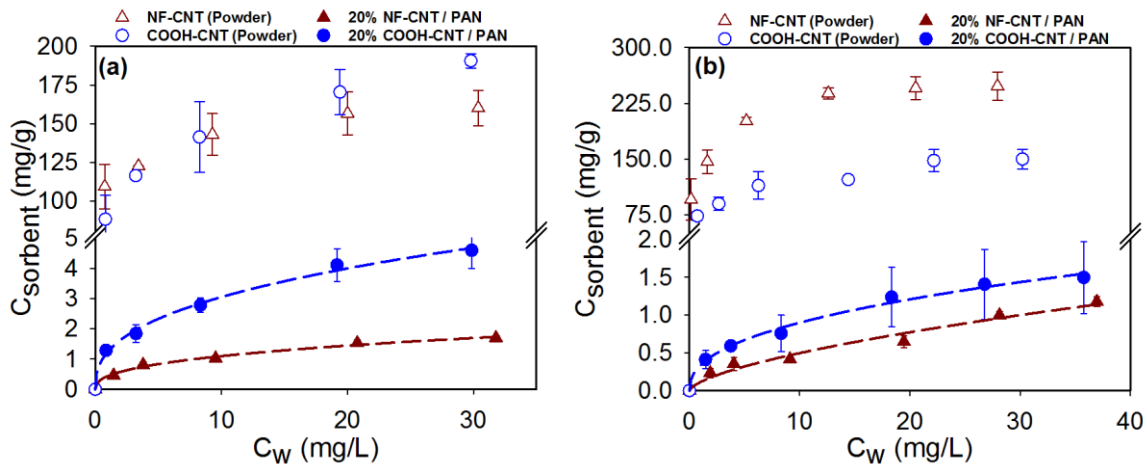


Figure 3-16. Sorption isotherms for (a) diuron and (b) caffeine. Data are shown for NF-CNT/PAN and COOH-CNT/PAN (solid symbols) as well as NF-CNT and COOH-CNT suspensions (open symbols). Please note that the y-axis is broken into two sections to span the range of sorbed concentrations measured across the different sorbents types. Dash lines represent Freundlich isotherm model fits, where K_f and n values are summarized in **Table 3-8**. Uncertainties associated with individual data points are standard deviations from at least three replicate experiments.

Beyond the large differences in capacity, another notable difference is the relative uptake of the target chemicals on NF-CNTs and COOH-CNTs in suspension versus when these materials are embedded within the PAN matrix. For caffeine, composites with COOH-CNT tended to result in greater uptake than composites with NF-CNTs. However, in suspension, NF-CNTs (capacity ~ 225 mg/g) clearly outperformed their oxidized counterparts (capacity ~150 mg/g). Likewise, while composites with COOH-CNT exhibited greater uptake of diuron than composites with NF-CNTs, there was little difference in uptake between the two types of CNT surface chemistries in suspensions. These relative sorption trends strongly suggest that the integration of CNTs into the polymer matrix produces a composite with behavior as a sorbent that is distinct and unique relative to the building blocks from which the composite is assembled.

To further explore how immobilization of CNTs within the polymer matrix altered CNT sorption behavior, we compared $\log K_{\text{ENM}}$ values from CNT/PAN composites to single-point partitioning coefficients ($\log K_d$ values) from CNT suspensions for our entire model compound suite ($n = 11$ organic targets). These sorption cross correlations are shown in **Figure 3-17**, but there is no apparent relationship between the extent of chemical uptake in CNT suspensions and that observed for CNT/PAN or CNT/PS, regardless of whether NF-CNTs or COOH-CNTs were used. Thus, the mechanisms and interactions responsible for organic chemical sorption on CNTs must be distinct from those in ENM-CNT composites. Rather, although the integration of CNTs is clearly responsible for increasing target analyte uptake in ENM composites relative to pure polymer ENMs, the composite materials behave as a new type of sorbent with binding sites distinct from the individual materials from which it was constructed.

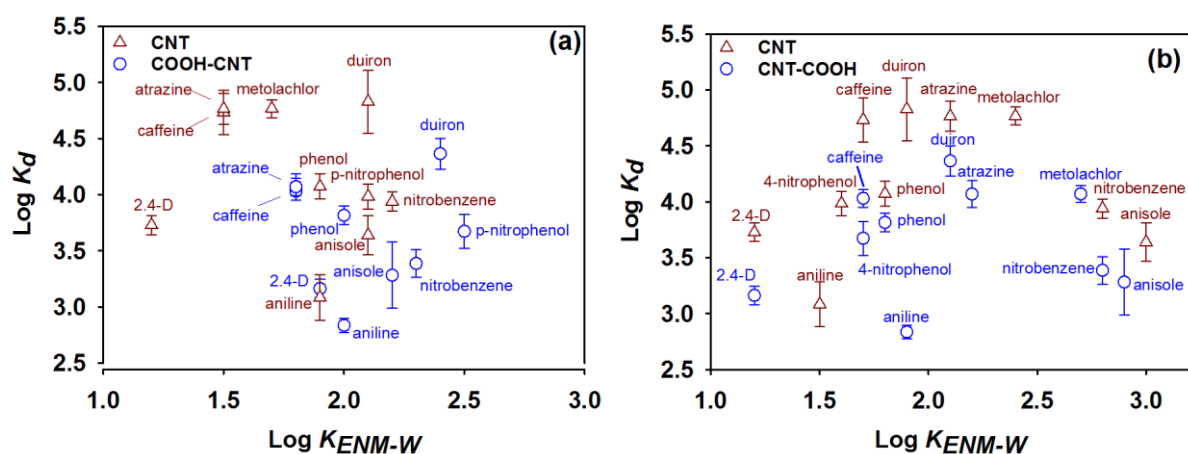


Figure 3-17. Reactivity cross correlations between $\log K_d$ values measured in CNT suspensions and $\log K_{ENM-W}$ values measured with CNT-ENM composites. Data are shown (a) CNT/PAN and (b) CNT/PS composites. Uncertainties associated with individual data points are standard deviations from at least three replicate experiments.

Practical considerations for ENM composite field applications. With the ultimate goal being the field deployment of optimal ENM-composites for testing as passive sampling devices, variables associated with their use in such applications were also considered. There are both environmental factors (e.g., temperature, aqueous pH) and design considerations (e.g., the amount of ENM deployed) that may influence performance, and select variables were experimentally assessed herein.

Influence of pH on ENM sorption performance. Solution pH may influence organic chemical partitioning into ENMs if the chemical is ionizable and/or the surface of the ENM has ionizable groups, as would be the case for COOH-CNTs (which are expected to be deprotonated at pH 7). We examined the uptake of 2,4-D, an anionic pesticide across environmentally relevant pH values (pK_a of 2.73),²³⁰ at pH 5 and 7. By all measures (e.g., C_W , C_{ENM} , and

$\log K_{ENM-W}$ values), 2,4-D uptake was unaffected across this pH range for PS- and PAN-based ENMs with either NF-CNT or COOH-CNTs (at 20% wt.) (see **Table 3-9**).

Table 3-9. Values of $\log K_{ENM-W}$ and C_{ENM} (measured after 48 h) for 2,4-D on CNT/PS and CNT/PAN composites at pH 5 and 7. Uncertainties are standard deviations obtained from the number of replicates (n) indicated.

	Log K_{ENM-W} (pH~5)	Log K_{ENM-W} (pH~7)	C_{ENM} (mg/g) (pH~5)	C_{ENM} (mg/g) (pH~7)
20% NF-CNT/PAN (n=4)	1.4 ± 0.07	1.4 ± 0.02	0.12 ± 0.04	0.09 ± 0.02
20% COOH-CNT /PAN (n=4)	1.9 ± 0.1	1.8 ± 0.03	0.6 ± 0.1	0.4 ± 0.02
20% NF-CNT/PS (n=3)	1.2 ± 0.06	1.2 ± 0.1	0.1 ± 0.005	0.1 ± 0.03
20% COOH-CNT /PS (n=3)	1.2 ± 0.07	1.2 ± 0.1	0.09 ± 0.02	0.09 ± 0.01

Influence of temperature on ENM sorption performance. Temperature, particularly the range experienced across seasons, may also influence passive sampler performance including chemical uptake rate, sorption capacity and equilibrium partitioning behavior.²³¹⁻²³⁴ We examined atrazine and 2,4-D uptake at temperatures of 4°C, 20°C and 35°C on PAN-based ENMs with both NF-CNTs and COOH-CNTs (at 20% wt.). From measured $\log K_{ENM-W}$ values across this temperature range (**Table 3-10**), equilibrium partitioning appears independent of temperature for PAN-based ENM-CNTs; although there were some slight fluctuations, all $\log K_{ENM-W}$ values were within the margin of error.

Table 3-10. Values of $\log K_{ENM-W}$ for atrazine and 2,4-D measured at different temperatures on CNT/PAN composites. Uncertainties associated represent standard deviations from at least three replicate experiments.

	Atrazine			2,4-D		
	4°C	20°C	35°C	4°C	20°C	35°C
20% NF-CNT/PAN	1.6 ± 0.06	1.5 ± 0.07	1.5 ± 0.1	1.4 ± 0.01	1.4 ± 0.02	1.4 ± 0.003
20% COOH-CNT/PAN	2.0 ± 0.02	1.8 ± 0.02	1.9 ± 0.06	1.7 ± 0.05	1.8 ± 0.03	1.7 ± 0.05

Influence of ENM mass loading on sorption performance. For chemical targets with a relatively low affinity for ENMs, a useful approach to increasing the target mass collected in the field would be the use of a higher total mass of passive sampling material. To confirm that $\log K_{ENM-W}$ values are independent of the mass of ENM deployed during field testing, we examined uptake of 2,4-D, diuron and atrazine on PS- and PAN-based ENMs with NF-CNTs and COOH-CNTs (at 20% wt.) in systems ranging from 25 to 100 mg of total ENM mass. As expected for a sorption process, doubling the mass of sorbent in the system resulted in more target analyte mass accumulating into the ENM and being drawn down from the aqueous phase (**Table 3-11** and

Table 3-12). Nevertheless, equilibrium partitioning scaled linearly with total ENM mass in all cases, producing $\log K_{ENM-W}$ values that were independent of total ENM mass. This is consistent with a linear regime for equilibrium partitioning and enables the use of higher ENM mass to increase the sensitivity and detection limits of results obtained during field deployments.

Table 3-11. Values of $\log K_{ENM-W}$ and total mass in ENM (M_{ENM} measured after 48 h) for 2,4-D on CNT/PS and CNT/PAN composites in systems with either 50 or 100 mg of ENM mass. Uncertainties are standard deviations obtained from the number of replicates (n) indicated.

	Log K_{ENM-W} (50 mg)	Log K_{ENM-W} (100 mg)	M_{ENM} (μ g) (50 mg)	M_{ENM} (μ g) (100 mg)
20% NF-CNT/PAN (n=4)	1.4 \pm 0.02	1.4 \pm 0.01	5.0 \pm 1.0	9.0 \pm 2.1
20% COOH-CNT/PAN (n=4)	1.8 \pm 0.03	1.8 \pm 0.02	19.5 \pm 1.9	43.5 \pm 2.9
20% NF-CNT/PS (n=3)	1.2 \pm 0.1	1.2 \pm 0.04	4.3 \pm 1.1	9.7 \pm 0.4
20% COOH-CNT/PS (n=3)	1.2 \pm 0.1	1.2 \pm 0.1	4.8 \pm 1.0	8.5 \pm 1.6

Table 3-12. Values of $\log K_{ENM-w}$ and total mass in ENM (M_{ENM} measured after 48 h) for diuron and atrazine COOH-CNT/PAN and NF-CNT/PAN in systems with either 25, 50 or 100 mg of ENM mass.

	Log K_{ENM-w} (25 mg)	Log K_{ENM-w} (50 mg)	Log K_{ENM-w} (100 mg)	M_{ENM} (μ g) (25 mg)	M_{ENM} (μ g) (50 mg)	M_{ENM} (μ g) (100 mg)
Diuron						
20% COOH-CNT PAN	3.37	3.41	3.38	61.9	103.2	196.4
Atrazine						
20% NF-CNT PAN	2.69	2.8	2.79	45.6	93.8	178.9

Note: Values of $\log K_{ENM-w}$ in this table are higher than others reported for diuron and atrazine with these same materials because a different batch of CNTs was used for synthesis of these materials. That batch of CNTs exhibited greater activity than the batch used in all other experiments conducted in this work.

Field demonstration of ENM-CNT composites as passive sampling materials. Before conducting an on-site deployment of ENM-CNT samplers, we first conducted uptake experiments with atrazine and 2,4-D using Iowa River water collected from the inlet of the University of Iowa water plant (**Figure 3-18**) to test performance in a more complex matrix.

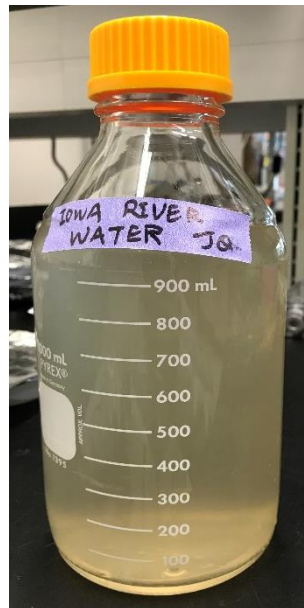


Figure 3-18. Iowa River water collected at the inlet to the University of Iowa Water Treatment Plant.

Table 3-13. Comparison of $\log K_{ENM-W}$ values for atrazine and 2,4-D on NF-CNT/PAN and COOH-CNT/PAN (20% wt.) measured in model phosphate buffer systems (DI water) and Iowa River Water.

	Atrazine		2,4-D	
	DI water (pH~7)	Iowa River water (pH~7.9)	DI water (pH~7)	Iowa River water (pH~7.9)
20% NF-CNT/PAN	1.5 ± 0.07	1.7 ± 0.1	1.4 ± 0.02	1.4 ± 0.06
20% COOH-CNT/PAN	1.8 ± 0.02	1.8 ± 0.07	1.8 ± 0.03	1.6 ± 0.1

The results of these experiments are summarized in **Table 3-13**. Generally, values of K_{ENM-W} for CNT/PAN ENMs did not change significantly in Iowa River water despite the higher pH (7.9) and high alkalinity, hardness, organic matter, and suspended solids concentration of the Iowa River water. Accordingly, the K_{ENM-W} values we report from model experimental systems as summarized in **Table 3-7** seem appropriate for use in estimating chemical concentrations in more complex aquatic environments via Equation 3-5:

$$C_{SW} = \frac{m_i}{m_{ENM}} \times K_{ENM-W} \quad (3-5)$$

where C_{SW} is the chemical concentration (ng/L) in the surface water, m_i is the mass (ng) of the chemical accumulated in the ENM, and m_{ENM} is the ENM mass used in the deployment (g).

Field deployment of CNT/PAN ENMs were conducted at Muddy Creek, Iowa for the measurement of atrazine. USGS measured atrazine concentrations at the Muddy Creek site obtained from grab sampling between September 2017 and February 2018 are shown in **Figure 3-19**, while the concentration data collected after 48 hour deployments of our ENMs are provided for comparison starting in December of 2017 through May 2018. Generally, both NF-CNT/PAN and COOH-CNT/PAN performed comparably during field deployment, producing

atrazine concentrations generally on the order of 40-60 ng/L across the sampling period. These ENM-measured concentrations agree well with those obtained through USGS grab sampling, which varies from ~15 to 65 ng/L over their sampling period. Notably, in December 2017, USGS data were collected at nearly the identical time as our ENM deployment, yielding atrazine concentrations of 18.2 ng/L (USGS grab sample), 55.4 ng/L (NF-CNT/PAN) and 27.3 ng/L (COOH-CNT/PAN). While more field validation is warranted, we are encouraged by these initial proof-of-concept deployment studies, where CNT-modified ENMs produced atrazine concentrations typical and as expected for Muddy Creek during the time of year corresponding to our deployment.

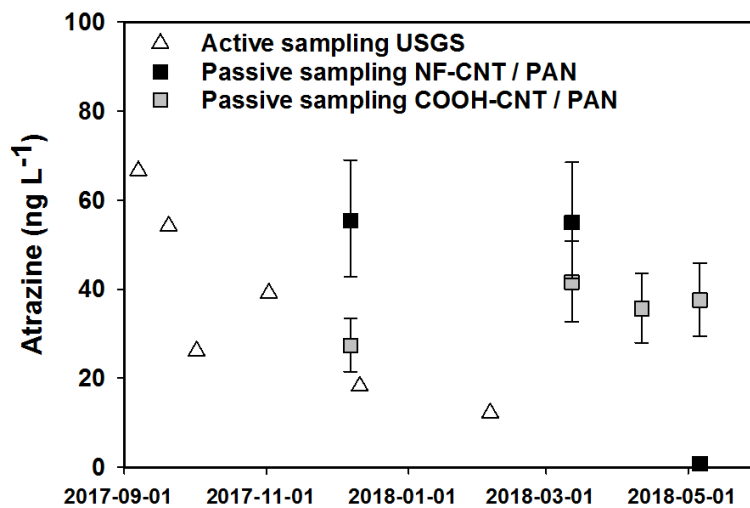


Figure 3-19. Atrazine concentration in Muddy Creek measured by ENM-CNT composites and active sampling methods. Uncertainties associated with individual data points are standard deviations reflecting the uncertainty associated with measured K_{ENM-W} values and instrument analytical error.

3.5 CONCLUSIONS AND ENVIRONMENTAL IMPLICATIONS

Carbon nanotubes (CNTs) provide a significant improvement in the uptake of polar and moderately hydrophobic organic pollutants on polymer electrospun nanofiber mats (ENMs). Not only is the extent of organic pollutant partitioning enhanced, but CNT-modified ENMs also exhibit fast uptake rates even in the absence of mixing (i.e., static sampling conditions). For nearly all organic targets, equilibrium is achieved over several hours, which will allow the optimally performing ENM-CNT composites to be used as equilibrium passive sampling devices for daily monitoring of organic pollutants in surface water and sediments.

Through complementary materials characterization, evidence suggests that CNTs represent the primary site for organic chemical uptake, while their inclusion also increases surface area and pore volume of the ENM. Accordingly, values of $\log K_{\text{ENM-w}}$, which reflect ENM uptake capacity, increase with increasing CNT mass loading in the composite. However, through the examination of reactivity cross-correlations, which compare the performance of ENM-CNT composites with the performance of either pure polymer ENMs or CNT suspensions, CNT/PAN and CNT/PS composites exhibit unique behavior as sorbents relative to the individual components from which they are constructed.

A field deployment in surface water to measure the concentration of atrazine illustrates that ENM-CNT composites can performance on par with more traditional sampling approaches (e.g., grab sampling), even in complex media and sampling conditions. Integration of CNTs enhances the mechanical strength and robustness of the composites, which helps maintain their integrity even in flowing surface water. Further, there was no evidence of biofouling, nor any confounding interference from other environment constituents (e.g., colloidal or dissolved organic matter, hardness, and alkalinity) anticipated at field sampling sites.

While the performance results for ENM-CNT composites toward polar and moderately hydrophobic organic compounds are promising, there remain opportunities for further improvements, especially where $\log K_{\text{ENM-w}}$ values remain relatively low (e.g., small, highly polar and/or ionic organic targets). Also, more field testing is required to validate our laboratory results, focusing on a broader suite of target organic pollutants expected in surface waters and sediment systems impacted by agricultural runoff and wastewater effluent discharges.

CHAPTER 4 SURFACTANT-ASSISTED FABRICATION OF POLYMERIC ELECTROSPUN NANOFIBERS (ENMS): INTEGRATION OF SURFACE FUNCTIONALITIES AND POROSITY TO IMPROVE ORGANIC CHEMICAL UPTAKE

4.1 ABSTRACT

We herein explore the use of surfactants to improve the performance of electrospun polymer nanofibers (e.g., polyacrylonitrile or PAN) and polymer-carbon nanotube composites (hereafter “CNT/PAN”) as passive sampling devices for trace organic micropollutants. Surface-segregating tetrabutyl ammonium bromide (TBAB) and cetrimonium bromide (CTAB) were used to impart positively charged quaternary ammonium surfaces sites on PAN and CNT/PAN nanofiber surfaces for targeting anionic pollutants. Alternatively, anionic sodium dodecyl sulfate (SDS) was used as a removable porogen, increasing the pore volume and specific surface area of PAN and CNT/PAN nanofibers as measured by N₂-BET by as much as 3-fold. Uptake studies with anionic [2,4-dichlorophenoxyacetic acid (2,4-D) and perfluorooctanoic acid (PFOA)] and neutral (atrazine, diuron and metolachlor) target analytes revealed that the changes imparted to PAN and CNT/PAN nanofibers by surfactants improved performance. Specifically, cationic TBAB and CTAB not only promoted uptake of anionic 2,4-D and PFOA, but also enhanced uptake of diuron and metolachlor, which we attribute to electron rich functionalities in their structure (e.g., carbonyl groups containing oxygen lone pairs of electrons). Similarly, pore volume and surface area increases arising from the intentional leaching of SDS from the nanofibers resulted in a corresponding increase, sometimes considerably (~2-fold), in target analyte uptake. Additional tests evaluated practical aspects of surfactant-modified electrospun nanofiber mats (ENMs) as passive sampling devices. Notably, uptake rates and capacities were mostly unchanged across a range of complex matrices (e.g., in the presence of model humic acid

and in Iowa River water). Our results illustrate the promise of surfactant-modified ENMs as next-generation equilibrium passive sampling materials for organic micropollutants, particularly those that are charged or highly polar and water soluble.

4.2 INTRODUCTION

In recent years, passive sampling devices have made great strides in development of new material platforms for targeting more diverse chemical suites. Most of these advances have been catalyzed by diversifying the types of materials used in passive sampler construction, where the physical and chemical nature of these materials ultimately dictates the types of chemicals that can be targeted during sampling events. For example, the commercially available Semipermeable Membrane Device (SPMD) passive sampler is based on triolein (**Figure 4-1**),⁵⁰ a monoacid triglyceride, and typically used for the sampling neutral, more hydrophobic ($\log K_{ow} > 3$) organic chemicals including polycyclic aromatic hydrocarbons (PAHs) and polychlorinated biphenyls (PCBs). More recently, the Polar Organic Chemical Integrative Sampler (POCIS) uses materials that can target polar, higher water solubility chemicals ($\log K_{ow} < 3$) including pharmaceuticals and pesticides. To do this, POCIS uses commercially available but proprietary functionalized resins (e.g., Isolute® ENV+ and Amborsorb® 1500, or Oasis HLB) commonly used for solid phase extraction.⁵⁰

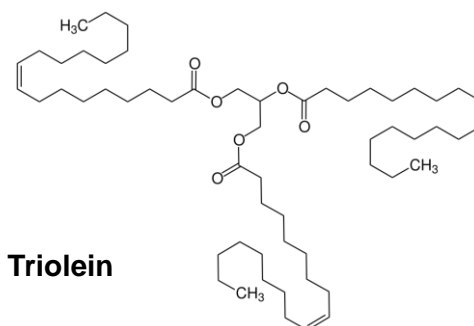


Figure 4-1. Chemical structure of Triolein

Despite these advances, there remain some important challenges in improving the effectiveness and versatility of passive samplers, particularly when considering characteristics of

emerging contaminant classes commonly encountered in water resources. The first challenge relates to increasing the material capacity for target analytes, which directly impacts the limits of detection for chemicals present in extracts collected from the sorbent material. For polar pharmaceutical and pesticide chemical classes typically targeted by POCIS, surface water concentrations often range from tens to thousands of ng/L.²³⁵⁻²³⁸ Although low (at parts per trillion levels), these exposures are still consequential for ecosystem, and in some cases human, health impacts.^{45, 239-243} Thus, passive sampling materials with greater capacities and fast uptake rates are most desirable, resulting in more sensitive quantification over shorter deployment timescales for emerging pollutant classes.

Another challenge in passive sampler development and application is the targeting of charged analytes.²⁴⁴⁻²⁴⁶ There are a growing number of high priority pollutants that are either charged across all environmentally relevant conditions, or that possess ionizable functionalities with acid dissociation constants (pK_a values) within the range of surface waters (pH values ~6 to 9) and thus may be present as ions in at least some environmental systems. Examples include 2,4-dichlorophenoxyacetic acid (2,4-D) and glyphosate, pesticides regulated under the Safe Drinking Water Act (SDWA), and per- and polyfluoroalkyl substances (PFAS), unregulated industrial chemicals commonly found in drinking water recourse for which EPA has established health advisories at 70 ng/L (or parts per trillion). Because of their charge, these compounds exhibit high water solubility, and it remains unclear if traditional passive sampler materials designed to target neutral compounds, including SMPD and POCIS, would be effective toward such charged analytes.²⁴⁴ While it is possible that alternative materials that exploit electrostatic interactions (e.g., ion exchange resins) could be used as passive sampling materials for these targets, a likely, and as yet unexplored, challenge is non-target interference from naturally

occurring co-solutes (e.g., natural organic matter, alkalinity, hardness causing cations) that may share the same charge as the desired analyte.

Herein, we aim to address these grand challenges in passive sampler development through the fabrication of new materials with physicochemical properties specifically tailored to promote uptake capacity and/or exploit selective chemical interactions with ionic target analytes. In prior Chapters, we have demonstrated that polymeric nanofibers, including their nanocomposites, fabricated via electrospinning hold several advantages with respect to tuning material properties to target a broader array of both legacy and emerging pollutant classes. For example, in Chapter 3, we found that integration of carbon nanotubes (CNTs) to produce polymer-CNT composites increases the uptake capacity through unique interactions of the target analyte with CNTs embedded at or near the nanofiber composite surface.

Another common approach that can be used to tailor polymer nanofiber composition and surface chemistry is the use of surfactants. Surfactants have commonly been used in electrospinning to improve synthesis, where the increase in conductivity imparted by anionic and cationic surfactants helps produce nanofibers of more uniform morphology and tighter diameter distributions within the deposited nonwoven mat.^{148, 247-251} Beyond these fabrication benefits, we, and others, have shown that some surfactants can impart other beneficial characteristics to nanofibers that are desirable for a range of possible applications.^{145, 252-254} For example, some surfactants, including quaternary ammonium salts (QAS), are surface segregating in electrospun polymers; thus, during synthesis, to minimize the free energy of interactions between the polymer and the surfactant, the surfactants migrate to the polymer-air interface. This, in turn, enriches the nanofiber surface concentration of the surfactant, such that their charged head introduces chemical functionality to the nanofiber surface (**Figure 4-2**, Scheme A). These

groups can then be exploited in various applications; for example, we have previously shown that cationic quaternary ammonium groups can be used to bind anionic metal species including chromate and arsenate from water in reactive filtration platforms.¹⁴⁵ Others have used this approach to generate antimicrobial nanofiber mats for various applications (e.g., wound dressings) via the antimicrobial activity of quaternary ammonium surfactants like tetrabutylammonium bromide (TBAB).^{255, 256} Notably, in our earlier work with metal oxyanion binding, we also discovered that the co-inclusion of nanoparticles with surface-segregating surfactants like TBAB resulted in the co-location of the nanoparticles to the nanofiber surface (**Figure 4-2**, Scheme B). This allows a simple, single-pot recipe for producing nanofiber surfaces enriched both with charged groups (e.g., quaternary ammonium) and nanoparticles (e.g., metal oxide nanoparticles), whose properties may also be exploited in environmental applications.

Another potentially beneficial use of surfactants for electrospun nanofiber mats is through their intentional removal after fabrication of the polymer to increase material surface area (**Figure 4-2**, Scheme C). Here, the surfactant, or micelles of the surfactant, acts as a porogen, where its removal via leaching from the polymer matrix leaves behind cavities that increase the pore volume, and in turn the specific surface area, of the fibers.^{141, 257, 258} In polymer-nanoparticle composites, the use of surfactant porogens can help to better expose embedded nanomaterials to targets dissolved in water, increasing uptake and improving sorbent capacity. Further, residual surfactant that is not fully leached from the polymer matrix may also impart charge to the nanofiber surface, promoting uptake of chemicals oppositely charged to the surfactant.

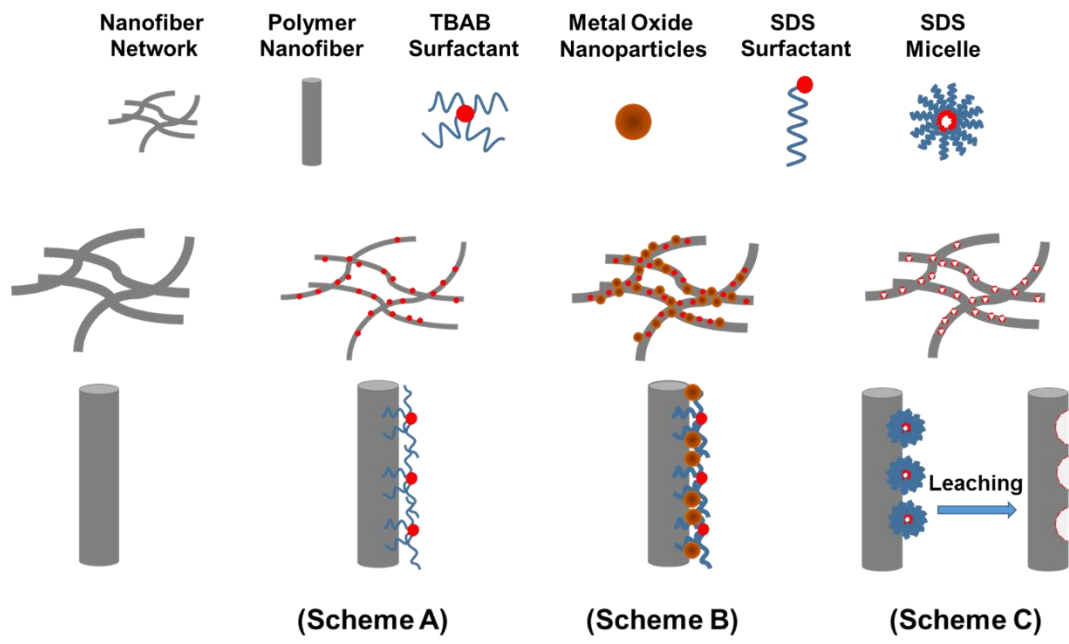


Figure 4-2. Schemes of using surfactants to modify nanofiber surface morphology and property

In this work, building off our prior studies with CNT-polymer composites (see Chapter 3), we integrate surfactants into nanofiber synthesis recipes for electrospinning to further improve the performance of polymer composite ENMs for passive sampling applications. The QAS cetrimonium bromide (CTAB) and tetra-n-butylammonium bromide (TBAB) were integrated during nanofiber synthesis to increase the positive charge on the nanofiber surface with the intent of improving performance toward common anionic pollutant targets including 2,4-D and PFAS. In polymer-CNT composites, we also explored the influence of TBAB and CTAB, both surface-segregating surfactants, on the surface-availability of embedded CNTs. Additionally, the anionic surfactant, sodium dodecyl sulfate (SDS), was used in polymer-CNT composites as a porogen, while also exploring whether it promotes the uptake of dissolved targets exhibiting partial positive charges through more favorable electrostatic interactions.

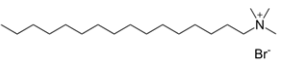
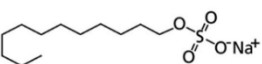
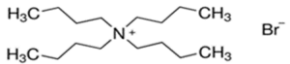
Beyond fundamental investigations of how surfactant inclusion alters nanofiber performance, another consideration was how the charge imparted to the nanofiber surface, particularly through positively charged CTAB and TBAB, influences interaction with non-target anionic species common in surface waters. Thus, experiments were conducted in more complex aqueous systems (e.g., Iowa River water) prior to field deployment to test the performance of surfactant amended nanofibers in the field.

4.3 MATERIALS AND METHODS

Reagents. All reagents for ENM fabrication were used as received, including polyacrylonitrile (PAN; MW ~150,000; Sigma Aldrich), polystyrene (PS; MW ~280,000; Sigma Aldrich), cetrimonium bromide (CTAB; $\geq 99\%$; Sigma Aldrich), sodium dodecyl sulfate (SDS; $\geq 99\%$; Sigma Aldrich), tetrabutylammonium bromide (TBAB; $\geq 99\%$; Sigma Aldrich), and N,N-dimethylformamide (DMF; 99.8%; VWR International). More details are listed in **Table 4-1**.

Carbon nanotubes (CNTs) were both non-functionalized (NF-CNT) and carboxylated (COOH-CNT), and acquired from Cheap Tubes Inc. (Cambridgeport, VT). CNTs were used as received, without any additional purification and their vendor-provided characteristics were previously summarized in **Table 3-1** of Chapter 3.

Table 4-1. Molecular structures and chemical properties of surfactants investigated herein.

Name	Cetrimonium Bromide (CTAB)	Sodium Dodecyl Sulfate (SDS)	Tetrabutylammonium Bromide (TBAB)
Structure			
Molecular formula	C ₁₉ H ₄₂ BrN	NaC ₁₂ H ₂₅ SO ₄	C ₁₆ H ₃₆ BrN
MW (g/mol)	364.45	288.37	322.37
Charge	positive	Negative	positive
Solubility in water (20°C)*	100 mg/mL	250 mg/mL	600 mg/mL
Solubility in DMF (20°C)**	Soluble	Soluble	Soluble

*Aqueous solubilities were reported in the manufacturer's product information sheet. **Qualitative evaluation of solubility in DMF was determined in our laboratory, and reflects the ability of at least 40 mg of surfactant to be dissolved in 100 mL of DMF.

For uptake experiments with surfactant-amended ENMs, target chemicals were atrazine (99.1%; Sigma Aldrich), 2,4-dichlorophenoxyacetic acid (2,4-D; ≥ 98.0%; Sigma Aldrich), Perfluorooctanoic acid (PFOA; 96%; Sigma Aldrich), metolachlor (≥ 99.9%; Sigma Aldrich) and diuron (powder, ≥ 98.0%; Sigma Aldrich). The structure and select chemical properties of these target analytes are summarized in **Table 4-2**. Stock solutions of each chemical (ranging in concentration from 5.4 to 7.1 g/L) were prepared in methanol (Optima grade, ≥ 99.9%; Sigma Aldrich) and stored in the refrigerator (~3 °C) until use. For experiments in more complex

aqueous systems, humic acid (Fluka, average molecular weight 500 – 1000 Da) was prepared at the concentration of 225 g/L in pH 10 aqueous solution, where the alkaline pH was used to promote the complete dissolution of the humic acid into water.

Electrospinning. All ENMs were fabricated from polyacrylonitrile (PAN). PAN-based ENMs were synthesized on a customized electrospinning apparatus using synthesis procedures as described in Chapters 2 and 3. Briefly, to minimize the presence of CNT aggregates in the final CNT-polymer nanofiber composites, CNT (17.5 mg/mL) suspensions in DMF were first sonicated (Branson 1510 Ultrasonic Cleaner; Yorba Linda, CA) for 5 hours. Then, selected polymer precursors and surfactant salts were added to CNT/DMF suspensions and thermally mixed (Eppendorf, ThermoMixer[®] C; Hauppauge, NY) at 60 °C for 5 hours to generate polymer sol-gel solutions for electrospinning. The obtained polymer sol-gel was transferred into a 12 mL syringe and pumped out through a 25G metal tip needle (note that a 23G needle was used for the 25% mass loading of carboxylated CNTs) at a flow rate of 0.5 mL/h. Depending on the mass ratio of polymer and CNT, a high voltage between 14 to 16 kV was applied to the needle tip using an Acopian Power Supply (Model P01.5HP40; Easton, PA). An aluminum foil covered, grounded spinning drum was used as the collector for nanofibers. The collector was positioned 10 cm away from the needle tip during synthesis. During electrospinning, humidity was controlled between 18 (\pm 2) % and the temperature was held constant at 28 °C.

For all SDS- containing ENMs, a post-synthesis leaching procedure was used to remove the SDS to facilitate its function as a porogen. ENMs were placed in a glass container filled with DI water (400 mL water per 1g ENM), which was then placed on a reciprocating shaker table (Precision Model 25; Marietta, Ohio) at 30 rpm for 24 hours at room temperature. The DI water

in the container was refreshed every 8 hours. In total, around 1.2 L DI water was used to treat 1 g of mat during this surfactant leaching process. After 24 hours of leaching, the ENM surface was rinsed with DI water prior to conducting uptake experiments or any other characterization measurements.

Table 4-2. Structure and select physicochemical properties of the organic chemical targets investigated here.

Chemical	Structure	MW (g/mol)	Log K_{ow}	Water solubility (25 °C; g 100 mL ⁻¹)*	Hydrogen bonds (count)**	pKa* (25 °C)	Charge @ pH ≈ 7	Molar refractivity (cm ³)*
Atrazine		215.68	2.6	0.007	H-donor (2) H- acceptor (5)	2.3	Neutral	59
Diuron		233.09	2.7	0.0042	H-donor (1) H- acceptor (3)	14	Positive	59
2,4-D		221.04	2.8	0.054	H-donor (1) H- acceptor (3)	2.98	Negative	49
Metolachlor		283.79	3.13	0.053	H-donor (0) H- acceptor (3)	1.45	Neutral	80.1
PFOA		414.07	4.81	0.33	H-donor (1) H- acceptor (16)	2.8	Negative	41.6

*Data were obtained from the PubChem database operating by National Center for Biotechnology Information (NCBI)

**Hydrogen bond is a chemical bond in which a hydrogen atom of one molecule is attached to an electronegative atom, especially a nitrogen, oxygen or fluorine atom, usually of another molecule. The number of electronegative atoms that accept covalent bonds and electropositive hydrogen atoms that participate covalent bonds in each chemical are listed in this table.

Nanofiber characterization. Nanofiber morphology and size distribution were determined using a Hitachi S-4800 scanning electron microscope (SEM). Histograms of nanofiber diameters were prepared through analysis of SEM images using the Image J software package (freely available through the National Institutes of Health). For each ENM sample, diameters of at least 200 nanofibers were measured to determine the average and standard

deviation. Specific surface area and total pore volume of ENMs were measured by a Micromeritics ASAP 2020 surface area and pore size analyzer using the analytical procedures described in Chapter 3.

Sorption and uptake experiments. All target analyte stock solutions were prepared in the methanol at a concentration of 25 mM (from 2.3 g/L to 7.1 g/L) and stored at 3 °C until use. To initiate uptake experiments, these stock solutions were diluted 1000-fold into 1 mM potassium phosphate buffer at pH 7 and room temperature (20 °C). This solution was then transferred into several 40 mL amber glass vials, where uptake data was collected over time via sacrificial sampling of these sets of identical reactors. Sorption experiments were conducted using both mixed (active uptake) and non-mixed (passive uptake) systems. For mixing, reactors were placed on a rotator (Barnstead/Thermolyne Model 415110; Dubuque, IA), and mixed end-over-end at 8 rpm for 2 days. Reactor sampling, as well as processing of aqueous and solid-phase (i.e., ENM) samples collected over time, was conducted as described in previous research chapters.

Experiment with humic acid and in environmental samples. Experiments were conducted to test performance in more complex systems. These involved experiments in the presence of 5 mg/L Fluke humic acid (FHA) in pH 7 phosphate buffer. Additional experiments were conducted using water samples collected on March 8, 2018 at the inlet of the University of Iowa Water Treatment Plant (UIWTP). The pH of these natural water samples was measured in our laboratory as 7.9. According to available USGS,²⁵⁹ and characterization at the UIWTP, the Iowa River water at this time of year has hardness in excess of 180 mg/L as CaCO₃ (very hard), alkalinity above 200 mg/L as CaCO₃, turbidity of ~75 NTU, and nitrate plus nitrite levels of ~3.4 mg/L as N. Experiments were conducted with atrazine and 2,4-D, and mostly followed the

experimental and sampling protocols described for model systems. We note that due to the possible presence of colloidal organic matter in both systems, water samples were passed through a 0.22 μm nylon filter (Celltreat Scientific Products) prior to analysis.

Analytical methods. For aqueous phase analysis, 1 mL of aqueous sample was removed from the reactors, transferred to an amber autosampler vial and immediately analyzed. For analysis of the sorbed phase, ENM-bound mass was extracted by mixing the ENM with 10 mL of methanol for 1 d, after which 1 mL of methanol was collected and analyzed.

The majority of aqueous samples and methanol extracts of ENMs were analyzed via high-performance liquid chromatography with a diode array detector (LC/DAD, Agilent 1100 series HPLC). Analysis of PFOA used liquid chromatography with high resolution mass spectrometry (LC/MS) at the University of Iowa High Resolution Mass Spectrometry Facility. All analyses were conducted on Waters Acquity TQD, which is a triple quadrupole mass spectrometer interfaced with a Water Acquity UPLC system, operating in negative electrospray ionization mode. HPLC and triple quadrupole LC/MS methods for each chemical were adapted from previously published methods.²⁶⁰⁻²⁶⁴

Field evaluation of ENM-CNT composites. A quadrate metallic frame (9.5 cm \times 9.5 cm) with a circular hole (diameter: 7 cm) in its middle was used to hold the ENM used in field testing. A piece of an ENM (approximately 11 cm \times 21cm; ~ 450 mg) was folded and sandwiched between the metal pieces, and the open edge of frame was tightened by two self-locking zip ties. After assembly, the frame with ENM was wrapped in aluminum foil and placed into a zip lock bag. An extra ENM of similar mass was also covered with aluminum foil and taken to the monitoring site for use as a blank reference sample.

The deployment location was chosen at 100 meters upstream from the Coralville wastewater treatment plant nearby Muddy Creek, Coralville, IA (USGS site: 05454090). The ENM-containing frame was tied to a metal rod that was then inserted into the sediment at the bottom of the creek. Once inserted, the ENM was in contact with the surface water of the creek, but not the underlying sediment. After 48 hours, the sampler was collected and once again covered in the aluminum foil during transport filed back to the laboratory.

For ENM processing and analysis, the field-recovered ENM was first rinsed by DI water to remove any coarse grain sandy particles or loose dirt on the material surface. Methanol was then used to extract the target organic analyte, atrazine and 2,4-D via immersion and mixing for 24 hours. The extract liquor was then filtered through a 0.22um Nylon filter prior to analysis by HPLC.

4.4 RESULTS AND DISCUSSION

Surfactant-Modified Material Characterization. SEM images of surfactant-modified PAN-CNT composites are shown in **Table 4-4**. Through SEM characterization and BET analysis, we found that inclusion of different surfactants influenced the nanofiber dimensions and surface area of the resulting ENMs. Results of these analyses are summarized in **Table 4-3**.

For the inclusion of quaternary ammonium salts CTAB and TBAB, the average diameter of the resulting nanofibers was not significantly changed for composites produced with either NF-CNTs or COOH-CNTs. However, the presence of these cationic surfactants resulted in a much broader distribution of nanofiber diameters (see the standard deviations for diameters in **Table 4-3** and histograms in **Figure 4-3**). We note that in Chapter 3, the size distribution of

CNT/PAN composites was effectively the same as that for unmodified PAN. Further, in our prior work with CTAB- and TBAB-modified PAN ENMs,¹⁴⁵ the inclusion of surfactants did not influence either the average or standard deviation of the resulting nanofibers. Thus, we presume that interactions between the quaternary ammonium surfactants and CNTs during electrospinning results in the much broader size distribution of CNT/PAN composite nanofibers. For example, surfactants can help to break apart CNT aggregates, improve their dispersion in both water and organic solvents.²⁶⁵⁻²⁶⁹ More work is merited (e.g., systematically varying the CNT to surfactant mass ratio) to better understand how CNT-surfactant interactions influence the morphology of the resulting nanofibers.¹⁴¹

Table 4-3. Surface area, pore volume and average diameters (with standard deviation) of surfactant-modified nanofibers fabricated herein.

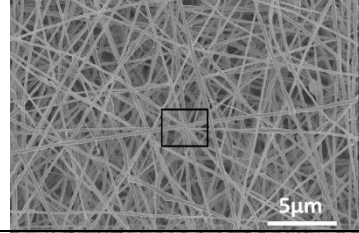
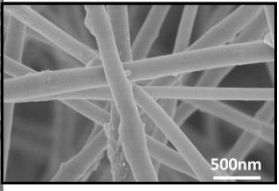
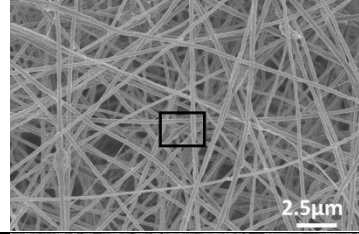
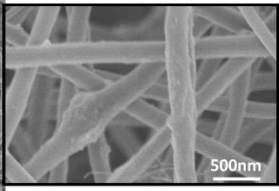
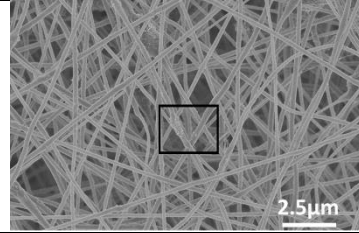
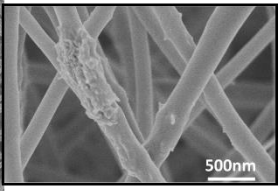
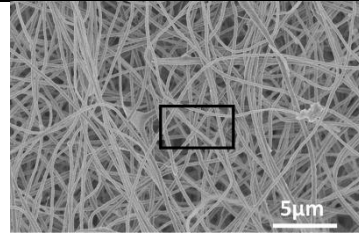
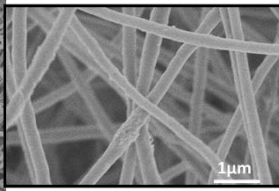
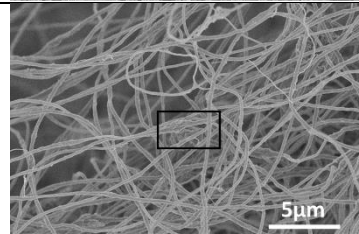
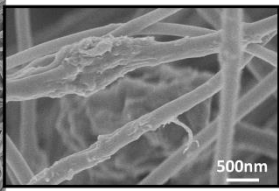
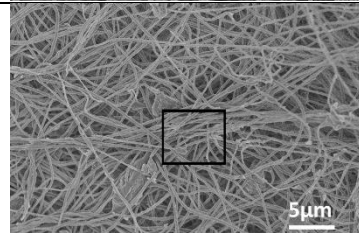
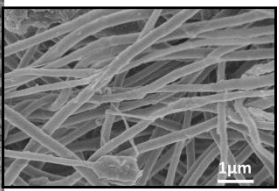
Sorbent	Surface Area (m ² /g) ^a <i>n</i> = 6	Pore Volume (10 ⁻³ mL/g) ^a <i>n</i> = 3	Diameter (nm) ^b <i>n</i> = 3
PAN	12 ± 0.5	23 ± 1.7	160 ± 30
20% NF-CNT/PAN	15 ± 2.4	37 ± 8.0	210 ± 50
20% CTAB/20% NF-CNT/PAN	N.M.	N.M.	220 ± 120
20% TBAB/20% NF-CNT/PAN	N.M.	N.M.	240 ± 110
20% SDS/20% NF-CNT/PAN ^L	21 ± 2.2	66 ± 7.7	290 ± 110
20% COOH-CNT/PAN	17 ± 2.0	43 ± 6.0	200 ± 40
20% CTAB/20% COOH-CNT/PAN	N.M.	N.M.	190 ± 100
20% TBAB/20% COOH-CNT/PAN	N.M.	N.M.	240 ± 130
20% SDS/20% COOH-CNT/PAN ^L	33 ± 3.0	103 ± 12	310 ± 140

^a Surface area and pore volume were measured by BET by using a seven-point adsorption isotherm, and BJH methods respectively; ^b Diameters were measured from SEM images using ImageJ software. ^c The presence of “L” indicates that the surfactant salts initially present in ENMs were intentionally leached out before analysis. Uncertainties represent the standard deviation from at least three replicate experiments. Typically, 100 nanofibers were measured per ENM sample. Values of *n* = number of replicate syntheses.

For SDS-modified CNT/PAN, we focused our attention on the characterization of nanofibers after SDS had been removed from the polymer matrix via leaching (samples noted by “L” in their name). The SDS-modified CNT/PAN had average diameters that were nominally

larger than unmodified CNT/PAN, but once again this increase was not statistically significant given the considerably broader distribution (i.e., standard deviation) of diameters after SDS integration. However, the SDS-leached materials exhibited specific surface areas nearly 3-fold greater than pure PAN and twice that of CNT/PAN for COOH-CNT composites. This increase in surface area appears to directly result from gains in pore volume after the release of SDS. For both NF-CNT and COOH-CNT composites, pore volumes more than doubled due to the use of SDS as a porogen. In fact, these gains in surface area and pore volume exceed those previously reported by our group for SDS-modified PAN-ferrihydrite nanocomposites.¹⁴¹ Unfortunately, pore formation was not evident in SEM images of SDS-leached materials (**Table 4-4**) because pore size is too small to be detected at the analytical resolution.

Table 4-4. Scanning electron microscopy images for surfactant-modified CNT/PAN composites. Both low (left) and high (right) magnification images are shown.

Low and High Magnification SEM Images		
20% CTAB/20% NF-CNT/PAN		
20% CTAB/20% COOH-CNT/PAN		
20% TBAB/20% NF-CNT/PAN		
20% TBAB/20% COOH-CNT/PAN		
20% SDS/20% NF-CNT/PAN		
20% SDS/20% COOH-CNT/PAN		

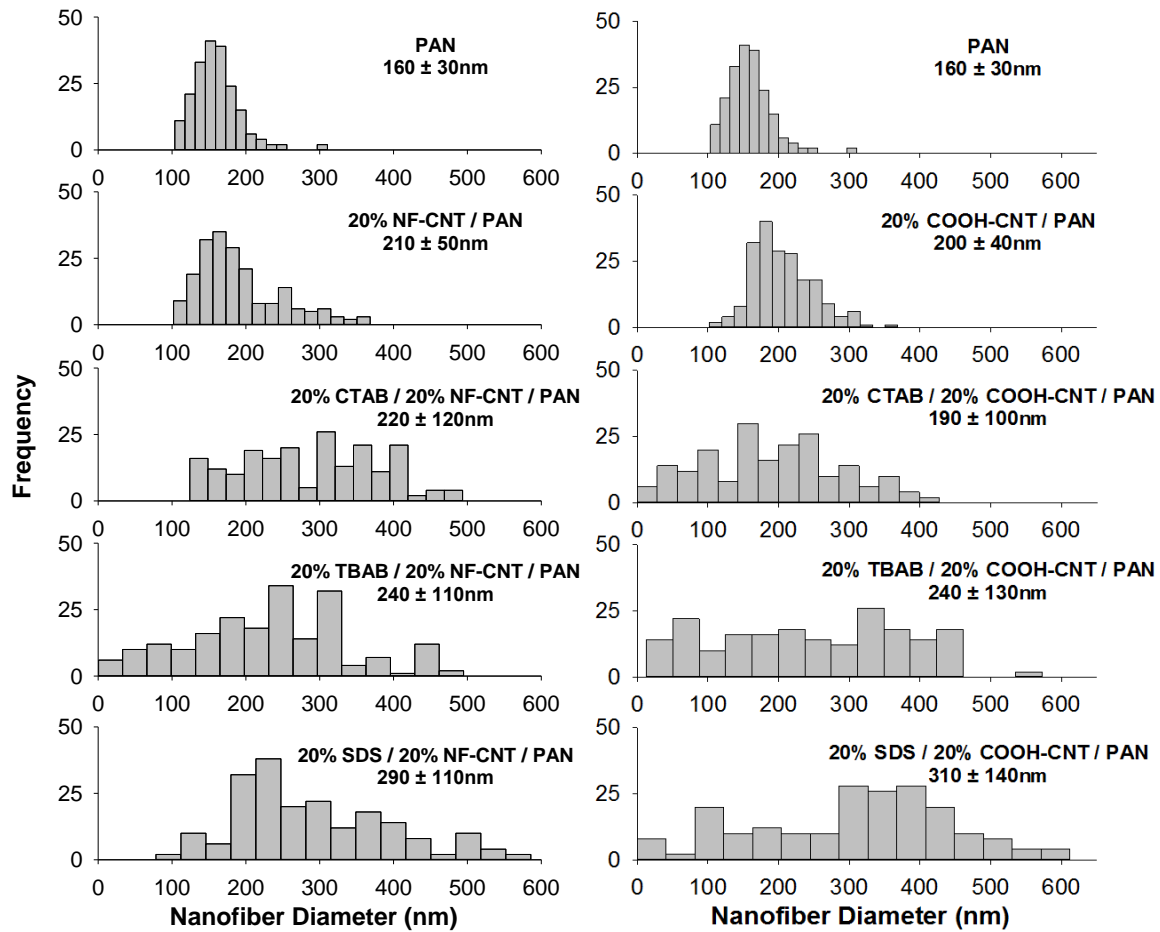


Figure 4-3. Histograms of nanofiber diameters for surfactant modified CNT/PAN. Data are shown for analysis of at least 200 nanofibers via SEM images. Average diameters (with standard deviation) are provided for each material.

Influence of quaternary ammonium surfactants on ENM performance toward 2,4-D. In **Figure 4-4a**, we show the influence of varying levels of TBAB (from 10-30% wt.) in PAN nanofibers (without CNTs) on the uptake of 2,4-D, which is an anion at the pH value investigated (pH 7). Despite relatively little partitioning of 2,4-D into PAN, uptake generally increased with increasing TBAB wt% in the nanofibers. Nanofibers with 20 and 30% wt. TBAB exhibited nearly equivalent performance, enhancing 2,4-D uptake by ~50-fold relative to unmodified PAN at equilibrium. Because these experiments used a much higher 2,4-D concentration (~5.5 mg/L) than would be encountered in the environment (typically ~100-1000 ng/L), these TBAB modified materials possess very high capacity not likely to be saturated during field applications. Equilibrium was also achieved quickly with these materials. Optimally performing 20% and 30% wt. TBAB materials reached equilibrium (i.e., the mass of 2,4-D in the ENM was constant over time) after 1 day, even in static (i.e., unmixed) experimental systems. Collectively, the inclusion of TBAB yields $\log K_{\text{ENM-w}}$ values that are roughly 2-log units higher than that obtained with unmodified PAN, which will improve the analytical detection limits associated with the use of these materials as equilibrium passive samplers.

Additional experiments compared the performance of TBAB with CTAB (**Figure 4-4b**), another surface-segregating quaternary ammonium surfactant.¹⁴⁵ As with TBAB, inclusion of CTAB increased 2,4-D uptake into the PAN-based ENM. We note that the slightly lower capacity of 2,4-D on 20% wt. CTAB/PAN relative to 20% wt. TBAB/PAN is likely attributable to differences in the available charge in each system. Specifically, differences in the molecular weights of TBAB (322.4 g/mol) and CTAB (364.5 g/mol) result in 1.13-fold greater moles of cationic charge in the TBAB/PAN system relative to CTAB/PAN when both QAS are present at the same mass loading (wt. %).

Our results with 2,4-D reveal a clear, beneficial effect on quaternary ammonium surfactants on the performance of PAN nanofibers. Both CTAB and TBAB are surface-segregating in polymers,^{252, 270} and their quaternary ammonium groups are often used as strong base ion exchange sites.^{145, 271-273} Taken together, it appears that positively charged quaternary ammonium groups on the surface of PAN nanofibers function as electrostatic binding sites for 2,4-D, presumably promoting uptake via a mechanism analogous to ion exchange.

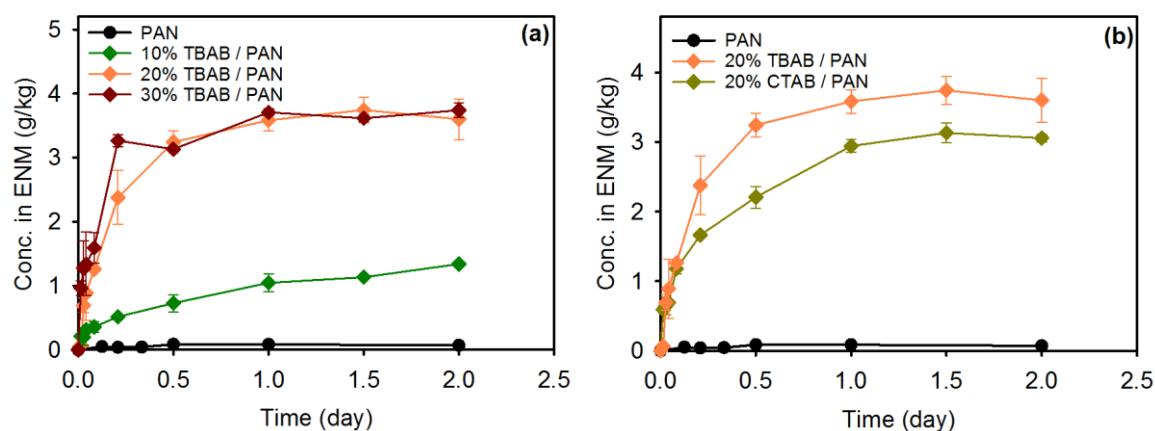


Figure 4-4. Uptake curves for 2,4-D on PAN ENMs with (a) different mass loadings (from 0-30% wt.) of TBAB and (b) 20% wt. of either TBAB or CTAB. Uncertainties represent the standard deviation from three replicate experiments. Experimental conditions: pH 7 (1 mM phosphate); initial 2,4-D concentration of 5.5 mg/L; ENM loading: ~1.5 g/L. Experiments with surfactant-modified PAN were carried out under a static (no mixing) condition, whereas data with unmodified PAN was collected in well-mixed reactor systems.

Influence of quaternary ammonium surfactants on ENM-CNT composite

performance toward 2,4-D. To explore potential synergies from the co-integration of CNTs and surfactants during electrospinning, as we observed with metal oxide nanoparticles and surfactants (e.g., both species co-locating to the nanofiber surface),¹⁴⁵ we examined 2,4-D uptake on CNT/PAN composites modified with 20% wt. of TBAB or CTAB (corresponding to a 1:1

mass ratio with CNTs). We considered CNT/PAN composites fabricated with both nonfunctional CNT (hereafter “NF-CNT”) and carboxylated CNTs (hereafter “COOH-CNT”).

Uptake curves for 2,4-D (**Figure 4-5**) revealed that surfactant-modified CNT/PAN composites, with either NF- and COOH-CNTs, exhibit comparable performance to that of surfactant modified PAN (without CNTs). Thus, the majority of the sorption activity exhibited toward 2,4-D remains attributable to the presence of CTAB and TBAB as cationic surfactants, and there does not appear to be any significant synergistic influence resulting from the co-inclusion of surface-segregating surfactants and CNTs. Notably, with co-integration of CNTs, TBAB- and CTAB-modified materials exhibited nearly identical sorption, indicating that CNTs help to improve modestly the performance of CTAB, although the cause of this behavior is not yet understood. We also note that while comparable uptake capacities were observed with these materials, the time to reach equilibrium appeared to increase for surfactant-modified CNT/PAN (i.e., equilibrium was not yet achieved at 2 days) relative to PAN modified with surfactants alone.

Stability of quaternary ammonium surfactants within ENMs during application. A concern we have previously identified with surfactant-modified nanofibers is their long-term stability during application. Specifically, we have observed declines in performance (for metal ion uptake) for certain surfactant-amended materials as a result of surfactant loss from the nanofibers over time.¹⁴⁵

To investigate the stability of CTAB and TBAB within CNT/PAN composites, we extensively washed surfactant-modified materials with DI water to promote surfactant leaching prior to conducting 2,4-D sorption experiments. The results for CTAB- and TBAB-modified PAN and CNT/PAN are shown in **Figure 4-6**. Performance of TBAB-modified materials

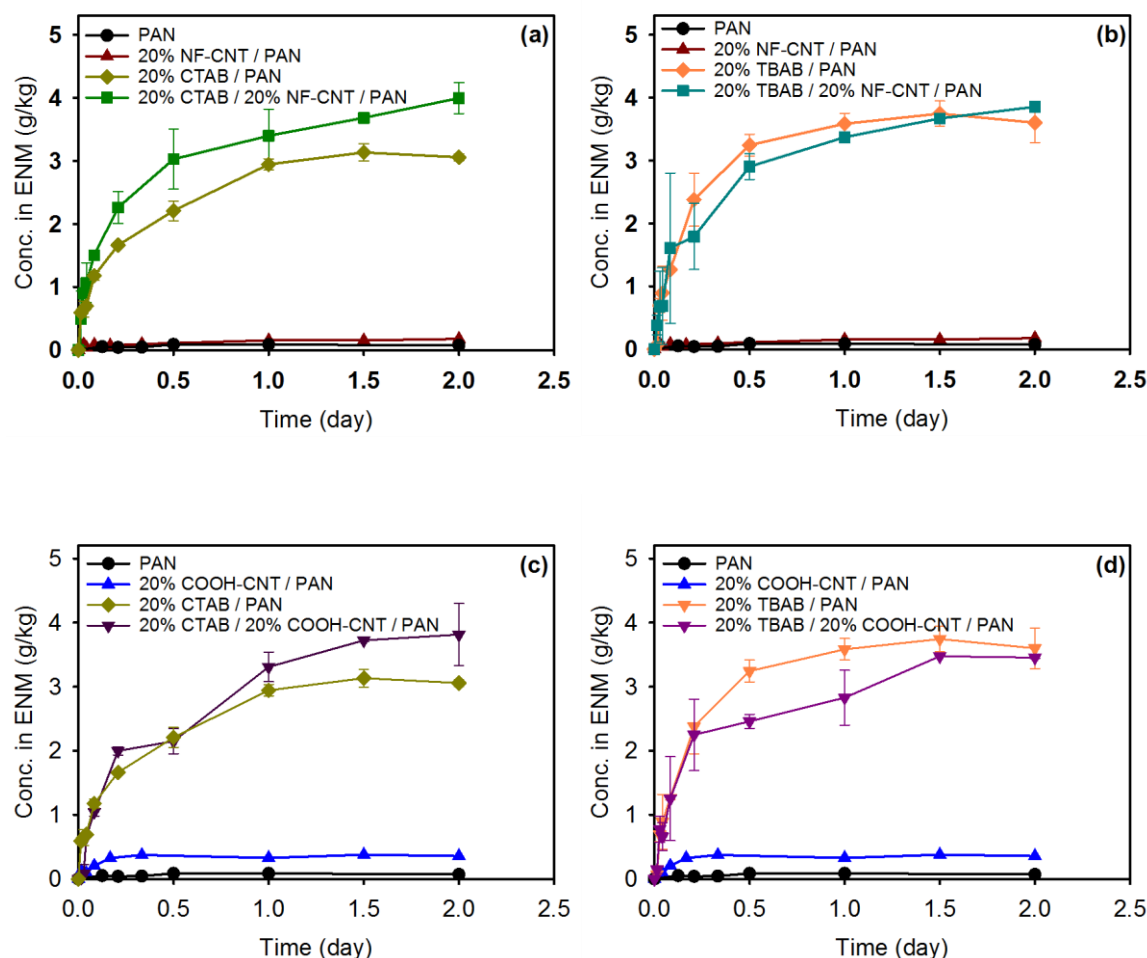


Figure 4-5. Uptake curves for 2,4-D on PAN-based ENMs modified with 20% wt. (a and c) CTAB and (b and d) TBAB. Data are shown for both PAN- and CNT/PAN composites, with composite data presented for both nonfunctionalized (NF-CNT) and carboxylated (COOH-CNT) CNTs. Uncertainties represent the standard deviation from three replicate experiments. Experimental conditions: pH 7 (1 mM phosphate); initial 2,4-D concentration of 5.5 mg/L; ENM loading: ~1.5 g/L. Experiments with surfactant-modified and CNT-modified PAN were carried out under a static (no mixing) condition, whereas data with unmodified PAN was collected in well-mixed reactor systems.

remained the same after extensive washing, with identical uptake curves and calculated K_{ENM-W} values. In contrast, the sorption capacity of all CTAB-modified materials decreased by ~50%, producing a corresponding decrease in measured K_{ENM-W} values. The relative stability of CTAB

and TBAB in PAN and CNT/PAN matches our earlier work,¹⁴⁵ where we attributed the greater stability of TBAB to better entanglement between the polymer and its four butyl tails (relative to the straight chain hydrocarbon tail on CTAB). Given its relative lack of stability in PAN matrices, CTAB was not included in any subsequent performance trials.

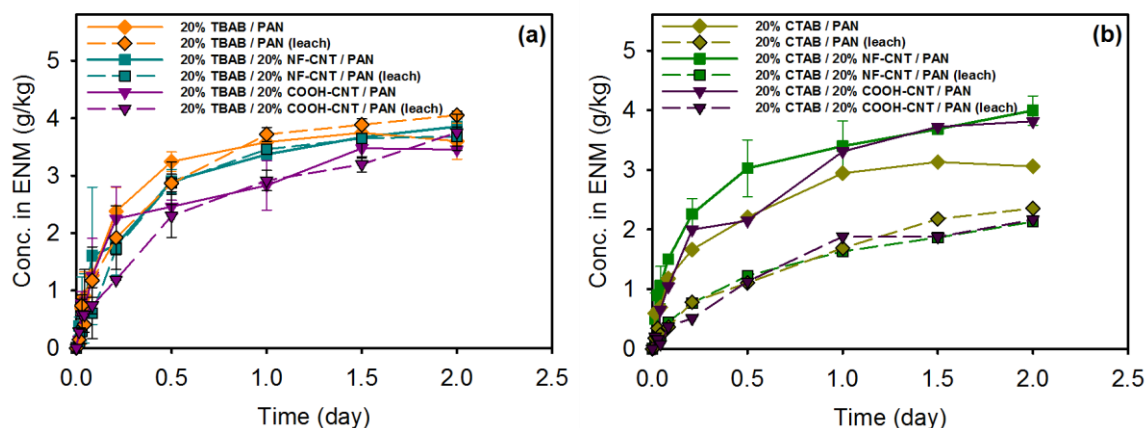


Figure 4-6. Uptake curves for 2,4-D on (a) TBAB and (b) CTAB modified PAN, NF-CNT/PAN and COOH-CNT/PAN. Data for all materials are shown before and after treatment to promote QAS leaching. Uncertainties represent the standard deviation from three replicate experiments. Experimental conditions: pH 7 (1 mM phosphate); initial 2,4-D concentration of 5.5 mg/L; ENM loading: ~1.5 g/L. Experiments were carried out under a static (no mixing) condition.

Influence of quaternary ammonium surfactants on ENM-CNT composite

performance toward PFOA. We also explored whether the beneficial influence of TBAB on 2,4-D uptake was generalizable for other anions. We explored uptake of perfluorooctanoic acid (PFOA), which is also negatively charged across environmentally relevant pH values. While PAN and COOH-CNT/PAN were ineffective for PFOA uptake, approximately 80% of the available aqueous mass of PFOA was taken up into PAN containing both COOH-CNTs and TBAB at pH 7 (**Figure 4-7**). Once again, equilibrium was rapidly achieved, with the ENM-associated PFOA concentration stabilizing in less than 0.5 days (which represents our first

sample point). Thus, we anticipate that the increased uptake afforded by inclusion of cationic TBAB will be generally observed across all anionic organic pollutant targets.

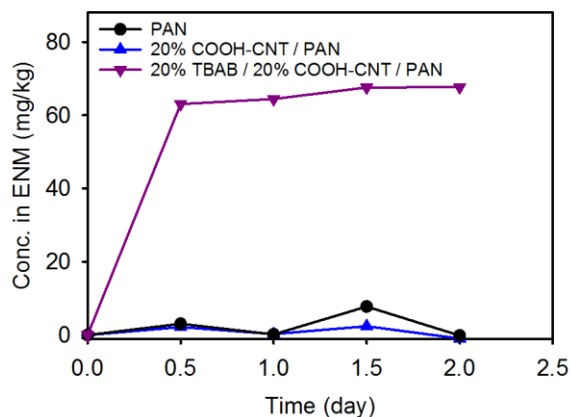


Figure 4-7. The uptake curve for PFOA on PAN, CNT/PAs, and TBAB-modified CNT/PAN. Experimental conditions: pH 7 (1 mM phosphate); initial PFOA concentration of 100 $\mu\text{g/L}$; ENM loading: ~ 1.5 g/L. Experiments were carried out in well-mixed reactor systems.

Influence of quaternary ammonium surfactants on uptake of neutral organic pollutants. Although TBAB improves uptake of anions, its integration into ENMs must not adversely impact the partitioning of other, neutral organic chemical targets. Indeed, while the inclusion of CNTs offered no clear benefit for 2,4-D sorption (see **Figure 4-5**), evidence in Chapter 3 suggests that CNTs will be the primary binding agent for most hydrophilic or moderately hydrophobic organic pollutant targets in PAN-based ENMs. Thus, for the most versatile sorbent, the inclusion of TBAB should not interfere with available CNT binding sites.

Sorption experiments were conducted with atrazine, diuron and metolachlor (**Figure 4-8**), three pesticides commonly detected in agriculturally impacted surface waters.^{274, 275} All of these compounds are neutrally charged. The presence of TBAB had no impact on atrazine partitioning, with uptake curves in TBAB-containing systems matching those for non-TBAB containing

analogs, where atrazine capacity followed: COOH-CNT/PAN >> NF-CNT/PAN >> PAN. This behavior matches that reported in Chapter 3, where the presence of CNTs improved uptake on PAN ENMs, and COOH-CNTs typically produced a greater partitioning than NF-CNTs. In contrast, the inclusion of TBAB had a positive impact on the uptake of both diuron and metolachlor. For diuron and metolachlor, the performance trend for materials without TBAB matched that observed for atrazine: COOH-CNT/PAN >> NF-CNT/PAN >> PAN. However, both TBAB-containing materials outperformed all other ENMs, with TBAB-modified COOH-CNT/PAN composites achieving the greatest chemical uptake overall. We note that diuron resulted in the largest amount of partitioning (up to almost 3 g/kg) compared to metolachlor (~0.6 g/kg) and atrazine (~0.4 g/kg), all on COOH-CNT containing sorbents.

We attribute the difference effect of TBAB on atrazine relative to diuron and metolachlor to differences in the chemical structure of these neutral target analytes. While all three targets share common functional groups (e.g., chlorine substituents, amine centers, and aromatic π -bonds), a key distinction in diuron and metolachlor is the presence of a ketone group, where the associated oxygen will possess lone electron pairs. We would anticipate an accumulation of partial negative charge on this oxygen, and this may promote interaction with surface quaternary ammonium groups. Additional work is needed to explore a broader range of neutral organic chemical targets and identify structural elements likely to benefit (or hinder) their interaction with positively charged quaternary ammonium sites on surfactant-modified ENM surfaces.

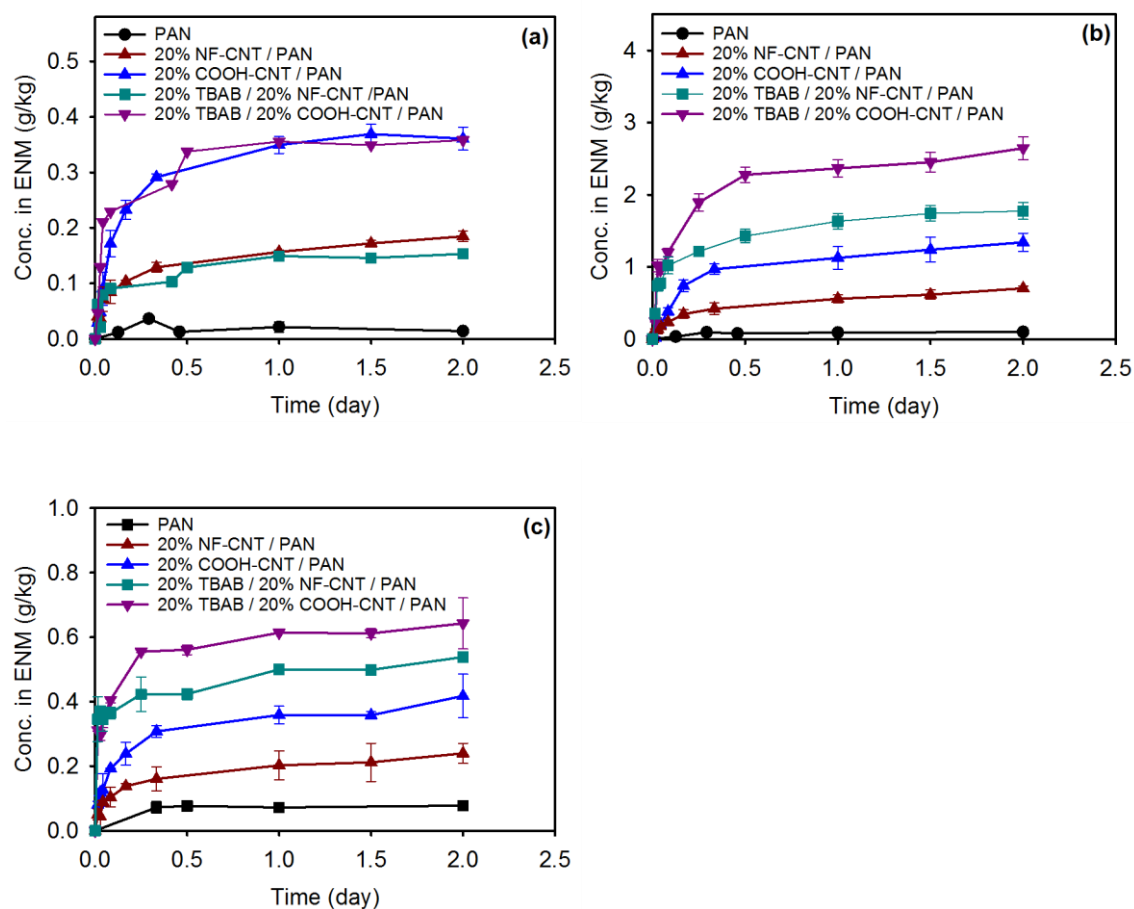


Figure 4-8. Uptake curves for (a) atrazine (b) diuron and (c) metolachlor on PAN, CNT/PAN, and TBAB-modified CNT/PAN. Uncertainties represent the standard deviation from three replicate experiments. Experimental conditions: pH 7 (1 mM Potassium phosphate DI in DI water); Initial concentration of atrazine: 5.4 mg/L, diuron: 5.8 mg/L, metolachlor: 7.1 mg/L; ENM loading: ~1.5 g/L. Experiments with surfactant-modified and CNT-modified ENMs were carried out under a static (no mixing) condition, whereas data with unmodified PAN were collected in well-mixed reactor systems.

Use of SDS as a porogen to improve PAN-ENM performance. To create more porous nanofibers,²⁷⁶ two mass ratios of SDS (20 and 40% wt.) were integrated into CNT/PAN during electrospinning. Then, these SDS-modified ENMs (2.5 g/L) were tumbled in DI water for 24 hours (with water replaced every 8 h) to remove the SDS via leaching. Washed ENMs were then

used in uptake experiments with atrazine to determine the influence of SDS mass loading on CNT/PAN performance (**Figure 4-9**).

For NF-CNT/PAN, 20 and 40% wt. of SDS exerted a similar, positive influence on atrazine uptake. The porosity induced in the material through SDS release resulted in a nearly 2-fold increase in atrazine uptake (from ~0.15 g/kg to ~0.3 g/kg) for both materials. These increases are on the order of those measured for pore volume and surface area after removal of 20% wt. SDS from CNT/PAN (see **Table 4-3**). Another noteworthy observation was the very rapid initial rate of atrazine uptake, with as much as 0.25 g/kg (a value nearly equivalent to equilibrium) partitioning in the first 2 hours, suggesting a positive influence of SDS-induced porosity on uptake rates.

For COOH-CNT/PAN, the influence of SDS mass loading was different. While 20% wt. SDS improved atrazine uptake by ~50%, achieving the highest level of atrazine uptake for any ENM we have thus far developed, there was little improvement in sorption capacity at 40% wt. At these higher surfactant loadings, we speculate that there may be interactions between SDS and the COOH-CNTs that negatively impact pore formation during our leaching process. Notably, while 40% wt. SDS in COOH-CNT/PAN had the same atrazine capacity as that of non-SDS treated materials, we observed much faster rates of atrazine uptake on the SDS-modified materials (see **Figure 4-9b**). Thus, there still may be a benefit of shorter equilibration times (i.e., shorter deployment times) for SDS-treated ENMs even when uptake capacity remains unchanged.

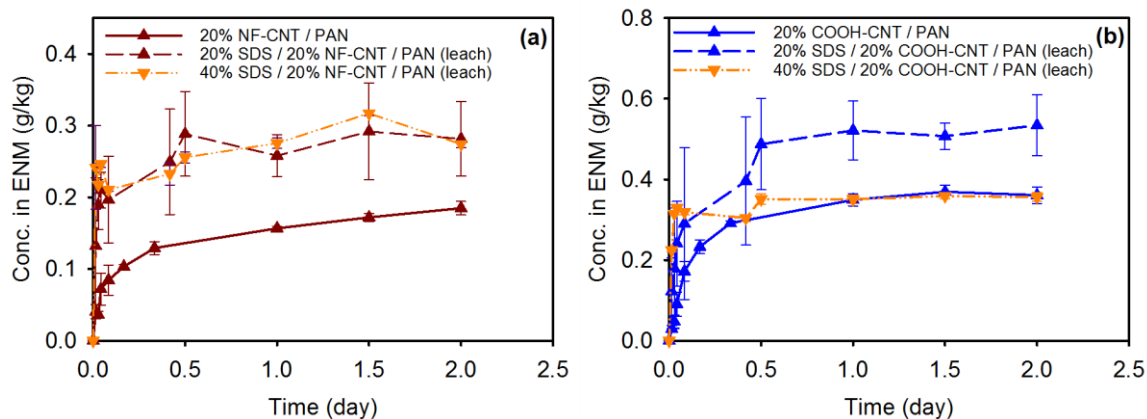


Figure 4-9. Uptake curves for atrazine on SDS-modified (a) NF-CNT/PAN and (b) COOH-CNT/PAN. Data are shown for two different mass loadings of SDS, 20% and 40% wt. Uncertainties represent the standard deviation from three replicate experiments. Experimental conditions: pH 7 (1 mM phosphate); initial concentration of atrazine: 5.4 mg/L; ENM loading: ~1.5 g/L. Experiments were carried out under a static (no mixing) condition.

Additional uptake experiments were conducted with diuron and metolachlor to ensure that the positive benefits of SDS-induced porosity observed for atrazine were generally applicable to other species (**Figure 4-10**). Indeed, for these other target analytes, comparable increases in sorption rate and capacity were observed for 20% wt. SDS-treated ENMs. Diuron exhibited behavior comparable to atrazine, with a nearly 2-fold increase in uptake capacity for both NF-CNT/PAN and COOH-CNT/PAN. Consistent with our findings in Chapter 3, COOH-CNT/PAN outperformed NF-CNT/PAN both before and after SDS treatment. Metolachlor, on the other hand, exhibited slightly different behavior; while COOH-CNT/PAN represents a better sorbent than NF-CNT/PAN, porosity induced by 20% wt. SDS resulted in both types of CNT composites exhibiting identical reactivity. Accordingly, SDS treatment resulted in a greater increase in metolachlor capacity for NF-CNT/PAN (~3-fold) relative to COOH-CNT/PAN (~1.5-fold). This suggests that the structure of the chemical target may influence the performance

of the SDS-treated materials. For example, the molecular size may influence what fraction of the SDS-induced pores are accessible. Alternatively, in our prior investigation using SDS as a porogen to improve metal cation (Pb^{2+} , Cu^{2+} and Cd^{2+}) uptake on iron oxide-PAN nanocomposites,¹⁴¹ we found that residual SDS retained in the polymer matrix after leaching can influence nanofiber surface chemistry. Accordingly, residual SDS may contribute a partial negative charge to the ENM surface that would also be expected to influence the uptake (potentially either favorably or unfavorably) of polar or ionizable organic targets.

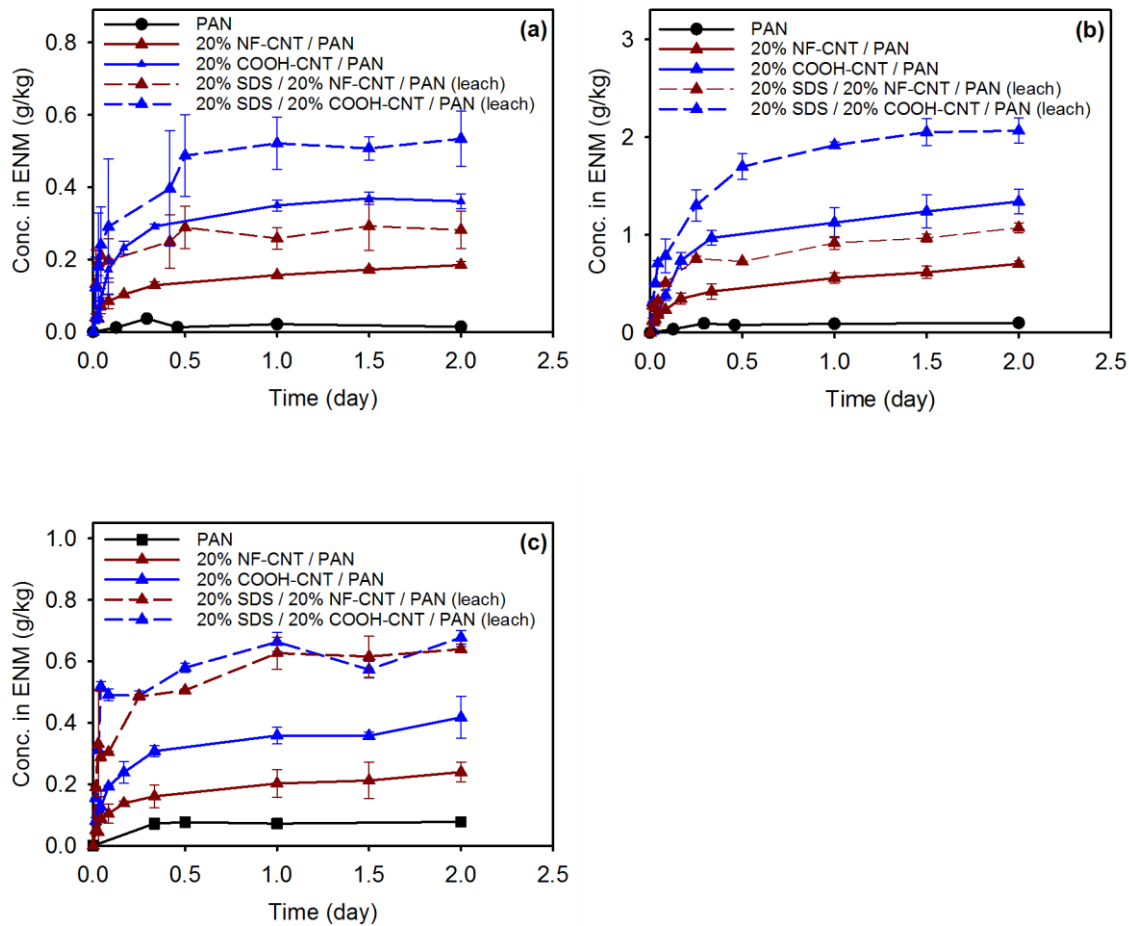


Figure 4-10. Uptake curves for (a) atrazine (b) diuron and (c) metolachlor on PAN, CNT/PAN, and SDS-modified CNT/PAN. Uncertainties represent the standard deviation from three replicate experiments. Experimental conditions: pH 7 (1 mM phosphate); initial concentration of atrazine: 5.4 mg/L, diuron: 5.8 mg/L, metolachlor: 7.1 mg/L; ENM loading: ~1.5 g/L. Experiments with

surfactant-modified and CNT-modified ENMs were carried out under a static (no mixing) condition, whereas data with unmodified PAN-ENMs was collected in well-mixed reactor systems.

Influence of environmental variables on surfactant-modified ENM performance. As a final performance consideration, we investigated the influence of several variables relevant to the field deployment of surfactant-modified ENMs. Of particular concern was evaluating how positively charged TBAB-modified materials would be influenced by the presence of common aqueous co-solutes including dissolved organic matter, which is generally anionic in nature.

Tests were conducted with 2,4-D and atrazine in solutions containing 5 mg/L of Fluka humic acid (FHA) (**Figure 4-11**). We note that because of the greater complexity of these solutions, the concentration of analyte associated with the ENM in **Figure 4-11** (the y-axis value) was estimated via mass balance from the difference between the initial aqueous concentration and the concentration measured at each sampling point ($C_{\text{ENM}} = C_{\text{w0}} - C_{\text{wt}}$).

As shown in **Figure 4-11**, all TBAB-modified ENMs (i.e., PAN, NF-CNT/PAN, and COOH-CNT/PAN) maintained their sorption capacity toward these target analytes in the presence of FHA at levels (5 mg/L) typical for many surface water sources. In fact, based on changes in solution phase concentration, there was greater uptake of atrazine by ENMs in the presence of FHA (**Figure 4-11b**). We speculate that uptake of atrazine is enhanced through its hydrophobic partitioning into FHA,²⁷⁷ which can then also attach to the ENM surface. Indeed, when $K_{\text{ENM-w}}$ values were calculated for these systems by extracting the ENM-bound atrazine using methanol, the values were identical to that measured in model (phosphate buffer) water systems (**Table 4-5**), suggesting the additional atrazine removed from solution was tightly associated with FHA. This scenario would also be consistent with why a similar increase in

uptake was not observed for anionic 2,4-D, which because of its charge is less likely to bind to FHA.

To further evaluate performance in complex matrices, we also conducted uptake studies with 2,4-D and atrazine in Iowa River water. Iowa River water contains many potential confounding species for passive sampler performance, including dissolved and colloidal organic matter, alkalinity (as HCO_3^-), and hardness causing ions (Ca^{2+} and Mg^{2+}).²⁷⁸⁻²⁸¹ The Iowa River is also located in an agriculturally impacted watershed, and would have many other agriculturally derived pollutants including nitrate and phosphate, as well as pesticides. Thus, the Iowa River represents a matrix in which passive sampling materials would likely be deployed for measurement of pesticides and related organic micropollutants (e.g., antibiotics used in animal agriculture).

As with results from FHA-containing systems, values of $K_{\text{ENM-W}}$ were identical in Iowa River water tests to those measured in FHA-containing and model (phosphate buffer) water systems (**Table 4-5**). The invariance in $K_{\text{ENM-W}}$ values for TBAB-modified EMMs as a function of solution complexity suggests they can be readily deployed in surface waters and sediments for measurement of target organic analytes.

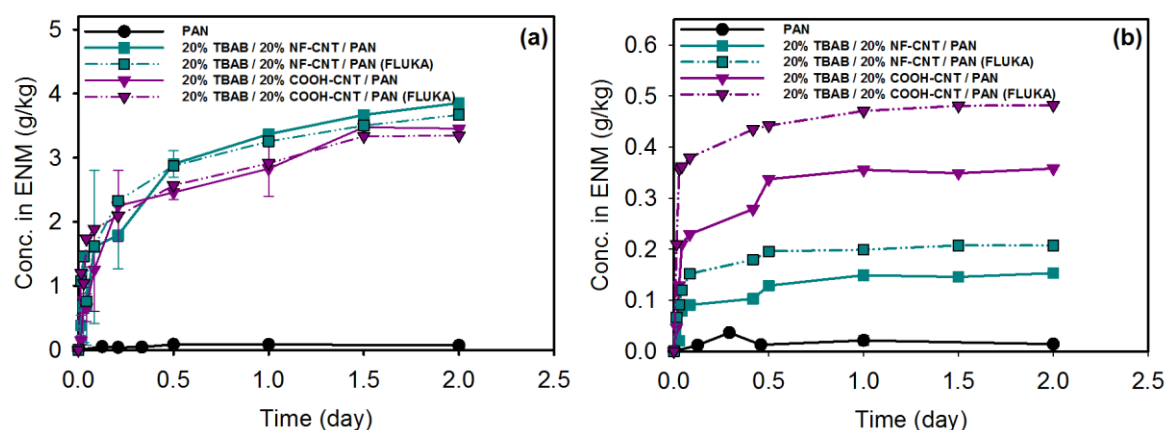


Figure 4-11. Uptake curves for (a) 2,4-D and (b) atrazine in solutions with 5 mg/L of Fluka Humic Acid (FHA). Because of the greater complexity of these solutions, the concentration of analyte associated with the ENM was estimated via mass balance from the difference between the initial aqueous concentration and the concentration measured at each sampling point. Experimental conditions: pH 7 (1 mM phosphate); initial concentration of atrazine: 5.4 mg/L, 2,4-D: 5.5 mg/L; ENM loading: ~1.5 g/L. Experiments with surfactant-modified and CNT-modified ENMs were carried out under a static (no mixing) condition, whereas data with unmodified PAN were collected in well-mixed reactor systems.

Table 4-5. Values of $\log K_{ENM-W}$ for atrazine and 2,4-D as measured in model DI water systems (i.e., 1 mM phosphate buffer), systems containing 5 mg/L of FHA, and in Iowa River water. Values represent mean and standard deviation on K_{ENM-W} values from at least two experiments.

Sorbent	Atrazine			2,4-D		
	DI water (n = 3)	FLUKA (n = 3)	Iowa River (n = 2)	DI water (n = 3)	FLUKA (n = 3)	Iowa River (n = 2)
20% TBAB PAN	1.5 ± 0.04	N.M.	1.6 ± 0.1	3.6 ± 0.1	N.M.	3.4 ± 0.2
20%TBAB 20% NF-CNT PAN	1.7 ± 0.03	1.7 ± 0.02	N.M.	3.6 ± 0.2	3.0 ± 0.06	N.M.
20%TBAB 20% COOH-CNT PAN	2.0 ± 0.08	2.0 ± 0.06	2.0 ± 0.1	3.2 ± 0.1	2.8 ± 0.07	3.1 ± 0.05

For equilibrium passive samplers, temperature represents another important environmental factor that can influence uptake rates, sorption capacity, and partitioning behavior.^{231, 234} Experiments with atrazine and 2,4-D were conducted with PAN-based ENMs at 4 °C, 20 °C and 35 °C to represent the seasonal (winter to summer) range of surface water temperatures. From the data in **Table 4-6**, we observed two different K_{ENM-W} behaviors for TBAB-modified ENMs. For the neutrally charged atrazine, where PAN and COOH-CNT surfaces represent the primary sorption site, K_{ENM-W} value were independent of temperature across this range. In contrast, for anionic 2,4-D, where surface quaternary ammonium sites of TBAB promote uptake via favorable electrostatic interactions and ion exchange, values of K_{ENM-W} were markedly lower at 4 °C compared to more elevated temperatures. Accordingly, the utility of TBAB-modified materials for anionic targets may be more limited in the winter, where less uptake would be expected.

Table 4-6. Values of $\log K_{ENM-W}$ for atrazine and 2,4-D as measured at 4 °C, 20 °C and 35 °C. Values represent mean and standard deviation on K_{ENM-W} values from three experiments.

Sorbent	Atrazine			2,4-D		
	4°C (n=3)	20°C (n=3)	35°C (n=3)	4°C (n=3)	20°C (n=3)	35°C (n=3)
20% TBAB PAN	1.4 ± 0.03	1.5 ± 0.04	1.5 ± 0.08	2.8 ± 0.2	3.6 ± 0.1	3.3 ± 0.3
20% TBAB 20% COOH-CNT PAN	2.0 ± 0.05	2.0 ± 0.08	1.9 ± 0.1	2.4 ± 0.2	3.2 ± 0.1	3.0 ± 0.3

As a final assessment of their performance in complex matrices, we deployed two TBAB-modified materials at Muddy Creek, Coralville, IA (USGS 05454090) for 2 days. Images of the freshly prepared, deployed, and cleaned materials are shown in **Table 4-7**. TBAB-modified ENMs recovered from the deployment site remained relatively clean during application and were

easily washed and processed to remove most of the colloidal debris or organic matter that accumulated over the monitoring period. Notably, TBAB is biocidal,^{252, 282} and thus we had expected that the ENMs would be less prone to biofouling (although longer deployments are needed to test whether this is indeed the case). Analysis of methanol extracts collected from these sampling devices via LC/MS/MS, as was conducted in Chapter 3 for comparison to USGS grab samples of surface water at the site, remains ongoing.

Table 4-7. Images of freshly prepared, field deployed, and washed TBAB-modified ENMs. Images are provided both for PAN and COOH-CNT/PAN ENMs. Samples were deployed for 2 days at Muddy Creek, Coralville, IA (USGS 05454090).

	20% TBAB/PAN	20%TBAB/20%COOH-CNT/PAN
Newly Prepared		
After deployment		
After Cleaning		

4.5 CONCLUSIONS AND ENVIRONMENTAL IMPLICATIONS

Herein, we have demonstrated that surfactants can be used to improve the uptake of organic compounds by electrospun polymer nanofibers (e.g., polyacrylonitrile or PAN) and polymer-carbon nanotube (CNT/PAN) composites. While surfactants have long been used to improve the fabrication of polymer nanofibers via electrospinning, recent advances by our group and others have shown that surfactants can also be used to increase the functionality of the resulting nanofibers.^{145, 252-254} Easily blended into sol gel precursors solutions, surfactants (e.g., TBAB and CTAB) can be used to impart surface charge, or be intentionally leached from the nanofiber framework to increase reactive surface area (SDS). The work herein represents the first demonstration of these approaches being exploited to improve the rate and extent of organic pollutant uptake by polymer ENMs and ENM nanocomposites. Accordingly, this work builds upon the works in Chapter 2 and 3, further illustrating our ability to tailor ENM physical and chemical properties so as to optimize their performance as equilibrium passive sampler materials. Indeed, **Table 4-8** summarizes the $\log K_{\text{ENM-W}}$ values measured with surfactant-modified materials, with maximum values representing the highest we have reported for these target analytes across our entire body of work with ENMs.

While surfactant-modified materials are certainly promising for future applications, additional work is needed to further optimize and validate the performance of these materials. Evidence suggests that for TBAB-containing ENMs, which are clearly beneficial for targeting dissolved anions, there are also more subtle, structure-dependent specific binding interactions that will help promote uptake of neutral species. A future investigation to establish such chemical structure-ENM activity relationship is needed to identify the range of chemical targets for which TBAB-modified materials would be well-suited (or alternatively, ill-suited). As

another example, in CNT-containing composites, a more systematic investigation of the interactions between surfactants and CNTs is warranted, as such interactions will influence the type and abundance of sites present on the ENM surface for chemical uptake. There may even exist an as yet unidentified optimal surfactant-to-CNT ratio that promotes the co-location of TBAB and CNTs to the nanofiber surface, as we have previously identified for TBAB and metal oxides nanoparticles in PAN.¹⁴⁵ Finally, field deployment and performance comparison to more traditional grab sampling are needed to verify that the promise of these innovative surfactant-modified materials can be transferred from the benchtop to the field.

Table 4-8. Summary of $\log K_{ENM-W}$ values measured herein with surfactant-modified materials across the target organic analyte suite.

Compound	Atrazine (n = 3)	2,4-D (n = 3)	Diuron (n = 3)	Metolachlor (n = 3)	PFOA (n=2)
PAN	1.2 ± 0.1 ^a	1.1 ± 0.2 ^a	1.4 ± 0.02 ^a	1.3 ± 0.03	1.7 ± 0.3 ^e
20% TBAB PAN	1.5 ± 0.04	3.6 ± 0.1	N.M.	N.M.	N.M.
20% CTAB PAN	N.M.	2.5 ± 0.03	N.M.	N.M.	N.M.
20% NF-CNT PAN	1.5 ± 0.07	1.4 ± 0.02	2.1 ± 0.1	1.8 ± 0.05	N.M.
20% TBAB 20% NF-CNT PAN	1.7 ± 0.03	3.6 ± 0.2	2.6 ± 0.03	1.9 ± 0.02	N.M.
20% CTAB 20% NF-CNT PAN	1.6 ± 0.02	3.3 ± 0.1	N.M.	N.M.	N.M.
20% SDS 20% NF-CNT PAN ^L	1.6 ± 0.1	N.M.	2.1 ± 0.03	1.9 ± 0.01	N.M.
20% COOH-CNT PAN	1.8 ± 0.02	1.8 ± 0.03	2.4 ± 0.1	1.6 ± 0.05	1.4 ± 0.03 ^e
20% TBAB 20% COOH-CNT PAN	2.0 ± 0.08	3.2 ± 0.1	2.9 ± 0.01	2.0 ± 0.03	3.5 ± 0.01 ^e
20% CTAB 20% COOH-CNT PAN	1.7 ± 0.03	3.1 ± 0.1	N.M.	N.M.	N.M.
20% SDS 20% COOH-CNT PAN ^L	1.9 ± 0.04	N.M.	2.6 ± 0.01	1.9 ± 0.02	N.M.

^a Less than 5% of the total aqueous mass was sorbed into the ENM. Initial Concentration of chemicals: 25µM; ENM loading: ~1.5 g/L. ^L Surfactant salts in ENM was leached out before measurement. ^e $\log K_{ENM-W}$ was estimated with mass balance number by assuming 100% recovery during the extraction procedure.

CHAPTER 5 CONCLUSIONS & FUTURE RESEARCH DIRECTIONS

5.1 Thesis overview

Thesis background and motivation. The use of nanomaterials to design environmental treatment and monitoring devices is an emerging trend in the fields associated with the study and protection of environmental quality. However, when focusing specifically on monitoring via passive sampling, which is the thrust of this thesis, while many polymer-based sampling devices have been developed and used in the field, very few have attempted to harness nanotechnology to improve performance. Because passive sampling materials operate through organic pollutant surface accumulation and/or bulk partitioning, use of high surface area to volume nanomaterials represents a promising way to explore more and better possibilities for passive sampler material development.

New passive sampling materials are needed because there are several opportunities to greatly increase the functionality and performance of these devices over what is currently available in commercial options. For example, a multi-target sampling device will not only improve the efficiency of passive sampler deployments but also help to better characterize contaminated sites plagued by complex and diverse pollutant mixtures. Equilibrium passive sampling devices would also represent a significant advancement, improving the spatial and temporal resolution of data available from passive sampling devices, while considerably simplifying analytical procedures by eliminating the need for reference compounds.

Overview of thesis approach. In this work, we intended to assemble all these benefits into a next-generation passive sampling device fabricated using electrospun polymer nanofibers and nanofiber composites. We chose this platform because the morphology, size, and inherent porous structure of electrospun nanofibers are likely to promote a fast uptake rate and facilitate device

operation by equilibrium partitioning,^{161, 283} which holds advantages over integrative passive samplers. Our initial focus on polymers was motivated by studies that have demonstrated that polymers including polyethylene and polystyrene,²⁸⁴ polydimethylsiloxane films,^{167, 285} and polyurethane foams²⁸⁶⁻²⁸⁸ exhibit good performance for passive sampling based monitoring of hydrophobic POPs.

Building off the baseline performance of these polymers, innovative aspects of our approach include exploring the performance of more hydrophilic polymers like polyacrylonitrile (PAN), and then tailoring the physical and chemical properties of these polymers through formation of CNT nanocomposites and surfactant-modified materials. In particular, we felt these additional approaches to material optimization were necessary to expand beyond monitoring of POPs and other legacy pollutants, and sensitively and selectively bind HMHCs. Notably, there are likely to be ancillary benefits of these approaches, including improved mechanical strength (through the integration of CNTs) and antifouling properties (through the inclusion of biocidal QAS). As a fundamental aim, we strived to establish the mechanism of target pollutant uptake (e.g., adsorption or absorption) and optimal application mode (e.g., integrative or equilibrium partitioning), as many theories have been proposed for existing passive sampling devices.^{289, 290} More practically, and in addition to laboratory optimization studies, this thesis also includes data from field deployment of select ENMs, which allows their performance to be compared to more traditional, active monitoring approaches (e.g., grab sampling).

5.2 Summary of key findings

There are three research chapters in this dissertation. Chapter 2 determined that polymer ENMs are a promising passive sampling material for both POPs and HMHC. Chapter 3 demonstrates that ENM/CNT nanocomposites exhibit improved sorption performance for a suite of HMHC targets, including high rates of uptake and high capacity. Chapter 4 illustrates that cationic and anionic surfactants can be used to change the bulk properties (e.g., porosity and surface area) and surface chemistry of ENM/CNT composites to further enhance their performance, including targeting their application to charged analytes. A more detailed summary of major findings from each Chapter is presented below.

5.2.1 Polymer electrospun nanofibers are a promising sampling material for both POPs and HMHC.

Chapter 2 serves as the foundation of this research because it confirmed the feasibility of using polymer ENMs as sorbents to design new passive sampling tools. Seven different polymers were used to fabricate nanofibers, which was accomplished with high reproducibility for the majority of polymers considered [ethylene-vinyl acetate (EVA) proved difficult to synthesize and polyvinyl acetate (PVAc) was water soluble and thus not well-suited for our target application.

The K_{ENM-W} of 19 hydrophobic and hydrophilic organic compounds were measured by the remaining five ENMs, polyacrylonitrile (PAN), Polymethyl methacrylate (PMMA), polystyrene (PS), polyvinylidene fluoride (PVDF) and polyethylene terephthalate (PET). Large partitioning coefficients greater than 3 log units were measured for all hydrophobic pollutants ($\log K_{ow} > 4.0$), and these values typically matched or exceed those reported for current commercially available passive samplers. Although we also report measured K_{ENM-W} values for several hydrophilic

targets ($\log K_{ow} < 2$), the extent of removal from the aqueous phase remained relatively low (~5% or less) for some of the more highly polar compounds. This result highlighted the need for additional optimization to increase uptake, particularly for hydrophilic species, and served as motivation for the tailoring of ENMs to improve performance in subsequent chapters.

In addition to reporting these K_{ENM-W} values for 5 polymers and 19 organic targets, Chapter 2 also contains several important results addressing both fundamental and practical performance insights. Values of K_{ENM-W} were found to be independent of pH, initial chemical concentration, polymer wettability (measured via contact angle), and ENM average nanofiber diameter. Notably, a smaller diameter produced a faster uptake rate, and suggests that nanofibers promote the use of ENMs as equilibrium passive sampling materials. We also presented the results of poly-parameter linear free energy relationships (pp-LFERs) that lend insight into the properties of the chemical target and the polymer ENM most beneficial for performance. More practically, the optimal ENMs (PS, PAN and PMMA) all performed well in both simulated (using model soils spiked with nitrobenzene) and real (nearly 30 d deployment at Indiana Harbor to measure PCBs) applications for measurement of sediment pore water concentration, with values determined via use of ENMs match more traditional sampling approaches.

5.2.2 Carbon nanotubes can be integrated into polymer ENMs to enhance performance.

In Chapter 3, to enhance ENM sorption performance toward HMHCs, CNTs were added to polymer nanofiber matrices to fabricate ENM-CNT nanocomposites. Two kinds of short, multi-wall CNTs were used: non-functionalized CNTs and oxidized CNTs primarily with surface carboxyl groups. The major outcome of Chapter 3 is that the integration of CNTs significantly increases both surface area and pore volume, which in turn enhanced uptake of our target analyte suite by as much as 50-fold relative to pure polymers. Additionally, the uptake rates achieved

with ENM-CNT composites was faster than a pure polymer ENM (typically less than 0.5 h), shortening the time that would be required for these materials to achieve equilibrium during deployment

Additional work explored how ENM-CNTs could be optimized, and sorption cross correlations and LFERs were developed to help identify the key material and chemical factors driving pollutant uptake. For example, higher CNT loadings produce larger sorption capacities (although we observed a practical limit to fabrication via electrospinning at 25% and 40% wt. for COOH-CNT and NF-CNTs, respectively). Also, K_{ENM-W} on all ENM-CNT composites were found to be independent of pH, temperature, and nanofiber diameter, and due to their high capacity, we also expect values of K_{ENM-W} will be independent of target analyte concentration at environmentally relevant values. More fundamentally, no correlation was observed between K_{ENM-W} values on ENM-CNTs and K_d values measured in CNT suspensions; thus while we suspect that the CNTs are the primary binding site for target analytes in these nanocomposites, the process of embedding the CNTs in polymer nanofibers generates a chemical environment where these embedded CNTs exhibit sorption distinct from their freely dispersed analogs. Using chemical predictors including $\log K_{ow}$ values, we find that CNT/PS composites are best suited for targeting hydrophobic pollutants, while uptake on CNT/PAN composites was largely independent of $\log K_{ow}$ values.

Finally, the versatility of these materials was demonstrated through field deployments of CNT/PAN composites at Muddy Creek, IA. Results from this deployment for atrazine agreed reasonably well with atrazine levels determined via grab sampling conducted by the USGS. Most notably, the materials were easily cleaned, and free of extensive colloidal or biological

fouling after deployment, resulting in relatively easy processing (e.g., cleaning and extraction) and liquid chromatography analysis after field deployment

5.2.3 Surfactants can be added to increase surface area and target charged analytes.

Chapter 4, we modified ENMs through the addition of surfactants. We selected quaternary ammonium salts CTAB and TBAB because they are (i) surface-segregating and (ii) their quaternary ammonium moiety is often exploited for ion exchange applications. Surfactant-modified ENMs exhibited a large increase in uptake of 2,4-D, an anionic pesticide, outperforming ENMs without surfactants by more than 50-fold. Similar improvements in uptake were also observed for anionic PFOA. Inclusion of these cationic surfactants even improved the partitioning of some neutral compounds, particularly those with electron-rich functional groups (e.g., carbonyl groups with oxygen lone pairs). TBAB appears more practically viable for tailoring ENM surface chemistry than CTAB, as CTAB is only weakly bound in the polymer matrix and can release or leach from the ENM over time.

In Chapter 4, we also used the anionic surfactant SDS as a removable porogen to increase ENM pore volume and surface area.¹⁴¹ Indeed, using atrazine as our target analyte, we saw increases in atrazine uptake on par with gains in surface area resulting from the intentional removal of SDS after initially integrating it into ENM synthesis.

An important consideration in using surfactant modified materials, particularly those relying on surface-enriched TBAB for target analyte uptake, is the impact of non-target solutes on performance. In more complex matrices including humic acid solutions and in Iowa River water, K_{ENM-W} values did not change. Some field testing with these materials were conducted. While analytical challenges have prevented us from quantifying target analytes using TBAB-modified materials (i.e., we suspect that trace amounts of TBAB leaching from the material are interfering with LC-MS/MS analysis), we found that these materials were not prone to fouling and could be easily cleaned and processed, as we also observed for ENM-CNT composites in Chapter 3.

5.3 Future research needs

Collectively, the final product of this thesis is a frame-designed passive sampling device using optimized ENMs as the sorbent phase. Several ENM formulations have been developed and validated, and some are specifically tailored for target analytes (e.g., CNT/PS for hydrophobic materials or TBAB-modified materials for anionic targets), while others exhibit a broad spectrum of target reactivity (e.g., CNT/PAN). In addition to our laboratory optimization experiments, environmental deployment with our materials reveals high versatility and good antifouling activity in different, complex environmental monitoring conditions. To date, we have successfully used our ENM passive sampler to monitor both POPs in sediment pore water (PCBs at Indiana Harbor) and HMHCs in surface water (atrazine at Muddy Creek) in the environment.

Nevertheless, opportunities exist to further investigate and improve the use of ENM in environmental monitoring, or related applications in environmental quality. For example, more

conventional polymer functionalization methods can be attempted to improve ENM selectivity, which remains a challenge when looking for a single analyte in a complex environmental mixture. As a result of their high rates and capacity for organic pollutant partitioning, we can envision new applications for ENMs as innovative filtration materials in water or air treatment. With our current materials, more field deployments are required to test their long term stability and performance in challenging environments such as high flow surface waters, winter, and in heavily contaminated systems (e.g., wastewater outfalls or agricultural runoff). Finally, the fundamental mechanisms driving ENM operation should be better understood, particularly for composites and surfactant modified materials where multiple characteristics of the chemical target and the ENM surface may influence partitioning. Some specific examples of future research in each of these areas are briefly discussed below.

5.3.1 Use molecular imprinting techniques to improve ENM selectivity.

Molecular imprinting technology (MIT) is a method to introduce predetermined functional groups into polymer matrices by binding active sites from template molecules.²⁹¹ The technology was first conceptualized in the 1970s and has developed quickly over the past 20 years.²⁹² The MIT tailored materials have a high selectivity due to its artificial recognition entities, thus people use them to mimic natural “lock-and-key” interactions like antibodies.^{293, 294} MIT is considered a promising technique for preparation of synthetic polymers that can specifically recognize both chemical and biological molecules and is widely used in many fields such as solid phase extraction,^{295, 296} membrane separation technology²⁹⁷ and pollutants sorption.^{298, 299} Accordingly, it has been demonstrated that MIT treated polymer nanofibers represent good sorbent materials to remove organic chemicals from the aqueous phase.^{300, 301} For passive sampling device applications, there are a few reports about using MIT to enhance the sensitivity of materials toward strongly polar organic compounds.³⁰² As such, integrating appropriate template

molecules for polar organic pollutants into our ENM may be a worthwhile way to enhance our sampling device selectivity, especially for hydrophilic chemicals.

5.3.2 Additional field testing.

So far, we have deployed our ENMs in fresh water sediment and in the surface water of a small creek. More field deployment should be done to demonstrate our sampling devices can be used in different, even more extreme, environments. Examples include application in surface waters with a range of discharge rates (from high flow to low flow), seasonal performance testing from winter through summer, and longer-term deployments in complex pollutant mixtures (e.g., wastewater outfalls and agricultural or urban runoff). Specific attempts should also be made to evaluate the antimicrobial activity of TBAB and/or CNT-containing ENMs. One place where this could be done is in systems with eutrophication and high rates of biological activity in surface water, where organic pollutants can be related to this phenomena.^{303, 304}

5.3.3 Mechanistic studies with optimized ENMs.

So far, pp-LFERs were only developed for pure polymer ENMs in Chapter 2. A deeper understanding of the mechanism of ENM-CNT composites and surfactant-modified ENMs would be helpful to determine the main factors influencing their performance and clarify the direction of further optimization. This will involve additional characterization of the modified-ENMs to develop variables for use in the pp-LFERs. For example, Fourier Transform Infrared (FTIR) and X-ray photoelectron spectroscopy could be used to measure the bulk and surface concentration of functional groups or bulk and surface atomic composition of our materials. For ENM-CNT composites, models have been proposed to describe the dispersion of CNT in polymer nanofibers based on CNT properties such as length, diameter and crystal habit.³⁰⁵⁻³⁰⁷ For

surfactant-modified materials, a useful metric is likely the amount of charged sites located on the ENM surface, which may be quantifiable through titrations or electrochemical characterization approaches. In this way, correlations between ENM chemical characteristics and sorption capacity for target analytes may be discovered.

5.3.4 Additional environmental applications of ENMs.

The high rates and uptake capacity of ENMs enable other potential applications in environmental management. Some possible examples include:

Water Filtration: The natural network of ENMs is an ideal structure for water filtration materials. The porous structure can provide thousands of micro-channels to let water flow through. During this process, the high surface-area of the polymer network will be in contact with the water. Besides physically filtering our solid particles, it may also be possible to kill bacteria and viruses, or remove organic pollutants or metals. Both goals could be achieved by integrating nanomaterials and/or charged surfactants onto the nanofiber surface.^{308, 309} Although we demonstrate a quick uptake rate of ENM as a passive sampling material in batch systems, a scaled-up experiment conducted under flow is required to evaluate the filtration efficiency. Also, more development of the mechanical properties of ENMs will be needed to optimize tensile strength, temperature expansion, and average pore radius, among others, for this application

Air sampling devices: In Chapter 2, a significant uptake of POPs was found on all tested pure polymer based ENMs. It is believed that most polymers (both bulk and nanofiber) have a high-performance adsorption to POPs due to the generally hydrophobic nature of their long carbon-carbon chain structure.³¹⁰ The porous structure of ENMs is the biggest advantage compared with other bulk sorbents, and the highly exposed nanofiber surface can likely shorten

the integration time of POPs relative to other materials. PCBs and other POPs can be transported through air,³¹¹⁻³¹³ thus an air equilibrium passive sampling tool can likely also be designed with ENMs to also take advantages of their beneficial properties. However, their application to a different environmental media may require some adaptations in application platforms. For example, the main challenge as an air sampler is the competition from small solid particles in the air, which can capture POPs. These particles could also be trapped in ENMs resulting in an illusory increase of POPs accumulation. A sandwich design by flatting ENMs in two protecting membranes would be a good solution.

LITERATURE CITED

1. About NTP. *National Toxicology Program* **2018**, <https://ntp.niehs.nih.gov/about/>.
2. Gascon, M.; Morales, E.; Sunyer, J.; Vrijheid, M., Effects of persistent organic pollutants on the developing respiratory and immune systems: A systematic review. *Environ. Int.* **2013**, *52*, 51-65.
3. Pappas, G. P.; Herbert, R. J.; Henderson, W.; Koenig, J.; Stover, B.; Barnhart, S., The respiratory effects of volatile organic compounds. *Int. J. Occup. Environ. Health* **2000**, *6*, (1), 1-8.
4. Carpenter, D. O. In *Organic chemicals and the immune system*, 2013; John Wiley & Sons, Inc.: 2013; pp 362-383.
5. Vested, A.; Giwercman, A.; Bonde, J. P.; Toft, G., Persistent organic pollutants and male reproductive health. *Asian J. Androl.* **2014**, *16*, (1), 71-80, 10 pp.
6. Grindler, N. M.; Allsworth, J. E.; Macones, G. A.; Kannan, K.; Roehl, K. A.; Cooper, A. R., Persistent Organic Pollutants and Early Menopause in US Women. *Plos One* **2015**, *10*, (1), 12.
7. Casals-Casas, C.; Desvergne, B., Endocrine Disruptors: From Endocrine to Metabolic Disruption. In *Annual Review of Physiology, Vol 73*, Julius, D.; Clapham, D. E., Eds. Annual Reviews: Palo Alto, 2011; Vol. 73, pp 135-162.
8. Kidd, K. A.; Paterson, M. J.; Rennie, M. D.; Podemski, C. L.; Findlay, D. L.; Blanchfield, P. J.; Liber, K., Direct and indirect responses of a freshwater food web to a potent synthetic oestrogen. *Philos. Trans. R. Soc. B-Biol. Sci.* **2014**, *369*, (1656), 11.
9. Howard, P. H.; Muir, D. C. G., Identifying New Persistent and Bioaccumulative Organics Among Chemicals in Commerce. *Environmental Science & Technology* **2010**, *44*, (7), 2277-2285.
10. Weber, R.; Watson, A.; Forter, M.; Oliaei, F., Persistent organic pollutants and landfills - a review of past experiences and future challenges. *Waste Manage. Res.* **2011**, *29*, (1), 107-121.
11. Geissen, V.; Mol, H.; Klumpp, E.; Umlauf, G.; Nadal, M.; van der Ploeg, M.; van de Zee, S. E. A. T. M.; Ritsema, C. J., Emerging pollutants in the environment: A challenge for water resource management. *International Soil and Water Conservation Research* **2015**, *3*, (1), 57-65.
12. Ren, J.; Wang, X.; Wang, C.; Gong, P.; Wang, X.; Yao, T., Biomagnification of persistent organic pollutants along a high-altitude aquatic food chain in the Tibetan Plateau: Processes and mechanisms. *Environmental Pollution* **2017**, *220*, 636-643.
13. Daley, J. M.; Paterson, G.; Drouillard, K. G., Bioamplification as a Bioaccumulation Mechanism for Persistent Organic Pollutants (POPs) in Wildlife. In *Reviews of Environmental Contamination and Toxicology, Vol 227*, Whitacre, D. M., Ed. Springer: New York, 2014; Vol. 227, pp 107-155.
14. White, S. S.; Birnbaum, L. S., An Overview of the Effects of Dioxins and Dioxin-Like Compounds on Vertebrates, as Documented in Human and Ecological Epidemiology. *J. Environ. Sci. Health Pt. C- Environ. Carcinog. Ecotoxicol. Rev.* **2009**, *27*, (4), 197-211.
15. Bakhiya, N.; Appel, K. E., Toxicity and carcinogenicity of furan in human diet. *Arch. Toxicol.* **2010**, *84*, (7), 563-578.
16. Ulbrich, B.; Stahlmann, R., Developmental toxicity of polychlorinated biphenyls (PCBs): a systematic review of experimental data. *Arch. Toxicol.* **2004**, *78*, (5), 252-268.
17. Jones, K. C.; de Voogt, P., Persistent organic pollutants (POPs): state of the science. *Environmental Pollution* **1999**, *100*, (1-3), 209-221.
18. Zaghi, C.; Conti, M. E.; Cecchetti, G., White Paper on chemicals and Stockholm convention on persistent organic pollutants: Perspectives for environmental risk management. *Int. J. Risk Assess. Manage.* **2002**, *3*, (2/3/4), 234-245.
19. Namiki, S.; Otani, T.; Seike, N., Fate and plant uptake of persistent organic pollutants in soil. *Soil Sci. Plant Nutr.* **2013**, *59*, (4), 669-679.

20. Muir, D. C. G.; Howard, P. H., Are there other persistent organic pollutants? A challenge for environmental chemists. *Environmental Science & Technology* **2006**, *40*, (23), 7157-7166.
21. Sinkkonen, S.; Paasivirta, J., Degradation half-life times of PCDDs, PCDFs and PCBs for environmental fate modeling. *Chemosphere* **2000**, *40*, (9-11), 943-949.
22. Hung, H.; Katsoyiannis, A. A.; Guardans, R., Ten years of global monitoring under the Stockholm Convention on Persistent Organic Pollutants (POPs): Trends, sources and transport modelling Preface. *Environmental Pollution* **2016**, *217*, 1-3.
23. Fisk, A. T.; Hobson, K. A.; Norstrom, R. J., Influence of chemical and biological factors on trophic transfer of persistent organic pollutants in the northwater polynya marine food web. *Environmental Science & Technology* **2001**, *35*, (4), 732-738.
24. Kelly, B. C.; Ikononou, M. G.; Blair, J. D.; Morin, A. E.; Gobas, F., Food web-specific biomagnification of persistent organic pollutants. *Science* **2007**, *317*, (5835), 236-239.
25. Abrahams, P. W., Soils: their implications to human health. *Sci. Total Environ.* **2002**, *291*, (1-3), 1-32.
26. Schwarzenbach, R. P.; Egli, T.; Hofstetter, T. B.; von Gunten, U.; Wehrli, B., Global Water Pollution and Human Health. In *Annual Review of Environment and Resources, Vol 35*, Gadgil, A.; Liverman, D. M., Eds. Annual Reviews: Palo Alto, 2010; Vol. 35, pp 109-136.
27. Li, Q. Q.; Loganath, A.; Chong, Y. S.; Tan, J.; Obbard, J. P., Persistent organic pollutants and adverse health effects in humans. *J. Toxicol. Env. Health Part A* **2006**, *69*, (21), 1987-2005.
28. Wania, F.; Mackay, D., A GLOBAL DISTRIBUTION MODEL FOR PERSISTENT ORGANIC-CHEMICALS. *Sci. Total Environ.* **1995**, *160-61*, 211-232.
29. Frimmel, F. H.; Assenmacher, M.; Sörensen, M.; Abbt-Braun, G.; Gräbe, G., Removal of hydrophilic pollutants from water with organic adsorption polymers: Part I. Adsorption behaviour of selected model compounds. *Chemical Engineering and Processing: Process Intensification* **1999**, *38*, (4), 601-610.
30. Leelamanie, D. A. L.; Karube, J., Effects of hydrophobic and hydrophilic organic matter on the water repellency of model sandy soils. *Soil Sci. Plant Nutr.* **2009**, *55*, (4), 462-467.
31. Gavrilescu, M.; Demnerová, K.; Aamand, J.; Agathos, S.; Fava, F., *Emerging Pollutants in the Environment: Present and Future Challenges in Biomonitoring, Ecological Risks and Bioremediation*. 2014; Vol. 32.
32. Gul, A., *Agricultural Pollution: An Emerging Issue*. 2014.
33. Zazouli, M. A.; Ulbricht, M.; Nasseri, S.; Susanto, H., EFFECT OF HYDROPHILIC AND HYDROPHOBIC ORGANIC MATTER ON AMOXICILLIN AND CEPHALEXIN RESIDUALS REJECTION FROM WATER BY NANOFILTRATION. *Iran. J. Environ. Health Sci. Eng.* **2010**, *7*, (1), 15-24.
34. Lamastra, L.; Balderacchi, M.; Trevisan, M., Inclusion of emerging organic contaminants in groundwater monitoring plans. *MethodsX* **2016**, *3*, 459-476.
35. Summary of the Safe Drinking Water Act. U.S. Environmental Protection Agency **1974**, <https://www.epa.gov/laws-regulations/summary-safe-drinking-water-act>.
36. Summary of the Clean Water Act. U.S. Environmental Protection Agency **1972**, <https://www.epa.gov/laws-regulations/summary-clean-water-act>.
37. Gavrilescu, M.; Demnerova, K.; Aamand, J.; Agathos, S.; Fava, F., Emerging pollutants in the environment: present and future challenges in biomonitoring, ecological risks and bioremediation. *New Biotech.* **2015**, *32*, (1), 147-156.
38. Daughton, C. G.; Ternes, T. A., Pharmaceuticals and personal care products in the environment: Agents of subtle change? *Environ. Health Perspect.* **1999**, *107*, 907-938.

39. Wilkinson, J. L.; Hooda, P. S.; Barker, J.; Barton, S.; Swinden, J., Ecotoxic pharmaceuticals, personal care products, and other emerging contaminants: A review of environmental, receptor-mediated, developmental, and epigenetic toxicity with discussion of proposed toxicity to humans. *Crit. Rev. Environ. Sci. Technol.* **2016**, *46*, (4), 336-381.
40. Fourth Unregulated Contaminant Monitoring Rule. *U.S. Environmental Protection Agency* **2016**, <https://www.epa.gov/dwucmr/fourth-unregulated-contaminant-monitoring-rule>.
41. Chiou, C. T.; Kile, D. E., EFFECTS OF POLAR AND NONPOLAR GROUPS ON THE STABILITY OF ORGANIC-COMPOUNDS IN SOIL ORGANIC-MATTER. *Environmental Science & Technology* **1994**, *28*, (6), 1139-1144.
42. Soderstrom, H.; Lindberg, R. H.; Fick, J., Strategies for monitoring the emerging polar organic contaminants in water with emphasis on integrative passive sampling. *Journal of Chromatography A* **2009**, *1216*, (3), 623-630.
43. Stuart, M.; Lapworth, D.; Crane, E.; Hart, A., Review of risk from potential emerging contaminants in UK groundwater. *Sci. Total Environ.* **2012**, *416*, 1-21.
44. Kuster, M.; de Alda, M. J.; Hernando, M. D.; Petrovic, M.; Martin-Alonso, J.; Barcelo, D., Analysis and occurrence of pharmaceuticals, estrogens, progestogens and polar pesticides in sewage treatment plant effluents, river water and drinking water in the Llobregat river basin (Barcelona, Spain). *J. Hydrol.* **2008**, *358*, (1-2), 112-123.
45. Westerhoff, P.; Yoon, Y.; Snyder, S.; Wert, E., Fate of endocrine-disruptor, pharmaceutical, and personal care product chemicals during simulated drinking water treatment processes. *Environmental Science & Technology* **2005**, *39*, (17), 6649-6663.
46. Bolong, N.; Ismail, A. F.; Salim, M. R.; Matsuura, T., A review of the effects of emerging contaminants in wastewater and options for their removal. *Desalination* **2009**, *239*, (1-3), 229-246.
47. Cwiertny, D. M.; Snyder, S. A.; Schlenk, D.; Kolodziej, E. P., Environmental Designer Drugs: When Transformation May Not Eliminate Risk. *Environmental Science & Technology* **2014**, *48*, (20), 11737-11745.
48. Brooks, B. W., Fish on Prozac (and Zoloft): Ten years later. *Aquat. Toxicol.* **2014**, *151*, 61-67.
49. Weinberger, J.; Klaper, R., Environmental concentrations of the selective serotonin reuptake inhibitor fluoxetine impact specific behaviors involved in reproduction, feeding and predator avoidance in the fish *Pimephales promelas* (fathead minnow). *Aquat. Toxicol.* **2014**, *151*, 77-83.
50. Alvarez, D. A. *Guidelines for the use of the semipermeable membrane device (SPMD) and the polar organic chemical integrative sampler (POCIS) in environmental monitoring studies*; 1-D4; Reston, VA, 2010; p 38.
51. Warren, J., Representativeness of Environmental Samples. *Environmental Forensics* **2005**, *6*, (1), 21-25.
52. Xie, Z. Y.; Ebinghaus, R., Analytical methods for the determination of emerging organic contaminants in the atmosphere. *Anal. Chim. Acta* **2008**, *610*, (2), 156-178.
53. Coes, A. L.; Paretto, N. V.; Foreman, W. T.; Iverson, J. L.; Alvarez, D. A., Sampling trace organic compounds in water: A comparison of a continuous active sampler to continuous passive and discrete sampling methods. *Sci. Total Environ.* **2014**, *473*, 731-741.
54. Hayward, S. J.; Gouin, T.; Wania, F., Comparison of Four Active and Passive Sampling Techniques for Pesticides in Air. *Environmental Science & Technology* **2010**, *44*, (9), 3410-3416.
55. Bronders, J., Fundamentals of Environmental Sampling and Analysis by Chunlong Zhang. *Int. J. Environ. Pollut.* **2008**, *35*, (2-4), 394-395.
56. Csuros, M., *Environmental Sampling and Analysis for Technicians*. Taylor & Francis: 1994.

57. Martinez, A.; Wang, K.; Hornbuckle, K. C., Fate of PCB Congeners in an Industrial Harbor of Lake Michigan. *Environmental Science & Technology* **2010**, *44*, (8), 2803-2808.
58. Albaiges, J., Passive Sampling Techniques in Environmental Monitoring edited by Richard Greenwood, Graham Mills and Bran Vrana. *Int. J. Environ. Anal. Chem.* **2008**, *88*, (9), 678.
59. Namiesnik, J.; Zabiegala, B.; Kot-Wasik, A.; Partyka, M.; Wasik, A., Passive sampling and/or extraction techniques in environmental analysis: a review. *Analytical and Bioanalytical Chemistry* **2005**, *381*, (2), 279-301.
60. Mackie, A.; Coggan, R.; Heteren, S., *Grab sampling*. 2007; p 152-165.
61. Vrana, B.; Mills, G. A.; Allan, I. J.; Dominiak, E.; Svensson, K.; Knutsson, J.; Morrison, G.; Greenwood, R., Passive sampling techniques for monitoring pollutants in water. *Trac-Trends Anal Chem* **2005**, *24*, (10), 845-868.
62. Yu, C. H.; Morandi, M. T.; Weisel, C. P., Passive dosimeters for nitrogen dioxide in personal/indoor air sampling: A review. *J. Expo. Sci. Environ. Epidemiol.* **2008**, *18*, (5), 441-451.
63. Ghosh, U.; Kane Driscoll, S.; Burgess, R. M.; Jonker, M. T. O.; Reible, D.; Gobas, F.; Choi, Y.; Apitz, S. E.; Maruya, K. A.; Gala, W. R.; Mortimer, M.; Beegan, C., Passive sampling methods for contaminated sediments: Practical guidance for selection, calibration, and implementation. *Integr Environ Assess Manag* **2014**, *10*, (2), 210-223.
64. Huang, J. Y.; Lyman, S. N.; Hartman, J. S.; Gustin, M. S., A review of passive sampling systems for ambient air mercury measurements. *Environ. Sci.-Process Impacts* **2014**, *16*, (3), 374-392.
65. Burton, G. A.; Rosen, G.; Chadwick, D. B.; Greenberg, M. S.; Taulbee, W. K.; Lotufo, G. R.; Reible, D. D., A sediment ecotoxicity assessment platform for in situ measures of chemistry, bioaccumulation and toxicity. Part 1: System description and proof of concept. *Environmental Pollution* **2012**, *162*, 449-456.
66. Rosen, G.; Chadwick, D. B.; Burton, G. A.; Taulbee, W. K.; Greenberg, M. S.; Lotufo, G. R.; Reible, D. D., A sediment ecotoxicity assessment platform for in situ measures of chemistry, bioaccumulation and toxicity. Part 2: Integrated application to a shallow estuary. *Environmental Pollution* **2012**, *162*, 457-465.
67. Gorecki, T.; Namiesnik, J., Passive sampling. *Trac-Trends Anal. Chem.* **2002**, *21*, (4), 276-291.
68. Harner, T.; Farrar, N. J.; Shoeib, M.; Jones, K. C.; Gobas, F., Characterization of polymer-coated glass as a passive air sampler for persistent organic pollutants. *Environmental Science & Technology* **2003**, *37*, (11), 2486-2493.
69. Vaes, W. H. J.; Hamwijk, C.; Urrestarazu Ramos, E.; Verhaar, H. J. M.; Hermens, J. L. M., Partitioning of Organic Chemicals to Polyacrylate-Coated Solid Phase Microextraction Fibers: Kinetic Behavior and Quantitative Structure–Property Relationships. *Anal. Chem.* **1996**, *68*, (24), 4458-4462.
70. Alvarez, D. A.; Petty, J. D.; Huckins, J. N.; Jones-Lepp, T. L.; Getting, D. T.; Goddard, J. P.; Manahan, S. E., Development of a passive, in situ, integrative sampler for hydrophilic organic contaminants in aquatic environments. *Environ Toxicol Chem* **2004**, *23*, (7), 1640-1648.
71. Vrana, B.; Komancova, L.; Sobotka, J., Calibration of a passive sampler based on stir bar sorptive extraction for the monitoring of hydrophobic organic pollutants in water. *Talanta* **2016**, *152*, 90-97.
72. Verweij, F.; Booij, K.; Satumalay, K.; van der Molen, N.; van der Oost, R., Assessment of bioavailable PAH, PCB and OCP concentrations in water, using semipermeable membrane devices (SPMDs), sediments and caged carp. *Chemosphere* **2004**, *54*, (11), 1675-1689.
73. Fries, E.; Zarfl, C., Sorption of polycyclic aromatic hydrocarbons (PAHs) to low and high density polyethylene (PE). *Environmental Science and Pollution Research* **2012**, *19*, (4), 1296-1304.

74. Mazzella, N.; Dubernet, J. F.; Delmas, F., Determination of kinetic and equilibrium regimes in the operation of polar organic chemical integrative samplers - Application to the passive sampling of the polar herbicides in aquatic environments. *Journal of Chromatography A* **2007**, *1154*, (1-2), 42-51.
75. Mayer, P.; Tolls, J.; Hermens, J. L. M.; Mackay, D., Equilibrium sampling devices (vol 37, pg 186, 2003). *Environmental Science & Technology* **2003**, *37*, (15), 270A-270A.
76. Sacks, V. P.; Lohmann, R., Development and Use of Polyethylene Passive Samplers To Detect Triclosans and Alkylphenols in an Urban Estuary. *Environ Sci Technol* **2011**, *45*, (6), 2270-2277.
77. Jonker, M. T. O.; van der Heijden, S. A.; Kotte, M.; Smedes, F., Quantifying the Effects of Temperature and Salinity on Partitioning of Hydrophobic Organic Chemicals to Silicone Rubber Passive Samplers. *Environmental Science & Technology* **2015**, *49*, (11), 6791-6799.
78. Ter Laak, T. L.; Agbo, S. O.; Barendregt, A.; Hermens, J. L. M., Freely dissolved concentrations of PAHs in soil pore water: Measurements via solid-phase extraction and consequences for soil tests. *Environmental Science & Technology* **2006**, *40*, (4), 1307-1313.
79. Cho, Y.-M.; Ghosh, U.; Kennedy, A. J.; Grossman, A.; Ray, G.; Tomaszewski, J. E.; Smithenry, D. W.; Bridges, T. S.; Luthy, R. G., Field Application of Activated Carbon Amendment for In-Situ Stabilization of Polychlorinated Biphenyls in Marine Sediment. *Environmental Science & Technology* **2009**, *43*, (10), 3815-3823.
80. Gorecki, T.; Yu, X. M.; Pawliszyn, J., Theory of analyte extraction by selected porous polymer SPME fibres. *Analyst* **1999**, *124*, (5), 643-649.
81. Mitra, S.; Winefordner, J. D., *Sample Preparation Techniques in Analytical Chemistry*. John Wiley & Sons Inc: 2003; p 400 pp.
82. Zhang, Z. Y.; Yang, M. J.; Pawliszyn, J., SOLID-PHASE MICROEXTRACTION. *Anal. Chem.* **1994**, *66*, (17), A844-A853.
83. Benotti, M. J.; Trenholm, R. A.; Vanderford, B. J.; Holady, J. C.; Stanford, B. D.; Snyder, S. A., Pharmaceuticals and Endocrine Disrupting Compounds in US Drinking Water. *Environmental Science & Technology* **2009**, *43*, (3), 597-603.
84. Ibrahim, I.; Togola, A.; Gonzalez, C., Polar organic chemical integrative sampler (POCIS) uptake rates for 17 polar pesticides and degradation products: laboratory calibration. *Environmental Science and Pollution Research* **2013**, *20*, (6), 3679-3687.
85. Charriau, A.; Lissalde, S.; Poulier, G.; Mazzella, N.; Buzier, R.; Guibaud, G., Overview of the Chemcatcher® for the passive sampling of various pollutants in aquatic environments Part A: Principles, calibration, preparation and analysis of the sampler. *Talanta* **2016**, *148*, 556-571.
86. Vrana, B.; Mills, G. A.; Dominiak, E.; Greenwood, R., Calibration of the Chemcatcher passive sampler for the monitoring of priority organic pollutants in water. *Environmental Pollution* **2006**, *142*, (2), 333-343.
87. Kingston, J. K.; Greenwood, R.; Mills, G. A.; Morrison, G. M.; Persson, L. B., Development of a novel passive sampling system for the time-averaged measurement of a range of organic pollutants in aquatic environments. *Journal of Environmental Monitoring* **2000**, *2*, (5), 487-495.
88. Allan, I. J.; Knutsson, J.; Guigues, N.; Mills, G. A.; Fouillac, A. M.; Greenwood, R., Evaluation of the Chemcatcher and DGT passive samplers for monitoring metals with highly fluctuating water concentrations. *Journal of Environmental Monitoring* **2007**, *9*, (7), 672-681.
89. Ahkola, H.; Herve, S.; Knuutinen, J., Overview of passive Chemcatcher sampling with SPE pretreatment suitable for the analysis of NPEOs and NPs. *Environmental Science and Pollution Research* **2013**, *20*, (3), 1207-1218.
90. Alvarez, D. A.; Huckins, J. N.; Petty, J. D.; Jones-Lepp, T.; Stuer-Lauridsen, F.; Getting, D. T.; Goddard, J. P.; Gravell, A., Tool for monitoring hydrophilic contaminants in water: polar organic chemical

- integrative sampler (POCIS). In *Passive Sampling Techniques in Environmental Monitoring, Vol 48*, Greenwood, R.; Mills, G.; Vrana, B., Eds. Elsevier Science Bv: Amsterdam, 2007; Vol. 48, pp 171-197.
91. Lapworth, D. J.; Baran, N.; Stuart, M. E.; Ward, R. S., Emerging organic contaminants in groundwater: A review of sources, fate and occurrence. *Environmental Pollution* **2012**, *163*, 287-303.
 92. Alvarez, D. A., Development of semipermeable membrane devices (SPMDs) and polar organic chemical integrative samplers (POCIS) for environmental monitoring. *Environ Toxicol Chem* **2013**, *32*, (10), 2179-2181.
 93. Gaffet, E., Nanomaterials: A review of the definitions, applications, health effects. How to implement secure development. *C. R. Phys.* **2011**, *12*, (7), 648-658.
 94. Boverhof, D. R.; Bramante, C. M.; Butala, J. H.; Clancy, S. F.; Lafranconi, M.; West, J.; Gordon, S. C., Comparative assessment of nanomaterial definitions and safety evaluation considerations. *Regulatory Toxicology and Pharmacology* **2015**, *73*, (1), 137-150.
 95. Ibrahim, R. K.; Hayyan, M.; AlSaadi, M. A.; Hayyan, A.; Ibrahim, S., Environmental application of nanotechnology: air, soil, and water. *Environmental Science and Pollution Research* **2016**, *23*, (14), 13754-13788.
 96. Mansoori, G. A.; Bastami, T. R.; Ahmadpour, A.; Eshaghi, Z., Environmental application of nanotechnology. *Annu. Rev. Nano Res.* **2008**, *2*, 439-493.
 97. Zhu, Z. G.; Garcia-Gancedo, L.; Flewitt, A. J.; Xie, H. Q.; Moussy, F.; Milne, W. I., A Critical Review of Glucose Biosensors Based on Carbon Nanomaterials: Carbon Nanotubes and Graphene. *Sensors* **2012**, *12*, (5), 5996-6022.
 98. Anon, Environmental Applications and Implications of Nanotechnology and Nanomaterials. *J. Environ. Eng. (Reston, VA, U. S.)* **2004**, *130*, (7), 723-724.
 99. Buzea, C.; Pacheco, II; Robbie, K., Nanomaterials and nanoparticles: Sources and toxicity. *Biointerphases* **2007**, *2*, (4), MR17-MR71.
 100. Hutchison, J. E., Greener nanoscience: A proactive approach to advancing applications and reducing implications of nanotechnology. *ACS Nano* **2008**, *2*, (3), 395-402.
 101. Persano, L.; Camposeo, A.; Tekmen, C.; Pisignano, D., Industrial Upscaling of Electrospinning and Applications of Polymer Nanofibers: A Review. *Macromol. Mater. Eng.* **2013**, *298*, (5), 504-520.
 102. Subbiah, T.; Bhat, G. S.; Tock, R. W.; Pararneswaran, S.; Ramkumar, S. S., Electrospinning of nanofibers. *J Appl Polym Sci* **2005**, *96*, (2), 557-569.
 103. Huang, Z. M.; Zhang, Y. Z.; Kotaki, M.; Ramakrishna, S., A review on polymer nanofibers by electrospinning and their applications in nanocomposites. *Compos Sci Technol* **2003**, *63*, (15), 2223-2253.
 104. Nataraj, S. K.; Yang, K. S.; Aminabhavi, T. M., Polyacrylonitrile-based nanofibers A state-of-the-art review. *Prog. Polym. Sci.* **2012**, *37*, (3), 487-513.
 105. Ma, Z. W.; Kotaki, M.; Yong, T.; He, W.; Ramakrishna, S., Surface engineering of electrospun polyethylene terephthalate (PET) nanofibers towards development of a new material for blood vessel engineering. *Biomaterials* **2005**, *26*, (15), 2527-2536.
 106. Qi, D. J.; Kang, X. J.; Chen, L. Q.; Zhang, Y. Y.; Wei, H. M.; Gu, Z. Z., Electrospun polymer nanofibers as a solid-phase extraction sorbent for the determination of trace pollutants in environmental water. *Analytical and Bioanalytical Chemistry* **2008**, *390*, (3), 929-938.
 107. Kang, X. J.; Pan, C.; Xu, Q.; Yao, Y. F.; Wang, Y.; Qi, D. J.; Gu, Z. Z., The investigation of electrospun polymer nanofibers as a solid-phase extraction sorbent for the determination of trazodone in human plasma. *Anal. Chim. Acta* **2007**, *587*, (1), 75-81.
 108. Patra, N.; Cernik, M.; Salerno, M., Advances in Electrospun Nanofibers. *Journal of Nanomaterials* **2016**, *2016*, 2.

109. Piperno, S.; Lozzi, L.; Rastelli, R.; Passacantando, M.; Santucci, S., PMMA nanofibers production by electrospinning. *Appl Surf Sci* **2006**, *252*, (15), 5583-5586.
110. Wang, T.; Kumar, S., Electrospinning of polyacrylonitrile nanofibers. *J Appl Polym Sci* **2006**, *102*, (2), 1023-1029.
111. Ghochaghi, N.; Taiwo, A.; Winkel, M.; Dodd, B.; Mossi, K.; Tepper, G., Electrospun Polystyrene Coatings with Tunable Wettability. *J Appl Polym Sci* **2015**, *132*, (10).
112. Uyar, T.; Besenbacher, F., Electrospinning of uniform polystyrene fibers: The effect of solvent conductivity. *Polymer* **2008**, *49*, (24), 5336-5343.
113. Veleirinho, B.; Lopes-da-Silva, J. A., Application of electrospun poly(ethylene terephthalate) nanofiber mat to apple juice clarification. *Process Biochem* **2009**, *44*, (3), 353-356.
114. Xu, C.; Xu, F.; Wang, B.; Lu, T., Electrospinning of Poly(ethylene-co-vinyl alcohol) Nanofibres Encapsulated with Ag Nanoparticles for Skin Wound Healing. *J Nanomater* **2011**.
115. Choi, S. S.; Lee, Y. S.; Joo, C. W.; Lee, S. G.; Park, J. K.; Han, K. S., Electrospun PVDF nanofiber web as polymer electrolyte or separator. *Electrochim Acta* **2004**, *50*, (2-3), 339-343.
116. Lee, J. S.; Choi, K. H.; Do Ghim, H.; Kim, S. S.; Chun, D. H.; Kim, H. Y.; Lyoo, W. S., Role of molecular weight of atactic poly(vinyl alcohol) (PVA) in the structure and properties of PVA nanofabric prepared by electrospinning. *J Appl Polym Sci* **2004**, *93*, (4), 1638-1646.
117. Jannesari, M.; Varshosaz, J.; Morshed, M.; Zamani, M., Composite poly(vinyl alcohol)/poly(vinyl acetate) electrospun nanofibrous mats as a novel wound dressing matrix for controlled release of drugs. *Int J Nanomedicine* **2011**, *6*, 11.
118. Leach, M. K.; Feng, Z.-Q.; Tuck, S. J.; Corey, J. M., Electrospinning fundamentals: optimizing solution and apparatus parameters. *J. Visualized Exp.* **2011**, (47), 2494/1-2494/4.
119. Babel, A.; Li, D.; Xia, Y. N.; Jenekhe, S. A., Electrospun nanofibers of blends of conjugated polymers: Morphology, optical properties, and field-effect transistors. *Macromolecules* **2005**, *38*, (11), 4705-4711.
120. Prabhakaran, M. P.; Ghasemi-Mobarakeh, L.; Ramakrishna, S., Electrospun Composite Nanofibers for Tissue Regeneration. *J. Nanosci. Nanotechnol.* **2011**, *11*, (4), 3039-3057.
121. Mo, X.; Wu, T.; Sun, B.; El-Hamshary, *Nanofiber composites in tendon tissue engineering*. 2017.
122. Varesano, A.; Carletto, R. A.; Mazzuchetti, G., Experimental investigations on the multi-jet electrospinning process. *J. Mater. Process. Technol.* **2009**, *209*, (11), 5178-5185.
123. Sun, Z. C.; Zussman, E.; Yarin, A. L.; Wendorff, J. H.; Greiner, A., Compound core-shell polymer nanofibers by co-electrospinning. *Adv. Mater.* **2003**, *15*, (22), 1929-+.
124. Nalbandian, M. J.; Greenstein, K. E.; Shuai, D.; Zhang, M.; Choa, Y.-H.; Parkin, G. F.; Myung, N. V.; Cwiertny, D. M., Tailored Synthesis of Photoactive TiO₂ Nanofibers and Au/TiO₂ Nanofiber Composites: Structure and Reactivity Optimization for Water Treatment Applications. *Environmental Science & Technology* **2015**, *49*, (3), 1654-1663.
125. Qian, J.; Jennings, B.; Cwiertny, D.; Martinez, A., Emerging investigator series: development and application of polymeric electrospun nanofiber mats as equilibrium-passive sampler media for organic compounds. *Environmental Science: Processes & Impacts* **2017**, *19*, (11), 1445-1456.
126. He, Y. M.; Chen, W. J.; Gao, C. T.; Zhou, J. Y.; Li, X. D.; Xie, E. Q., An overview of carbon materials for flexible electrochemical capacitors. *Nanoscale* **2013**, *5*, (19), 8799-8820.
127. Chae, H. G.; Sreekumar, T. V.; Uchida, T.; Kumar, S., A comparison of reinforcement efficiency of various types of carbon nanotubes in poly acrylonitrile fiber. *Polymer* **2005**, *46*, (24), 10925-10935.
128. De Volder, M. F. L.; Tawfick, S. H.; Baughman, R. H.; Hart, A. J., Carbon Nanotubes: Present and Future Commercial Applications. *Science* **2013**, *339*, (6119), 535-539.

129. Saeed, K.; Ibrahim, Carbon nanotubes-properties and applications: a review. *Carbon Lett.* **2013**, *14*, (3), 131-144.
130. Das, R.; Ali, M. E.; Abd Hamid, S. B.; Ramakrishna, S.; Chowdhury, Z. Z., Carbon nanotube membranes for water purification: A bright future in water desalination. *Desalination* **2014**, *336*, 97-109.
131. Al-Jumaili, A.; Alancherry, S.; Bazaka, K.; Jacob, M. V.; Bazaka, K., Review on the Antimicrobial Properties of Carbon Nanostructures. *Materials (Basel)* **2017**, *10*, (9).
132. Zhang, M.; Li, J., Carbon nanotube in different shapes. *Materials Today* **2009**, *12*, (6), 12-18.
133. Tanaka, K., Chapter 1 - Classification of Carbon. In *Carbon Nanotubes and Graphene (Second Edition)*, Tanaka, K.; Iijima, S., Eds. Elsevier: Oxford, 2014; pp 1-5.
134. Dumas, L.; Bonnaud, L.; Dubois, P., Chapter 38 - Polybenzoxazine Nanocomposites: Case Study of Carbon Nanotubes A2 - Ishida, Hatsuo. In *Advanced and Emerging Polybenzoxazine Science and Technology*, Froimowicz, P., Ed. Elsevier: Amsterdam, 2017; pp 767-800.
135. Karimi, M.; Solati, N.; Amiri, M.; Mirshekari, H.; Mohamed, E.; Taheri, M.; Hashemkhani, M.; Saeidi, A.; Asghari Estiar, M.; Kiani, P.; Ghasemi, A.; Moosavi, M.; Aref, A. R.; Hamblin, M., *Carbon nanotubes part I: Preparation of a novel and versatile drug-delivery vehicle*. 2015; Vol. 12, p 1-17.
136. Savage, N.; Diallo, M. S., Nanomaterials and water purification: Opportunities and challenges. *J. Nanopart. Res.* **2005**, *7*, (4-5), 331-342.
137. Kang, S.; Herzberg, M.; Rodrigues, D. F.; Elimelech, M., Antibacterial effects of carbon nanotubes: Size does matter. *Langmuir* **2008**, *24*, (13), 6409-6413.
138. Lam, C. W.; James, J. T.; McCluskey, R.; Arepalli, S.; Hunter, R. L., A review of carbon nanotube toxicity and assessment of potential occupational and environmental health risks. *Crit. Rev. Toxicol.* **2006**, *36*, (3), 189-217.
139. Wu, H.-C.; Chang, X.; Liu, L.; Zhao, F.; Zhao, Y., Chemistry of carbon nanotubes in biomedical applications. *Journal of Materials Chemistry* **2010**, *20*, (6), 1036-1052.
140. Margam, C.; William, B. A.; Lam, L. N., *Materials Degradation And Its Control By Surface Engineering (3rd Edition)*. World Scientific Publishing Company: 2011.
141. Peter, K. T.; Myung, N. V.; Cwiertny, D. M., Surfactant-assisted fabrication of porous polymeric nanofibers with surface-enriched iron oxide nanoparticles: composite filtration materials for removal of metal cations. *Environ. Sci.: Nano* **2018**, *5*, (3), 669-681.
142. Fingas, M., Use of Surfactants for Environmental Applications. In *Surfactants: Fundamentals and Applications in the Petroleum Industry*, Schramm, L. L., Ed. Cambridge University Press: Cambridge, 2000; pp 461-540.
143. Guermouche, M. H.; Habel, D.; Guermouche, S., Theoretical aspects of micellar liquid chromatography using C(12)DAPS surfactant. *Fluid Phase Equilib.* **1998**, *147*, (1-2), 301-307.
144. Hunley, M. T.; Harber, A.; Orlicki, J. A.; Rawlett, A. M.; Long, T. E., Effect of Hyperbranched Surface-Migrating Additives on the Electrospinning Behavior of Poly(methyl methacrylate). *Langmuir* **2008**, *24*, (3), 654-657.
145. Peter, K. T.; Johns, A. J.; Myung, N. V.; Cwiertny, D. M., Functionalized polymer-iron oxide hybrid nanofibers: Electrospun filtration devices for metal oxyanion removal. *Water Res.* **2017**, *117*, 207-217.
146. Silhavy, T. J.; Kahne, D.; Walker, S., The Bacterial Cell Envelope. *Cold Spring Harbor Perspect. Biol.* **2010**, *2*, (5), 16.
147. Banerjee, S.; Cazeneuve, C.; Baghdadli, N.; Ringeissen, S.; Leermakers, F. A. M.; Luengo, G. S., Surfactant-polymer interactions: molecular architecture does matter. *Soft Matter* **2015**, *11*, (12), 2504-2511.

148. Aykut, Y.; Pourdeyhimi, B.; Khan, S. A., Effects of surfactants on the microstructures of electrospun polyacrylonitrile nanofibers and their carbonized analogs. *J. Appl. Polym. Sci.* **2013**, *130*, (5), 3726-3735.
149. Datta, P.; Chatterjee, J.; Dhara, S., Electrospun nanofibers of a phosphorylated polymer-A bioinspired approach for bone graft applications. *Colloid Surf. B-Biointerfaces* **2012**, *94*, 177-183.
150. Choi, J.; Ide, A.; Truong, Y. B.; Kyratzis, I. L.; Caruso, R. A., High surface area mesoporous titanium-zirconium oxide nanofibrous web: a heavy metal ion adsorbent. *J. Mater. Chem. A* **2013**, *1*, (19), 5847-5853.
151. Jung, Y. H.; Kim, H. Y.; Lee, D. R.; Park, S. Y.; Khil, M. S., Characterization of PVOH nonwoven mats prepared from Surfactant-Polymer system via electrospinning. *Macromolecular Research* **2005**, *13*, (5), 385-390.
152. Uykun, N.; Ergal, I.; Kurt, H.; Gokceoren, A. T.; Gocek, I.; Kayaoglu, B. K.; Akarsubasi, A. T.; Sarac, A. S., Electrospun antibacterial nanofibrous polyvinylpyrrolidone/cetyltrimethylammonium bromide membranes for biomedical applications. *J. Bioact. Compat. Polym.* **2014**, *29*, (4), 382-397.
153. Nitanan, T.; Opanasopit, P.; Akkaramongkolporn, P.; Rojanarata, T.; Ngawhirunpat, T.; Supaphol, P., Effects of processing parameters on morphology of electrospun polystyrene nanofibers. *Korean J. Chem. Eng.* **2012**, *29*, (2), 173-181.
154. Horzum, N.; Shahwan, T.; Parlak, O.; Demir, M. M., Synthesis of amidoximated polyacrylonitrile fibers and its application for sorption of aqueous uranyl ions under continuous flow. *Chem Eng J* **2012**, *213*, 41-49.
155. Han, Z. B.; Han, X.; Zhao, X. M.; Yu, J. T.; Xu, H., Iron phthalocyanine supported on amidoximated PAN fiber as effective catalyst for controllable hydrogen peroxide activation in oxidizing organic dyes. *J. Hazard. Mater.* **2016**, *320*, 27-35.
156. Lu, G.; Johns, A. J.; Neupane, B.; Phan, H. T.; Cwiertny, D. M.; Forbes, T. Z.; Haes, A. J., Matrix-Independent Surface-Enhanced Raman Scattering Detection of Uranyl Using Electrospun Amidoximated Polyacrylonitrile Mats and Gold Nanostars. *Anal. Chem.* **2018**, *90*, (11), 6766-6772.
157. Das, S.; Brown, S.; Mayes, R. T.; Janke, C. J.; Tsouris, C.; Kuo, L. J.; Gill, G.; Dai, S., Novel poly(imide dioxime) sorbents: Development and testing for enhanced extraction of uranium from natural seawater. *Chem. Eng. J.* **2016**, *298*, 125-135.
158. Puliyalil, H.; Cvelbar, U., Selective Plasma Etching of Polymeric Substrates for Advanced Applications. *Nanomaterials* **2016**, *6*, (6), 24.
159. Chen, H. T.; Lin, H. L.; Kuo, C.; Chen, I. G., UV-induced synthesis of silver nanofiber networks as transparent electrodes. *J. Mater. Chem. C* **2016**, *4*, (32), 7675-7682.
160. Savoji, H.; Lerouge, S.; Ajji, A.; Wertheimer, M. R., Plasma-Etching for Controlled Modification of Structural and Mechanical Properties of Electrospun PET Scaffolds. *Plasma Process. Polym.* **2015**, *12*, (4), 314-327.
161. Peter, K. T.; Vargo, J. D.; Rupasinghe, T. P.; De Jesus, A.; Tivanski, A. V.; Sander, E. A.; Myung, N. V.; Cwiertny, D. M., Synthesis, Optimization, and Performance Demonstration of Electrospun Carbon Nanofiber-Carbon Nanotube Composite Sorbents for Point-of-Use Water Treatment. *Acs Applied Materials & Interfaces* **2016**, *8*, (18), 11431-11440.
162. Prilutsky, S.; Zussman, E.; Cohen, Y., Carbonization of Electrospun Poly(acrylonitrile) Nanofibers Containing Multiwalled Carbon Nanotubes Observed by Transmission Electron Microscope with In Situ Heating. *J. Polym. Sci. Pt. B-Polym. Phys.* **2010**, *48*, (20), 2121-2128.
163. Rasheed, A.; Howe, J. Y.; Dadmun, M. D.; Britt, P. F., The efficiency of the oxidation of carbon nanofibers with various oxidizing agents. *Carbon* **2007**, *45*, (5), 1072-1080.

164. Rasheed, A.; Dadmun, M. D.; Brittz, P. F., Polymer-nanofiber composites: Enhancing composite properties by nanofiber oxidation. *J. Polym. Sci. Pt. B-Polym. Phys.* **2006**, *44*, (21), 3053-3061.
165. Greenwood, R.; Mills, G.; Vrana, B., *Comprehensive Analytical Chemistry: Passive sampling techniques in environmental monitoring*. Elsevier Publishing Company: 2007.
166. Jonker, M. T. O.; Koelmans, A. A., Polyoxymethylene solid phase extraction as a partitioning method for hydrophobic organic chemicals in sediment and soot. *Environ Sci Technol* **2001**, *35*, (18), 3742-3748.
167. Martinez, A.; O'Sullivan, C.; Reible, D.; Hornbuckle, K. C., Sediment pore water distribution coefficients of PCB congeners in enriched black carbon sediment. *Environ Pollut* **2013**, *182*, (0), 357-363. PMID: 23974165: PMC3833079.
168. Mayer, P.; Wania, F.; Wong, C. S., Advancing passive sampling of contaminants in environmental science. *Env Sci Process Impact* **2014**, *16*, (3), 366-368.
169. George, T. S.; Vlahos, P.; Harner, T.; Helm, P.; Wilford, B., A rapidly equilibrating, thin film, passive water sampler for organic contaminants; characterization and field testing. *Environ Pollut* **2011**, *159*, (2), 481-486.
170. Lao, W. J.; Hong, Y. W.; Tsukada, D.; Maruya, K. A.; Gan, J., A New Film-Based Passive Sampler for Moderately Hydrophobic Organic Compounds. *Environ Sci Technol* **2016**, *50*, (24), 13470-13476.
171. Metcalfe, C.; Hoque, M. E.; Sultana, T.; Murray, C.; Helm, P.; Kleywegt, S., Monitoring for contaminants of emerging concern in drinking water using POCIS passive samplers. *Env Sci Process Impact* **2014**, *16*, (3), 473-481.
172. Mills, G. A.; Gravell, A.; Vrana, B.; Harman, C.; Budzinski, H.; Mazzella, N.; Ocelka, T., Measurement of environmental pollutants using passive sampling devices - an updated commentary on the current state of the art. *Env Sci Process Impact* **2014**, *16*, (3), 369-373.
173. Macleod, S. L.; McClure, E. L.; Wong, C. S., Laboratory calibration and field deployment of the polar organic chemical integrative sampler for pharmaceuticals and personal care products in wastewater and surface water. *Environ Toxicol Chem* **2007**, *26*, (12), 2517-2529.
174. Harman, C.; Allan, I. J.; Vermeirssen, E. L. M., Calibration and use of the polar organic chemical integrative sampler-a critical review. *Environ Toxicol Chem* **2012**, *31*, (12), 2724-2738.
175. Morin, N.; Miege, C.; Randon, J.; Coquery, M., Chemical calibration, performance, validation and applications of the polar organic chemical integrative sampler (POCIS) in aquatic environments. *Trac-Trends Anal Chem* **2012**, *36*, 144-175.
176. Magner, J. A.; Alsberg, T. E.; Broman, D., Evaluation of Poly(ethylene-co-vinyl acetate-co-carbon monoxide) and Polydimethylsiloxane for equilibrium sampling of polar organic contaminants in water. *Environ Toxicol Chem* **2009**, *28*, (9), 1874-1880.
177. Ajayan, P. M.; Schadler, L. S.; Braun, P. V., *Nanocomposite Science and Technology*. Wiley-VCH Verlag GmbH & Co. KGaA: 2003; p 230 pp.
178. Mayer, P.; Tolls, J.; Hermens, J. L. M.; Mackay, D., Peer Reviewed: Equilibrium Sampling Devices. *Environ Sci Technol* **2003**, *37*, (9), 184A-191A.
179. ter Laak, T. L.; Busser, F. J. M.; Hermens, J. L. M., Poly(dimethylsiloxane) as passive sampler material for hydrophobic chemicals: Effect of chemical properties and sampler characteristics on partitioning and equilibration times. *Anal. Chem.* **2008**, *80*, (10), 3859-3866.
180. Persano, L.; Camposeo, A.; Tekmen, C.; Pisignano, D., Industrial Upscaling of Electrospinning and Applications of Polymer Nanofibers: A Review. *Macromol Mater Eng* **2013**, *298*, (5), 504-520.
181. Kim, S.; Thiessen, P. A.; Bolton, E. E.; Chen, J.; Fu, G.; Gindulyte, A.; Han, L.; He, J.; He, S.; Shoemaker, B. A.; Wang, J.; Yu, B.; Zhang, J.; Bryant, S. H., PubChem Substance and Compound databases. *Nucleic Acids Research* **2016**, *44*, (Database issue), D1202-D1213.

182. Bauerlein, P. S.; Mansell, J. E.; ter Laak, T. L.; de Voogt, P., Sorption Behavior of Charged and Neutral Polar Organic Compounds on Solid Phase Extraction Materials: Which Functional Group Governs Sorption? *Environ Sci Technol* **2012**, *46*, (2), 954-961.
183. Qu, S.; Kolodziej, E. P.; Cwiertny, D. M., Sorption and Mineral-Promoted Transformation of Synthetic Hormone Growth Promoters in Soil Systems. *J. Agric. Food Chem.* **2014**, *62*, (51), 12277-12286.
184. Caceci, M. S., Estimateing the error limits in parametric curve fitting. *Anal Chem* **1989**, *61*, (20), 2324-2327.
185. Wolfe, N. L.; Carreira, L. H.; Delgado, M. C., Method and composition for remediating environmental contaminants. In Google Patents: 2000.
186. Riggin, R. M.; Lucas, S. V.; Cole, T. F.; Birts, M. A. *Analytical procedures for aniline and selected derivatives in wastewater and sludge*; Battelle: 1984; p 231 pp.
187. Paruta, A. N.; Irani, S. A., Solubility profiles for the xanthenes in aqueous alcoholic mixtures. I. Ethanol and methanol. *J. Pharm. Sci.* **1966**, *55*, (10), 1055-9.
188. Van Boven, M.; Laruelle, L.; Daenens, P., HPLC analysis of diuron and metabolites in blood and urine. *J Anal Toxicol* **1990**, *14*, (4), 231-4.
189. Cledera-Castro, M. d. M.; Santos-Montes, A. M.; Izquierdo-Hornillos, R., Method development and validation for phenol and nitrophenols in tap water by HPLC using a monolithic column. *LC-GC Eur* **2006**, *19*, (7), 424-426,428-431.
190. Lang, M. J.; Burns, S. E., Improvement of EPA method 8330: complete separation using a two-phase approach. *J. Chromatogr. A* **1999**, *849*, (2), 381-388.
191. Euerby, M.; Petersson, P., Chromatographic classification and comparison of commercially available reversed-phase liquid chromatographic columns using principal component analysis. *J. Chromatogr. A* **2003**, *994*, (1-2), 13-36.
192. Lambert, M. K.; Friedman, C.; Luey, P.; Lohmann, R., Role of Black Carbon in the Sorption of Polychlorinated Dibenzo-p-dioxins and Dibenzofurans at the Diamond Alkali Superfund Site, Newark Bay, New Jersey. *Environ Sci Technol* **2011**, *45*, (10), 4331-4338.
193. Duffel, M. W., Review of organic functional groups: Introduction to medicinal organic chemistry. By Thomas L. Lemke. Lea and Febiger, Philadelphia, PA. 1983. 131 pp. 15 × 23 cm. Price \$10.50. *J Pharm Sci* **1984**, *73*, (8), 1188-1188.
194. Adams, R. G.; Lohmann, R.; Fernandez, L. A.; Macfarlane, J. K.; Gschwend, P. M., Polyethylene devices: Passive samplers for measuring dissolved hydrophobic organic compounds in aquatic environments. *Environ Sci Technol* **2007**, *41*, (4), 1317-1323.
195. Arp, H. P. H.; Hale, S. E.; Krusa, M. E.; Cornelissen, G.; Grabanski, C. B.; Miller, D. J.; Hawthorne, S. B., Review of polyoxymethylene passive sampling methods for quantifying freely dissolved porewater concentrations of hydrophobic organic contaminants. *Environ Toxicol Chem* **2015**, *34*, (4), 710-720.
196. Belles, A.; Alary, C.; Mamindy-Pajany, Y., Thickness and material selection of polymeric passive samplers for polycyclic aromatic hydrocarbons in water: Which more strongly affects sampler properties? *Environ Toxicol Chem* **2016**, *35*, (7), 1708-1717.
197. Yang, Z. Y.; Zeng, E. Y.; Xia, H.; Wang, J. Z.; Mai, B. X.; Maruya, K. A., Application of a static solid-phase microextraction procedure combined with liquid-liquid extraction to determine poly(dimethyl)siloxane-water partition coefficients for selected polychlorinated biphenyls. *J Chromatogr A* **2006**, *1116*, (1-2), 240-247.
198. Kaserzon, S. L.; Hawker, D. W.; Kennedy, K.; Bartkow, M.; Carter, S.; Booi, K.; Mueller, J. F., Characterisation and comparison of the uptake of ionizable and polar pesticides, pharmaceuticals and personal care products by POCIS and Chemcatchers. *Env Sci Process Impact* **2014**, *16*, (11), 2517-2526.

199. Cornelissen, G.; Pettersen, A.; Broman, D.; Mayer, P.; Breedveld, G. D., Field testing of equilibrium passive samplers to determine freely dissolved native polycyclic aromatic hydrocarbon concentrations. *Environ Toxicol Chem* **2008**, *27*, (3), 499-508.
200. Booij, K.; Hofmans, H. E.; Fischer, C. V.; Van Weerlee, E. M., Temperature-dependent uptake rates of nonpolar organic compounds by semipermeable membrane devices and low-density polyethylene membranes. *Environ Sci Technol* **2003**, *37*, (2), 361-366.
201. Booij, K.; Sleiderink, H. M.; Smedes, F., Calibrating the uptake kinetics of semipermeable membrane devices using exposure standards. *Environ Toxicol Chem* **1998**, *17*, (7), 1236-1245.
202. Huckins, J. N.; Petty, J. D.; Orazio, C. E.; Lebo, J. A.; Clark, R. C.; Gibson, V. L.; Gala, W. R.; Echols, K. R., Determination of uptake kinetics (Sampling rates) by lipid-containing semipermeable membrane devices (SPMDs) for polycyclic aromatic hydrocarbons (PAHs) in water. *Environ Sci Technol* **1999**, *33*, (21), 3918-3923.
203. Lohmann, R., Critical Review of Low-Density Polyethylene's Partitioning and Diffusion Coefficients for Trace Organic Contaminants and Implications for Its Use As a Passive Sampler. *Environ Sci Technol* **2012**, *46*, (2), 606-618.
204. Nataraj, S. K.; Yang, K. S.; Aminabhavi, T. M., Polyacrylonitrile-based nanofibers A state-of-the-art review. *Prog Polym Sci* **2012**, *37*, (3), 487-513.
205. Endo, S.; Brown, T. N.; Watanabe, N.; Ulrich, N.; Bronner, G.; Abraham, M. H.; Goss, K. U. UFZ-LSER database v 3.1 [Internet], Leipzig, Germany, Helmholtz Centre for Environmental Research-UFZ.
206. Hale, S. E.; Martin, T. J.; Goss, K. U.; Arp, H. P. H.; Werner, D., Partitioning of organochlorine pesticides from water to polyethylene passive samplers. *Environ Pollut* **2010**, *158*, (7), 2511-2517.
207. Lapworth, D. J.; Baran, N.; Stuart, M. E.; Ward, R. S., Emerging organic contaminants in groundwater: A review of sources, fate and occurrence. *Environ. Pollut.* **2012**, *163*, 287-303.
208. Postigo, C.; Barcelo, D., Synthetic organic compounds and their transformation products in groundwater: Occurrence, fate and mitigation. *Sci. Total Environ.* **2015**, *503*, 32-47.
209. Luo, Y. L.; Guo, W. S.; Ngo, H. H.; Nghiem, L. D.; Hai, F. I.; Zhang, J.; Liang, S.; Wang, X. C. C., A review on the occurrence of micropollutants in the aquatic environment and their fate and removal during wastewater treatment. *Sci. Total Environ.* **2014**, *473*, 619-641.
210. Ghattas, A. K.; Fischer, F.; Wick, A.; Ternes, T. A., Anaerobic biodegradation of (emerging) organic contaminants in the aquatic environment. *Water Res.* **2017**, *116*, 268-295.
211. Alvarez, D. A.; Maruya, K. A.; Dodder, N. G.; Lao, W. J.; Furlong, E. T.; Smalling, K. L., Occurrence of contaminants of emerging concern along the California coast (2009-10) using passive sampling devices. *Mar. Pollut. Bull.* **2014**, *81*, (2), 347-354.
212. Zhang, Z. L.; Hibberd, A.; Zhou, J. L., Analysis of emerging contaminants in sewage effluent and river water: Comparison between spot and passive sampling. *Anal. Chim. Acta* **2008**, *607*, (1), 37-44.
213. Liu, X.; Wang, M.; Zhang, S.; Pan, B., Application potential of carbon nanotubes in water treatment: A review. *J Environ Sci (China)* **2013**, *25*, (7), 1263-80.
214. Zhang, S. J.; Shao, T.; Bekaroglu, S. S. K.; Karanfil, T., Adsorption of synthetic organic chemicals by carbon nanotubes: Effects of background solution chemistry. *Water Res.* **2010**, *44*, (6), 2067-2074.
215. Pan, B.; Xing, B. S., Adsorption Mechanisms of Organic Chemicals on Carbon Nanotubes. *Environ. Sci. Technol.* **2008**, *42*, (24), 9005-9013.
216. Barrett, E. P.; Joyner, L. G.; Halenda, P. P., THE DETERMINATION OF PORE VOLUME AND AREA DISTRIBUTIONS IN POROUS SUBSTANCES .1. COMPUTATIONS FROM NITROGEN ISOTHERMS. *J. Am. Chem. Soc.* **1951**, *73*, (1), 373-380.
217. The DRAFT 2016 Iowa List of Clean Water Act Section 303(d) Impaired Waters. *Water Quality Monitoring & Assessment Section, Water Quality Bureau, Iowa Department of Natural Resources* **2017**.

218. Kalkhoff, S. J., Barnes, K.K., Becher, K.D., Savoca, M.E., Schnoebelen, D.J., Sadorf, E.M., Porter, S.D., and Sullivan, D.J., Water Quality in the Eastern Iowa Basins, Iowa and Minnesota, 1996–98. *U.S. Geological Survey Circular* **2000**, 1210, 37 p.
219. Reeves, R. A.; Pierce, C.; Vandever, M.; Muths, E. L.; Smalling, K., Amphibians, pesticides, and the amphibian chytrid fungus in restored wetlands in agricultural landscapes. *Herpetological Conservation and Biology* **2017**, 12, 68-77.
220. Hruby, C. E.; Libra, R. D.; Fields, C. L.; Kolpin, D. W.; Hubbard, L. E.; Borchardt, M. R.; Spencer, S. K.; Wichman, M. D.; Hall, N.; Schueller, M. D.; Furlong, E. T.; Weyer, P. J. *2013 Survey of Iowa groundwater and evaluation of public well vulnerability classifications for contaminants of emerging concern*; 57; 2015.
221. Villacanas, F.; Pereira, M. F. R.; Orfao, J. J. M.; Figueiredo, J. L., Adsorption of simple aromatic compounds on activated carbons. *J. Colloid Interface Sci.* **2006**, 293, (1), 128-136.
222. Connick, W. J.; Simoneaux, J. M., DETERMINATION OF (2,4-DICHLOROPHENOXY)ACETIC ACID AND OF 2,6-DICHLOROBENZONITRILE IN WATER BY HIGH-PERFORMANCE LIQUID-CHROMATOGRAPHY. *Journal of Agricultural and Food Chemistry* **1982**, 30, (2), 258-260.
223. Ma, J.; Graham, N. J. D., Degradation of atrazine by manganese-catalysed ozonation - Influence of radical scavengers. *Water Res.* **2000**, 34, (15), 3822-3828.
224. Yokley, R. A.; Mayer, L. C.; Huang, S. B.; Vargo, J. D., Analytical method for the determination of metolachlor, acetochlor, alachlor, dimethenamid, and their corresponding ethanesulfonic and oxanillic acid degradates in water using SPE and LC/ESI-MS/MS. *Analytical Chemistry* **2002**, 74, (15), 3754-3759.
225. Yang, C.; Wang, X.; Du, P. C.; Liu, P., Polyaniline/carbon nanotube multi-layered hollow microspheres with sandwich structure and their electrochemical performance. *Synth. Met.* **2013**, 179, 34-41.
226. Li, X. Y.; Pignatello, J. J.; Wang, Y. Q.; Xing, B. S., New Insight into Adsorption Mechanism of Ionizable Compounds on Carbon Nanotubes. *Environ. Sci. Technol.* **2013**, 47, (15), 8334-8341.
227. Hale, S. E.; Martin, T. J.; Goss, K.-U.; Arp, H. P. H.; Werner, D., Partitioning of organochlorine pesticides from water to polyethylene passive samplers. *Environmental Pollution* **2010**, 158, (7), 2511-2517.
228. Han, Y.; Zhang, X. H.; Yu, X. P.; Zhao, J. N.; Li, S.; Liu, F.; Gao, P.; Zhang, Y. Y.; Zhao, T.; Li, Q. W., Bio-Inspired Aggregation Control of Carbon Nanotubes for Ultra-Strong Composites. *Sci Rep* **2015**, 5, 9.
229. Kizildag, N.; Ucar, N., Electrospinning Functional Polyacrylonitrile Nanofibers with Polyaniline, Carbon Nanotubes, and Silver Nitrate as Additives. In *Electrospinning - Material, Techniques, and Biomedical Applications*, Haider, S.; Haider, A., Eds. InTech: Rijeka, 2016; p Ch. 02.
230. Cabral, M. G.; Viegas, C. A.; Teixeira, M. C.; Sa-Correia, I., Toxicity of chlorinated phenoxyacetic acid herbicides in the experimental eukaryotic model *Saccharomyces cerevisiae*: role of pH and of growth phase and size of the yeast cell population. *Chemosphere* **2003**, 51, (1), 47-54.
231. Jakubov, T. S.; Kabanova, O. N.; Serpinsky, V. V., TEMPERATURE-DEPENDENCE OF ADSORPTION. *Journal of Colloid and Interface Science* **1981**, 79, (1), 170-177.
232. Haftka, J. J. H.; Govers, H. A. J.; Parsons, J. R., Influence of temperature and origin of dissolved organic matter on the partitioning behavior of polycyclic aromatic hydrocarbons. *Environmental Science and Pollution Research* **2010**, 17, (5), 1070-1079.
233. Zhao, Z. G.; Nagai, N.; Kodaira, T.; Hukuta, Y.; Bando, K.; Takashima, H.; Mizukami, F., Surface treatment- and calcination temperature-dependent adsorption of methyl orange molecules in wastewater on self-standing alumina nanofiber films. *Journal of Materials Chemistry* **2011**, 21, (38), 14984-14989.

234. Booij, K.; Hofmans, H. E.; Fischer, C. V.; Van Weerlee, E. M., Temperature-dependent uptake rates of nonpolar organic compounds by semipermeable membrane devices and low-density polyethylene membranes. *Environmental Science & Technology* **2003**, *37*, (2), 361-366.
235. Carlson, J. C.; Challis, J. K.; Hanson, M. L.; Wong, C. S., Stability of pharmaceuticals and other polar organic compounds stored on polar organic chemical integrative samplers and solid-phase extraction cartridges. *Environ. Toxicol. Chem.* **2013**, *32*, (2), 337-344.
236. Aisha, A. A.; Hneine, W.; Mokh, S.; Devier, M.-H.; Budzinski, H.; Jaber, F., Monitoring of 45 pesticides in Lebanese surface water using Polar Organic Chemical Integrative Sampler (POCIS). *Ocean Science Journal* **2017**, *52*, (3), 455-466.
237. Loos, R.; Wollgast, J.; Huber, T.; Hanke, G., Polar herbicides, pharmaceutical products, perfluorooctanesulfonate (PFOS), perfluorooctanoate (PFOA), and nonylphenol and its carboxylates and ethoxylates in surface and tap waters around Lake Maggiore in Northern Italy. *Analytical and Bioanalytical Chemistry* **2007**, *387*, (4), 1469-1478.
238. Ebele, A. J.; Abou-Elwafa Abdallah, M.; Harrad, S., Pharmaceuticals and personal care products (PPCPs) in the freshwater aquatic environment. *Emerging Contaminants* **2017**, *3*, (1), 1-16.
239. Tiam, S. K.; Fauvelle, V.; Morin, S.; Mazzella, N., Improving Toxicity Assessment of Pesticide Mixtures: The Use of Polar Passive Sampling Devices Extracts in Microalgae Toxicity Tests. *Front. Microbiol.* **2016**, *7*, 17.
240. Lindstrom, A. B.; Strynar, M. J.; Libelo, E. L., Polyfluorinated Compounds: Past, Present, and Future. *Environmental Science & Technology* **2011**, *45*, (19), 7954-7961.
241. Steenland, K.; Fletcher, T.; Savitz, D. A., Epidemiologic Evidence on the Health Effects of Perfluorooctanoic Acid (PFOA). *Environ. Health Perspect.* **2010**, *118*, (8), 1100-1108.
242. Jorgenson, Z. G.; Thomas, L. M.; Elliott, S. M.; Cavallin, J. E.; Randolph, E. C.; Choy, S. J.; Alvarez, D. A.; Banda, J. A.; Gefell, D. J.; Lee, K. E.; Furlong, E. T.; Schoenfuss, H. L., Contaminants of emerging concern presence and adverse effects in fish: A case study in the Laurentian Great Lakes. *Environmental Pollution* **2018**, *236*, 718-733.
243. Brox, S.; Seiwert, B.; Kuster, E.; Reemtsma, T., Toxicokinetics of Polar Chemicals in Zebrafish Embryo (*Danio rerio*): Influence of Physicochemical Properties and of Biological Processes. *Environmental Science & Technology* **2016**, *50*, (18), 10264-10272.
244. Bäuerlein, P. S.; Mansell, J. E.; ter Laak, T. L.; de Voogt, P., Sorption Behavior of Charged and Neutral Polar Organic Compounds on Solid Phase Extraction Materials: Which Functional Group Governs Sorption? *Environ. Sci. Technol.* **2012**, *46*, (2), 954-961.
245. Vermeirssen, E. L. M.; Dietschweiler, C.; Escher, B. I.; van der Voet, J.; Hollender, J., Transfer Kinetics of Polar Organic Compounds over Polyethersulfone Membranes in the Passive Samplers POCIS and Chemcatcher. *Environmental Science & Technology* **2012**, *46*, (12), 6759-6766.
246. Kaserzon, S. L.; Hawker, D. W.; Kennedy, K.; Bartkow, M.; Carter, S.; Booij, K.; Mueller, J. F., Characterisation and comparison of the uptake of ionizable and polar pesticides, pharmaceuticals and personal care products by POCIS and Chemcatchers. *Environmental Science: Processes & Impacts* **2014**, *16*, (11), 2517-2526.
247. Kriegel, C.; Kit, K. M.; McClements, D. J.; Weiss, J., Electrospinning of chitosan-poly(ethylene oxide) blend nanofibers in the presence of micellar surfactant solutions. *Polymer* **2009**, *50*, (1), 189-200.
248. Zheng, J. Y.; Zhuang, M. F.; Yu, Z. J.; Zheng, G. F.; Zhao, Y.; Wang, H.; Sun, D. H., The Effect of Surfactants on the Diameter and Morphology of Electrospun Ultrafine Nanofiber. *Journal of Nanomaterials* **2014**, *9*.

249. Lin, T.; Wang, H. X.; Wang, H. M.; Wang, X. G., The charge effect of cationic surfactants on the elimination of fibre beads in the electrospinning of polystyrene. *Nanotechnology* **2004**, *15*, (9), 1375-1381.
250. Hu, J.; Prabhakaran, M. P.; Ding, X.; Ramakrishna, S., Emulsion electrospinning of polycaprolactone: influence of surfactant type towards the scaffold properties. *J. Biomater. Sci.-Polym. Ed.* **2015**, *26*, (1), 57-75.
251. Yang, D. Y.; Wang, Y.; Zhang, D. Z.; Liu, Y. Y.; Jiang, X. Y., Control of the morphology of micro/nanostructures of polycarbonate via electrospinning. *Chin. Sci. Bull.* **2009**, *54*, (17), 2911-2917.
252. Lundin, J. G.; Coneski, P. N.; Fulmer, P. A.; Wynne, J. H., Relationship between surface concentration of amphiphilic quaternary ammonium biocides in electrospun polymer fibers and biocidal activity. *Reactive and Functional Polymers* **2014**, *77*, 39-46.
253. Zhu, L. L.; Hong, M. H.; Ho, G. W., Hierarchical Assembly of SnO₂/ZnO Nanostructures for Enhanced Photocatalytic Performance. *Sci Rep* **2015**, *5*, 11.
254. Suslu, A.; Albayrak, A. Z.; Urkmez, A. S.; Bayir, E.; Cocen, U., Effect of surfactant types on the biocompatibility of electrospun HAp/PHBV composite nanofibers. *J. Mater. Sci.-Mater. Med.* **2014**, *25*, (12), 2677-2689.
255. Jonn, J.; Quintero, J.; Hoskin, G.; Roweton, S. L. Adhesive-containing wound closure device and method. US20060009099A1, 2006.
256. Majtan, V.; Majtanova, L.; Hostacka, A.; Hybenova, D.; Mlynarcik, D., Effect of quaternary ammonium salts and amine oxides on *Pseudomonas aeruginosa*. *Microbios* **1995**, *84*, (338), 41-51.
257. Long, Y. Y.; Chen, H. B.; Yang, Y.; Wang, H. M.; Yang, Y. F.; Li, N.; Li, K. A.; Pei, J.; Liu, F., Electrospun Nanofibrous Film Doped with a Conjugated Polymer for DNT Fluorescence Sensor. *Macromolecules* **2009**, *42*, (17), 6501-6509.
258. Huang, K.; Li, M.; Chen, Z.; Yao, Y.; Yang, X., Nitrogen-enriched porous carbon nanofiber networks for binder-free supercapacitors obtained by using a reactive surfactant as a porogen. *Electrochim. Acta* **2015**, *158*, 306-313.
259. Ito, A.; Tanaka, K., Chapter 11 - Applications of Carbon Nanotubes and Graphene in Spin Electronics. In *Carbon Nanotubes and Graphene (Second Edition)*, Tanaka, K.; Iijima, S., Eds. Elsevier: Oxford, 2014; pp 253-278.
260. Vaughan, C. W., Determination of 2,4-dichlorophenoxyacetic acid and silvex in water with high-performance liquid chromatography. *Anal. Chim. Acta* **1981**, *131*, 307-310.
261. Yokley, R. A.; Mayer, L. C.; Huang, S.-B.; Vargo, J. D., Analytical Method for the Determination of Metolachlor, Acetochlor, Alachlor, Dimethenamid, and Their Corresponding Ethanesulfonic and Oxanillic Acid Degradates in Water Using SPE and LC/ESI-MS/MS. *Anal. Chem.* **2002**, *74*, (15), 3754-3759.
262. van boven, M.; Laruelle, L.; Daenens, P., *HPLC Analysis of Diuron and Metabolites in Blood and Urine*. 1990; Vol. 14, p 231-4.
263. Paiano, V.; Fattore, E.; Carra, A.; Generoso, C.; Fanelli, R.; Bagnati, R., Liquid Chromatography-Tandem Mass Spectrometry Analysis of Perfluorooctane Sulfonate and Perfluorooctanoic Acid in Fish Fillet Samples. *J. Anal. Methods Chem.* **2012**, *5*.
264. van Leeuwen, S. P. J.; Kärrman, A.; van Bavel, B.; de Boer, J.; Lindström, G., Struggle for Quality in Determination of Perfluorinated Contaminants in Environmental and Human Samples. *Environmental Science & Technology* **2006**, *40*, (24), 7854-7860.
265. Cui, H. Z.; Yan, X. T.; Monasterio, M.; Xing, F., Effects of Various Surfactants on the Dispersion of MWCNTs-OH in Aqueous Solution. *Nanomaterials* **2017**, *7*, (9), 14.

266. Wang, B. M.; Han, Y.; Song, K.; Zhang, T. T., The Use of Anionic Gum Arabic as a Dispersant for Multi-Walled Carbon Nanotubes in an Aqueous Solution. *J. Nanosci. Nanotechnol.* **2012**, *12*, (6), 4664-4669.
267. Clark, M. D.; Subramanian, S.; Krishnamoorti, R., Understanding surfactant aided aqueous dispersion of multi-walled carbon nanotubes. *Journal of Colloid and Interface Science* **2011**, *354*, (1), 144-151.
268. Nguyen, T. T.; Nguyen, S. U.; Phuong, D. T.; Nguyen, D. C.; Mai, A. T., Dispersion of denatured carbon nanotubes by using a dimethylformamide solution. *Adv. Nat. Sci.: Nanosci. Nanotechnol.* **2011**, *2*, (3), 035015/1-035015/4.
269. Vaisman, L.; Wagner, H. D.; Marom, G., The role of surfactants in dispersion of carbon nanotubes. *Adv. Colloid Interface Sci.* **2006**, *128-130*, 37-46.
270. Lundin, J. G.; Giles, S. L.; Yesinowski, J. P.; Rasley, B. T.; Wynne, J. H., Nature of Polyoxometalate Intramolecular Coordination to Quaternary Ammonium Salts from Paramagnetic Relaxation Enhancement. *J. Phys. Chem. C* **2016**, *120*, (31), 17767-17776.
271. Ishikawa, A.; Hanai, T.; Koizumi, N., DIELECTRIC-PROPERTIES OF QUATERNARY AMMONIUM ION-EXCHANGE BEADS DISPERSED IN AQUEOUS PHASES. *Colloid Polym. Sci.* **1984**, *262*, (6), 477-480.
272. Bolto, B.; Dixon, D.; Eldridge, R.; King, S.; Linge, K., Removal of natural organic matter by ion exchange. *Water Research* **2002**, *36*, (20), 5057-5065.
273. Bolto, B.; Dixon, D.; Eldridge, R., Ion exchange for the removal of natural organic matter. *React. Funct. Polym.* **2004**, *60*, 171-182.
274. Metcalfe, C. D.; Sultana, T.; Li, H. X.; Helm, P. A., Current-use pesticides in urban watersheds and receiving waters of western Lake Ontario measured using polar organic chemical integrative samplers (POCIS). *J. Gt. Lakes Res.* **2016**, *42*, (6), 1432-1442.
275. Pasquarell, G. C.; Boyer, D. G., Herbicides in karst groundwater in southeast West Virginia. *J. Environ. Qual.* **1996**, *25*, (4), 755-765.
276. Li, J. H.; Zhou, B. X.; Cai, W. M., The solubility behavior of bisphenol A in the presence of surfactants. *J. Chem. Eng. Data* **2007**, *52*, (6), 2511-2513.
277. Chiou, C. T.; Malcolm, R. L.; Brinton, T. I.; Kile, D. E., WATER SOLUBILITY ENHANCEMENT OF SOME ORGANIC POLLUTANTS AND PESTICIDES BY DISSOLVED HUMIC AND FULVIC-ACIDS. *Environmental Science & Technology* **1986**, *20*, (5), 502-508.
278. Sadorf, E. M.; Linhart, S. M., Ground-Water Quality in Alluvial Aquifers in the Eastern Iowa Basins, Iowa and Minnesota. *U.S. Geological Survey Water-Resources Investigations Report 00-4106 46 p* **2000**.
279. Jacobson, R. B.; Colvin, M. E.; Bulliner, E. A.; Pickard, D.; Elliott, C. M. *Bend-scale geomorphic classification and assessment of the Lower Missouri River from Sioux City, Iowa, to the Mississippi River for application to pallid sturgeon management*; 2018-5069; Reston, VA, 2018; p 46.
280. Linhart, S. M. *Ammonia in ground water from the Mississippi River alluvium, Fort Madison, Iowa*; 2001-4062; Reston, VA, 2001.
281. Littin, G. R. *Selected water-quality data from the Cedar River and Cedar Rapids well fields, Cedar Rapids, Iowa, 2006-10*; 657; Reston, VA, 2012.
282. Gerba, C. P., Quaternary Ammonium Biocides: Efficacy in Application. *Appl. Environ. Microbiol.* **2015**, *81*, (2), 464-469.
283. Mousavi, S.; Deuber, F.; Petrozzi, S.; Federer, L.; Aliabadi, M.; Shahraki, F.; Adlhart, C., Efficient dye adsorption by highly porous nanofiber aerogels. *Colloid Surf. A-Physicochem. Eng. Asp.* **2018**, *547*, 117-125.

284. Lee, H.; Shim, W. J.; Kwon, J. H., Sorption capacity of plastic debris for hydrophobic organic chemicals. *Sci. Total Environ.* **2014**, *470*, 1545-1552.
285. Jahnke, A.; Mayer, P.; Broman, D.; McLachlan, M. S., Possibilities and limitations of equilibrium sampling using polydimethylsiloxane in fish tissue. *Chemosphere* **2009**, *77*, (6), 764-770.
286. Harner, T.; Shoeib, M.; Diamond, M.; Stern, G.; Rosenberg, B., Using passive air samplers to assess urban - Rural trends for persistent organic pollutants. 1. Polychlorinated biphenyls and organochlorine pesticides. *Environmental Science & Technology* **2004**, *38*, (17), 4474-4483.
287. Zhang, G.; Chakraborty, P.; Li, J.; Sampathkumar, P.; Balasubramanian, T.; Kathiresan, K.; Takahashi, S.; Subramanian, A.; Tanabe, S.; Jones, K. C., Passive Atmospheric Sampling of Organochlorine Pesticides, Polychlorinated Biphenyls, and Polybrominated Diphenyl Ethers in Urban, Rural, and Wetland Sites along the Coastal Length of India. *Environmental Science & Technology* **2008**, *42*, (22), 8218-8223.
288. Martinez, A.; Hadnott, B. N.; Awad, A. M.; Herkert, N. J.; Tomsho, K.; Basra, K.; Scammell, M. K.; Heiger-Bernays, W.; Hornbuckle, K. C., Release of Airborne Polychlorinated Biphenyls from New Bedford Harbor Results in Elevated Concentrations in the Surrounding Air. *Environmental Science & Technology Letters* **2017**, *4*, (4), 127-131.
289. Team, T. I. T. R. C. D. S., Technology Overview of Passive Sampler Technologies. **2006**.
290. Namiesnik, J.; Zabiegala, B.; Kot-Wasik, A.; Partyka, M.; Wasik, A., Passive sampling and/or extraction techniques in environmental analysis: a review. *Anal. Bioanal. Chem.* **2005**, *381*, (2), 279-301.
291. Chen, L.; Wang, X.; Lu, W.; Wu, X.; Li, J., Molecular imprinting: perspectives and applications. *Chemical Society Reviews* **2016**, *45*, (8), 2137-2211.
292. Vlatakis, G.; Andersson, L. I.; Muller, R.; Mosbach, K., DRUG ASSAY USING ANTIBODY MIMICS MADE BY MOLECULAR IMPRINTING. *Nature* **1993**, *361*, (6413), 645-647.
293. Ye, L.; Mosbach, K., Molecular imprinting: Synthetic materials as substitutes for biological antibodies and receptors. *Chem. Mat.* **2008**, *20*, (3), 859-868.
294. Mosbach, K.; Ramstrom, O., The emerging technique of molecular imprinting and its future impact on biotechnology. *Bio-Technology* **1996**, *14*, (2), 163-170.
295. Muldoon, M. T.; Stanker, L. H., Molecularly imprinted solid phase extraction of atrazine from beef liver extracts. *Anal. Chem.* **1997**, *69*, (5), 803-808.
296. Yi, L.-X.; Fang, R.; Chen, G.-H., Molecularly Imprinted Solid-Phase Extraction in the Analysis of Agrochemicals. *J. Chromatogr. Sci.* **2013**, *51*, (7), 608-618.
297. Yoshikawa, M., Molecularly imprinted polymeric membranes. *Bioseparation* **2001**, *10*, (6), 277-286.
298. Dai, C.; Zhang, J.; Zhang, Y.; Zhou, X.; Liu, S., Application of molecularly imprinted polymers to selective removal of clofibric acid from water. *PLoS One* **2013**, *8*, (10), e78167.
299. Cao, F.; Wang, L.; Tian, Y.; Wu, F.; Deng, C.; Guo, Q.; Sun, H.; Lu, S., Synthesis and evaluation of molecularly imprinted polymers with binary functional monomers for the selective removal of perfluorooctanesulfonic acid and perfluorooctanoic acid. *J. Chromatogr. A* **2017**, *1516*, 42-53.
300. Ruggieri, F.; D'Archivio, A. A.; Di Camillo, D.; Lozzi, L.; Maggi, M. A.; Mercurio, R.; Santucci, S., Development of molecularly imprinted polymeric nanofibers by electrospinning and applications to pesticide adsorption. *J. Sep. Sci.* **2015**, *38*, (8), 1402-1410.
301. Sharma, S.; Balasubramanian, K., Molecularly imprinted and nanoengineered camphor soot functionalized PAN-nanofibers for effluent treatment. *RSC Adv.* **2015**, *5*, (40), 31732-31741.
302. Berho, C.; Claude, B.; Coisy, E.; Togola, A.; Bayoudh, S.; Morin, P.; Amalric, L., Laboratory calibration of a POCIS-like sampler based on molecularly imprinted polymers for glyphosate and AMPA sampling in water. *Anal. Bioanal. Chem.* **2017**, *409*, (8), 2029-2035.

303. Gunnarsson, J. S.; Rosenberg, R., Eutrophication increases the association of PCB to dissolved organic matter in marine microcosms. *Mar. Pollut. Bull.* **1996**, *33*, (1-6), 100-111.
304. Vitousek, P. M.; Aber, J. D.; Howarth, R. W.; Likens, G. E.; Matson, P. A.; Schindler, D. W.; Schlesinger, W. H.; Tilman, D., Human alteration of the global nitrogen cycle: Sources and consequences. *Ecol. Appl.* **1997**, *7*, (3), 737-750.
305. Yeo, L. Y.; Friend, J. R., Electrospinning carbon nanotube polymer composite nanofibers. *Journal of Experimental Nanoscience* **2006**, *1*, (2), 177-209.
306. Liu, Y.; Kumar, S., Polymer/Carbon Nanotube Nano Composite Fibers—A Review. *ACS Applied Materials & Interfaces* **2014**, *6*, (9), 6069-6087.
307. Silva, J.; Lanceros-Mendez, S.; Simoes, R., Effect of cylindrical filler aggregation on the electrical conductivity of composites. *Physics Letters A* **2014**, *378*, (40), 2985-2988.
308. Zhang, L.; Jiao, L.; Zhong, J.; Guan, W.; Lu, C., Lighting up the interactions between bacteria and surfactants with aggregation-induced emission characteristics. *Materials Chemistry Frontiers* **2017**, *1*, (9), 1829-1835.
309. Ahn, C. K.; Park, D.; Woo, S. H.; Park, J. M., Removal of cationic heavy metal from aqueous solution by activated carbon impregnated with anionic surfactants. *J. Hazard. Mater.* **2009**, *164*, (2-3), 1130-1136.
310. Zhang, H. J.; Wang, J. H.; Zhang, Y. H.; Hu, T. L., Hollow Porous Organic Polymer: High-Performance Adsorption for Organic Dye in Aqueous Solution. *J. Polym. Sci. Pol. Chem.* **2017**, *55*, (8), 1329-1337.
311. Hu, D.; Martinez, A.; Hornbuckle, K. C., Discovery of Non-Aroclor PCB (3,3'-Dichlorobiphenyl) in Chicago Air. *Environmental Science & Technology* **2008**, *42*, (21), 7873-7877.
312. Hu, D.; Lehmler, H.-J.; Martinez, A.; Wang, K.; Hornbuckle, K. C., Atmospheric PCB congeners across Chicago. *Atmospheric Environment* **2010**, *44*, (12), 1550-1557.
313. Kallenborn, R.; Christensen, G.; Evenset, A.; Schlabach, M.; Stohl, A., Atmospheric transport of persistent organic pollutants (POPs) to Bjornoya (Bear island). *Journal of Environmental Monitoring* **2007**, *9*, (10), 1082-1091.